The role of Nr4a1 in the development of Ly6Clow monocytes

Garner, Hannah Claire

Awarding institution:
King's College London

KING'S College LONDON

The role of *Nr4a1* in the development of Ly6C^{low} monocytes

By Hannah Claire Garner

This thesis is submitted to King's College London for the degree of Doctor of Philosophy

October 2015

Abstract

Monocytes are haematopoietic stem cell-derived, immune effector cells. In mice, monocytes consist of two principal subsets: the classical Ly6C-expressing subset and the patrolling Ly6C^{low} subset. The origin and fate of Ly6C^{low} monocytes remains a topic of debate, as does their interrelationship with Ly6C^{+} monocytes. The current model of Ly6C^{low} monocyte development suggests that Ly6C^{+} monocytes are the obligate, steady state precursors of the Ly6C^{low} subset, undergoing conversion or maturation within the blood. However, several studies have reported differing genetic dependencies of monocyte subsets that are in conflict with this model of Ly6C^{low} monocyte development.

To re-investigate monocyte precursor-product relationships, this project combined genetic, kinetic and adoptive transfer studies to probe the interrelationships between bone marrow precursors, blood monocytes and tissue macrophages. This study firstly confirms the existence of a third, minor monocyte subset that expresses MHC II and varying levels of Ly6C and is found in the blood, spleen and bone marrow monocyte compartments. Secondly, this study establishes that all three monocyte subsets arise in the bone marrow from a proliferating common pro-monocyte via two genetically distinct lineages. This study demonstrates that Ly6C^{low} MHC II^{-} monocytes arise from a novel *Nr4a1*-dependent, *Irf8*-independent intermediate population in the bone marrow compartment under steady state conditions, whereas. Thirdly, *Nr4a1*-dependent monocytes have a long half-life and circulate within the systemic and splenic vasculature, contributing minimally to tissue macrophage populations under steady state conditions. The findings in this thesis clarify and extend our understanding of monocyte genetic and functional heterogeneity.

Acknowledgements

I am grateful to my supervisors Frédéric Geissmann and Arnaud Didierlaurent for the opportunities and guidance they have given throughout the course of my PhD.

I would like to say a special thank you to Helen, Céline, Elisa, Katrin and Lucile for their amazing help and support over the past 4 years. Thanks also go to members of CMCBI past and present for help, support and encouragement at various points over the last 4 years.

To Nik, I couldn't have done this without you, thank you for believing in me and making everything better. To my family, for their unwavering love, support and encouragement.

From my time in Norwich, I would like to thank Penny, Jane "O", Debs and Justin.

This PhD was funded by the BBSRC

Declaration

I declare that I have personally prepared this thesis and that the work included is my own, unless otherwise stated. All information sources included in this thesis are referenced accordingly.

Hannah C Garner

October 2015

Table of Contents

Table of Figures

Table of Tables

Abbreviations

2N	Diploid
4N	Tetraploid
7AAD	7-aminoactinomycin D
AAMø	Alternatively activated macrophage
AGM	Aorta-gonad-mesonephros
apoE	Apolipoprotein E
ATAC-seq	Assay for trasnposase accessible chromatin sequencing
Aβ	Amyloid β
BAC	Bacterial artificial chromosome
BM	Bone marrow
BrdU	5'-bromo-2'-deoxyuridine
cDC	Conventional dendritic cell
CDP	Common dendritic cell precursor
ChIP-seq	Chromatin immunoprecipitation sequencing
CLP	Common lymphoid precursor
cMoP	Common monocyte progenitor
CMP	Common myeloid progenitor
CO_2	Carbon dioxide
cProM	Common pro-monocyte
CSF1	Colony stimulating factor 1 (also called MCSF)
DAPI	4',6-diamidino-2-phenylindole
DC	Dendritic cells
DETC	Resident dendritic γ/δ T cells
dNTPs	Deoxyribonucleotides
E	Embryonic day
EDTA	Ethylenediaminetetraacetic acid
TBE	Tris/borate/ethylenediaminetetraacetic
FACS	Fluorescently activated cell sorting
FBS	Foetal bovine serum
FcγR	Fc (fragment, crystallisable region) gamma receptor
FMO	Fluorescence minus one
GFP	Green fluorescent proteins

GM	Granulocyte/macrophage lineage
GMP	Granulocyte macrophage progenitor
GPI	Glycosylphosphatidyl-inositol
HLA-DR	Human leukocyte antigen, DR
HSCs	Haematopoietic stem cell
i.p.	Intraperitoneal
IFN	Interferon
IFNAR	Type I interferon receptor
IFNγ	Interferon gamma
IgG	Immunoglobulin G
IL	Interleukin
iNOS	Inducible nitric oxide synthase
IRF8	Interferon regulatory factor 8
KLF4	Kruppel-like factor 4
LMPP	Lymphoid primed multipotent progenitors
LPM	Large peritoneal macrophage
LPS	Lipopolysaccharide
LT-HSC	Long-term haematopoietic stem cell
M1	Classically activated macrophage
M2	Alternatively activated macrophage
MCMV	Murine cytomegalovirus
MCSF	Macrophage colony stimulating factor
MDP	Macrophage dendritic cell precursor
MegE	Megakaryocyte/erythrocyte lineage
MEP	Megakaryocyte/erythrocyte progenitor
MHC II	Major histocompatibility complex, class II
Mø	Macrophage
MPP	Multipotent progenitor
MPS	Mononuclear Phagocyte System
MTb	Mycobacterium tuberculosis
MyRP	Myeloid restricted progenitors with long term repopulating activity
NK cell	Natural killer cell
NO	Nitric oxide
oxLDL	Oxidised low-density lipoproteins

P/S	Penicillin and streptomycin
PCR	Polymerase chain reaction
pDC	Plasmacytoid dendritic cell
PMNs	Polymorphonuclear leukocytes
PRR	Pattern recognition receptor
RBC	Red blood cells
RES	Reticuloendothelial system
RNA-seq	RNA sequencing
RNI	Reactive nitrogen intermediates
ROS	Reactive oxygen species
RPM	Red pulp macrophages
RT qPCR	Real time quantitative polymerase chain reaction
RXR	Retinoid X receptor
S1PR5	Sphingosine-1 phosphate receptor 5
SD	Standard deviation
SLE	Systemic lupus erythematosus
SPF	Specific pathogen free
SPM	Small peritoneal macrophage
ST-HSC	Short-term haematopoietic stem cell
T2D	Type 2 diabetes
TAMs	Tumour associated macrophages
TF	Transcription factor
T_H1	T-helper 1
T_H2	T-helper 2
TIM4	T-cell immunoglobin mucin
Tip-DC	TNF/iNOS producing dendritic cell
TLR	Toll-like receptor
TNFα	Tumour necrosis factor α
TRM	Tissue resident macrophage
w/v	Weight / volume
WBC	White blood cell
WNV	West Nile Virus
YFP	Yellow fluorescent protein
YS	Yolk sac

1 Introduction

1.1 Historical perspectives of monocyte biology

Almost all metazoan organisms present some form of defence against invading pathogens. Versions of the innate immune system can be seen in invertebrates, such as *Drosophila melanogaster,* and vertebrates including mice and humans. The innate immune system consists of both humoral agents, such as antimicrobial peptides, complement proteins and opsonins, and cellular mechanisms to fight invading pathogens, such as bacteria, fungi and parasites. The cellular arm of the innate immune system consists mainly of specialised cells known as phagocytes. Russian zoologist, Elie Metchnikoff, was the first person to combine the observation of phagocytosis with a detailed hypotheses of the protective role this process could have (Gordon, 2008).

Phagocytes can be found across animal phyla and appear, in evolutionary terms, before the development of the vascular system. Interestingly, specialised phagocytic cells capable of detoxification and immune-like functions can be found in colonies of the social amoeba *Dictyostelium discoideum* (Chen et al., 2007). This indicates phagocytosis is an ancient and conserved scavenging mechanism that has been adapted for protective functions prior to the expansion of animal phyla.

The highly conserved nature of phagocytes allowed Metchnikoff to utilise transparent cells, in particular of starfish larvae and water fleas, as models for early intravital microscopy. During these experiments, he noted that if he pierced the larvae with a foreign object, he could observe the recruitment of amoeboid cells around the foreign object (Gordon, 2008; Metchnikoff, 1891; Metchnikoff, 1892, 1893). Metchnikoff continued to use simple, transparent organisms and directly observed under the microscope the engulfment of particulate matter. The term phagocyte was eventually coined by Professor Carl Friedrich Wilhelm Claus, with whom Metchnikoff discussed his ideas of cellular defence against invading pathogens (Gordon, 2008).

Figure 1-1 Metchnikoff's drawing of phagocytes during inflammation
Reproduced from (Metchnikoff, 1968).

In addition to noting their role as defence against microbial pathogens, Metchnikoff was also the first person to postulate, using Echinoderm larvae, the contribution of phagocytes to the maintenance and renewal of tissues (Metchnikoff, 1884b; Metchnikoff, 1968). These observations led Metchnikoff to suggest that phagocytes seen outside of the vascular system participated in the remodelling of tissue and in

recruiting leucocytes to the point of tissue injury (Metchnikoff, 1884a, b; Metchnikoff, 1892, 1893).

Metchnikoff defined two types of phagocyte, the smaller polymorphonuclear (PMN) leukocyte that he named a "microphage" and the larger mononuclear leukocyte he termed "macrophage" (Gordon, 2008; Metchnikoff, 1968; Yona and Gordon, 2015).

The incredible diversity in anatomical location and functionality is part of what makes macrophages so fascinating, has led to great confusion in the classification of these cells and their interrelationships (Yona and Gordon, 2015). Ehrlich, an early advocate of humoral immunology who was awarded the Nobel Prize jointly with Metchnikoff, pioneered the classification of blood cells based on their nuclear morphology stained with dyes (Ehrlich, 1956; Silverstein, 2009). The pathologist Ludwig Aschoff built upon the early work by Ehrlich by the systematic cellular classification that he termed the "reticuloendothelial system" (RES) (Halpern, 1959). This classification unified phagocytes from diverse tissues into a single system (Halpern, 1959). Aschoff hypothesised that phagocytes belonged in a single system on the basis that these cells had the shared ability to ingest and accumulate particulate matter (Halpern, 1959). Furthermore, he divided cells of the RES into "sessile" and "wandering" and suggested that the cells of the RES derived from their anatomical location (Halpern, 1959).

However mounting evidence accumulated, from the use of experimental inflammation models both *in vitro* (Carrel and Ebeling, 1926; Lewis, 1925) and *in vivo* (Ebert and Florey, 1939; Marchesi and Florey, 1960) that demonstrated monocytes giving rise to macrophages. These observations led to the development of a new framework postulating that macrophages belonged to the haematopoietic system and that they arose from blood monocytes. Consequently, the RES model seemed inaccurate and out-dated

and was eventually replaced by the concept of the mononuclear phagocyte system (MPS).

The MPS, is a model established by van Furth and Cohn (van Furth and Cohn, 1968; van Furth et al., 1972) which hierarchically organised macrophages, monocytes and, after their discovery in 1975, dendritic cells (Steinman et al., 1975) in a single system. This system regarded monocytes as the circulating precursors to tissue resident macrophages, providing an intermediate between cycling bone marrow (BM) progenitors and effector macrophages in tissues. Thus, the MPS outlined a linear model of macrophage development (van Furth, 1970, 1980; van Furth et al., 1972) that has proved to be highly effective and persistent. However, the majority of the experiments that led to the establishment of the MPS relied upon investigating monocytes and macrophages under inflammatory conditions and not in steady state. In addition, many studies have published observations that are at odds with the linear concept of the MPS. For example, during embryogenesis, macrophages can be seen before the emergence of HSCs at embryonic day 10.5 (E10.5) (Boisset et al., 2010; Sorokin et al., 1992) and tissue resident macrophage populations are unaffected by in monocytopenic mice (Yamada et al., 1990). Consequently, yolk sac origins of tissue resident macrophages in steady state has begun to be realised (see section 1.5) and the effector functions of monocytes in their own right is being appreciated.

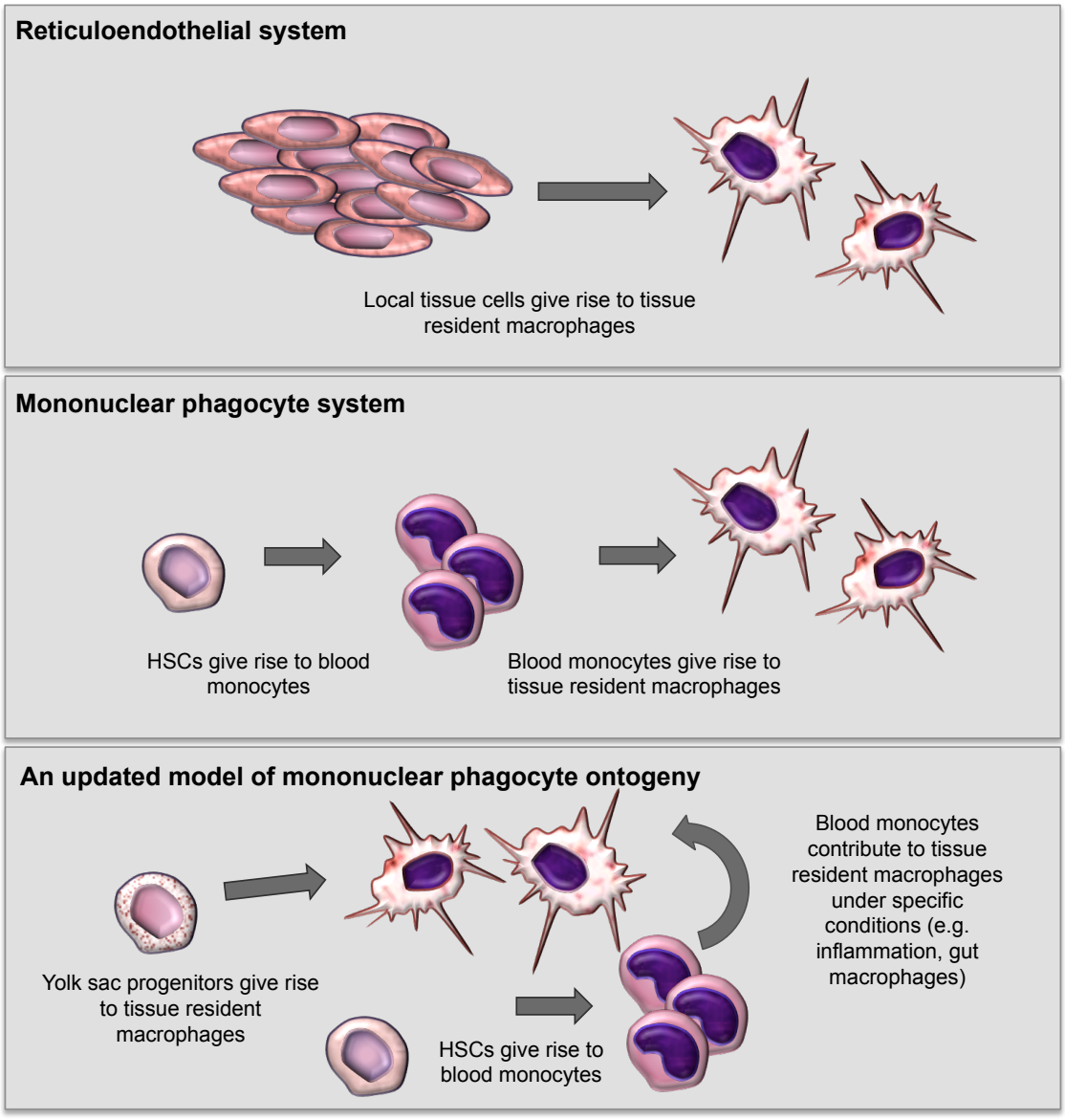

Figure 1-2 A schematic illustrating different models of monocyte and macrophage ontogeny

As can be seen in Figure 1-2, recent advances in our understanding of monocyte and macrophage ontogeny and functionality do not invalidate the model of the mononuclear phagocyte system, rather adds an additional layer of complexity.

1.2 Blood monocytes

1.2.1 Monocyte subsets

Monocytes belong to the myeloid arm of the immune system. They develop normally in lymphoid deficient mice harbouring combined mutations in recombinase activating gene-2 (*Rag2*$^{-/-}$) and common cytokine receptor γ chain (*Il2rg*$^{-/-}$ or *γc*) (Auffray et al., 2007; Mazurier et al., 1999).

Amongst blood cells, monocytes can be defined by high expression of CSF1R (CD115^{+}) and the integrin CD11b (CD11b^{+}) (MacDonald et al., 2005; Sasmono et al., 2003), and do not express CD3, CD19, Ly6G and NK cell markers. Morphologically, monocytes can be identified by their high cytoplasm-to-nucleus ratio and their distinctive bean shaped nuclei (Auffray et al., 2009b) (Figure 1-3).

Table 1-1 Blood cellular morphology

Cell type	Cytospin	Mouse markers	Human markers
Erythrocyte	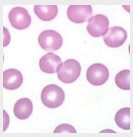	CD235a Ter119	CD235a
Megakaryocyte/ platelet	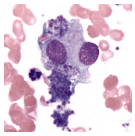	CD41 CD61 CD62P	CD41 CD61 CD62
Granulocyte	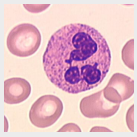	Ly6G Ly6C Gr1 CD66b	CD66b
Monocyte	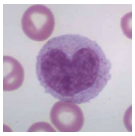	CD115 CD11b Ly6C	CD14 CD16
Lymphocytes	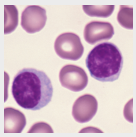	T cells: CD3, CD4, CD8 B cells: CD19, B220	T cells: CD3, CD4, CD8 B cells: CD19, CD20

Monocytes represent ~10% of human blood leukocytes (Kratz et al., 2004) and 1.5-5% of murine blood leukocytes (http://phenome.jax.org). Research over the last 30 years has provided considerable insight into the blood monocyte compartment, revealing that these cells do not represent a homogeneous population, but display considerable heterogeneity, both phenotypically and functionally. In both humans and mice, two principal monocyte subsets have been described (Geissmann et al., 2003; Passlick et al., 1989). In humans, these subsets are defined as $CD14^{+}$ $CD16^{-}$ "classical" monocyte and the $CD14^{dim}$ $CD16^{+}$ "non-classical" monocyte (Ziegler-Heitbrock et al., 2010). In mice, the two principal monocyte subsets are defined as $Ly6C^{+}$ ($GR\text{-}1^{+}$) "classical" or "inflammatory" monocyte and the $Ly6C^{low}$ ($GR\text{-}1^{low}$) "non-classical", "patrolling" or "resident" subset (Figure 1-3) (Geissmann et al., 2003; Ziegler-Heitbrock et al., 2010).

Furthermore, in both the human and mouse blood monocyte compartment, a third minor subset can be seen (Figure 1-3). In humans this is the double positive $CD14^+$ $CD16^+$ population. In murine blood, there is a third subset with varying levels of Ly6C expression that also expresses MHC II^+ (major histocompatibility complex, class II) population (Carlin et al., 2013; Jakubzick et al., 2013). Whilst the main subsets have been relatively well defined phenotypically, there remains some debate as to how they interrelate with each other *in vivo* and how these, poorly characterised, minor subsets relate to the major monocyte subsets.

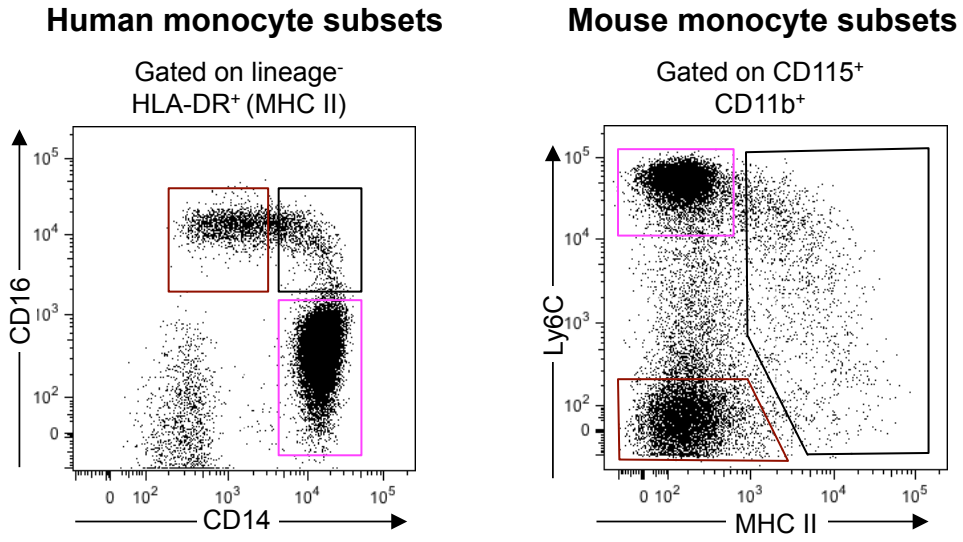

Figure 1-3 Human and mouse monocyte subsets

Human monocyte populations are $CD14^+$ $CD16^-$ "classical" monocytes, which are analogous to murine $Ly6C^+$ monocytes (pink gate); $CD14^{dim}$ $CD16^+$ "patrolling" monocytes, which are thought to be analogous to murine $Ly6C^{low}$ MHC II^- monocytes (red gate). Both humans and mice have a third, intermediate monocyte population that are $CD14^+$ $CD16^+$ in humans and $Ly6C^{int}$ MHC II^+ in mice. These intermediate populations remain to be fully characterised.

1.2.1.1 Human blood monocytes

Traditionally, human monocytes were thought to be a homogeneous blood circulating cell type, defined by expression of CD14 and HLA-DR (Human Leukocyte Antigen-DR) whose principal function was considered to be replenishment of tissue macrophages in homeostasis and under pathological conditions.

The work of Passlick, Flieger and Ziegler-Heitbrock in the late 1980's shed light on the heterogeneity of the human monocyte compartment in terms of size, morphology, phagocytic and adherence capability as well as cell surface markers by identifying a population of $CD14^{dim}$ $CD16^{+}$ monocytes (Passlick et al., 1989; Ziegler-Heitbrock et al., 1988).

At the time, the identification of monocyte heterogeneity was considered to be a reflection of tissue macrophage heterogeneity (Passlick et al., 1989). As a result there were many attempts to clearly discriminate and characterise monocyte subtypes, leading to an appreciation of heterogeneity within the $CD16^{+}$ monocyte compartment. Consequently, the intermediate $CD14^{+}$ $CD16^{+}$ monocyte population was identified as a subset in their own right (Ancuta et al., 2003; Grage-Griebenow et al., 2001b; Moniuszko et al., 2009; Skrzeczynska-Moncznik et al., 2008).

"Classical" $CD14^{+}$ $CD16^{-}$ monocytes make up around 85% of human blood monocytes (Cros et al., 2010; Ziegler-Heitbrock, 2014); they are large (approximately 18-20μm in diameter) (Cros et al., 2010; Passlick et al., 1989), and express CSF1R (CD115), CD11b, CD64 (FcγRI), high levels of the chemokine receptor CCR2, L-selectin (CD62L), and low levels of the chemokine receptor CX_3CR1 (Cros et al., 2010; Grage-Griebenow et al., 2001a; Grage-Griebenow et al., 2000).

In contrast, the "non-classical" $CD14^{dim}$ $CD16^{+}$ monocyte subset is smaller (around 15μm in diameter) and less granular (Cros et al., 2010; Passlick et al., 1989) and make up approximately 7% of human blood monocytes (Cros et al., 2010). This population, by definition, expresses CD16 (FcγRIII) as well as CD115 and high levels of CX_3CR1. Unlike classical monocytes, $CD14^{dim}$ $CD16^{+}$ monocytes do not express CD62L or CD64 and express lower levels of CD11b, HLA-DR and the scavenger receptor CD163 (Cros et al., 2010; Grage-Griebenow et al., 2001a; Grage-Griebenow et al., 2000; Passlick et al., 1989).

The third subset of human monocytes, the $CD14^{+}$ $CD16^{+}$ monocytes, display an intermediate phenotype between the classical and non-classical subsets however gene expression profiling studies have shown that this subset selectively expresses markedly higher levels of HLA-DR compared to $CD14^{+}$ $CD16^{-}$ and $CD14^{dim}$ $CD16^{+}$ subsets. In addition, double positive monocytes express a variety of MHC II-restricted antigen processing genes such as CD74 (class II invariant chain) as well as the co-stimulatory molecule CD40 (Wong et al., 2011; Zawada et al., 2011). An overview of human monocyte subsets is set out in Table 1-2.

Table 1-2 Human blood monocyte subsets

Human monocyte subsets	Frequency of total monocytes	Phenotype	Main functions
$CD14^+ CD16^-$	85%	$CCR2^+$ $CD62L^+$ $CD163^+$ $HLA\text{-}DR^+$ CX_3CR1^{low}	Classical "inflammatory" monocytes Respond to fungi and LPS stimulation
$CD14^+ CD16^+$	~5%	$CCR2^{int}$ $CD62L^{low}$ $CD163^{int}$ $HLA\text{-}DR^{++}$ CX_3CR1^+	Unknown
$CD14^{dim} CD16^+$	~7-10%	$CCR2^-$ $CD62L^-$ $CD163^-$ CX_3CR1^{++}	Patrolling microvasculature, surveying endothelium Respond to TLR-7/TLR-8 stimulus

The differences observed in gene and protein expression patterns reflect functional differences of the three human monocyte subsets. Side by side gene expression profiling of human and mouse monocyte subsets has lent support to the contention that functionally, human $CD14^+ CD16^-$ cells are analogous to murine $Ly6C^+$ classical monocytes (see Figure 1-3) and that human $CD14^{dim} CD16^+$ monocytes are analogous to murine $Ly6C^{low}$ monocytes, although both with important differences. This analogy was extended with intravital imaging demonstrating $CD14^{dim} CD16^+$ monocytes exhibiting patrolling behaviour when transferred to blood vessels in the mouse ear (Cros et al., 2010).

Functionally, human monocyte subsets have distinct responses to infectious agents. Serbina *et al.,* demonstrated that in response to *Aspergillus fumigatus conidia,* $CD14^+ CD16^-$ classical monocytes could inhibit fungal growth but produced little tumour necrosis factor α (TNFα), whereas the double positive, $CD14^+ CD16^+$ subset secreted

considerable quantities of TFNα but were unable to inhibit fungal growth (Serbina et al., 2009).

In response to LPS stimulation, $CD14^+$ $CD16^-$ monocytes produce high levels of reactive oxygen species (ROS), CCL2, CCL3, IL-6 and IL-8 but secreted comparatively low levels of TNFα and IL-1β. In contrast, $CD14^+$ $CD16^+$ monocytes produced very high levels of TNFα, IL-1β and IL-6 but lower levels of CCL3, IL-6 and IL-8 and considerably reduced CCL2 and ROS. In addition, both $CD14^+$ monocyte subsets are highly efficient at phagocytosing latex beads and capable of producing the anti-inflammatory cytokine IL-10 but with differing kinetics (Cros et al., 2010).

Conversely, human $CD14^{dim}$ $CD16^+$ monocytes do not respond strongly to LPS stimulation or phagocytose latex beads efficiently, however, they selectively respond to viral stimulation via TLR7 and TLR8 (Ancuta et al., 2006; Cros et al., 2010). In addition to their patrolling behaviour, this subset expresses very high levels of the fractalkine receptor CX_3CR1 and is shown to traffic in response to CX_3CL1 (fractalkine) in transendothelial migration assays (Ancuta et al., 2004; Ancuta et al., 2003). In contrast, $CD14^+$ monocytes express high levels of chemokine receptors CCR1, CCR2 and CXCR2 but lower levels of CX_3CR1 (Weber et al., 2000) and therefore selectively traffic in response to the chemokine CCL2 (MCP-1).

However, whether these differences in cell surface marker expression and functionality represent separate, bona fide monocyte subsets or different activation states within a single subset remains to be elucidated. To better understand the origin, function and interrelationship of monocyte subsets, the tools available within mouse models have been invaluable. Mouse models allow the use of several genetic approaches as well as *in*

vivo methods of tracing and labelling monocyte subsets. Therefore, the majority of this thesis will focus on murine monocyte subsets.

1.2.1.2 Murine monocyte subsets

The first indication of heterogeneity in murine monocyte subsets came from Palframan *et al.,* based on the differential expression of CX_3CR1-promoter driven green fluorescent protein (GFP) (Jung et al., 2000; Palframan et al., 2001). In 2003, Geissmann et al. described that in both murine and human blood two monocyte subsets could be identified by their expression level of CX_3CR1 and other cell surface markers as well as by their migratory properties (Geissmann et al., 2003). Here it was observed for the first time that the heterogeneity in mouse monocyte subsets was related to function. In addition, it was shown that differential expression of CX_3CR1 and Ly6C allowed the distinction between two major monocyte subsets. $Ly6C^+$ monocytes express low/intermediate levels of CX_3CR1 but high levels of the chemokine receptor CCR2, which they depend upon for their egress from the BM (Serbina and Pamer, 2006). Conversely $Ly6C^{low}$ monocytes express high levels of CX_3CR1 and low to negligible levels of CCR2. Further evidence of murine monocyte heterogeneity was demonstrated in 2013 when both Carlin *et al*., and Jakubzick *et al*., showed that a minority of blood monocytes express MHC II and are have high to intermediate expression of Ly6C (Carlin et al., 2013; Jakubzick et al., 2013).

The CX_3CR1^{low} $Ly6C^+$ $CCR2^+$ monocyte subset was shown to preferentially home to inflamed tissues and have the capacity to differentiate into macrophages and dendritic cells thus they have subsequently become known as “inflammatory monocytes” (Geissmann et al., 2003). This study characterised for the first time the CX_3CR1^{high} $Ly6C^{low}$ $CCR2^{low}$ monocyte subset.

Table 1-3: Murine blood monocyte subsets

Mouse monocyte subset	Frequency of total monocytes	Phenotype	Main functions
$Ly6C^+$ MHC II^-	~50%	$Ly6C^+$ MHC II^- $CCR2^+$ CX_3CR1^{int} $CD11c^-$ $CD11b^+$ $CD115^+$	Classical "inflammatory" monocytes Extravasate in response to inflammatory signals, produce inflammatory mediators and differentiate into DCs and macrophages
$Ly6C^{int}$ MHC II^+	~10%	$Ly6C^{int / low}$ MHC II^+ CCR2? CX_3CR1^{int} $CD11c^{low}$ $CD11b^+$ $CD115^+$	Unknown
$Ly6C^{low}$ MHC II^-	~40%	$Ly6C^{low}$ MHC II^- $CCR2^{low}$ CX_3CR1^{++} $CD11c^+$ $CD11b^+$ $CD115^+$	Patrolling microvasculature assessing endothelial integrity and scavenging microparticles

As $Ly6C^+$ monocytes have been observed giving rise to tissue resident cells in inflammatory conditions (Serbina et al., 2008; Serbina et al., 2003b), have a short half-life (van Furth and Cohn, 1968; Yona et al., 2013) and the capacity to differentiate in dendritic cells (Serbina et al., 2008), it was often assumed that these cells were the blood circulating precursors for tissue macrophages and dendritic cells. In recent years, it has become clear that classical dendritic cells can be maintained independently of monocyte contribution (Liu et al., 2009; Liu et al., 2007; Varol et al., 2009). Furthermore, recent studies have demonstrated that tissue resident macrophages develop prior to the development of monocytes in embryogenesis and many tissue resident macrophage populations are maintained with little contribution from monocytes in the steady state (Gomez Perdiguero et al., 2015; Gomez Perdiguero et al., 2013; Kierdorf et al., 2013a; Schulz et al., 2012; Yona et al., 2013).

However, there are some tissue macrophage populations to which Ly6C^{+} monocytes contribute to in the steady state. For example, at the time of weaning, Ly6C^{+} monocytes colonise the gut lamina propria and differentiate into mature anti-inflammatory macrophages (Bain et al., 2014; Varol et al., 2007). This macrophage pool is constantly replenished throughout life by circulating Ly6C^{+} monocytes (Bain et al., 2014).

The CX_3CR1^{high} Ly6C^{low} $CCR2^{low}$ MHC II^{-} monocyte subset differs from Ly6C^{+} "inflammatory" monocytes: they are smaller in size, as well as the high expression level of CX_3CR1. In addition, this subset expresses high levels of the orphan nuclear receptor NR4A1 and is highly dependent upon it for their development. Further, this subset requires the sphingosine 1 phosphate receptor 5 (S1PR5) for their egress from the BM (Debien et al., 2013). Ly6C^{low} monocytes have been shown to crawl along the luminal side of endothelium where they scavenge microparticles, the behaviour that earned the name "patrolling monocytes" (Auffray et al., 2007; Carlin et al., 2013). Thus, recent work has established that this subset has intravascular effector functions in their own right.

In addition to being referred to as "patrolling" monocytes, this subset is sometimes known as "resident" monocytes. This is due to the observation that this subset persisted longer in tissues in the absence of inflammation and were shown to express CD11c and MHC II after adoptive transfer (Geissmann et al., 2003). These data were interpreted at the time as suggesting that Ly6C^{low} monocytes were a blood circulating precursor for tissue resident dendritic cells (DCs) and could potentially also represent a blood-circulating progenitor population for tissue resident macrophages (Geissmann et al., 2003). Despite the identification of the yolk sac origin of most tissue macrophages, this hypothesis of monocytes giving rise to tissue macrophages has persisted in the literature and will be addressed in this thesis.

1.2.1.3 Monocytes and dendritic cells

The interrelationship between monocytes and DCs has become considerably clearer over the last two decades. DCs belong to the myeloid branch of the immune system and are specialised antigen presenting cells. DCs were originally described as cells enriched in the mouse spleen (Steinman and Cohn, 1973; Steinman et al., 1974) that were the most potent stimulators of T cells in primary mixed leucocyte reactions (Steinman and Witmer, 1978). DCs have now been identified in almost every tissue that has been studied, with the exception of the brain parenchyma, all of which are highly efficient at the uptake and processing of antigens for presentation to naïve T cells (Mildner and Jung, 2014). Broadly, DCs can be subdivided into three main categories: conventional DCs (cDCs), monocyte-derived DCs, known as TNFα/iNOS producing DCs (Tip-DCs) and plasmacytoid DCs (pDCs).

After the identification of dendritic cells by Steinman *et al.,* in 1973 (Steinman and Cohn, 1973) there was some controversy as to whether they should be included in the MPS, but eventually, van Furth included them and subsequent studies identified a common developmental pathway with monocytes (Fogg et al., 2006).

Monocytes are highly plastic cells that have the potential to give rise to monocyte-derived Tip-DCs (Auffray et al., 2009b; Gordon and Taylor, 2005; Randolph et al., 1999; Serbina et al., 2008; Taylor and Gordon, 2003). Among circulating monocytes the $Ly6C^+$ subset is the proposed precursor of Tip-DCs the in models of infection and tissue damage (Auffray et al., 2009b; Dominguez and Ardavin, 2010; Serbina et al., 2003b). However, differentiation of $Ly6C^+$ monocytes into DCs is observed, for the most part, under inflammatory conditions. For example, in the context of *Listeria monocytogenes* infection, $Ly6C^+$ monocytes are recruited to the site of infection, where they produce

high levels of TNFα and iNOS, earning them the name Tip-DCs (Serbina et al., 2008; Serbina et al., 2003b). In addition, these monocyte-derived cells are efficient at priming naïve T cells, express high levels of MHC II and morphologically resemble DCs (Serbina et al., 2003b; Serbina et al., 2012). However, it has become clear in recent years that in steady state "classical" cDCs arise from the common dendritic cell precursor (CDP), independently of any monocyte contribution (Liu et al., 2009; Varol et al., 2007; Waskow et al., 2008).

1.3 Monocyte development

1.3.1 Haematopoiesis

1.3.1.1 Haematopoietic stem cells

The classical model of adult haematopoiesis is a hierarchical model of haematopoietic stem cell (HSC) commitment (Morrison and Weissman, 1994; Spangrude et al., 1988; Weissman, 2000). As far as we currently know, haematopoietic stem cells and their progenitors give rise to all immune cells with the exception of yolk sac derived macrophages. The sequence of differentiation that links multipotent HSCs, with their capacity for self-renewal, to terminally differentiated, mature cells that have lost the ability to self-renew, is still a matter of great discussion despite being extensively studied.

However, the identification of a series of intermediates, characterised by their surface marker expression and clonogenic ability, has provided the foundation on which the classical model of haematopoiesis has been built. In this model, HSCs give rise to progeny that progressively become more restricted to a single lineage whilst losing their capacity for self-renewal. The definition of a haematopoietic stem cell in this context is

a self-renewing cell that can be transplanted to a lethally irradiated mouse and rescue this mouse from lethality by re-establishing long-term blood production (Eaves, 2015; Spangrude et al., 1988; Weissman, 2000).

This stochastic model of haematopoiesis argues that a very small number of quiescent, self-renewing, long-term haematopoietic stem cells (LT-HSC) self-renew throughout the whole life of an organism (Christensen and Weissman, 2001; Laiosa et al., 2006; Morrison and Weissman, 1994; Osawa et al., 1996). These give rise to short-term HSCs (ST-HSC), which have limited capacity for self-renewal (Morrison and Weissman, 1994; Yang et al., 2005). In contrast with these results obtained mostly by transplantation of HSCs, recent pulse labelling studies of adult HSCs *in situ* have demonstrated that such ST-HSCs nearly fully self-renew, sustain most adult haematopoiesis, only receiving rare but polyclonal input from LT-HSCs (Busch et al., 2015).

The next step in this model of haematopoiesis are multipotent progenitors (MPP) found within the HSC compartment (Morrison et al., 1997). These are the progeny of ST-HSCs, which have to make a binary decision regarding the fate of their progeny, either to the lymphoid or myeloid lineage. Such fate decisions have been proposed to be a result of activation of lineage specific transcription factors (TF), triggering different genetic programmes. This will be discussed further in section 1.3.

Classically, the progeny of MPPs are either the common lymphoid progenitor (CLP) or the common myeloid progenitor (CMP). Interestingly, whilst HSCs have the potential to give rise to all blood cells, they preferentially express more myeloid associated genes rather than lymphoid associated genes until the fate decision of CLP or CMP is made

(Miyamoto et al., 2002). This is in accordance with the strong myeloid bias observed in adult HSCs *in vivo* (Busch et al., 2015).

The clonogenic progenitor common for cells of the lymphoid lineage was the first lineage-restricted MPP identified (Kondo et al., 1997). This IL-7Rα^{+} progenitor was shown to give rise to T cells, B cells and natural killer (NK) cells but could not give rise to cells of the myeloid lineage (Akashi et al., 1999; Kondo et al., 1997). This raised the obvious question of identifying a clonogenic progenitor that could give rise to cells of the myeloid lineage and in 2000, work from the Weissman lab demonstrated the presence of a common myeloid progenitor (CMP) (Akashi et al., 2000). Within the IL-7Rα^{-} fraction of murine BM cells, the CMP had the potential to give rise to either granulocyte/macrophage (GM) progenitors or megakaryocyte/erythrocyte (MegE) progenitors. From this work, it was proposed that commitment to the GM lineage was mutually exclusive from commitment to the MegE lineage.

Whilst this model has been vital for our conceptual understanding of haematopoiesis and HSC commitment further studies and improving analytical techniques as well as experimental models have provided evidence for further hypotheses to emerge. For example, in 2005 work by the lab of Jackobsen and colleagues demonstrated the presence of a population within the HSC compartment, resembling MPPs but expressing high levels of Flt3. This population does not have the potential to generate megakaryocytes or erythrocytes but has the capacity to generate T-, B-, and myeloid-cell restricted progenitors. This population is the most primitive HSC with lymphoid gene expression thus it was termed “lymphoid primed multipotent progenitor” (LMPP) (Adolfsson et al., 2005). While they can give rise to all lineages they are not bona fide HSCs as they only have a limited capacity of self-renewal – capable of short-term (up to 8 weeks) multilineage repopulation. These studies indicated that a loss of MegE

potential is accompanied by a gain of expression of lymphoid associated genes and maintenance of myeloid potential, a phenomenon known as multilineage priming (Adolfsson et al., 2005; Hu et al., 1997; Mansson et al., 2007; Miyamoto et al., 2002). Importantly, no co-expression of lymphoid- and MegE-associated genes was observed, indicating that commitment of these cell fates is mutually exclusive.

A recent study by Yamamoto *et al.,* further challenged the step-wise hierarchical model of haematopoiesis by the identification of myeloid-restricted progenitors with long-term repopulating activity (MyRP). The authors in this study showed that HSCs could differentiate directly into MyRP via asymmetric cell division. By using single cell transplantation systems and paired daughter analysis the authors were able to show lineage commitment at the level of the HSC and bypass the step-wise lineage commitment steps of the classical model of HSC differentiation (Yamamoto et al., 2013).

To add a supplemental layer of complexity, HSCs found in the developing embryo (foetal HSCs) are not equivalent to their adult counterparts, as evidenced by their balanced or unbiased output (Crisan et al., 2015). In 1989, Leonore and Leonard Herzenberg (Herzenberg and Herzenberg, 1989) proposed that the immune system gives rise to distinct and successive waves ("layers") of immune and progenitor cells during development and adulthood. In accordance, foetal HSCs are the only source for several foetal (B-1 B cells (Montecino-Rodriguez et al., 2006) and γ/δ T cells (Havran and Allison, 1988; Ikuta et al., 1990)) and adult lymphoid populations (resident dendritic γ/δ T cells (DETCs) in the adult mouse epidermis (Havran and Allison, 1990).

These findings are intriguing and provide insights into the fine nuances of how HSCs give rise to lineage committed progenitors and are helping to redraw our understanding of haematopoiesis from a hierarchical model to a networked model.

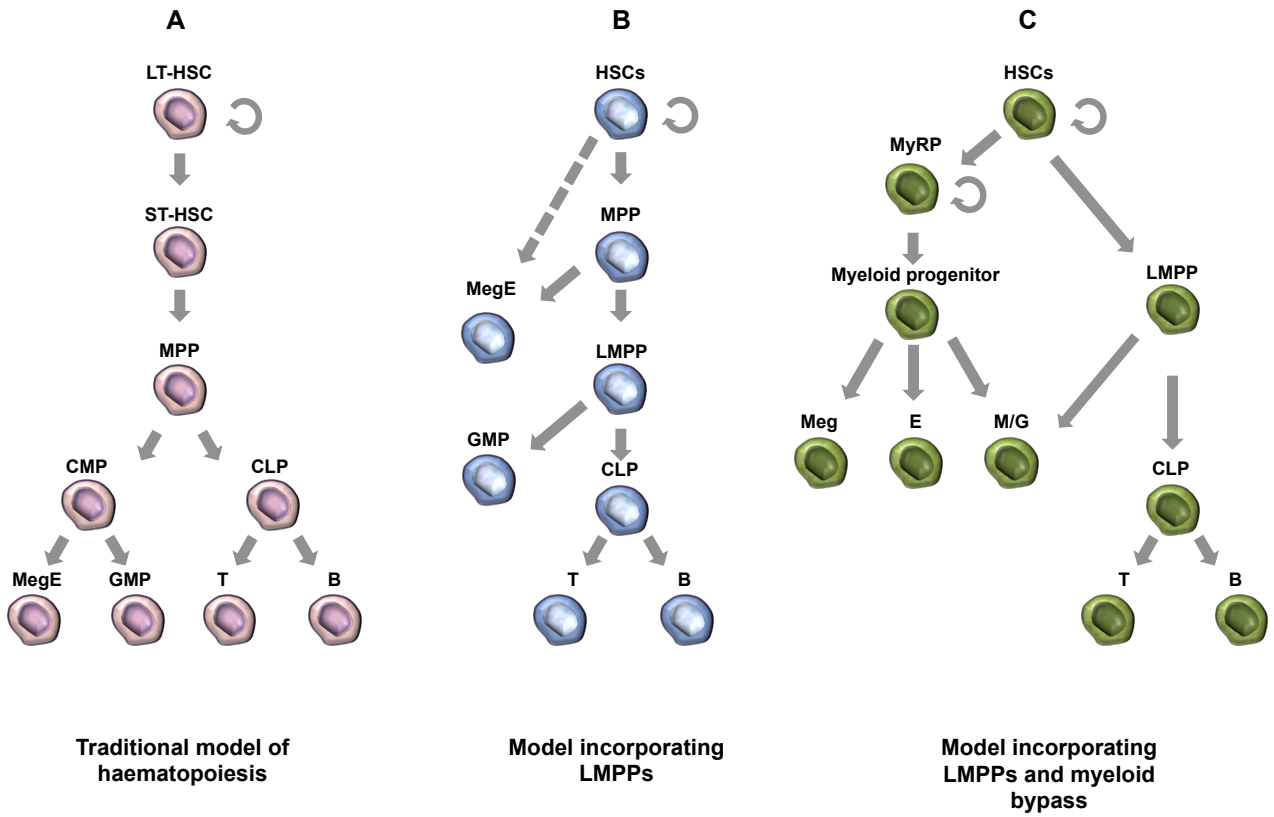

Figure 1-4 A schematic illustrating different models of haemoatopoiesis

(A) Illustrates the traditional, linear model of haematopoiesis that suggests a strict separation between myelopoiesis and lymphopoiesis; **(B)** illustrates the revised view of the haematopoietic model after the identification of LMPPs; **(C)** illustrates the myeloid bypass model (Yamamoto et al., 2013) which suggests that multipotentiality and the ability to self-renew can be disassociated.

1.3.1.2 Macrophage and dendritic cell precursor (MDP) and common monocyte progenitor (cMoP)

A major step forward in our understanding of monocyte development was the identification of the macrophage and dendritic cell precursor (MDP) in mouse BM (Fogg et al., 2006). The MDP was so called because at the time of its identification, monocytes were still considered the obligate precursors to all tissue resident macrophage populations in steady state. While they are still the main source of "infiltrating" macrophages, most macrophages found in tissues are not maintained by differentiation of monocytes, but rather develop from yolk sac derived progenitors. However, the name macrophage and dendritic cell precursor has persisted although perhaps a more accurate name for this population now would be "monocyte and dendritic cell precursor".

The MDP is downstream of the common myeloid progenitor (CMP) and the granulocyte/macrophage progenitor (GMP), having lost granulocyte potential. MDPs express KIT (CD117), CSF1R (CD115) and FLT3 (CD135) whilst they are negative for lymphoid lineage markers such as CD3 and CD19. The MDP has been shown to be a proliferating subset of BM cells that can give rise to monocytes and the common dendritic cell progenitor (CDP) (Auffray et al., 2009a; Fogg et al., 2006; Naik et al., 2007; Onai et al., 2007; Varol et al., 2007).

The chemokine receptor CX_3CR1 is not expressed on early haematopoietic progenitors but is subsequently upregulated on the MDP (Fogg et al., 2006), and its expression, using the CX_3CR1^{GFP} knock-in mouse (Jung et al., 2000) was instrumental in identifying the MDP population (Fogg et al., 2006). Thus, expression of CX_3CR1 is

associated with commitment to monocyte and dendritic cell lineages (Auffray et al., 2009a; Fogg et al., 2006).

In 2013, the next commitment step along the pathway of monocyte development was elucidated. Hettinger *et al.,* showed that the upregulation of Ly6C and loss of Flt3 expression identified a monocyte-committed, proliferating BM population that the authors called the common monocyte progenitor (cMoP) (Hettinger et al., 2013). In this paper, the authors show the existence of heterogeneity within the KIT^+ $CD115^+$ compartment that has previously been considered to contain only the MDP/CDP, there is heterogeneity. By including Ly6C as a marker when investigating this compartment, the cMoP can be identified. Adoptive transfer in non-irradiated mice confirmed that this population could give rise to monocytes *in vivo* (Hettinger et al., 2013).

1.3.2 Molecular control of monocyte development

Commitment to the myeloid lineage and the subsequent development of blood monocytes is under tight control by both intrinsic and extrinsic factors. A number of transcription factors have been found to be key regulators in monocyte development; furthermore, extrinsic signals have been shown to be vital molecular cues directing the development of monocytes from multipotent progenitors. The understanding of these molecular cues remains incompletely elucidated, however, there have been several genetic models that have provided significant insight in to the molecular requirements for monocyte development.

The cues and signals that push HSCs along the myeloid lineage as opposed to the lymphoid lineage are incompletely understood but genetic models have provided the tools to better understand myeloid lineage commitment. Disruption of specific myeloid-associated genes is one of the most powerful tools available for understanding the

molecular requirements for monocyte development. Both naturally occurring mutations and laboratory engineered disruption of genes, either by complete ablation or by conditional deletion, has provided significant insights into the molecular control of monocyte development.

1.3.2.1 cMyb

During embryogenesis, there are three waves of haematopoiesis (Golub and Cumano, 2013): an initial yolk sac (YS) primitive wave followed by two successive definitive waves, the definitive YS-derived progenitors and the foetal HSCs. During the latter, HSCs generated in the aorta-gonad-mesonephros (AGM) region of the embryo seed the foetal liver, where they expand (Golub and Cumano, 2013; Medvinsky and Dzierzak, 1996; Muller et al., 1994). The proto-oncogene cMyb is required for expansion, self-renewal and maintenance both foetal and adult HSCs, and a lack of cMyb expression leads to rapid HSC-derived haematopoiesis failure, including a complete absence of adult monocytes (Mucenski et al., 1991; Mukouyama et al., 1999; Schulz et al., 2012).

Whilst cMyb is expressed by all definitive haematopoietic progenitors (both YS-progenitors and HSCs) (Kierdorf et al., 2013a; Mucenski et al., 1991; Soza-Ried et al., 2010), primitive haematopoiesis and YS-definitive myelopoeisis are unaffected in cMyb-deficient animals (Gomez Perdiguero et al., 2015; Schulz et al., 2012; Soza-Ried et al., 2010; Sumner et al., 2000; Tober et al., 2008). Thus, dependency on cMyb genetically separates the first two YS waves from the intra-embryonic HSC wave of haematopoiesis.

1.3.2.2 PU.1

PU.1 is a transcription factor belonging to the E-twenty six or E26 transformation-specific (Ets) family of transcription factors, encoded by the *Sp1* gene. Sometimes

considered the "master regulator" of lineage commitment, PU.1 is dispensable for the generation of HSCs but it is required for commitment to myeloid or lymphoid lineages (Dakic et al., 2005). PU.1 deficiency is lethal and mice lacking PU.1 die either at a late embryonic stage or shortly after birth. Analysis of these animals revealed severely impaired development of monocytes, granulocytes, T-cells, and B-cells (McKercher et al., 1996; Scott et al., 1994; Spain et al., 1999) and to a lesser extent, NK cells (Colucci et al., 2001). However, cells of the megakaryocyte/erythrocyte (MegE) lineage are intact in these animals (McKercher et al., 1996; Scott et al., 1994). Furthermore, conditional deletion of PU.1 in adult mice uncovers a complete ablation of the CLP, CMP and GMP and an increased frequency of megakaryocyte/erythrocyte progenitors (MEPs) (Dakic et al., 2005; Iwasaki et al., 2005). These studies show that PU.1 has an important role in the lineage commitment of MPPs to proceed to CMPs and CLPs but it is redundant for the development of cells in the MegE lineage.

1.3.2.3 The role of Irf8 in determining monocytic and ganulocytic fates

The decision to commit to monocytic versus granulocytic fates at the GMP is determined by PU.1 and it's DNA binding partners. For cells to commit to the monocytic lineage, one such binding partner is IRF8 (Tamura et al., 2000). *Irf8* is expressed by progenitors, monocytes and macrophages but not granulocytes. Indeed *Irf8*-deficient mice show increased susceptibility to intracellular infections such as vaccinia virus or tuberculosis (Holtschke et al., 1996; Marquis et al., 2009; Turcotte et al., 2007) which has been linked to reduced expression of IL-12p40 by monocytic cells resulting in impaired T cell activation (Giese et al., 1997; Scharton-Kersten et al., 1997). Interestingly, immunodeficient humans with IRF8 mutations that affect DNA binding are also susceptible to tuberculosis infections, which are associated with impaired IL-12 production (Hambleton et al., 2011).

Furthermore, *Irf8*-deficiency is associated with a myeloproliferative syndrome that results marked increase in granulocyte numbers but significantly reduced monocytes and macrophages (Holtschke et al., 1996; Kierdorf et al., 2013a). Holtschke *et al.,* demonstrated that *Irf8*-deficient mice have a differentiation block during haematopoiesis, which manifests in a myeloproliferative syndrome resembling human chronic myeloid leukaemia (Holtschke et al., 1996). *Irf8* and its role in monocyte development will be discussed in more detail below.

1.3.2.4 The role of Csf1r (CD115) signalling in myeloid development

Monocyte development in mice is completely dependent upon *Csf1r* (also known as CD115 and M-Csfr) encoded by the proto-oncogene *c-fms.* Deficiency in *Csf1r (Csf1r*$^{-/-}$ *)* results in a severe phenotype: small, toothless animals with shortened limbs due to a failure in osteoclast development that results in impaired bone remodelling finally resulting in a shortened adult life span (Dai et al., 2002). Furthermore, these mice are devoid of circulating monocytes and have significantly depleted F4/80^{+} tissue macrophage populations in many tissues (Dai et al., 2002).

Csf1r$^{-/-}$ mice have a more severe phenotype than with the naturally occurring *op/op* mice, which have a mutation in the coding region of one of the *Csf1r* ligands, *Csf1*, and consequently, no CSF1 (also known as MCSF) protein can be detected in these animals (Wiktor-Jedrzejczak et al., 1990; Yoshida et al., 1990). Similarly to the *Csf1r*$^{-/-}$ mouse, the *op/op* mouse has a marked deficiency in osteoclasts that renders them osteopetrotic, a lack of circulating monocytes and a reduction in macrophage populations compared with littermates. The reduction of macrophages observed in these mice, rather than complete absence, is attributed to the fact that *Csf1r* has another ligand, IL-34 (Auffray et al., 2009b; Lin et al., 2008). Dai *et al.,* showed in 2002 that mice with one copy of

Csf1r but with the *op/op* mutation (*Csf1r*$^{+/-}$ / *Csf1*$^{op/op}$) showed the same phenotype as the *op/op* mice and not the same severity as *Csf1r*$^{-/-}$ which suggested that *Csf1r* was responding to second ligand. Consequently, IL-34 was identified by using a functional high-throughput screen of human monocytes (Lin et al., 2008).

As discussed above, HSC lineage commitment decisions are usually explained by stochastic models (Till et al., 1964) and the prevailing model is that cytokines have little direct influence on HSC commitment (Cross and Enver, 1997; Enver et al., 1998; Metcalf, 2007). However, it was shown that under conditions of haematopoietic stress that induce systemically high levels CSF1 such as infection and inflammation, CSF1 can directly influence differentiation of HSCs to a myeloid bias (Mossadegh-Keller et al., 2013). The authors demonstrate that CSF1 has the ability to directly induce PU.1, which instructs a transient and reversible change of HSC differentiation preference to a myelo-monocytic fate regardless selective survival or proliferation (Mossadegh-Keller et al., 2013).

Thus, monocyte development is regulated by a number of genetic signals. However, different monocyte subsets have their own genetic requirements. The next section of this thesis will discuss the genetic requirements of the two principal murine monocyte subsets.

1.3.2.5 Ly6C^{+} monocyte specific transcription factors

The current model of monocyte development suggests that the MDP gives rise to the cMoP, which gives rise to Ly6C^{+} monocytes, which mature or undergo conversion into Ly6C^{low} monocytes (Sunderkotter et al., 2004; Varol et al., 2007; Yona et al., 2013; Yrlid et al., 2006). However, analysis of various genetic models have provided insights

that seemly contradict this model or at least bring into question some of the nuances of monocytes development.

The Kruppel-like factor 4 (KLF4) was shown by Feinberg *et al.,* to be a critical regulator of monocyte differentiation (Feinberg et al., 2007). In this study, it was demonstrated that KLF4 is a downstream target of PU.1 and KLF4 deficiency is associated with impaired monocyte development but increased granulocyte development. However, detailed *in vivo* studies of the role *Klf4* plays in monocyte development were hampered by lethality shorty after birth in KLF4-deficient animals due to an inability of these mice to establish the barrier function of the skin (Segre et al., 1999).

In a study by Alder *et al.,* (Alder et al., 2008), the authors were surprised to observe that $Ly6C^{low}$ monocytes were still evident, albeit reduced; in $KLF4^{-/-}$ chimeras that were completely ablated of blood $Ly6C^{+}$ monocytes. This was surprising given the current model of $Ly6C^{low}$ monocyte development relies upon blood $Ly6C^{+}$ monocytes maturing into $Ly6C^{low}$.

Further investigations by Kurotaki *et al.,* into the role of KLF4 in monocyte development by identified that $Irf8^{-/-}$ mice displayed similar but even more severe abnormalities than those observed in the KLF4 chimeras, most notably $Irf8^{-/-}$ mice are also devoid of blood $Ly6C^{+}$ monocytes (Kurotaki et al., 2013). The authors demonstrated that KLF4 is directly induced by IRF8, thus identifying a KLF4-IRF8 axis vital for $Ly6C^{+}$ monocyte development (Kurotaki et al., 2013). Of note, this study also observed blood $Ly6C^{low}$ monocytes developing in the absence of $Ly6C^{+}$, although reduced in numbers.

1.3.2.6 Ly6C^{low} monocyte specific transcription factors

In 2011, Hanna *et al.,* showed that mice lacking the transcription factor *Nr4a1* have a defect in BM Ly6C^{low} monocyte development and survival, resulting in a lack of Ly6C^{low} monocytes in the blood, patrolling microvasculature and in the spleen (Hanna et al., 2011). This study demonstrated that *Nr4a1*$^{-/-}$ mice were unable to develop Ly6C^{low} monocytes whilst having normal numbers of myeloid progenitors including the MDP and Ly6C^{+} monocytes compared to wild type animals (Hanna et al., 2011). Furthermore, the few remaining patrolling monocytes that were observed in the BM of *Nr4a1*$^{-/-}$ mice were unable to complete cell cycle and accumulated in S phase of proliferation where they underwent apoptosis (Hanna et al., 2011). In addition, the few remaining Ly6C^{low} monocytes from *Nr4a1*$^{-/-}$ animals expressed lower levels of CX_3CR1 and were larger in size (Hanna et al., 2011).

This led to the hypothesis that Ly6C^{low} monocytes develop independently of Ly6C^{+} monocytes in the BM, arising via a distinct differentiation pathway. This paper raised the possibility that, although it is accepted that both monocyte subsets arise from the MDP, the intermediate steps between MDP and mature blood monocytes remains unclear as both subsets require different molecular input for their differentiation and maturation.

1.3.2.7 Ly6C^{+} and Ly6C^{low} monocytes rely on different mechanisms for bone marrow egress

Ly6C^{+} monocytes are reduced in the periphery of *Ccr2*$^{-/-}$ mice whereas their BM contains normal or slightly increased Ly6C^{+} monocyte numbers (Tsou et al., 2007). Thus, *Ccr2*-deficiency causes a defect in Ly6C^{+} monocyte mobilisation, resulting in impaired BM Ly6C^{+} monocyte egress to the periphery (Serbina and Pamer, 2006; Tsou

et al., 2007). The principal chemokines responsible for Ly6C^{+} monocyte mobilisation from the BM are CCL1 (MCP-1) and CCL7 (MCP-3) and animals that lack either of these chemokines also have impaired monocyte mobilisation in response to inflammatory stimuli (Tsou et al., 2007). In addition, infection with *Listeria monocytogenes* results in BM accumulation of activated Ly6C^{+} monocytes in *Ccr2*-deficient mice (Serbina et al., 2008; Serbina and Pamer, 2006).

In a similar manner to Ly6C^{+} monocytes having an impaired egress from the BM to the periphery in *Ccr2*$^{-/-}$ mice, Ly6C^{low} monocytes require sphingosine-1 phosphate receptor 5 (S1PR5) to mediate their egress from the BM (Debien et al., 2013). Debien *et al*., showed that *S1pr5*$^{-/-}$ mice had normal frequencies of Ly6C^{low} monocytes in the BM but significantly reduced frequencies of this subset in the periphery. Furthermore, the Ly6C^{+} monocyte frequency was unaffected by this mutation in the BM and in the periphery, arguing against the current model of monocyte development in which Ly6C^{+} monocytes give rise to the Ly6C^{low} subset in the blood.

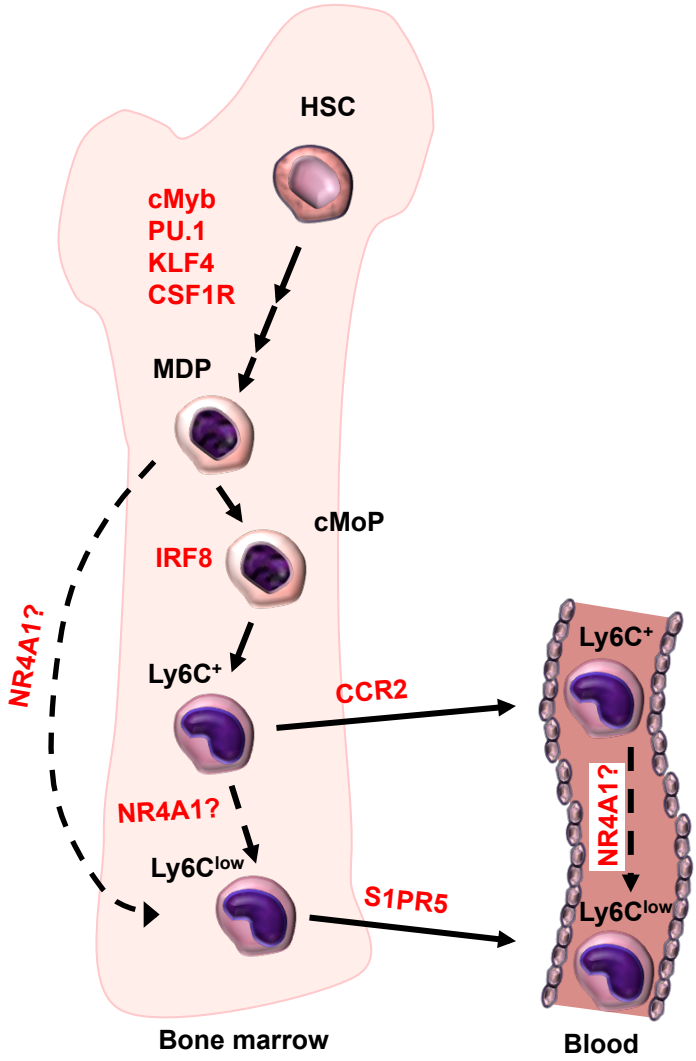

Figure 1-5 Molecular control of monocyte development

Commitment to the myelo-monocytic lineage is under the control of cMyb, PU.1, KLF4, and CSF1R. Ly6C^{+} monocyte development requires the transcription factor IRF8 for their development and CCR2 for their BM egress whereas Ly6C^{low} monocytes are selectively dependent on NR4A1 for their development and S1PR5 for their BM egress.

1.4 Monocyte effector functions

As long ago as 1939, it was observed, *in vivo*, that monocytes could extravasate in response to acute tissue injury by Ebert and Florey (Ebert and Florey, 1939). Using a chamber to observe monocyte extravascular development in response to tissue injury in rabbit ears, they directly observed monocytes leaving blood vessels and transforming into monocyte-derived macrophages and phagocytosing debris. Whilst early studies

such as these (Ebert and Florey, 1939) aided the misconception that monocytes are solely the blood circulating precursors of tissue resident macrophages, they also provided early insight into the effector functions of monocytes *in vivo*.

1.4.1 Ly6C$^+$ monocyte effector functions

Ly6C$^+$ monocytes have been known to be involved in the inflammatory process for many years now and the majority of what is known about monocyte effector functions arises from studies investigating this subset using various inflammatory models, including infection, high fat diet and cancer (Auffray et al., 2009b; Gordon and Taylor, 2005; Wynn et al., 2013).

Both monocyte subsets have been shown to traffic to sites of infection but rely on different cues (Ancuta et al., 2003; Auffray et al., 2007; Serbina and Pamer, 2006; Tacke and Randolph, 2006) and with vastly different efficiencies.

1.4.1.1 Bacterial infections

As previously mentioned, Ly6C$^+$ monocytes are frequently referred to in the literature as "inflammatory" monocytes reflecting their responsiveness to inflammatory stimuli including cytokine production and their readiness to extravasate. Ly6C$^+$ monocytes have a pivotal role in immunity against pathogens and their recruitment and activation is required for effective control and clearance of many pathogens and their role has been extensively studied in particular, the work of Pamer's lab has provided considerable insight into Ly6C$^+$ monocyte effector functions particularly in the context of *L. monocytogenes* infection (Pamer, 2004; Serbina et al., 2008; Serbina and Pamer, 2006).

L. monocytogenes is a facultative intracellular, Gram-positive bacterium that is acquired through the gastrointestinal tract. Innate immune responses in mice are quickly

triggered after infection, acting to restrict bacterial growth in the spleen and liver, the main infection sites (Rosen et al., 1989). Ly6C$^+$ monocytes and Ly6C$^+$ monocyte-derived Tip-DCs are recruited to infection foci where they produce TNFα and iNOS (Kurihara et al., 1997; Serbina et al., 2003b). Ly6C$^+$ monocyte mobilisation in response to infection is dependent upon the chemokine receptor CCR2 interacting with its ligands, the chemokines CCL2 and CCL7 (also known as MCP-1 and MCP-3, respectively) (Tsou et al., 2007). Thus, *Ccr2*$^{-/-}$ mice are less able to clear infections such as *L. monocytogenes* where in *Ccr2*$^{-/-}$ mice, activated Ly6C$^+$ monocytes accumulate in the BM (Serbina and Pamer, 2006).

Infection with *L. monocytogenes* induces the CCR2 ligands CCL2 and CCL7. Mice that lack these chemokines have reduced monocyte recruitment to the sites of infection and, like the *Ccr2*$^{-/-}$ animals, retain Ly6C$^+$ monocytes in the BM (Jia et al., 2008). Thus, CCR2 signalling is critical for monocyte emigration from the BM into the blood.

CCL2 production is induced in a wide variety of cell types in response to inflammatory stimuli via MyD88 and type I interferon (IFN) mediated signalling. Moreover, CCL2 production is unaffected in MyD88-deficient (Serbina et al., 2003a) and the type I interferon receptor (IFNAR)-deficient animals (Jia et al., 2009). However, combining the two mutations to generate animals deficient for both genes (*MyD88*$^{-/-}$ and *IFNAR*$^{-/-}$) results in a dramatic reduction of Ly6C$^+$ monocyte recruitment during the early stages of infection (Jia et al., 2009). This indicates a level of redundancy in the molecular mechanisms leading to Ly6C$^+$ monocyte mobilisation, highlighting the critical importance to host immunity of CCR2 signalling and Ly6C$^+$ monocyte recruitment to sites of inflammation.

Whether CCR2 signalling is required for tissue infiltration of monocytes is less clear, data from Serbina and Pamer demonstrates that monocyte/Tip-DC localisation within spleens of CCR2-deficient animals infected with *L. monocytogenes* is comparable to wild type littermates (Serbina and Pamer, 2006). This suggests that within the context of infection, $Ly6C^{+}$ migration from the blood to infected tissue is *Ccr2*-independent.

Monocytes themselves are capable of producing reactive oxygen species and reactive nitrogen intermediates (ROS and RNI, respectively) (Fang, 2004) during *L. monocytogenes* infection, in addition to differentiating into Tip-DCs. The TNFα and iNOS produced by these cells contributes significantly to the innate defence against *L. monocytogenes*, (Pamer, 2004; Serbina et al., 2008; Serbina et al., 2003a).

Whilst it is clear that $Ly6C^{+}$ monocytes are reduced in the periphery of $Ccr2^{-/-}$ mice, there have been some inconsistencies in the reported effect of *Ccr2*-deficiency on $Ly6C^{low}$ monocytes. Tsou *et al.,* reported a small but significant reduction of $Ly6C^{low}$ monocytes (Tsou et al., 2007) under physiological conditions, whereas Qu *et al.,* reported similar frequencies of $Ly6C^{low}$ monocytes in $Ccr2^{-/-}$ and littermate controls (Qu et al., 2004). Thus, further clarification is required to ascertain whether this subset is affected by *Ccr2*-deficiency: a question this thesis aims to address.

Another bacterial infection model in which the role of monocytes has been well characterised is *Mycobacterium tuberculosis* (MTb). MTb is an airborne pathogen that infects dendritic cells and macrophages (Cooper, 2009). Whilst $Ccr2^{-/-}$ mice respond normally when given a low-dose inoculation of *M. tuberculosis*, they present with a more severe phenotype to high dose infection with MTb. The *Ccr2*-dependent $Ly6C^{+}$ monocyte recruitment protects mice after a high-dose inoculum of MTb (Scott and Flynn, 2002). During MTb infection, $Ly6C^{+}$ monocytes are thought to differentiate into

F4/80^{dim} and CD11c$^{dim/+}$ cell populations, expand and subsequently activate T cells (Peters et al., 2004). *Ccr2*-deficiency markedly reduces the expansion of these populations in the lung and consequently T cell responses to MTb in these mice are defective (Peters et al., 2004).

1.4.1.2 Viral infections

Murine cytomegalovirus (MCMV) is possibly one of the most widely studied murine models of viral infection. Ly6C^{+} monocytes are essential for the recruitment of NK cells to the foci of infection in the liver via production of CCL3 (MIP-1α) (Salazar-Mather et al., 1998). Both MCMV and vaccinia virus stimulate the expression of type I interferons (IFNs) in Ly6C^{+} monocytes via a TLR2 mediated signalling pathway (Barbalat et al., 2009). As TLR2 is endosomal, viral ligands within infected cells stimulate the TLR2 pathway and induce type I IFNs expression by Ly6C^{+} monocytes. This contrasts with bacterial infections in which the Ly6C^{+} monocytes produce TNFα and iNOS.

Ly6C^{+} monocytes are also implicated in West Nile Virus (WNV), where they are recruited to the brain and aid viral clearance (Lim et al., 2011). *Ccr2*-deficient mice studied in the context of both WNV and MCMV are less efficient at viral clearing, however, as discussed above, this is due to defective egress from the BM into the blood whereas migration from the blood to infected tissues is *Ccr2*-independent.

The role of classical monocytes in infection is not without collateral damage. Using influenza virus as a model, *Ccr2*-deficient mice have decreased mortality and immunopathology, associated with their impaired recruitment of Ly6C^{+} monocytes, and therefore Tip-DCs to the lungs (Aldridge et al., 2009; Dawson et al., 2000). Conversely, these mice show delayed viral clearance and priming of virus-specific T cells is impaired (Aldridge et al., 2009).

1.4.1.3 Fungal and parasitic infections

A model for fungal infection, *Cryptococcus neoformans,* has been investigated in *Ccr2*-deficient mice and it has been demonstrated that impaired BM egress of Ly6C$^+$ monocytes results in more severe and prolonged pulmonary infection. This is thought to be due to a shift in CD4-T cell polarisation from a mainly T helper 1 (T_H1) response to a T helper 2 (T_H2) bias (Traynor et al., 2000).

Further investigations using the *Ccr2*-deficient animals have provided insight into the role of Ly6C$^+$ monocytes in parasitic infections. The parasitic protozoa, *Plasmodium chabaudi* are used extensively as a murine model of malaria. *Ccr2*$^{-/-}$ mice have considerably higher parasitemia during acute stages of malarial infection due to reduced Ly6C$^+$ monocyte derived iNOS and ROS (Sponaas et al., 2009).

Infection with the helminth parasite *Schistosoma mansoni* is characterised by granulomatous lesions, which form around eggs that get trapped within organs such as the intestines. Granulomas are macrophage-dense, nodular aggregations that are protective to the host due to their role in skewing T cell responses towards T_H2-type during infection with *S. mansoni* (Herbert et al., 2010; Pesce et al., 2009). Hallmarks T_H2-type responses are the cytokines IL-4 and IL-13 produced by T helper 2 (T_H2) cells and expanded populations such as mast cells, eosinophils, basophils and "alternatively activated macrophages" (AAMø). AAMø's can be defined as macrophages that respond to signalling via IL-4Rα (Gordon and Martinez, 2010). Two recent studies demonstrated that, in the context of *S. mansoni* infection, recruitment of Ly6C$^+$ monocytes from the blood was principally responsible for macrophage accumulation around schistosome eggs forming granulomas in the liver, and were critical for host survival (Girgis et al., 2014; Nascimento et al., 2014). However, Ly6C$^+$ monocytes are not always critical for

macrophage accumulation during helminth infection. For example, in the filarial nematode *Litomosoides sigmodontis* infection model, it has been demonstrated that AAMø arise by local proliferation of resident macrophages rather than recruited monocytes (Jenkins et al., 2011; Jenkins et al., 2013).

1.4.1.4 Sterile inflammation

Just as monocyte infiltration is a common feature of infection, Ly6C$^+$ monocytes are also associated with sterile inflammation including cardiovascular disease, adipose tissue inflammation in models of obesity and related metabolic disorders such as type 2 diabetes (T2D).

For some time now, it has been recognised that proportion of macrophages in the adipose tissue of obese mice is significantly increased (Weisberg et al., 2003; Xu et al., 2003). This observation was key to advancing our understanding how of obesity propagates inflammation via macrophage-derived pro-inflammatory cytokine production (Olefsky and Glass, 2010). This is as a result of chronic stimulation of pattern recognition receptors (PRRs) and the subsequent activation of the AP-1 and NF-κB signalling pathways, crucial for the initiation of adipose tissue inflammation, which can lead to insulin resistance and T2D (Gordon and Taylor, 2005; Olefsky and Glass, 2010). Evidence from the *Ccr2*$^{-/-}$ mice fed high fat diet has demonstrated that, in contrast to infection models described above, this accumulation of macrophages is due to the recruitment of Ly6C$^+$ monocytes in a *Ccr2*-dependent manner (Kanda et al., 2006; Weisberg et al., 2006). Furthermore, *Ccr2*-deficient mice are less likely to develop insulin resistance and obesity (Chawla et al., 2011; Weisberg et al., 2006), indicting a crucial role for Ly6C$^+$ monocytes in the development of metabolic disease.

Atherosclerosis has long been considered an inflammatory disease, with monocytes and macrophages being the first immune cells described within atherosclerotic plaques in pigs (Gerrity et al., 1979; Ross, 1999). Atherosclerotic plaques are well-defined structures that can develop in mammals with hyperlipidaema and local endothelial cell dysfunction within arteries, particularly at branch points of the arterial tree (Hahn and Schwartz, 2009). These plaques consist of a necrotic core surrounded by accumulated lipids, areas of calcified tissue, inflamed smooth muscle cells, foam cells, endothelial cells and immune cells (Woollard and Geissmann, 2010). In recent years, various studies have demonstrated the close relationship between monocytes and atherosclerotic plaque formation (Galkina and Ley, 2009; Ley et al., 2011; Weber et al., 2008), in particular $Ly6C^+$ monocytes (Robbins et al., 2012; Swirski et al., 2007). The macrophage populations that reside in atherosclerotic plaques are $Ly6C^+$ monocyte derived cells recruited during early pathogenesis (Robbins et al., 2012), process sustained by splenic extramedullary haematopoiesis (Leuschner et al., 2012; Robbins et al., 2012). As atherosclerotic plaques mature, local macrophage proliferation is thought to contribute to the vast macrophage pool within the lesions (Robbins et al., 2013). The recruited blood monocytes scavenge cell-activating oxidised low-density lipoproteins (oxLDL) and other lipids and then accumulate, forming lesions in the arterial wall, which develop into plaques (Weber et al., 2008; Woollard and Geissmann, 2010).

A key mediator of lipid metabolism and removal from the blood is apolipoprotein E (apoE) (Plump and Breslow, 1995) and mice deficient in apoE have been used extensively as a model to study atherosclerosis because they develop more atherosclerotic lesions when fed a high fat diet compared to controls (Combadiere et al., 2008; Zernecke et al., 2008; Zhang et al., 1992). A study by Swirski *et al.,* demonstrated that $Ly6C^+$ monocyte numbers expanded dramatically in $apoE^{-/-}$ mice fed on a high fat

diet. Furthermore, it was observed that Ly6C$^+$ monocytes adhered to activated endothelium and infiltrated atherosclerotic lesions where they differentiated into atherosclerotic macrophages (Swirski et al., 2007).

A further important role of Ly6C$^+$ monocytes is their differentiation into tumour-associated macrophages (TAMs). Again, this is an example of a sterile, inflammatory microenvironment. A study by Franklin *et al.,* demonstrated that, in a murine mammary gland cancer model, TAMs were Ly6C$^+$ monocyte-derived and distinct from tissue resident mammary macrophages (Franklin et al., 2014). Furthermore this study demonstrated that monocyte-derived TAMs were critical for tumour growth due to their role in inhibiting lymphocyte-mediated responses to tumour inflammation (Franklin et al., 2014).

1.4.2 Ly6C^{low} monocyte effector functions

The Ly6C^{low} monocyte subset effector functions remain more elusive, they do not share the functional characteristics that define classical Ly6C$^+$ monocytes, as they extravasate rarely in comparison to Ly6C$^+$ monocytes in steady state and do not differentiate into inflammatory macrophages or dendritic cells in response to *Listeria* infection (Auffray et al., 2007). However, in recent years, a number of studies have provided significant insight into the functional roles of Ly6C^{low} monocytes *in vivo.*

1.4.2.1 Patrolling and scavenging

A major advance in our understanding of the role of Ly6C^{low} monocytes *in vivo* and in steady state came in 2007 with the observation that Ly6C^{low} monocytes appear to "patrol" vasculature by slowly crawling along endothelium, against the direction of blood flow in an LFA-1 integrin dependent manner (Auffray et al., 2007). Carlin *et al.,* demonstrated that a functional contribution of this behaviour, showing that this subset is

continuously scanning endothelial cells lining the capillaries and scavenging microparticles from the luminal side of the microvasculature in steady state (Carlin et al., 2013).

In response to TLR7-specific nucleic acid stimulation in the kidney, Ly6C^{low} monocytes were recruited to the damaged kidney endothelium and increased the length of time they adhered to the endothelium, a process referred to as "retention". TLR7 stimulation of the kidney cortex was shown to result in endothelial fractalkine (CX_3CL1) expression followed by retention of Ly6C^{low} monocytes by the endothelium in a process that requires both CX_3CR1 and CD11b. Once recruited and retained, Ly6C^{low} monocytes initiate necrosis of the endothelial cells, by in turn recruiting neutrophils (Carlin et al., 2013).

Thus, this crawling and scavenging behaviour of Ly6C^{low} monocytes suggests an important role as caretakers of the endothelium, carefully and safely orchestrating endothelial cell death in response to danger signals. However, in pathogenic contexts, it has been suggested that this process could become damaging to the kidney vasculature (Carlin et al., 2013). Indeed, it has been suggested by several studies that Ly6C^{low} monocytes or their human counterparts, the CD14^{dim} monocyte subset, are activated in several murine models of systemic lupus erythematosus (SLE) or human SLE patients (Amano et al., 2005; Carlin et al., 2013; Cros et al., 2010; Nakatani et al., 2010; Santiago-Raber et al., 2009; Santiago-Raber et al., 2011). These studies raise the hypothesis that Ly6C^{low} monocytes, whilst protecting against endothelial damage in healthy individuals, may contribute to tissue and vascular injury in pathological conditions.

Furthermore, a recent study highlighted a potential role for Ly6C^{low} monocytes in the initiation and propagation of rheumatoid arthritis in a murine model during the effector phase of the disease (Misharin et al., 2014). In this study they demonstrated that Ly6C^{low} monocytes were recruited to the joint during inflammation and may have roles both in promoting tissue injury during the early stage of disease and then tissue repair during later stages of disease (Misharin et al., 2014).

In line with this functional behaviour, Ly6C^{low} monocytes express a full set of FcγR (Biburger et al., 2011), vital for facilitating IgG-dependent effector functions, such as phagocytosis. The family of FcγR consists of four members: three activating (FcγRI, FcγRIII and FcγRIV) and one inhibitory member (FcγRIIB), which are involved in mediating the activity of different IgG subclasses. (Nimmerjahn and Ravetch, 2008). Biburger *et al.,* demonstrated that Ly6C^{low} monocytes were unique among innate immune cells in their expression of both FcγRI and FcγRIV and their data suggested a selective role for Ly6C^{low} monocytes in antibody-mediated phagocytosis of platelets (Biburger et al., 2011). This may provide a hypothesis as to why FcγRIV-positive monocytes are selectively increased in murine lupus models (Santiago-Raber et al., 2009), if this cell population is fundamentally involved in IgG-dependent tissue damage.

The patrolling behaviour of Ly6C^{low} monocytes is also implicated in Alzheimer's disease (Michaud et al., 2013; Michaud et al., 2011). Michaud *et al.,* demonstrated that Ly6C^{low} monocytes targeted veins with amyloid-β (Aβ) deposition within the central nervous system where they scavenged and facilitated Aβ removal.

Thus, since the demonstration of Ly6C^{low} monocytes ability to patrol by Auffray *et al.,* in 2007 (Auffray et al., 2007), it has become clear that Ly6C^{low} monocytes have effector

functions in their own right and are implicated as having both beneficial roles, for example in Alzheimer's disease, as well as potentially detrimental pathogenic roles in other contexts such as Lupus nephritis.

1.4.2.2 Ly6C^{low} monocytes in MCMV infection

Consistent with their close interplay between patrolling monocytes and endothelial cells (Carlin et al., 2013), Ly6C^{low} monocytes have been implicated in the dissemination of the murine cytomegalovirus (MCMV) as mediators of systemic infection (Daley-Bauer et al., 2014). This study demonstrated that MCMV uses virus-encoded chemokines to recruit Ly6C^{low} monocytes to infection sites, where they become infected and then disseminate the virus through the body, thus hijacking the early immune response as a strategy for viral dissemination (Daley-Bauer et al., 2014). Whether Ly6C^{low} monocytes become infected directly by the virus or indirectly by phagocytosing infected endothelial cells remains unclear.

Thus, it can be seen that a diverse range of studies utilising a variety of models, have demonstrated subset specific functions for Ly6C^{+} and Ly6C^{low} monocytes. However, the relationship between Ly6C^{+} and Ly6C^{low} monocytes remains to be fully clarified. Because of the subset specific roles of monocytes in inflammatory conditions, a more refined understanding of their development pathways could have important therapeutic implications. This thesis aims to analyse monocyte interrelationships and improve our understanding of the monocyte development *in vivo* and in the steady state.

1.5 Tissue resident macrophages

For many years, peripheral blood monocytes were considered the obligate precursor to tissue resident macrophages as a result of studying inflammatory models and BM irradiation chimeras. Irradiation generates an inflammatory-like setting by causing

tissue damage in addition to a loss of vascular and basal membrane integrity (Diserbo et al., 2002; Kierdorf et al., 2013b; Mildner et al., 2007). Thus, both inflammatory and irradiation models cause monocyte recruitment and their subsequent differentiation into macrophages or DCs. In recent years, it has become increasingly clear that macrophages appear in the embryo before the emergence of haematopoietic stem cells and monocytes and that these YS derived macrophages persist into adulthood.

1.5.1 Macrophage development

1.5.1.1 Embryonic haematopoiesis

During embryogenesis, there are three waves of haematopoiesis termed the primitive and the definitive waves (Cumano and Godin, 2007). Within the latter, the first wave of definitive haematopoiesis originates in the YS and is dedicated to erythromyeloid development. This is followed by the intra-embryonic wave of definitive haematopoiesis after the foetal liver is colonised by HSCs generated in the AGM region of the embryo at around E10.5 (Cumano and Godin, 2007). The first primitive haematopoietic wave starts as early as E7.5 in the YS blood islands, a transient structure before vascularisation of the YS (Golub and Cumano, 2013; Gomez Perdiguero et al., 2015). Primitive progenitors are mono-potent and comprise primitive erythrocyte progenitors and restricted macrophage progenitors (Gomez Perdiguero et al., 2015). Whilst primitive haematopoiesis is fairly well understood in the zebrafish model (Herbomel et al., 1999), it is technically very challenging to investigate in mouse development *in vivo* and has been rather evidenced *in vitro* (Bertrand et al., 2005; Palis et al., 1999). Primitive and definitive haematopoiesis have differing transcription factor requirements as definitive haematopoiesis is absent from Runx1-defincient embryos while primitive haematopoiesis is unaffected (Chen et al., 2009; Lacaud et al., 2002; Lancrin et al., 2010)

YS macrophages appear in mice around E8.5-E9.0 (Takahashi et al., 1989). Moreover, these primitive macrophages do not require the transcription factor cMyb (Schulz et al., 2012), which is essential for the development of BM, HSC-derived cells (see section 1.3.2.1).

Use of tamoxifen inducible *Csf1r*$^{Mer\text{-}iCre\text{-}Mer}$ mouse model with pulse labelling *in utero* at E8.5 provided a model in which to trace into adulthood, cells and/or their progeny that expressed CSF1R at E8.5, prior to the start of definitive haematopoiesis thus, HSC-derived, Myb-dependent cells are not labelled (Schulz et al., 2012). These data showed that tissue resident macrophages, including microglia, Langerhans cells and Kupffer cells arose from cells expressing CSF1R at E8.5 (Schulz et al., 2012). Complementary approaches in which HSCs can be pulse-labelled with an inducible *Tie2*^{Cre} model or where HSC-derived cells and monocytes can be genetically labelled in a *Flt3*^{Cre} mouse model further demonstrated that foetal and adult HSCs are not the main contributor to tissue resident macrophage pools (Gomez Perdiguero et al., 2015; Schulz et al., 2012). These studies and others have shown that tissue resident macrophages arise early in embryogenesis and independently of monocyte contribution in the steady state (Kierdorf et al., 2013a; Schulz et al., 2012; Yona et al., 2013).

1.5.1.2 Macrophage maintenance throughout life

In parallel with the evidence of YS derived macrophages, is the question as to whether these cells self maintain in steady state throughout life or if they are constantly being replenished by haematopoietic stem cell derived populations. As macrophages are an extremely diverse group of cells, the answer to this question is also diverse. A pioneering study established that most adult tissue resident macrophages persist in tissues after birth without further input from HSC-derived progenitors under steady

state conditions (Schulz et al., 2012). These findings have subsequently been independently confirmed using a wide array of different techniques (Hashimoto et al., 2013; Hoeffel et al., 2015; Sheng et al., 2015; Yona et al., 2013). For many tissue resident macrophage populations, it seems clear that they self maintain throughout life through local proliferation both in the steady state and under inflammatory conditions (Bruttger et al., 2015; Chorro et al., 2009; Davies et al., 2013b; Davies et al., 2011; Hashimoto et al., 2013; Jenkins et al., 2011; Yona et al., 2013). However, this is not the case for all tissue macrophage populations, for example, lamina propria macrophages in the gut. Bain *et al.,* demonstrated that embryonic macrophages seed the foetal gut, however unlike other tissue resident macrophage populations, they did not persist into adulthood. At the point of weaning, the lamina propria is colonised by an influx of CCR2-dependent Ly6C^{+} monocytes, which differentiate *in situ* into mature gut macrophages (Bain et al., 2014). This pool of intestinal macrophages is constantly being replenished by Ly6C^{+} monocytes throughout life; indeed, gut macrophages have a very short half-life, compared to other macrophage populations, of around three weeks (Varol et al., 2009).

Importantly for this thesis, Ly6C^{low} monocytes have often been thought of as contributing to the tissue macrophage pool in the steady state. Fate-mapping studies have demonstrated that macrophage populations within adult tissues are heterogeneous populations comprising both YS- and HSC- derived macrophages (Gomez Perdiguero et al., 2015). Currently, there are no known cell surface markers that would allow the discrimination between YS- and HSC-derived macrophages. Thus this thesis aims to use genetic models to understand the contribution of Ly6C^{low} monocytes to tissue macrophage populations.

1.5.2 Tissue resident macrophage activation

Appreciation of macrophage activation is vital for our understanding of tissue homeostasis, disease pathogenesis, the mechanisms of acute and chronic inflammation and what makes the difference between resolving and non-resolving inflammatory responses (Biswas and Mantovani, 2010; Gordon and Martinez, 2010; Lawrence and Natoli, 2011; Murray et al., 2014). Over recent years, macrophage activation has been intensively studied, arising from the observations that macrophages stimulated *in vitro* with interferon γ (IFNγ) and IL-4 or IL-13 became polarised metabolically and in terms of anti-microbial activity (Doyle et al., 1994; Nathan et al., 1983; Stein et al., 1992).

The balance between iNOS and arginase within macrophages was shown to be directly related T_H1 or T_H2 polarisation, respectively (Munder et al., 1998). From this, and from studies into mice with differing genetic backgrounds, the concept of the M1/M2 dichotomy arose (Mills et al., 2000).

Based on the T_H1/T_H2 model of T cell polarisation (Gazzinelli et al., 1993; Mosmann and Coffman, 1989; O'Garra and Murphy, 1994), Mills *et al.,* demonstrated that macrophages from mouse strains with T_H1 (C57BL/6; B10D2) background behaved in a metabolically distinct way to macrophages from mice with T_H2 background (Balb/c). On stimulation with LPS or IFNγ, T_H1 mouse strains produced more nitric oxide (NO), a metabolic process that requires L-arginine as a substrate. In contrast, macrophages from mice with T_H2 background increased their metabolism of L-arginine to ornithine production in response to LPS (Mills et al., 2000).

It has subsequently been realised that the differences in arginine metabolism by C57BL/6 and Balb/c mice are due C57BL/6 mice harbouring a deletion in the promoter region of a key macrophage arginine transporter, *Slc7a2* (Sans-Fons et al., 2013),

which, in part, is attributable for the strain-specific arginine utilisation. Nonetheless, the M1/M2 dichotomy persists: classical macrophage activation is associated with increased antigen presenting function coupled with increased production of IL-1β, IL-6 and TNFα, all of which can contribute to driving a T_H1 polarised T cell response (Martinez and Gordon, 2014; Mosser and Edwards, 2008). Whereas alternatively activated macrophages (MMAø) are associated with IL-4 and IL-10, and T_H2-polarised responses.

Whilst it has been suggested that AAMø represent a transition from inflammatory to reparative phenotype (Mills, 2012), *in vivo* data of AAMø during helminth infections has demonstrated a distinct molecular signature and a vital role in T_H2 environments, such as allergy or helminth infection (Loke et al., 2002; Nair et al., 2003; Raes et al., 2002). These data illustrate that alternative activation is not a transition state, rather a distinct molecular signature of effector functions that are not fully understood.

Furthermore it is now appreciated that, just as T cell responses cannot be confined solely to T_H1 and T_H2 activation, macrophage activation cannot be considered purely classical or alternative states. More accurately, there is a spectrum of macrophage activation and activated macrophages are associated with substantial changes in gene expression profiles depending upon the stimulus to which they are exposed (Murray et al., 2014).

1.6 Thesis outline

1.6.1 The origin and fate of Ly6C^{low} monocytes

This thesis focuses on the development and fate of Ly6C^{low} monocytes under physiological conditions. Of particular interest is the interrelationship between monocyte subsets in the blood and BM. Previous studies have divided the murine

monocyte compartment into two subsets (Geissmann et al., 2003; Hanna et al., 2011; Yona et al., 2013). Strong evidence has been provided indicating that Ly6C^{low} monocytes develop from Ly6C^{+} monocytes in the blood (Sunderkotter et al., 2004; Yona et al., 2013; Yrlid et al., 2006). However, some genetic studies appear to contradict these data. The study presented here uses a combination of fate mapping approaches and genetic tools to dissect and further clarify the murine monocyte interrelationships.

1.6.2 General hypothesis

Blood Ly6C^{low} monocytes develop independently of blood Ly6C^{+} monocytes in the BM from an *Nr4a1*-dependent precursor population.

1.6.3 Thesis structure

The materials and methods used during the course of this study are described in Chapter 2. Chapter 3 describes in depth phenotypic analysis of blood and BM monocyte compartments of wild type animals in the steady state. Chapter 3 confirms the presence of a third monocyte subset that expresses MHC II (Carlin et al., 2013; Jakubzick et al., 2013). Chapter 3 also introduces the cell cycle analysis and kinetic analysis of monocyte dynamics in wild type animals. These techniques are used again in genetic models described in the next chapter.

Chapter 4 describes the thorough characterisation of different genetic models, confirming the dependence of Ly6C^{low} monocytes on *Nr4a1* for their development but their development is independent of *Ccr2* and *Irf8*. Furthermore, the analytical techniques introduced in Chapter 3 of cell cycle and kinetic analyses are applied to genetic mutants in order to further understand monocyte interrelationships.

Chapter 5 asks the question of whether Ly6C^{low} monocytes contribute to tissue resident macrophage populations *in vivo* and under steady state conditions. In addition, Chapter 5 investigates the ontogeny of macrophage populations from two tissues in greater depth.

Chapter 6 is a discussion of the data presented in this thesis in relation to what is known in the literature, and comparatively to human myeloid biology.

2 Materials and methods

2.1 Mice

2.1.1 Animal strains used in this thesis

Nr4a1$^{-/-}$ animals (Lee et al., 1995), which lack Ly6C^{low} monocytes (Hanna et al., 2011), were purchased commercially from Jackson Laboratories (B6.129S2-Nr4a1$^{tm1Jmi/J}$) as frozen embryos and re-derived in-house. These mice were bred on a C57BL/6J background as heterozygotes to produce homozygous *Nr4a1*-knockout animals, along with heterozygous and wild type littermate controls.

Csf1r^{iCre} animals (Deng et al., 2010) were generated and bred on an FVB/N background and kindly provided by Jeffery W. Pollard.

Nr4a1$^{f/f}$ mice (Kadkhodaei et al., 2009) were generated on a C57BL/6 (CD45.2) background and were provided by Pierre Chambon. The *Nr4a1* locus (chromosome 15) was engineered with two LoxP recognition sites flanking exons 2 and 4. In the presence of CRE recombinase, the LoxP sites are cleaved deleting the *N*-terminus and functional DNA binding domain of *Nr4a1*. This results in a truncated 3' region of the gene sequence lacking an in-frame ATG for the translation of any remaining protein coding sequence (Boudreaux et al., 2012; Kadkhodaei et al., 2009). *Nr4a1*$^{fl/fl}$ mice were bred and maintained as homozygotes.

Nr4a1^{GFP} reporter mice (Moran et al., 2011) were generated by Kristin A. Hogquist and provided by George Kassiotis (NIMR). These *Nr4a1*^{GFP} reporter mice are a bacterial artificial chromosome (BAC) transgenic line that were developed by obtaining a ~170kbp C57BL/6J mouse BAC #RP24-366J14 which contained the entire *Nr4a1* locus. A GFP-Cre fusion protein was inserted to the ATG start site of the BAC *Nr4a1* gene along with an *frt*-flanked neomycin cassette and a TGA-STOP codon via homologous recombination. Subsequently, the *frt*-flanked neo cassette was removed

and a ~135kbp fragment from the modified BAC containing the targeted *Nr4a1* locus was purified and microinjected into C57BL/6J embryos (Moran et al., 2011) (Figure 2-2).

A ~135kb fragment from the modified BAC containing the targeted *Nr4a1* locus as well as 60kb sequence flanking each side of the *Nr4a1* locus was purified and then microinjected into C57BL/6J embryos.

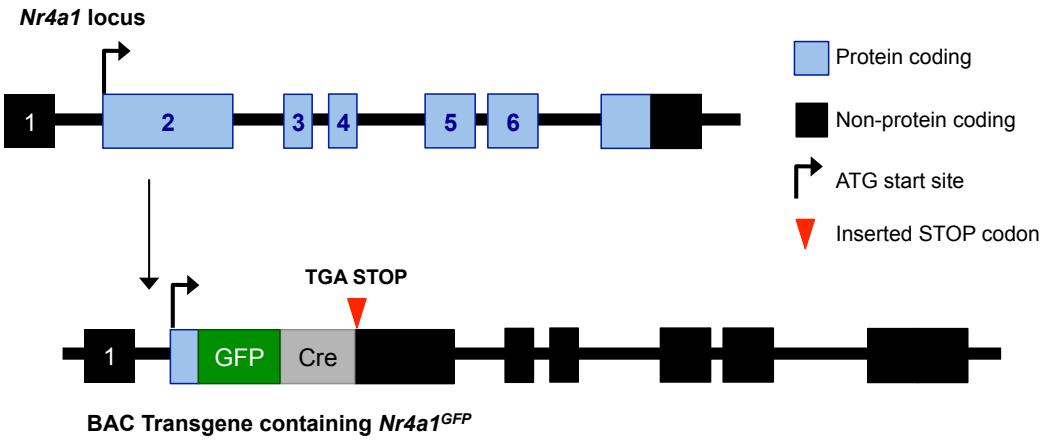

Figure 2-1 Generation of *Nr4a1*^{GFP} BAC

The BAC contains the whole *Nr4a1* locus and a GFP-Cre fusion protein was inserted into the ATG start site of *Nr4a1* along with a TGA stop codon.

Flt3^{Cre} mice (Benz et al., 2008) were generated on a C57BL/6 background by Conrad Bleul and provided by Sten-Eirik Jacobsen. The *Flt3*^{Cre} containing BAC is on the Y chromosome therefore only males are FLT3^{CRE+}.

Rosa26^{YFP} reporter mice (Srinivas et al., 2001) (B6.129X1-Gt(Rosa)26Sor$^{tm1(EYFP)Cos/J}$) were purchased from Jackson Laboratories and maintained on a C57BL/6 background.

Cx3cr1$^{GFP/+}$, *Rag2*$^{-/-}$, *Il2rg*$^{-/-}$ mice, which are devoid of all lymphoid cells and the only circulating cells expressing GFP are monocytes (Auffray et al., 2007) were generated in-house and maintained on a C57BL/6 background.

Ccr2$^{-/-}$ mice were generated as previously described (Boring et al., 1997) and were provided by Israel Charo and maintained on a C57BL/6 background.

Irf8$^{-/-}$ were provided by Marco Prinz (University of Freiburg) were maintained on a C57BL/6 background and generated as previously described (Holtschke et al., 1996).

2.2 Animal crosses used in this thesis

2.2.1 *Csf1r*^{iCre} *Rosa26*^{YFP} and *Flt3*^{Cre} *Rosa26*^{YFP} reporter mice

Csf1r^{iCre} mice (FVB/N) were crossed to *Rosa26*^{YFP} (C57BL/6) reporter mice (Srinivas et al., 2001), generating *Csf1r*^{iCre} *Rosa26*^{YFP} reporter strain (FVB/N: C57BL/6 mixed background) to assess *Csf1r*^{iCre} mediated recombination.

Flt3^{Cre} mice (C57BL/6) were crossed to *Rosa26*^{YFP} (C57BL/6) reporter mice as a reporter of *Flt3*^{Cre} mediated recombination.

2.2.2 *Nr4a1* conditional knockout

In order to generate animals in which Nr4a1 is deleted only within the haematopoietic system, *Nr4a1*$^{f/f}$ mice were crossed with *Csf1r*^{iCre} animals (FVB/N background) to generate conditional deletion of *Nr4a1*. Thus, *Csf1r*^{iCre} *Nr4a1*$^{f/f}$ animals analysed in this thesis are a mixed background of C57BL/6J and FVB/N.

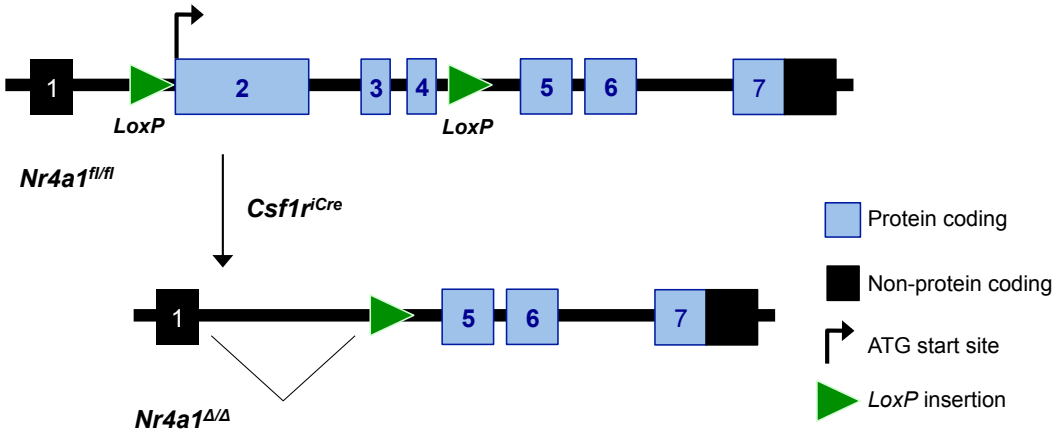

Figure 2-2 *Csf1r*^{iCre} conditional *Nr4a1* deletion

Nr4a1 locus was engineered with LoxP recognition sites for CRE recombinase flanking exons 2 - 4. In the presence of CRE recombinase the *N*-terminus and functional DNA binding domain of *Nr4a1* are excised.

2.2.3 Generation of *Nr4a1*^{GFP} *Nr4a1*$^{-/-}$ double mutants

To generate *Nr4a1*^{GFP} *Nr4a1*$^{-/-}$ mice, *Nr4a1*$^{-/-}$ animals were crossed with *Nr4a1*^{GFP} animals. The F1 breeding produced animals heterozygous for endogenous *Nr4a1* and positive for the *Nr4a1*^{GFP} BAC construct (*Nr4a1*^{GFP} *Nr4a1*$^{+/-}$). These F1 animals heterozygous for endogenous *Nr4a1* (*Nr4a1*^{GFP} *Nr4a1*$^{+/-}$) were crossed together and the F2 breeding produced the following genotypes used for experimental purposes: *Nr4a1*^{GFP} *Nr4a1*$^{+/+}$; *Nr4a1*^{GFP} *Nr4a1*$^{+/-}$ and *Nr4a1*^{GFP} *Nr4a1*$^{-/-}$ offspring.

2.3 Genotyping

2.3.1 DNA isolation

Genomic DNA was isolated from ear biopsies by incubating the tissue with 300µl 50mM NaOH at 97˚C for 1 hour before being neutralised with 30µl Tris-HCl. The extract was vortexed and subsequently centrifuged at 20,000 x g for 5 minutes. Samples were stored at 4˚C until analysis.

Post-PCR reaction, all samples were run on a 2% agarose gel made with Tris/borate/Ethylenediaminetetraacetic acid (EDTA) (TBE) containing ethidium bromide. Gels were imaged using a Bio-Rad Gel Doc EZ system.

2.3.1.1 Csf1r^{iCre} Genotyping protocol

Csf1r^{iCre} mice were genotyped as previously described (Deng et al., 2010). Briefly, one PCR reaction per mouse with 2 primers per tube was carried out. Each tube contained 12.5µl of HotStartTaq (Qiagen) master mix, 2.5µl of CoralLoad DNA loading buffer (Qiagen), 7µl of RNAse and DNase free water and with 2µl of genomic DNA extracted as above and 0.5µl each of the following two primers:

Csf1r^{iCre} Forward (10µM): 5'TCTCTGCCCAGAGTCATCCT3'

Csf1r^{iCre} Reverse (10µM): 5'CTCTGACAGATGCCAGGACA3'

The PCR reaction was carried out for 30 cycles, performed at the following reaction conditions: denaturing temperature of 95˚C for 45 seconds, annealing temperature of 60˚C for 45 seconds and elongation temperature of 72˚C for 45 seconds.

The expected band size for this PCR is 400bp.

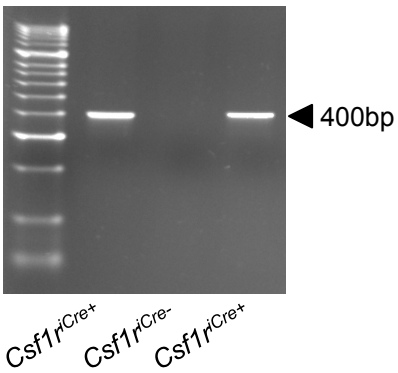

Figure 2-3 *Csf1r^{iCre}* genotyping PCR gel

2.3.1.2 Nr4a1$^{-/-}$ Genotyping protocol

One PCR reaction per mouse with 3 primers per tube was carried out to genotype *Nr4a1*$^{-/-}$ animals. Each tube contained 10µl of HotStartTaq (Qiagen) master mix, 2µl of CoralLoad DNA loading buffer (Qiagen), 4µl of RNAse and DNase free water and with 2µl of genomic DNA extracted as above and the following three primers:

Nr4a1$^{-/-}$ common primer: 1µl (10µM): 5' CCACGTCTTCCTCATCC 3'

Nr4a1$^{-/-}$ wild type reverse primer: 0.5µl (10µM): 5' TGAGCAGGGACTATAGT 3'

Nr4a1$^{-/-}$ mutant primer: 1.5µl (10µM): 5' CACGAGACTAGTGAGACGTG 3'

The PCR reaction was carried out for 35 cycles, performed with the following reaction conditions: denaturing temperature of 94˚C for 30 seconds, annealing temperature of 62˚C for 1 minute and elongation temperature of 72˚C for 1 minute.

Wild type band is 180bp and the mutant band is 350bp.

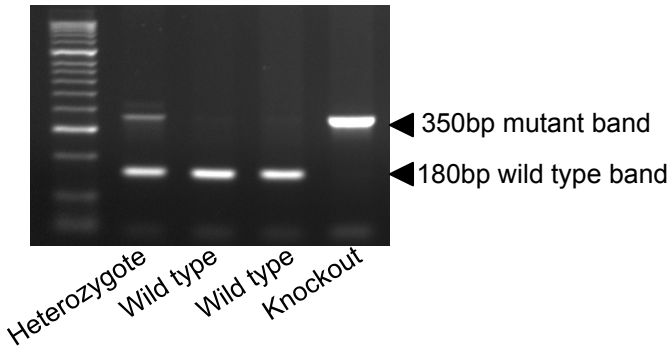

Figure 2-4 *Nr4a1*$^{-/-}$ genotyping PCR gel

2.3.1.3 Flt3^{Cre} Genotyping protocol

One PCR reaction was carried out per mouse containing 2 primers per tube for the dentification of *Flt3*^{Cre} mice. Each tube contained 12.5µl of HotStartTaq (Qiagen)

master mix, 2.5µl of CoralLoad DNA loading buffer (Qiagen), 7µl of RNAse and DNase free water and with 2µl of genomic DNA extracted as above and 0.5µl each the following two primers:

Flt3^{Cre} forward (10µM): 5'ACGGAGTCCAGGCAACTTCC 3'

Flt3^{Cre} reverse (10µM): 5'GAAGCATGTTTAGCTGGCCC 3'

The PCR reaction was performed for 44 cycles with the following reaction conditions: denaturing temperature of 95˚C for 30 seconds, annealing temperature of 58˚C for 35 seconds and elongation temperature of 72˚C for 60 seconds.

Expected band size for this PCR is 400bp.

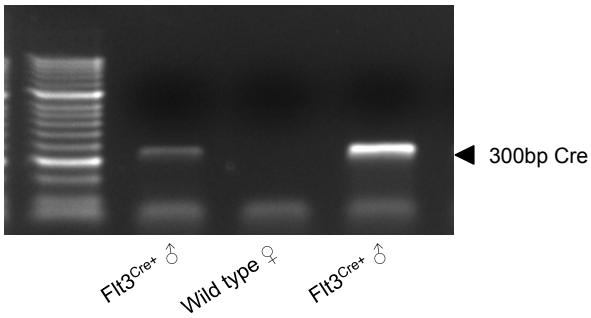

Figure 2-5 *Flt3*^{Cre} genotyping gel

The *Flt3*^{Cre} is inserted on the Y chromosome: all males are Cre^{+} and all females are Cre.

2.3.1.4 Nr4a1$^{fl/fl}$ *genotyping protocol*

One PCR reaction per mouse with 2 primers per tube was carried out for the identification of *Nr4a1*$^{fl/fl}$ animals. Each tube contained 10µl of HotStartTaq (Qiagen) master mix, 2µl of CoralLoad DNA loading buffer (Qiagen), 4µl of RNAse and DNase free water and with 2µl of genomic DNA extracted as above and 1µl each of the following two primers:

Nr4a1$^{fl/fl}$ Forward (10µM): 5' TTTTGAGAGTTGTCTTTTCTCCAGT 3'

Nr4a1$^{fl/fl}$ Reverse (10µM): 5' TCTGTAACTCTAGCTCCAGGACATC 3'

The PCR reaction was carried out for 35 cycles, performed at the following reaction conditions: denaturing temperature of 94˚C for 45 seconds, annealing temperature of 60˚C for 56 seconds and elongation temperature of 72˚C for 1 minute.

The expected band sizes for this PCR are:

Wild type (unfloxed): 215bp

Floxed: 300bp

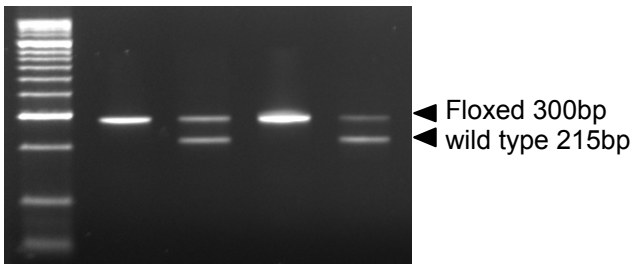

Figure 2-6 *Nr4a1*$^{fl/fl}$ genotyping PCR

2.3.1.5 Genotyping Ccr2$^{-/-}$ *mice*

One PCR reaction per mouse with 4 primers per tube was carried out for the identification of *Ccr2*$^{-/-}$, *Ccr2*$^{-/+}$ and *Ccr2*$^{+/+}$ animals. Each tube contained 12.5µl of HotStartTaq (Qiagen) master mix, 2.5µl of CoralLoad DNA loading buffer (Qiagen), 6µl of RNAse and DNase free water and with 2µl of genomic DNA extracted as above and 1µl each of the following two primers:

Ccr2$^{+/+}$ Forward (10µM): 5' CCACAGAATCAAAGGAAATGG 3'

Ccr2$^{+/+}$ Reverse (10µM): 5' CCAATGTGATAGAGCCCTGTA 3'

Ccr2$^{-/-}$ Forward (10µM): 5' CTTGGGTGGAGAGGCTATTC 3'

Ccr2$^{-/-}$ Reverse (10μM): 5' AGGTGAGATGACAGGAGATC 3'

The PCR reaction was carried out for 35 cycles, performed at the following reaction conditions: denaturing temperature of 94˚C for 30 seconds, annealing temperature of 60˚C for 30 seconds and elongation temperature of 72˚C for 1 minute.

The expected band sizes for this PCR are:

Wild type: 424bp

Mutant: 280bp

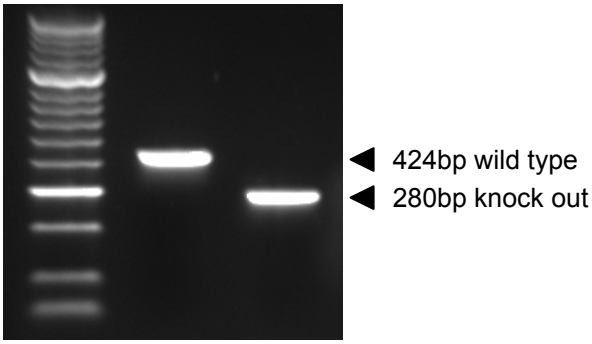

Figure 2-7 *Ccr2*$^{-/-}$ genotyping gel

2.3.1.6 Phenotyping Nr4a1^{GFP} *animals*

Tail vein bleeding and analysis by flow cytometry detected the presence or absence of GFP in *Nr4a1*^{GFP} animals crossed to C57BL/6J (see section 2.3.1.1). This was carried out at least 1 week before experimental use.

2.3.1.7 Genotyping Nr4a1^{GFP} *Nr4a1*$^{-/-}$ *animals*

To identify the double mutant *Nr4a1*^{GFP} *Nr4a1*$^{-/-}$ animals, genotyping of the *Nr4a1* deletion was assessed using the *Nr4a1*$^{-/-}$ as outlined above.

The BAC has been inserted to generate *Nr4a1*^{GFP} mice contains the whole NR4A1 locus although the insertion of a STOP codon ensures that the protein is not transcribed from the BAC. However, this means that all animals will express the wild type band (see figures 2-1 and 2-4), regardless of genotype. Thus, the genotyping PCR was carried out to detect presence of the mutant allele (see section 2.3.1.2).

Once the presence of the mutant allele was obtained, mice were blood phenotyped to assess presence or absence of GFP and to detect presence or absence of Ly6C^{low} monocytes.

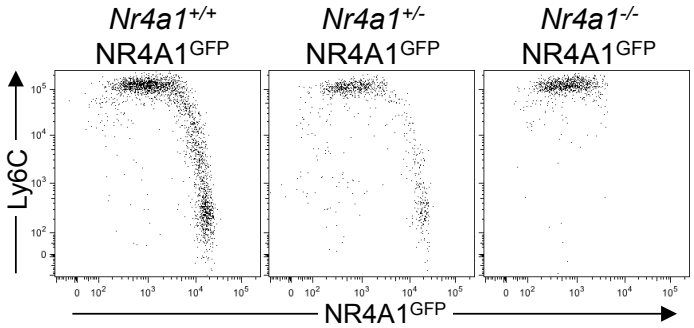

Figure 2-8 Blood phenotyping of *Nr4a1*^{GFP} *Nr4a1*$^{-/-}$ mice and littermates.
Double mutant mice were assessed by flow cytometry for presence of GFP and Ly6C^{low} monocytes to confirm genotyping results.

2.3.1.8 Nr4a1 deletion PCR

To assess genetic *Nr4a1* deletion in the *Csf1r*^{iCre} *Nr4a1*$^{f/f}$ animals a three-primer reaction was carried out with 1µl each of the following oligonucleotides:

p1 (10µM): 5' TTTTGAGAGTTGTCTTTTCTCCAGT 3'

p2 (10µM): 5' TCTGTAACTCTAGCTCCAGGACATC 3'

p3 (10µM): 5' AAAGCCTACACAAGCTGCATTAC 3'

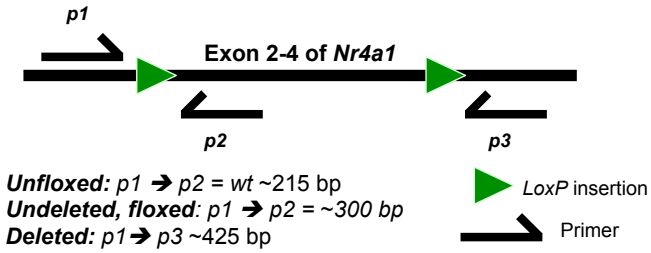

Figure 2-9 Schematic of 3-primer *Nr4a1* deletion PCR

Each tube contained 10µl of HotStartTaq (Qiagen) master mix, 2µl of CoralLoad DNA loading buffer (Qiagen), 3µl of RNAse and DNase free water and with 2µl of genomic DNA extracted as above.

The PCR was performed for 35 cycles with the following reaction conditions: denaturing temperature of 94˚C for 45 seconds, annealing temperature of 56˚C for 45 seconds, elongation temperature of 72˚C for 1 minute.

2.4 Flow cytometry

2.4.1 Blood Isolation for flow cytometry

Mice were bled either from the tail vein or by intra-cardiac puncture.

2.4.1.1 Tail vein bleeding

For tail vein bleeding: animals were heated to 38˚C before being bled from the tail vein using a micro-lance. Blood was collected into pediatric EDTA-containing blood tubes and subsequently resuspended in 1ml of RBC lysis buffer (8.3g NH_4Cl, 1g $NaHCO_3$, 1ml EDTA (100mM) in 1L of dH_2O) and incubated on ice for 5 minutes. After which, the lysis reaction is stopped by the addition of 1ml of PBS 1X; 0.5% BSA (w/v); 2mM EDTA (staining buffer). Cells were centrifuged at 400 x g for 10 minutes (4˚C) and the

supernatant removed by aspiration. Lysis was repeated with a further 1ml RBC lysis buffer, on ice.

2.4.1.2 Intracardiac puncture

For intra-cardiac puncture: animals were lethally anaesthetised by intaperitoneal injection of anaesthetic cocktail containing ketamine (50 mg/kg), xylazine (10 mg/kg), and acepromazine (1.7 mg/kg). Anaesthetised mice were kept warm on a heating pad and between 0.5ml and 1ml of blood was collected using a 25-gauge x 16mm needle and syringe containing 50µl of EDTA (100mM) by intracardiac puncture. Blood was then transferred to a 15ml tube containing a further 50µl of 100mM EDTA. Blood was resuspended in 5ml RBC lysis buffer and incubated on ice for 5 minutes. Subsequently, 5ml of staining buffer was added to stop the lysis reaction and cells were centrifuged at 400 x g for 10 minutes (4˚C) and the supernatant removed by aspiration. The lysis reaction was repeated twice more, firstly with a further 3ml RBC lysis buffer and secondly with 1ml of RBC lysis buffer.

After the final lysis step, cells were resuspended in 50µl of Fc block (FcγRIII/II; clone 2.4G2) diluted 1/50 in staining buffer for 15 minutes in round-bottomed 96 well plates on ice. Blocking was carried out to avoid non-specific binding of the staining antibodies to Fc receptors on the surface of cells. Cells were then stained for surface markers by incubating for 30 minutes, on ice, protected from the light with fluorochrome-conjugated antibodies (see table 2-1).

2.4.2 Tissue isolation for flow cytometry

Mice were culled by cervical dislocation, lethal anaesthesia (intaperitoneal injection of anaesthetic cocktail containing ketamine (50 mg/kg), xylazine (10 mg/kg), and acepromazine (1.7 mg/kg)) or CO_2 inhalation.

2.4.2.1 Peritoneal lavage

Animals were culled using CO_2 inhalation, after which the outer skin was cut to expose the inner skin. 5ml of PBS + 3% foetal bovine serum was gently injected into the peritoneal cavity using a 27-gauge needle, being careful not to pierce any internal organs in the process. The peritoneum was then massaged for 30 seconds before the fluid aspirated using a 25-gauge needle. The process was repeated once more before cells were centrifuged at 320 x g for 7 minutes at 4˚C. The supernatant was then discarded and cells resuspended in cells 50µl of Fc block (FcγRIII/II; clone 2.4G2) diluted 1/50 in staining buffer for 15 minutes. Cells were then stained for surface markers by incubating for 30 minutes, on ice, protected from the light with fluorochrome-conjugated antibodies (see table 2-1).

2.4.2.2 Isolation of macrophages from internal organs

After cervical dislocation or lethal anaesthesia brain, spleen, left liver lobe, right lung lobe, thymus and inguinal lymph nodes were harvested and placed immediately in ice cold PBS. To obtain single cell suspensions, organs were finely chopped and incubated for 30 minutes at 37˚C in PBS containing 1mg/ml Collagenase D (Roche), 100U/ml Deoxyribnuclease I (DNAse I, Sigma), 2.5mg/ml Dispase (Invitrogen) and 3% foetal bovine serum (Invitrogen).

Ears were excised from mice, separated into dorsal and ventral halves and placed dermis side down in PBS containing 2.4mg/ml Dispase (Invitrogen) for 1 hour at 37˚C or overnight at 4˚C. The dermis and epidermis were then carefully separated before digestion at 37˚C for 30 minutes in 1ml PBS containing 1mg/ml Collagenase D (Roche, Burgess Hill, UK), 100U/ml Deoxyribonuclease I (DNAse I, Sigma), 2.4mg/ml Dispase (Invitrogen, Paisley, UK) and 3% foetal bovine serum. The digestion mix was then

diluted in 6ml of staining buffer. The tissues were then mechanically dissociated by passing through a 100µm cell strainer (BD). Cells were centrifuged at 320 x g for 7 minutes at 4˚C before proceeding to staining as described above in section 2.3.2.1.

2.4.2.3 Isolation of monocytes from the spleen

For analysis of monocytes subsets in the spleen, half of the spleen was directly mechanically dissociated through a 100µm strainer without being digested to preserve CD115 expression. After dissociation, the cell suspension was filtered again through a 70µm filter before being spun down at 320 x g for 7 minutes, 4˚C. Cells were further prepared and stained for flow cytometry as described above.

2.4.2.4 Bone marrow isolation

Hind limbs were excised, cleaned of muscle tissue and the ends of the bones, including the iliac crest, were trimmed. BM was flushed using a 27-guage needle and 10ml syringe containing RPMI-1% penicillin/streptomycin. Cells were pelleted at 320 x g for 10 minutes (4˚C) and then resuspended in staining buffer before being passed through a 100µm filter. Cells were spun down at 320 x g for 5 minutes, supernatant discarded and cells resuspended in staining buffer containing 10µM/ml of rat anti-mouse 1A8 and 20µM/ml of rat anti-mouse Ter119 to deplete granulocytes and erythrocytes, respectively.

BM was depleted of 1A8 and Ter119 expressing cells using sheep anti-rat Dynabeads (Life Technologies). Depleted BM cells were counted prior to blocking with anti-CD16/32 (FcγRIII/II; clone 2.4G2) diluted 1/50 in staining buffer for 15 minutes in round-bottomed 96 well plates. Antibody mixes were added and cells were incubated for 30 minutes on ice, protected from light. Where appropriate, cells were incubated

with a secondary streptavidin conjugate for a further 20 minutes (see antibody list below).

2.4.3 Flow cytometry

Unstained samples and single stained cells were passed to set up photomultiplier tube (PMT) voltages. Single stained cells were used to compensate on the flow cytometer and recorded for post-acquisition compensation during analysis.

Fluorescence minus one (FMO) controls were acquired for each fluorochrome used during the optimisation of all new antibody panels.

Flow cytometry was performed using BD Biosciences Aria II, BD Biosciences FACSCanto II or BD Biosciences LSR Fortessa.

All data were analysed using FlowJo version 9.5 (Tree Star Inc.).

2.4.3.1 Antibodies for flow cytometry

The antibodies used in this thesis are listed in table 2.1.

It was important to exclude NK cells from the analyses presented in this thesis, however, in setting up the antibody panels it was observed the NK1.1 antibody was non-specifically staining the Ly6C^{low} monocyte subset, whereas NKp46 did not. Therefore, throughout this study, NKp46 was used to exclude NK cells rather than NK1.1. This phenomenon has subsequently been observed by others (Biburger et al., 2015).

Using Ly6C to differentiate between the two principal monocyte subsets was critical for the analysis in this thesis. The monoclonal antibody Gr1 recognises both Ly6C and Ly6G epitopes, expressed on both granulocytes and monocytes. These are

glycosylphosphatidyl-inositol (GPI) linked proteins that were first reported on murine lymphocytes in the 1977 (McKenzie et al., 1977) and are part of the wider Ly6 superfamily. In this thesis, monocytes were distinguished from granulocytes by CD115 and CD11b staining and from each other by expression of Ly6C. Whilst the Ly6C epitope is expressed on both granulocytes and monocytes, Ly6G is not expressed by monocytes; consequently Ly6C and Ly6G antibodies were preferentially used over Gr1 so that granulocytes could be excluded

Furthermore, there are two clones available for Ly6C, HK1.4 and AL-21. Both clones were tested in setting up antibody panels and HK1.4 was chosen to be preferable over AL-21 due to much brighter staining and therefore better separation of the $Ly6C^{+}$ and $Ly6C^{low}$ monocyte subsets.

All antibodies were titrated to find the optimal dilution for staining 5 million cells. Titrations were done starting with 10µl/ 100µl of cell suspension containing 5 million cells and titrated down to identify the optimal concentration for use.

2.4.3.2 Fluorescently Activated Cell Sorting

Cells were sorted using BD Biosciences Aria II into tubes containing RPMI medium supplemented with 10% foetal bovine serum (FBS) and 1% penicillin/streptomycin (P/S), TRIzol (Life Technologies) or Cell Lysis Solution (DNA Purification KIT, Promega). For every sort, unstained samples were analysed first in order to calibrate the sorter for detection of fluorochromes. Single stained cells were acquired for compensation, which was carried out on the sorter prior to starting the sort to ensure any spectral overlap between fluorochromes was corrected.

To ensure that the sort streams were correctly aligned, 200 cells of each population were sorted and reacquired to ensure 100% purity. In addition, for adoptive transfer, 10µl of the sorted sample was reacquired post-sort to ensure purity.

Table 2-1: Murine antibodies used for flow cytometry

Antibody	Clone	Conjugate	Company
CD3e	145-2C11	Biotin	BD Pharmingen
CD3e	145-2C11	PE	Biolegend
CD3e	145-2C11	FITC	ebioscience
CD4	H129.19	PE or FITC	Biolegend
CD8a	53-6.7	PE	Biolegend
CD8a	53-6.7	FITC	ebioscience
CD11b	M1/70	PE or PE Cy7	BD Pharmingen
CD11b	M1/70	BV605 or BV711 or FITC	Biolegend
CD11c	N418	PerCP Cy5.5 or APC	ebioscience
CD16/32	2.4G2	uncoupled	BD Pharmingen
CD19	1D3	Biotin or PE or PE Cy7	BD Pharmingen
CD45	30-F11	APC Cy7	Biolegend
CD45.1	A20	PE	BD Pharmingen
CD45.2	104	APC Cy7	BD Pharmingen
CD48	HM48-1	APC	Biolegend
CD64	X54-5/7.1	PE	BD Pharmingen
CD103	M290	Biotin or APC	BD Pharmingen
CD104	346-11A	Biotin	Biolegend
CD115	AFS98	PE or APC	ebioscience
CD117 (c-KIT)	2B8	BV605	BD Pharmingen
CD117 (c-KIT)	2B8	APC Cy7	Biolegend
CD135	A2F10	PerCP eFluor 710	ebioscience
CD150	TC15-12F12.2	PE Cy7	Biolegend
CD326 (EpCAM)	G8.8	PE Cy7	ebioscience
CD335 (NKp46)	29A1.4	PE or FITC	ebioscience
F4/80	2M8	e450	ebioscience
Ki67	B56	PE	BD Pharmingen
Ly-6A/E (Sca-1)	D7	PE or FITC or PerCP Cy5.5	ebioscience
Ly-6A/E (Sca-1)	D7	BV421	Biolegend
Ly-6C	HK1.4	PE Cy7 or BV421	Biolegend
Ly-6C/6G (Gr-1)	RB6-8C5	APC	BD Pharmingen
Ly-6C/6G (Gr-1)	RB6-8C5	PE or FITC	Biolegend
Ly-6G	1A8	PE or FITC	BD Pharmingen
Ly-76	Ter119	PE	Biolegend
MHC class II	M5/114.15.2	FITC or PE Cy7	BD Pharmingen
MHC class II	M5/114.15.2	PerCP eFluor 710	ebioscience
Siglec F	E50-2440	PE	BD Pharmingen
TIM4	RMT4-54	Alexa Fluor 647	Biolegend
DAPI	-	-	Invitrogen
Streptavidin	-	Pacific Blue	Invitrogen
Streptavidin	-	APC	BD Pharmingen

2.5 Absolute cell counts

To obtain absolute cell counts to measure the size of haematopoietic compartments and compare absolute cell numbers between different genetic models, an automated cell counter was used. A Sysmex KX-21N Haematology cell counter was used throughout the experiments presented in this thesis.

Whole blood samples or diluted samples were aspirated by the haemocytometer, which then feeds the sample through transducers. Each transducer chamber has an aperture with electrodes on both sides between which direct current flows. As the cell suspension passes through the aperture, the electrical resistance between the two electrodes changes creating pulses. The size of these pulses allow discrimination between red and white blood cells (RBC and WBC respectively) and cell counts are calculated by counting the pulses.

The reliability and accuracy of this machine for WBC counts was assessed by comparison with manual counting using a Malessez counting chamber.

2.5.1 Blood cell counts

To obtain total RBC and WBC counts, an aliquot of 10µl of whole (unlysed) blood was diluted and analysed on the Sysmex KX-21N Haematology cell counter using the programmed pre-diluted mode. This pre-diluted mode requires a 1/26 dilution of whole blood prior to sample aspiration and provides a read-out of cells per µl.

To obtain a count for the number of individual cell populations per µl of blood, the volume of blood taken from each animal was recorded. After lysis, (as described above) cell pellets are resuspended in an appropriate volume of Fc block from which a 10µl was taken and diluted 1/10. This 1/10 dilution was measured using the Sysmex KX-21N

haemocytometer. The following formula was applied to the reading from the automated cell counter:

$Cell\ count = (10x)V_{FC}$

Where: x = reading from automated cell counter (cells/µl)

10 = dilution factor

V_{FC} = volume of FC block used for cell pellet was resuspension

Thus providing a post-lysis cell count. After analysis of samples, the post-lysis cell count was multiplied by the frequency of each population as determined by flow cytometry in order to calculate relative compartment size.

To calculate relative compartment size of blood monocytes, it was considered that the total blood volume an adult mouse was 80ml/kg and that adult C57BL/6 mice weighted 25g (Harkness and Wagner, 1995; Mitruka and Rawnsley, 1981). Consequently, it was considered that the total blood volume per mouse was 2ml.

2.5.2 Bone marrow cell counts

After isolation of BM cells, an aliquot was taken BM cell suspension was taken for pre-depletion count. After depletion of 1A8 and Ter119 expressing cells, BM cells were resuspended in an appropriate volume of FC block and a 10µl aliquot was taken and diluted 1/10. A cell count per µl of this dilution was acquired using the Sysmex automated cell counter. The total number of cells for 2 hind limbs (minus iliac crests) was calculated with the following formula:

$Cell\ count = (10x)V_{FC}$

Where: x = reading from automated cell counter (cells/µl)

10 = dilution factor

V_{FC} = volume of FC block used for cell pellet was resuspension

The cell count was then multiplied by the frequency of each population as determined by flow cytometry in order to calculate relative compartment size.

To calculate relative compartment size of BM populations, the cell count two hind limbs was taken to represent ~20% of total BM cellularity (Colvin et al., 2004; Colvin et al., 2000; Lambert et al., 2000).

2.6 Cell cycle analysis

After staining with surface marker antibodies, cells were fixed in 4% formaldehyde solution weight/volume (w/v) for 20 minutes on ice. Cells were then permeabilised with PBS 1X; 0.5% BSA (w/v); 2mM EDTA; 0.5% saponin (w/v). Cells were blocked with anti-CD16/32 (FcγRIII/II; clone 2.4G2) diluted 1/50 in saponin buffer (PBS 1X; 0.5% BSA (w/v); 2mM EDTA; 0.5% saponin (w/v)) for 30 minutes prior to incubation with Ki67 (BD Pharmingen) and 0.05ng/ml of DAPI (Invitrogen) for 1 hour on ice. DAPI signal was acquired on a linear scale and used to quantify total DNA levels, 2N was defined as fluorescence=50 (x1000). Diploid (2N) were defined as G0/G1 and either $Ki67^-$ or $Ki67^+$. G2M phase cells were defined as $Ki67^+$ with 4N (tetraploid). S-phase cells were characterized by $Ki67^+$ staining and >2N<4N ploidy.

2.7 BrdU incorporation

Mice were treated with a single i.p. injection of 1.5mg BrdU (bromodeoxyuridine) (BD Pharmingen FITC BrdU Flow KIT). To assess BrdU incorporation, blood, BM and spleen cells were isolated as above, stained with primary antibodies. Samples were then fixed with BD Cytofix/Perm buffer for 20 minutes on ice then washed with BD Perm/Wash Buffer. Samples were re-fixed with BD Cytoperm Plus buffer for 10 minutes on ice before treatment of cells with DNase (300µg/ml) for 1 hour at 37˚C. Samples were then stained with FITC-conjugated anti-BrdU for 20 minutes at room

temperature. After which, samples were washed, supernatant discarded and cells were resuspended in 20µl 7-aminoactinomycin D (7AAD). A further 200µl of staining buffer was added and samples were acquired on a BD FACS Aria II.

2.7.1 Measurement of apoptosis

Apoptotic cells have incomplete DNA content due to losing chromatin in apoptotic bodies and because fragmented DNA is extracted during the staining procedure (Pozarowski and Darzynkiewicz, 2004). Thus, they can be quantified as samples with DNA content $<G_0G_1$. During processing of samples for kinetic analysis, cells were additionally stained with 7AAD and analysed on BD Biosciences LSR Fortessa. 7AAD signal was acquired on a linear scale and used to quantify total DNA levels. 2N was defined as fluorescence=50 (x1000) and apoptotic cells were defined as sub-2N.

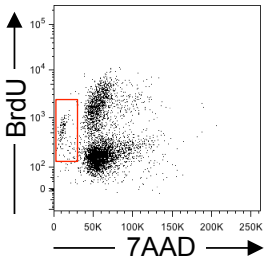

Figure 2-10 Gating of apoptotic cells using BrdU and 7AAD

2.8 Feeder culture

Unfractionated BM from CD45.1 mice were plated out into flat-bottomed 96-well plates at a density of $50x10^4$ cells/ml in RPMI medium supplemented with 10% FBS and 1% P/S.

Cell populations of interest were FACS sorted from *Nr4a1*^{GFP} (CD45.2) animals into RPMI medium supplemented with 10% FBS and 1% P/S. Post sort, cells were washed by centrifugation at 320 x g for 7 minutes at 4˚C and then resuspended at a density of

$5x10^4$ cells/ml. Aliquots of 100µl were added to 96-well plates containing 100µl of CD45.1 feeder cell suspension. Populations were plated in triplicate.

Cells were incubated at 37˚C, 5% carbon dioxide (CO_2) for 1, 12, 24 and 48 hours before washing and staining for reanalysis.

2.9 Adoptive transfer

Populations for adoptive transfer were FACS sorted as above into RMPI medium supplemented with 10% FBS 1% P/S. Post sort, cells were washed, supernatant discarded and resuspended in RPMI with 1%P/S (no FBS) at a density of 200,000 cells per 100µl. 200,000 cells (100µl) were injected directly into the tail vein of congenic animals. Animals were sacrificed 3.5 days post transfer and blood and spleen were prepared as above (see sections 2.3.1.2 and 2.3.2.3 respectively).

2.10 Quantitative real-time PCR

2.10.1 cDNA preparation

Cells were sorted directly into Eppendorf tubes containin 500µl TRIzol (Life Technologies) at 4˚C. Once the sort was complete, the samples were vortexed and incubated for 5 minutes at room temperature. Phenol-chloroform-isoamyl alcohol was added to each sample, shaken vigorously and incubated at room temperature for 2 minutes before being centrifuged at 12,000 x g for 15 minutes at 4˚C.

The upper aqueous phase of the sample was transferred to a new Eppendorf tube to which 5µg of RNase-free glycogen (Invitrogen) was added. 250µl of isopropanol was added and the samples were incubated at -20˚C overnight for maximal RNA precipitation.

Samples were then centrifuged for 10 minutes at 12,000 x g 4˚C and the supernatant was removed and discarded. Subsequently, the pellet was washed in 250µl of 75% ethanol before repeating centrifugation (10 minutes, 12,000 x g, 4˚C) after which the supernatant was discarded. The pellet was then allowed to air dry and then resuspended in 17µl of RNase- and DNase-free water.

RNA was then treated for 30 minutes with DNase I (Fermentas) at 37˚C to remove any residual genomic DNA. cDNA synthesis was carried out using the First Strand cDNA Synthesis KIT (Fermentas). First, samples were primed with random hexamers for 5 minutes at 70˚C before being treated with M-MuLV Reverse Transcriptase (Fermentas), 10mM deoxyribonucleotides (dNTPs) and RNasin (Fermentas) RNAse inhibitors for 1 hour at 37˚C. Finally, heating samples to 70˚C for 10 minutes inactivated enzymes and cDNA samples were stored at -20˚C until use in RT qPCR experiments.

2.10.2 RT qPCR

The resulting cDNA from the protocol described above was used to generate a 1:3 serial dilution, resulting in a set of 7 standards before being diluted 1:5 in RNase- and DNase-free water and run alongside a no-template control. RT qPCR was carried out using Sensimix SYBR Green No-Rox (Bioline) on a Corbett Rotor Gene 600. The cycling settings were: 95˚C hold for 10 minutes followed by 35 cycles of 95˚C for 15 seconds, 63˚C for 30 seconds, 70˚C for 30 seconds. RT-qPCR primer sequences are found in the table below and were used at a concentration of 10µM.

Table 2-2 RT-qPCR Primers

Gene	Forward Primer	Reverse Primer
18S	5'-AACGGCTACCACATCCAAGG	5'-GGGAGTGGGTAATTTGCGC
CD115	5’- AAACTGCATCCACCGGGAC	5’-GTCCGCTGGTCAACAGCAC

2.11 Immunofluorescence

2.11.1 Epidermis

Ears were harvested from sacrificed mice and any hair was removed using hair removal cream (Veet). Ears were separated into dorsal and ventral halves and placed dermis side down into PBS (1X) containing 2.4mg/ml Dispase; 3% foetal bovine serum. The epidermal sheets were carefully separated from the dermis and placed on slides. Epidermal sheets were fixed for 10 minutes with 4% formaldehyde before blocking overnight with PBS (1X) containing 5% normal goat serum (Invitrogen), 0.5% BSA (w/v) and 0.1% Triton X-100. Epidermal sheets were stained with primary antibody over night at 4˚C, followed by secondary antibody for 2 hours at room temperature.

Table 2-3 Antibodies for epidermal immunofluorescence

Primary antibody	Dilution	Secondary antibody	Dilution
Rabbit anti-GFP	1/200	Goat anti-Rabbit Alexa fluor 488	1/200
Rat anti-IA/IE (clone 2G9)	1/100	Donkey anti-Rat Cyanine Cy3	1/100

Sheets were post-fixed with 1% formaldehyde for 1 minute and mounted with mounting medium (Vector Laboratories). Images were acquired using a Leica TCS SP5 confocal microscope. Image analysis was performed using the Image J software (National Institute of Health) or Imaris (Bitplane) software.

2.11.2 Spleen

Spleens were fixed for 4 hours in 4% formaldehyde, incubated overnight in 30% sucrose and embedded in OCT compound (Sakura Finetek). Cryoblocks were cut at a thickness of 15µm and then blocked with Streptavidin/Biotin blocking KIT (Vector laboratories) followed by further blocking with 1X PBS containing 5% normal goat

serum (Invitrogen); 0.5% BSA (w/v); 0.3% Triton X-100 for 1 hour at room temperature. Samples were incubated overnight at 4˚C with primary antibodies. Samples were washed and incubated with secondary antibodies for 2 hours at room temperature. Samples were then mounted with mounting medium (Vector Laboratories). Images were acquired using a Leica TCS SP5 confocal microscope. Image analysis was performed using the Image J software (National Institute of Health) or Imaris (Bitplane) software.

Table 2-4 Antibodies for spleen immunofluorescence

Primary antibody	Dilution	Secondary antibody	Dilution
Rat anti-MARCO	1/50	Anti-Rat Alexa fluor 555	1/100
Rat anti-CD169	1/50	Anti-Rat Alexa fluor 555	1/100
Biotin-conjugated anti-F4/80	1/100	Streptavidin Alexa fluor 488	1/100

2.12 Statistical analysis

2.12.1 Statistical significance

In all experimental figures included in this thesis, statistical significance is indicated by stars or with the p value written above. Statistical significance was considered to be $p<0.05$.

Table 2-5 Levels of statistical significance

Statistical significance	Wording	Summary
≥0.05	Not significant	ns (or blank)
0.01 to 0.05	Significant	*
0.001 to 0.01	Very significant	**
0.0001 to 0.001	Highly significant	***
<0.0001	Highly significant	****

2.12.2 Statistical analysis of flow cytometry data

Flow cytometry data was analysed using FlowJo (Tree Star Inc) and population frequencies amongst $CD45^+$ cells were exported from FlowJo. Data were graphically visualised with error bars representing standard deviation (SD) using GraphPad Prism 6. Normal distribution of samples was assessed using D'Agostino-Pearson normality test (D'Agostino and Stephens, 1986) to confirm Guassian distribution and unpaired t-tests were applied to data using GraphPad Prism 6 (GraphPad Software Inc).

2.12.3 Half-life calculations from BrdU experiments

To calculate the half-lives of monocytes and their progenitors, exponential trend lines were fitted to the data using the following one-phase exponential decay equation:

$$Y = (Y0\text{-}Plateau) * exp^{(-K*X)} + Plateau$$

Where: X = time

Y = $BrdU^+$ cells

K= Rate constant

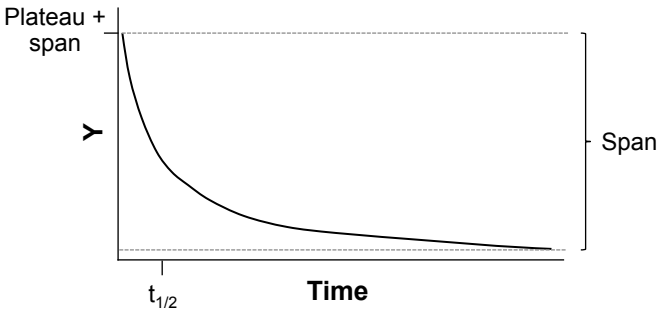

Figure 2-11 One phase exponential decay trendline fitting

Half-life of the decay is computed as ln(2)/K *(ln(2)=0.6932)*.

3 Wild-type monocyte dynamics

3.1 Introduction, aims and objective

3.1.1 Introduction

Monocytes belong to the myeloid arm of the immune system and develop normally in lymphocyte deficient *Rag2*$^{-/-}$ *Il2rg*$^{-/-}$ animals (Auffray et al., 2007; Mazurier et al., 1999). Monocytes can be defined by expression of CD115 (also called *Csf1r* or *M-csfr*) and CD11b (MacDonald et al., 2005; Sasmono et al., 2003), together with the lack of expression of T cell, B cell, granulocyte and NK cell markers. In mice, two principal subsets have been described (Geissmann et al., 2003): the "inflammatory" Ly6C^{+} CX_3CR1^{int} subset which are thought to correlate to the human CD14^{+} monocytes and the "patrolling" Ly6C^{low} CX_3CR1^{bright} subset which are thought to be analogous to human CD14^{dim} CD16^{+} monocytes.

This chapter establishes that murine monocytes in the blood and BM can be separated into three subsets monocyte based on their cell surface expression of Ly6C and MHC II in the blood and BM.

The chemokine receptor *Cx3cr1* is widely expressed within myeloid lineages and *Cx3xr1*^{GFP} knock-in mice (Jung et al., 2000) have been a vital tool in the identification and characterisation of myeloid BM progenitors (Fogg et al., 2006; Liu et al., 2009) and monocyte subsets (Geissmann et al., 2003; Yona et al., 2013). However, *Cx3cr1* expression is not exclusive to myeloid cells (Auffray et al., 2007; Jung et al., 2000). Accordingly, experiments using *Cx3cr1*^{GFP} animals should be carried out on mice with a lymphocyte-deficient *Rag2*$^{-/-}$ *Il2rg*$^{-/-}$ background to confirm if cells belong to the myeloid lineage, however, it is important to analyse these animals bearing in mind the caveat it is not technically steady state conditions.

This chapter validates the third, minor Ly6C^{int} MHC II^{+} monocyte subset by analysing *Cx3cr1*$^{GFP/+}$ animals on a lymphocyte-deficient *Rag2*$^{-/-}$ *Il2rg*$^{-/-}$ background (Auffray et al., 2007; Jung et al., 2000). In addition, *Nr4a1*^{GFP} mice were analysed to assess the level of NR4A1 expression in different monocyte subsets in the blood and BM and their progenitors, confirming and building upon the work by Hanna *et al.,* (Hanna et al., 2011). Furthermore, this chapter uses to C57BL/6 wild type mice to analyse the cell cycle dynamics of the monocytes in the blood and BM along with their progenitors. In conjunction with this, the dynamics of monocyte subsets were interrogated using BrdU incorporation pulse-chase analysis. This enabled the establishment monocyte half-lives *in vivo* when three separate subsets are considered.

3.1.2 Objective and aims

Chapter 3 objective: Detailed definition of the murine monocyte compartment and the interrelationships between different monocyte subsets in the blood and BM of wild type adult mice.

The aims of this chapter are:

1. Characterisation of blood and BM monocyte subsets and their BM progenitor/ precursor populations in adult, wild type mice

2. Investigate blood and BM monocyte subsets and their BM progenitor/ precursor populations proliferation using Ki-67 and DAPI staining

3. Investigate monocyte and monocyte progenitor dynamics using BrdU pulse-chase labelling

3.2 Characterisation of monocyte subsets and their precursors

3.2.1 Blood monocytes

3.2.1.1 Blood monocyte subsets

Blood monocytes express the growth factor receptor CD115 (also known as CSF1R and M-CSFR) and the integrin CD11b (also known as Mac-1). For isolating blood monocyte subsets in this thesis, an antibody mix was developed, excluding $CD3^+$, $CD19^+$ and $Ly6G^+$ cells and selecting the $CD115^+$ $CD11b^+$ population (Figure 3-1). To confirm this antibody mix was identifying monocytes as have previously been described, blood from CX_3CR1^{GFP} reporter mice on a *Rag2*$^{-/-}$ *Il2rg*$^{-/-}$ background was analysed using C57BL/6 wild type mice as a control (Figure 3-1).

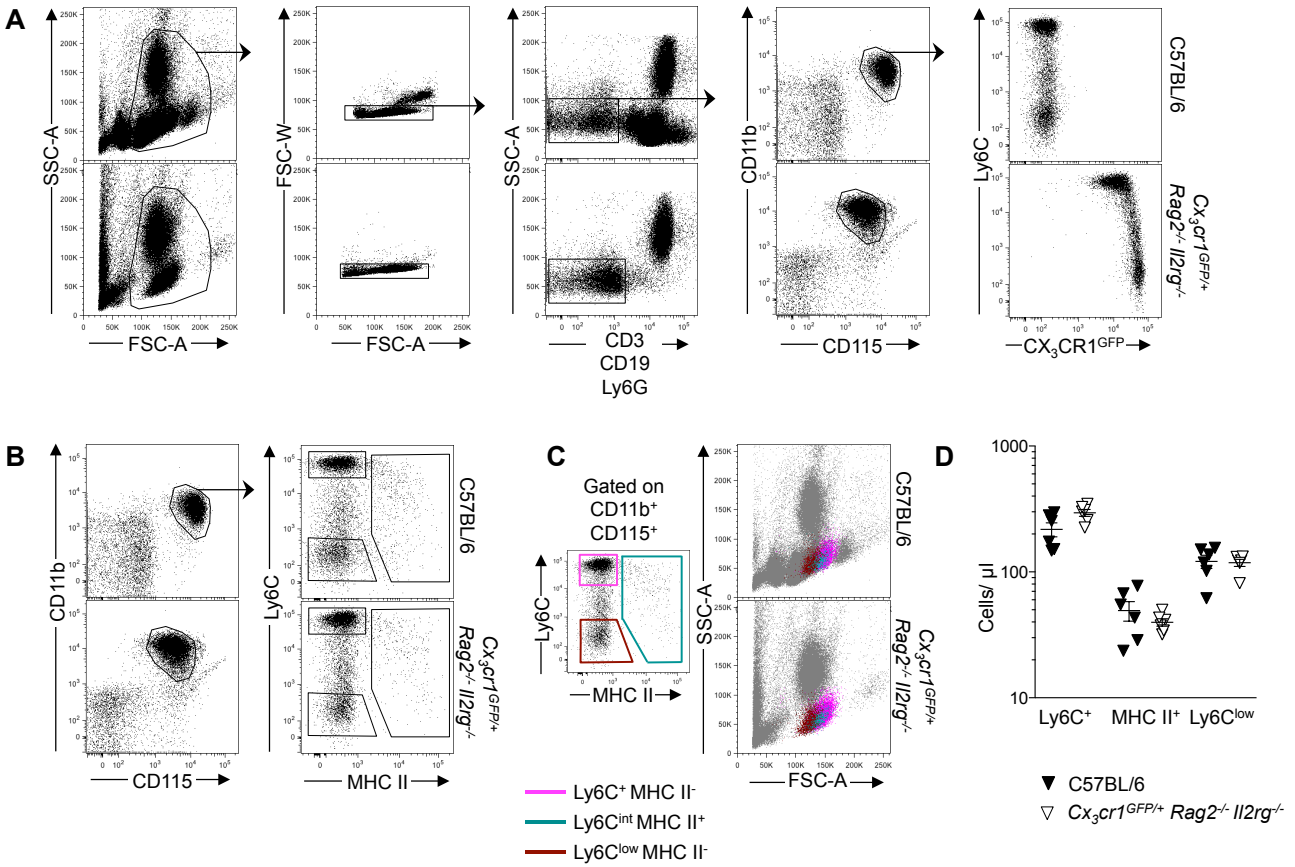

Figure 3-1 Isolation of blood monocyte subsets

(A) Blood monocyte isolation by selection of CD11b^{+} CD115^{+} cells and exclusion of doublets, T cells, B cells and granulocytes in C57BL/6 wild type mice and *Cx3cr1*$^{GFP/+}$ *Rag2*$^{-/-}$ *Il2rg*$^{-/-}$ animals. **(B)** Blood monocytes can be divided into three subsets based on expression of Ly6C and MHC II. **(C)** Backgating of 3 monocyte subsets on to forward- and side-scatter dot plot. **(D)** Frequencies of all three monocyte subsets in *Rag2*$^{-/-}$ *Il2rg*$^{-/-}$ animals.

Figure 3-1 shows the gating strategy used to isolate blood monocytes. In 3-1a, it can be seen that monocytes were selected as $CD11b^+$ $CD115^+$ cells after exclusion of doublets, $CD3^+$, $CD19^+$ and $Ly6CG^+$ cells. Furthermore, in the *Cx3xr1*$^{GFP/+}$ *Rag2*$^{-/-}$ *Il2rg*$^{-/-}$ animals, CX_3CR1 expression demonstrates $Ly6C^{low}$ monocytes express this reporter very strongly and GFP expression is lower in $Ly6C^+$ monocytes as has previously been described (Geissmann et al., 2003).

Within the $CD115^+$ $CD11b^+$ compartment a third monocyte subset, characterised by the expression of MHC II and variable levels of Ly6C, could be identified (Figure 3-1b), as was previously shown by both Jakubzick *et al*., and Carlin *et al.,* (Carlin et al., 2013; Jakubzick et al., 2013). This $CD11b^+$ $CD115^+$ MHC II^+ population was found in lymphocyte deficient mice showing that this population develops in the absence of the common gamma chain (*Il2rg*) and backgating shows characteristic monocyte forward and side scatter profiles in both wild type and *Rag2*$^{-/-}$ *Il2rg*$^{-/-}$ animals (Figure 3-1c). Henceforth throughout this thesis, this population will be referred to as $Ly6C^{int}$ MHC II^+ monocytes. Finally, Figure 3-1d demonstrates that no differences were observed in the frequencies of all three monocyte subsets between C57BL/6 mice and *Rag2*$^{-/-}$ *Il2rg*$^{-/-}$ animals.

Collectively, these data confirm the presence of a third blood monocyte subset that can be identified by expression of MHC II and intermediate expression of Ly6C. In addition, this population develops normally in *Rag2*$^{-/-}$ *Il2rg*$^{-/-}$ animals. Consequently, to fully understand wild type monocyte dynamics, monocytes were analysed as three separate subsets throughout this study.

3.2.1.2 Blood monocyte subset characterisation

To characterise the three separate monocyte subsets, expression levels of CX_3CR1 and NR4A1 were investigated using GFP reporter mice (Figure 3-2). Blood cells were additionally stained with CD11c and Flt3 (CD135) or an appropriate isotype control. It was observed that expression of both CX_3CR1^{GFP} and $NR4A1^{GFP}$ increase incrementally from $Ly6C^{+}$ MHC II^{-} to $Ly6C^{int}$ MHC II^{+} and again from $Ly6C^{int}$ MHC II^{+} to $Ly6C^{low}$ MHC II^{-}. Thus, $Ly6C^{low}$ MHC II^{-} monocytes in the blood express high levels of NR4A1, in addition to their requirement of this transcription factor for their development (Hanna et al., 2011).

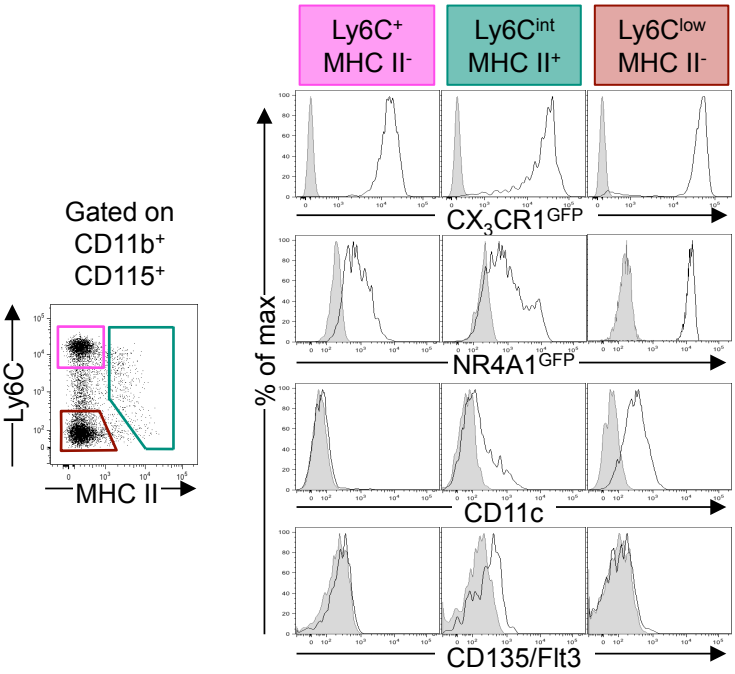

Figure 3-2 Blood monocyte subset characterisation

Expression patterns of CX_3CR1^{GFP}, $NR4A1^{GFP}$, CD11c and Flt3 in blood monocyte subsets when separated into three populations as indicated in the dot plot on the left-hand side. White histograms represent GFP reporter signal or antibody staining, grey histograms represent GFP^{-} controls or isotype controls.

The level of expression for both CX_3CR1^{GFP} and $NR4A1^{GFP}$ increases as Ly6C expression decreases between subsets. The most probable explanation for this is a reflection of higher gene expression levels in $Ly6C^{int}$ MHC II^+ and $Ly6C^{low}$ MHC II^- monocyte subsets; however, an alternative interpretation should also be considered. GFP has a long half-life in cells (~26 hours (Corish and Tyler-Smith, 1999)), and one could speculate that the inverse correlation of both NR4A1 and CX_3CR1 with Ly6C could be that the GFP is accumulating over time as $Ly6C^+$ monocytes convert into $Ly6C^{low}$ monocytes. This could potentially lend support to the current model of $Ly6C^{low}$ monocytes maturation from blood $Ly6C^+$ monocytes (Sunderkotter et al., 2004; Varol et al., 2007; Yona et al., 2013). However, this interpretation of the data would suggest that such a conversion requires $Ly6C^+$ monocytes passing through an MHC II^+ intermediate step; and the biological rationale for MHC II^+ upregulation followed by downregulation is not obvious. Conversely, the same reasoning could be applied when considering that $Ly6C^{low}$ monocytes have a significantly longer life span compared to the $Ly6C^+$ subset (Yona et al., 2013) and brighter GFP signals in the $Ly6C^{low}$ subset could also be a reflection of their longer half-life in which to accumulate GFP.

In addition, CD11c staining shows a successive increase in expression as monocytes lose expression of Ly6C, which could be interpreted, along with the GFP observations, to fit the maturation hypothesis or alternatively, these data together could be indicative of three distinct subsets and not a maturation pathway. Interestingly, $Ly6C^{int}$ MHC II^+ population only expresses Flt3 (CD135), albeit at very low levels, in addition to MHC II, which may point towards a dendritic cell-like function, a hypothesis that requires investigating. Purely phenotypical data such as these are not sufficient to answer questions of blood monocyte interrelationships however it provides insight into the

subtle differences in cell surface marker expression which may provide clues as to functional differences between subsets.

3.2.2 Bone marrow monocytes and their progenitors

3.2.2.1 MDP, cMoP and bone marrow monocyte definitions

In this thesis, one of the principal aims is to clarify the development pathway of Ly6C^{low} monocytes. There have been some seemingly contradictory results regarding the immediate precursor cell to Ly6C^{low} monocytes. Some studies have indicated that Ly6C^{+} blood monocytes are the immediate precursor cell of Ly6C^{low} blood monocytes (Hettinger et al., 2013; Sunderkotter et al., 2004; Varol et al., 2007; Yona et al., 2013; Yrlid et al., 2006). However, genetic studies have also reported Ly6C^{low} monocytes develop in the absence of Ly6C^{+} monocytes in *Irf8*- and *Klf4*-deficient mice (Alder et al., 2008; Kurotaki et al., 2013). Furthermore, Ly6C^{low} monocyte development and/or survival is dependent upon the transcription factor *Nr4a1* (Hanna et al., 2011), and their egress from the BM is selectively dependent upon sphingosine-1 phosphate receptor 5 (S1pr5) (Debien et al., 2013). Thus, uniting these observations into a single hypothesis has proved problematic and this thesis proposed to re-examine the development pathways of Ly6C^{+} and Ly6C^{low} MHC II^{-} monocytes and shed new light on the interrelationships by including the Ly6C^{int} MHC II^{+} monocyte subset.

Ly6C^{+} monocytes have been shown to differentiate from BM myeloid progenitors from the CX_3CR1^{+} MDP (Fogg et al., 2006). The MDP, defined as CD115^{+} KIT^{+} Flt3^{+} (CD135) CD11b^{low}, is a clonogenic BM progenitor population capable of giving rise to both monocytes and dendritic cells but has lost the ability to give rise to granulocytes (Auffray et al., 2009a; Fogg et al., 2006).

Subsequently, in 2013, the monocyte-restricted precursor population, the cMoP, was described (Hettinger et al., 2013). This population of BM cells is one step further along the differentiation pathway, having lost expression of Flt3 (CD135) and the capacity to give rise to DCs, the cMoP is a Ly6C-expressing dedicated monocyte precursor.

Thus, an important starting point for BM analysis in this thesis was to develop an antibody panel that enabled analysis of the MDP and cMoP along with BM monocyte populations. Whilst the MDP was identified using CX_3CR1^{GFP} reporter mice, deficient of lymphocytes (Fogg et al., 2006), for this thesis it was necessary to isolate the MDP without the use of CX_3CR1^{GFP} and in animals with lymphocytes. The development an antibody panel that isolated the MDP, cMoP and BM monocytes without the aid of CX_3CR1^{GFP} and in immunocompetent mice was necessary to allow consistent analysis of BM populations between different genetic models and reporter strains.

Figure 3-3 shows the gating strategies used for identifying these BM populations throughout the thesis. Gating on $CD45^+$ and lineage negative cells isolated myeloid populations of interest. The lineage in this antibody panel contained CD3, CD19, Ly6G, NKp46 and Sca-1 to exclude T cells, B cells, granulocytes, NK cells and HSCs, respectively. Considering $CD45^+$ lineage negative cells in terms of KIT and CD115 expression allowed the isolation of the populations of interest. Within the KIT^+ $CD115^+$ compartment were the MDP (lineage negative, KIT^+ $CD115^+$ $CD11b^{low}$ $Ly6C^-$) and the cMoP (lineage negative, KIT^+ $CD115^+$ $Flt3^-$ $CD11b^{low}$ $Ly6C^+$) (Figure 3-3).

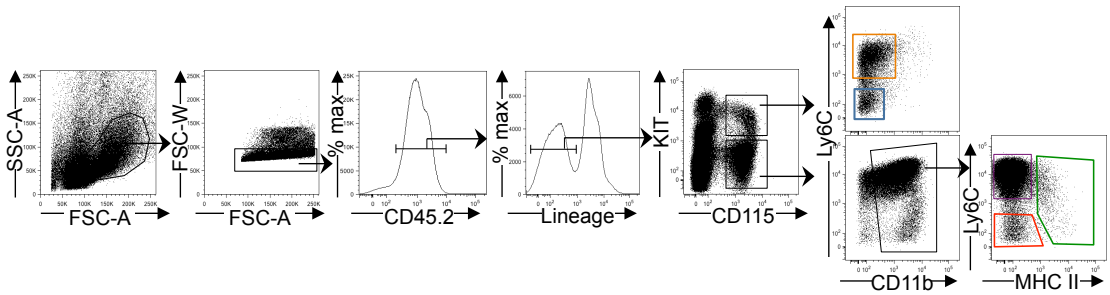

Figure 3-3 BM monocyte and progenitor gating strategy

Gating strategy for selecting BM monocytes and their progenitors by gating on $CD45^+$ lineage (CD3 CD19 NKp46 Sca-1 Ly6G) negative cells and selecting either KIT $CD115^+$ for the MDP (light blue) and cMoP (orange) or KIT^- $CD115^+$ for BM monocytes: $Ly6C^+$ $MHC\ II^-$ (purple) $Ly6C^{int}$ $MHC\ II^+$ BM (green) and $Ly6C^{low}$ $MHC\ II^-$ (red).

BM monocytes were identified as KIT^- $CD115^+$ $CD11b^+$. All three monocyte subsets that were identified in the blood were also found in the BM (Figure 3-3). BM monocytes were previously described as pro-monocytes (Shand et al., 2014) as they were shown to be proliferating, but considered by others as mature monocytes (Hettinger et al., 2013; Yona et al., 2013) because they lack KIT (also known as c-KIT or CD117) expression. In this thesis, they will be referred to as BM monocytes but their precursor potential shall be further investigated.

3.2.2.2 Bone marrow myeloid population characterisation

To further characterise the BM myeloid populations, expression levels of CX_3CR1 and NR4A1 were assessed using GFP reporter mice. The MDP and the cMoP express intermediate levels of CX_3CR1 and low levels of NR4A1 (Figure 3-4). As in the blood, expression of both CX_3CR1^{GFP} and $NR4A1^{GFP}$ increased as Ly6C expression reduced among the three BM monocyte subsets. Thus, $Ly6C^{low}$ monocytes express the highest levels of both proteins in both the blood (Figure 3-2) and the BM (Figure 3-4).

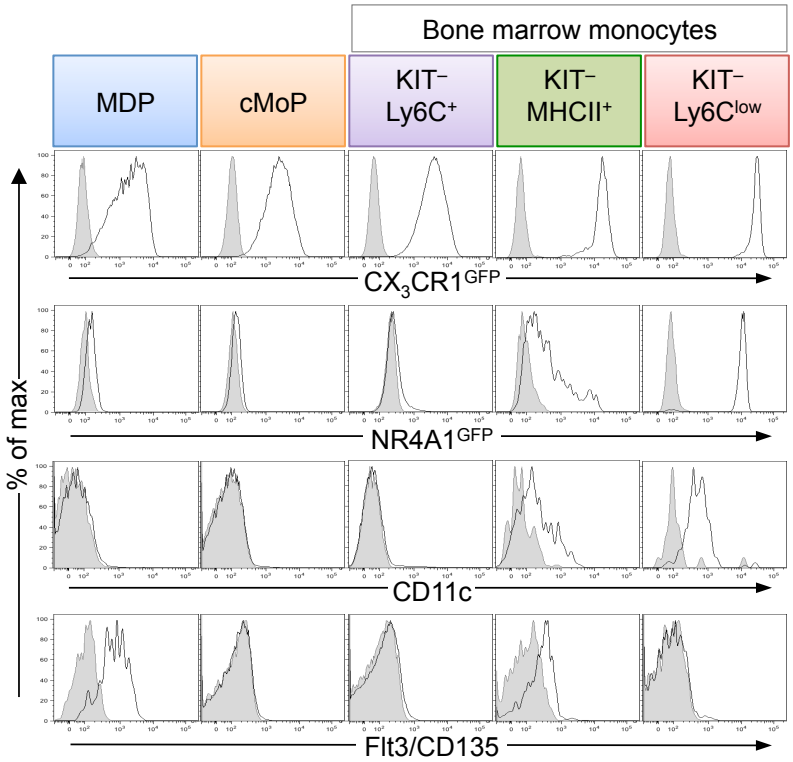

Figure 3-4 Characterisation of BM monocyte progenitors and BM monocytes

Expression of CX_3CR1^{GFP} and $NR4A1^{GFP}$ (white histograms) in BM myeloid progenitors and BM monocytes compared to GFP-negative controls (grey histograms). Expression of CD11c and Flt3 (white histograms) compared to isotype controls (grey histograms).

BM $Ly6C^+$ monocytes were not found to express CD11c or Flt3, whereas the $Ly6C^{low}$ monocytes express CD11c and the $Ly6C^{int}$ MHC II^+ subset expresses both CD11c and Flt3, showing a very similar expression pattern to the blood monocyte subsets (Figure 3-4).

Interestingly, within the BM lineage negative $Ly6C^{low}$ $CD11b^+$ compartment, a second cell population could be identified that expressed high levels of GFP in $NR4A1^{GFP}$ animals as well as high GFP expression in CX_3CR1^{GFP} animals, in a very similar manner to $Ly6C^{low}$ MHC II^- monocytes (Figure 3-5a and 3-5b). However, this population did not express high levels of the monocyte marker CD115. Backgating analysis demonstrated that this population has very similar forward and side scatter profile to $Ly6C^{low}$ BM monocytes (Figure 3-5c).

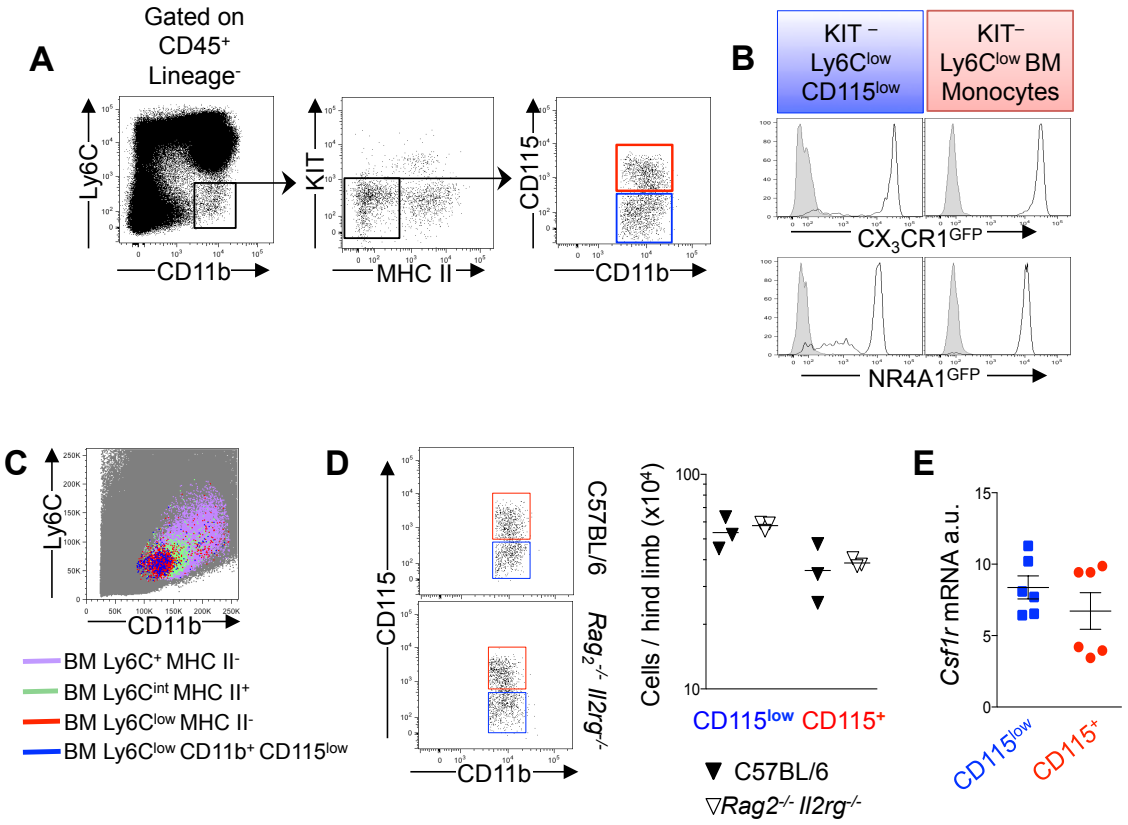

Figure 3-5 Identification and characterisation of a Ly6C^{low} CD11b^{+} CD115^{low} myeloid population

(A) Gating strategy to identify Ly6C^{low} CD11b^{+} CD115^{low} population (blue) and Ly6C^{low} BM monocytes (red). **(B)** Expression of CX_3CR1^{GFP} (top) and $NR4A1^{GFP}$ (bottom) in both Ly6C^{low} CD11b^{+} CD115^{low} (blue) and Ly6C^{low} BM monocytes (red). **(C)** Backgating analysis of BM monocytes and Ly6C^{low} CD11b^{+} CD115^{low} population. **(D)** Analysis and quantification of Ly6^{low} CD11b^{+} CD115^{low} (blue) and Ly6C^{low} BM monocytes (red) in *Rag2*$^{-/-}$ *Il2rg*$^{-/-}$ animals n=3 per genotype, symbols represent individual animals **(E)** RT-qPCR analysis of CD115 (*Csf1r*) in sorted Ly6^{low} CD11b^{+} CD115^{low} (blue) and Ly6C^{low} BM monocytes, n=6, symbols represent individual animals, error bars represent standard deviation (SD).

This population was found to be present in normal numbers in *Rag2*$^{-/-}$ *Il2rg*$^{-/-}$ animals indicating it develops independently of *Il2rg* (Figure 3-5d). In addition, RT-qPCR analysis carried out on FACS sorted cells from this compartment revealed similar CD115 mRNA levels in both the NR4A1^{bright} CD115^{low} novel population and in the NR4A1^{bright} CD115^{+} BM Ly6C^{low} monocytes (Figure 3-5e).

All together, these data demonstrate the presence of an *Il2rg*-independent CX_3CR1^{bright} $NR4A1^{bright}$ $Ly6C^{low}$ $CD11b^{+}$ bona fide myeloid population that only expresses CD115 at the mRNA level. As this population was novel and potentially related to $Ly6C^{low}$ monocytes, it was included in all further analysis carried out in this thesis and henceforth referred to as $CD11b^{+}$ $CD115^{low}$ cells.

3.2.3 Dynamics of blood and bone marrow subsets

3.2.3.1 Proliferation rates of monocytes and their precursors in vivo

To understand the dynamics of BM myeloid progenitors, as well as BM and blood monocytes in wild type animals under steady state conditions, it was necessary to assess what proportion of each population was actively cycling at a single time point. Staining with the nuclear dye 4',6-diamidino-2-phenylindole (DAPI) allows measurement of DNA content, revealing the percentage of cells in G_0/G_1 (2N) vs S phase (>2N<4N) vs. G_2M (4N) (Pozarowski and Darzynkiewicz, 2004). All cells in G_0/G_1 phases have uniform DNA content that can be set to 50,000 DAPI fluorescence (2N) and cells in G_2M should have exactly twice this much (4N DAPI fluorescence = 100,000) (Figure 3-6a and b). However, in reality, there is some variation in the spread of cells representing 2N DNA content. This variation can be measured when DAPI fluorescence is represented as a histogram and width of the G_0/G_1 peak is measured (coefficient of variation, CV). The CV is a direct reflection of the accuracy of DNA measurement, thus to ensure maximal accuracy, only samples with DAPI CV of <6% were considered.

Using DAPI in conjunction with Ki-67, a marker expressed during the active phases of the cell cycle (G_1, S and G_2M phases) but not resting cells (G_0) (Challen et al., 2009), it is possible to determine what proportion of a population is in a particular phase of cell cycle at any given time point (Figure 3-6).

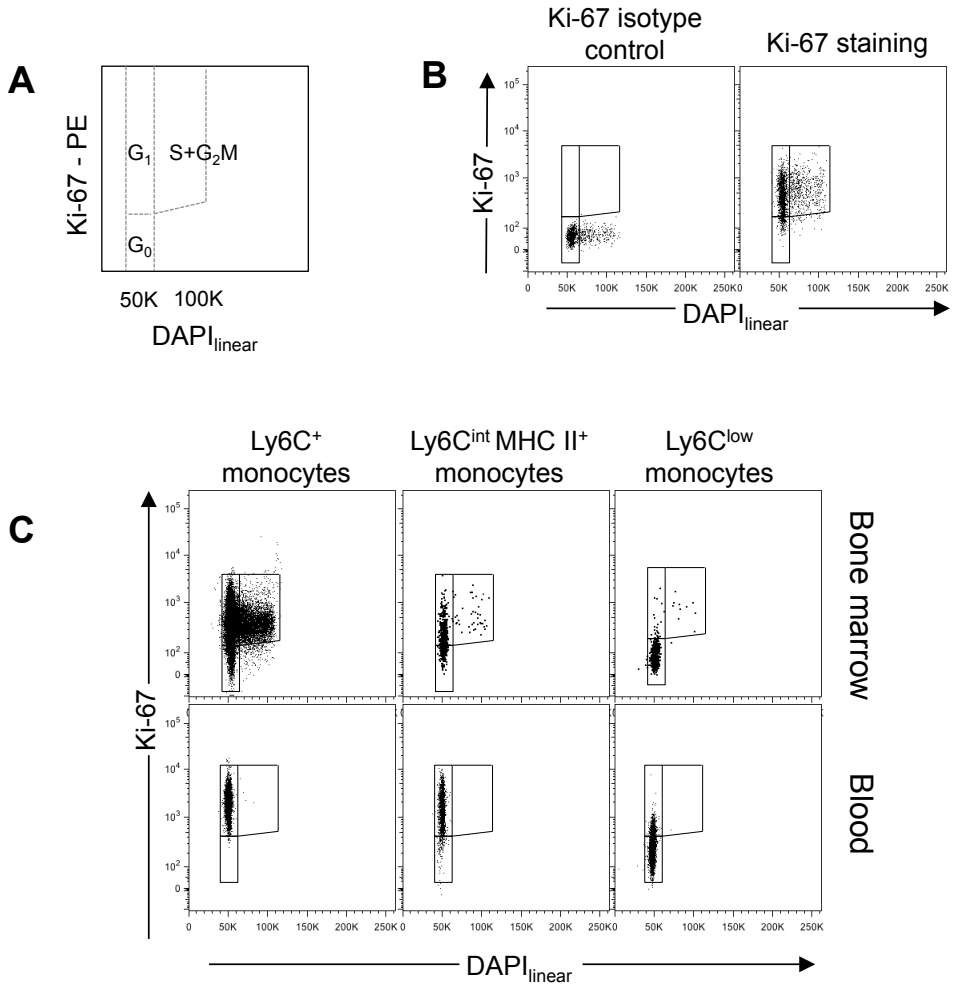

Figure 3-6 Cell cycle analysis

The phase of cell cycle a cell is in can be ascertained by staining with Ki-67 and DAPI **(A).** Representative dot plots of cell cycle analysis gating from a Ki-67 isotype control staining (left) and Ki-67 antibody staining (right) from C57BL/6 BM **(B). (C)** Representative dot plots of Ki-67 and DAPI staining of monocyte subsets from the BM (top panel) and blood (lower panel) in C57BL/6 mice.

This analysis revealed that the MDP was highly active with 36.03±3.68% (±standard deviation, SD) in S+G_2M phases and 87.81±1.53% of the MDP compartment was positive for Ki-67. The cMoP was similarly found to be highly active with 46.5±9.13% of cells in S+G_2M phases and with 87.67±3.09% of the cMoP population expressing Ki-67 (Figure 3-7a).

BM Ly6C$^+$ monocytes were also still actively cycling despite loss of KIT expression with 15.85±1.83% of the population in S+G_2M phases and more than 76.65±5.55% Ki-67$^+$ (Figure 3-6c and 3-7a). Thus, these data confirmed the observations of Shand *et al.,* who referred to BM Ly6C$^+$ monocytes as "pro-monocytes" after demonstrating their proliferation using Fucci mice (Shand et al., 2014).

The Ly6C^{int} MHC II$^+$ BM monocyte population showed an intermediate phenotype with 46.83±7.38% of the compartment quiescent (Ki-67$^-$ and 2N DNA content) and 6.68±1.83% of the population actively cycling in S+G_2M phase (Figure 3-6c and 3-7a).

In contrast, the majority of BM Ly6C^{low} MHC II$^-$ monocytes were quiescent with 91.62±2.94% of the population lacking expression of Ki-67 and having 2N DNA content and only 1±0.27% of the Ly6C^{low} MHC II$^-$ BM compartment was actively cycling (Figure 3-6c and 3-7b).

Interestingly, the CD11b$^+$ CD115^{low} population was also mostly quiescent with 70.37±7.96% of the population in G_0 and this population only had slightly more cells actively cycling (3±1.1%) in G_2M. Whilst this is a very small proportion of the population, it could be indicative of a slowly proliferating population that might replenish a long-lived cell type.

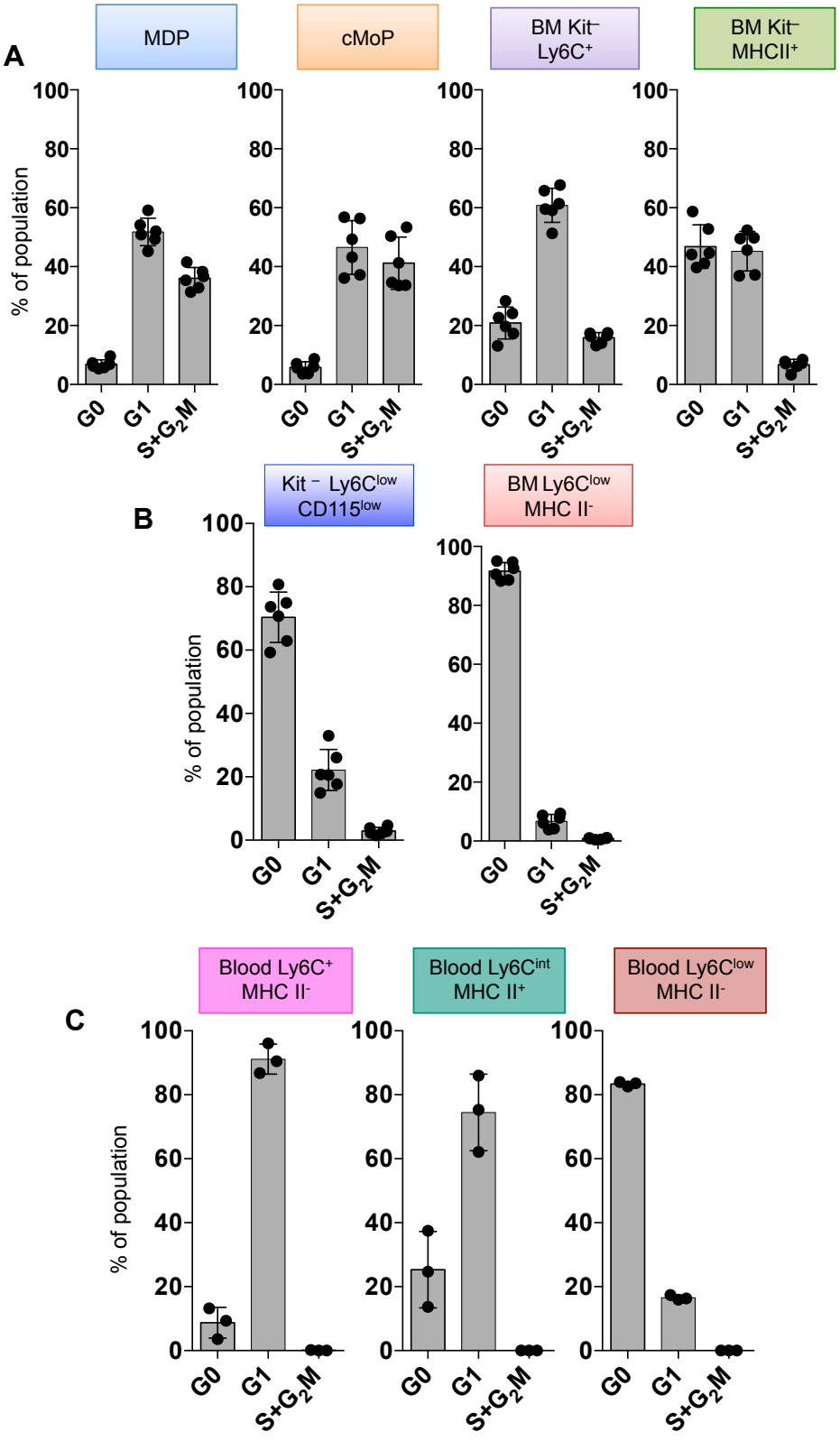

Figure 3-7: Cell cycle analysis of blood and BM monocytes and their progenitors

(A) Frequency of BM monocyte progenitors and BM Ly6C^{+} and Ly6C^{int} MHC II^{+} monocytes in cell cycle phases G_0 (2N Ki-67^{-}), G_1 (2N Ki-67^{+}) and S+G_2M (>2N Ki-67^{+}) n=6 **(B)** Percentage of BM CD11b^{+} Ly6C^{low} cells and Ly6C^{low} MHC II^{-} BM monocytes in G_0, G_1 and S+G_2M, n=6 **(C)** Percentage of blood monocytes in G_0, G_1 and S+G_2M, n=3. Symbols represent individual animals, error bars represent SD.

As expected, cells were observed to be in G_0 or G_1 phase in blood monocyte subsets. Interestingly, 91.24±4.76% of the Ly6C$^+$ monocyte subset was positive for Ki-67 whereas in the blood Ly6C^{low} MHC II$^-$ monocyte compartment only around 16.54±0.77% of the population still expressed Ki-67 (Figure 3-6c and 3-7c). This is could be due to Ly6C^{low} MHC II$^-$ monocytes being out of active cell cycle for long enough to down regulate Ki-67 expression. But whether this is a reflection of their longer half-life (Yona et al., 2013) or because they are further differentiated remains to be clarified. In contrast, Ly6C$^+$ monocytes have a short life span, and having recently finished cycling, it is possible that they have not yet lost expression of Ki-67.

3.2.3.2 Half-lives of monocytes and their progenitors/precursors

Whilst the "snapshot" measurement of a single time point that Ki-67 and DAPI analysis provides, it does not inform on cell cycle kinetics, and in particular, the length of time different populations remain in each phase of the cell cycle. In order to evaluate the dynamics and establish half-lives of monocyte progenitors and the three separate monocyte subsets, both in the blood and BM, a pulse-chase labelling protocol was used. Wild type mice were pulsed with the synthetic nucleoside, 5'-bromo-2'-deoxyuridine (BrdU) which, as an analogue of the pyrimidine deoxy-nucleoside thymidine, is permanently incorporated into DNA of actively dividing cells. This was followed by a chase to examine rate of BrdU dilution over time, either by subsequent cell divisions during the chase phase or by death of labelled daughter cells.

As proliferation in blood monocytes was undetectable using Ki-67 and DAPI (Figure 3-6c and 3-7c) (Shand et al., 2014), time-lapse analysis of blood monocyte BrdU content following a single pulse should allow to measure their rate of production and their half-life *in vivo* (Yona et al., 2013). C57BL/6 wild type mice were given a single dose of

1.5mg BrdU by intraperitoneal (i.p.) injection. Blood and BM were analysed for BrdU incorporation in the different myeloid subsets at regular intervals from 1-hour post-injection through to 240-hours post-injection (10 days), with three animals per time point.

Visually, it can be seen from the graphs in Figure 3-8 that Ly6C^{low} MHC II^{-} monocytes, both in the BM and the blood, have a much slower rate of BrdU incorporation and subsequent loss of BrdU signal (decay) compared to the other subsets analysed. The MDP, the cMoP and the Ly6C expressing monocyte populations appear to follow a similar pattern of incorporation and rapid decay of BrdU signal consistent with a short life span.

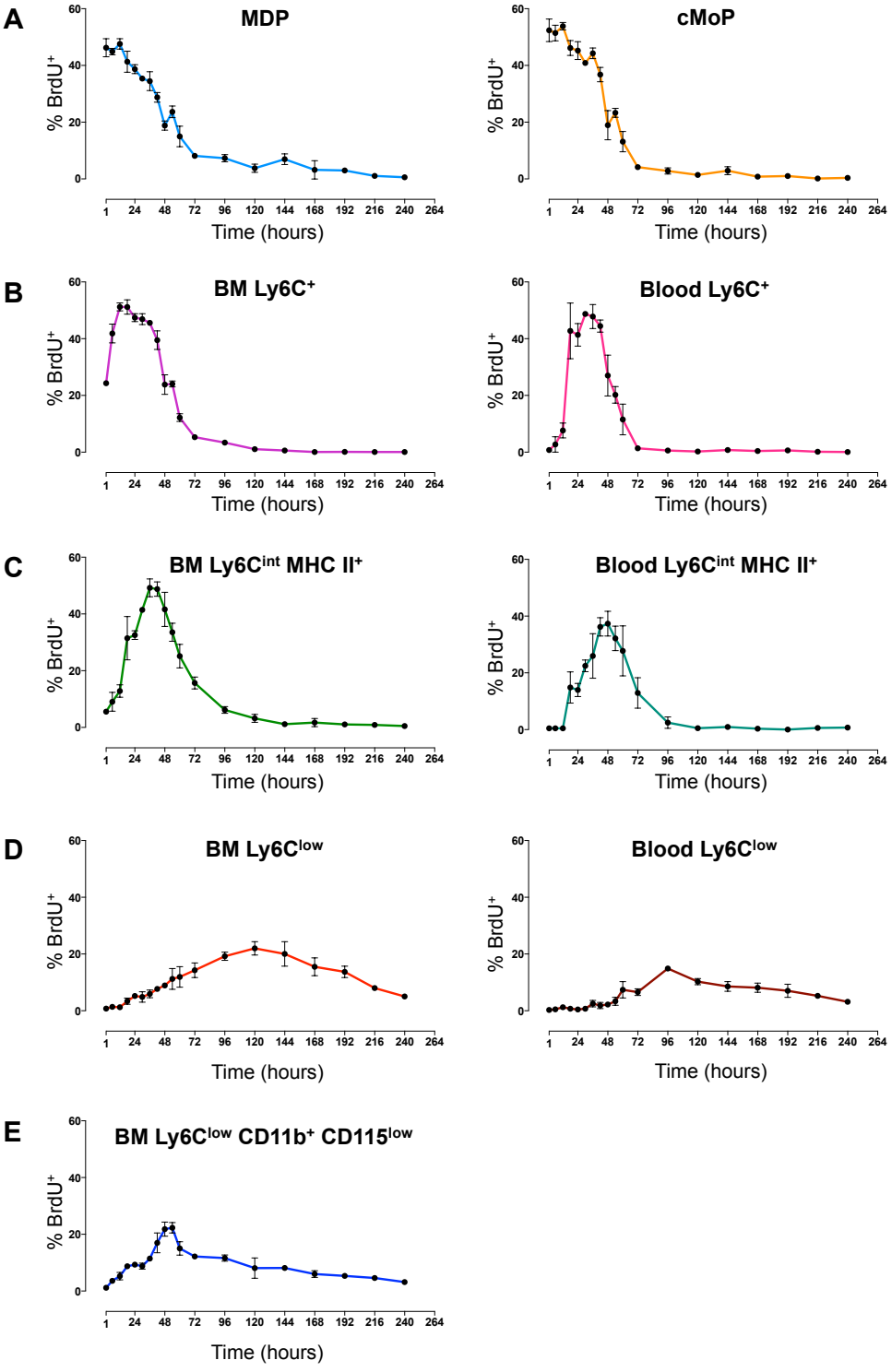

Figure 3-8: BrdU incorporation in monocytes and their progenitors from wild type mice

BrdU incorporation after 1.5mg i.p. injection. **(A)** Frequency of $BrdU^+$ cells among MDP (left, light blue) and cMoP (right, orange) **(B)** Frequency of $BrdU^+$ cells among $Ly6C^+$ monocyte populations in the BM (left, purple) and blood (right, pink). **(C)** Frequency of $BrdU^+$ cells among $Ly6C^{int}$ MHC II^+ cells in the BM (left, green) and blood (right, turquoise) **(D)** BrdU incorporation within the BM (left, red) and blood (right, burgundy) $Ly6C^{low}$ monocytes populations **(E)** BM $Ly6C^{low}$ $CD11b^+$ $CD115^{low}$ cells BrdU incorporation; n=3 mice per time point, error bars represent standard deviation.

Fitting exponential trend lines from the peak of BrdU incorporation and measuring the rate of decay provides an estimation of half-life. The results indicated that the steady state half-life the MDP was 39.99 hours or 1.7 days ($r^2 = 0.94$), the half-life of the cMoP was similar at 35.67 hours or 1.49 days ($r^2 = 0.90$). Interestingly, the steady state half-life of the BM Ly6C$^+$ monocyte was much shorter at 13.81 hours or 0.58 days ($r^2 = 0.98$) and similarly, blood Ly6C$^+$ monocytes were calculated to have a half-life of 12.31 hours or 0.51 days ($r^2 = 0.95$). The Ly6C^{int} MHC II$^+$ BM monocytes were found to have a slightly longer half-life of 18.79 hours or 0.78 days ($r^2 = 0.98$) and the corresponding MHC II$^+$ blood population had a half-life of 16.38 hours or 0.68 days ($r^2 = 0.94$).

In stark contrast, BM Ly6C^{low} MHC II$^-$ monocytes were calculated as having a half-life of 80.6 hours or 3.36 days ($r^2 = 0.91$) and in the blood the Ly6C^{low} monocyte half-life was 77.21 hours or 3.2 days ($r^2 = 0.88$), 6 times longer than that of blood Ly6C$^+$ monocyte subset (Figure 3-8). The half-life of Ly6C^{low} MHC II$^-$ monocytes was therefore found to be longer than previously calculated (Yona et al., 2013). A possible explanation for this could be the separation of MHC II$^+$ monocytes from the Ly6C^{low} compartment, as MHC II$^+$ monocytes have a shorter half-life and their kinetic seems to be much more closely related to the kinetic of the Ly6C$^+$ subset. Furthermore, investigating the BrdU incorporation of the BM Ly6C^{low} CD11b$^+$ population revealed this population also has a long half-life of 66.41 hours or 2.8 days ($r^2 = 0.89$). Again, this lends support to the conjecture that this population may be related to BM Ly6C^{low} MHC II$^-$ monocytes and is worthy of continued investigation.

The kinetics of BrdU incorporation and loss for each blood monocyte subset was very similar to its corresponding BM counterpart albeit with a slight delay, validating the concept that all monocyte populations differentiate in the BM before their egress into the periphery.

These data demonstrate a very different kinetic for Ly6C^{low} MHC II^{-} monocytes, both in the BM and in the blood, compared to Ly6C^{+} monocytes. This prompted further probing into the interrelationships of monocyte subsets using genetic models.

3.3 Overview and Discussion

3.3.1 Rationale for considering three monocyte subsets

Traditionally, murine monocytes are divided into two subsets based on expression of Ly6C and CX_3CR1 (Geissmann et al., 2003; Gordon and Taylor, 2005; Yona et al., 2013) although the presence of intermediate populations has previously been alluded to (Carlin et al., 2013; Jakubzick et al., 2013; Sunderkotter et al., 2004). Flow cytometry analysis of monocyte subsets including MHC II as a marker allows the separation of a third, minor monocyte population.

Monocytes expressing intermediate levels of Ly6C have been considered representative of the transition or maturation of Ly6C^{+} monocytes into Ly6C^{low} however; the expression of MHC II on this subset does not fit comfortably with this interpretation. The expression of MHC II could be indicative of activation or of unique effector functions for this subset. Both possibilities require investigation to fully understand whether or not this is monocyte differentiation/maturation from Ly6C^{+} or Ly6C^{low} MHC II^{-} monocytes or a fully separate subset. However, the additional heterogeneity inferred by the presence of a third, phenotypically distinct subset might explain the conflicting reports regarding monocyte interrelationships.

3.3.2 Bone marrow monocytes and their progenitors

All three monocytes can be identified in the BM, which could indicate that monocyte subsets differentiate in the BM before their egress to the periphery. Furthermore blood

monocyte BrdU incorporation mirrored bone monocyte incorporation with a slight delay, which suggests BM origin of all three subsets.

This interpretation is in contrast to previous reports which suggest that BM and blood Ly6C^{low} monocytes are independent. Yona *et al.,* demonstrated that BrdU incorporation into Ly6C^{low} monocytes was reduced after treatment with a Ly6C^{+} monocyte ablation strategy using the CCR2 antibody, MC21 (Bruhl et al., 2007; Yona et al., 2013). MC21 depletes blood Ly6C^{+} monocytes but not Ly6C^{+} BM monocytes, in line with Ly6C^{+} monocytes dependency on CCR2 for their BM egress. Treatment with MC21 was found to reduce BrdU incorporation in the blood Ly6C^{low} monocytes but not in the BM Ly6C^{low} monocytes which indicated that Ly6C^{+} monocytes controlled development of Ly6C^{low} monocytes in both the blood and BM.

In light of data presented here of increased monocyte heterogeneity, in both the blood and BM, a new hypothesis was developed in which Ly6C^{+} monocytes give rise to MHC II^{+} monocytes in both the blood and BM whereas Ly6C^{low} MHC II^{-} monocytes develop independently in the BM via a CD11b^{+} CD115^{low} intermediate before egressing to the periphery. This hypothesis will be explored and interrogated further in the next chapter using different genetic models.

4 The genetics of Ly6C^{low} monocyte development

4.1 Introduction, aims and objectives

4.2 Genetics of Monocyte development in mice

There are several known mutations that affect the development of monocytes. Mice deficient in *Csf1r* (also called *c-fms*, *M-Csfr* or CD115) have a severe reduction in blood monocytes (Dai et al., 2002). Furthermore, animals that are deficient in *Csf1*, a ligand of *Csf1r*, are also deficient in blood monocytes (Kodama et al., 1991; Wiktor-Jedrzejczak and Gordon, 1996).

Adult monocytes arise from BM haematopoietic stem cells, which have to pass through various stages of commitment before they mature to blood circulating monocytes. It is known that at several of these commitment steps, the Ets family transcription factor, PU.1 is required as PU.1 can induce commitment to the myeloid lineage in HSCs (Mossadegh-Keller et al., 2013) and in immature multi-potent progenitors (Nerlov and Graf, 1998). These genetic requirements occur early in cell fate decisions and commit cells to the myeloid lineage.

Of particular interest to this thesis is the analysis of different genetic mouse models in which monocyte subsets show differing genetic requirements. This chapter will focus mainly on the nuclear receptor *Nr4a1*, an ideal example of a selective genetic requirement in monocyte development.

Nr4a1 belongs to a family of orphan nuclear receptors, known as the NR4A-subfamily. This subfamily consists of three members: NR4A1 (also known as Nur77, TR3 and NGFI-B), NR4A2 (also known as Nurr1) and NR4A3 (also known as NOR-1). These receptors are considered “orphan” as they have no known ligands.

Nr4a1 is known to act as a transcription factor, directly binding to DNA either as a monomer or as a homodimer (Kurakula et al., 2014). *Nr4a1* can also form heterodimers with retinoid X receptors (RXRs) and has been shown to interact with both RXRα and RXRγ (Kurakula et al., 2014; Roszer et al., 2013). Thus, *Nr4a1* has the capacity to influence gene expression in multiple ways, many of which remain to be elucidated. As a consequence, *Nr4a1* has been implicated in many different biological processes including cell survival, proliferation and apoptosis in a vast array of cell types, both haematopoietic and non-haematopoietic.

This chapter will focus on understanding the differentiation pathway of Ly6C^{low} MHC II^{-} monocytes in light of the heterogeneity described in Chapter 3, using a variety of genetic models to facilitate unravelling the intricacies of monocyte development. In particular, this chapter and the next will fully characterise a novel conditional *Nr4a1*-knock out model developed for this project, *Csf1r*^{iCre} *Nr4a1*$^{fl/fl}$ animals, which confines *Nr4a1* deletion to the haematopoietic compartment thus minimising the possibility that the loss of Ly6C^{low} MHC II^{-} monocytes observed in *Nr4a1*$^{-/-}$ mice is due to deletion of *Nr4a1* in stromal cells.

4.3 *Nr4a1* and Ly6C^{low} MHC II^{-} monocyte development

The current model of Ly6C^{low} monocyte development proposes that blood Ly6C^{+} classical monocytes undergo a maturation or "conversion" step into Ly6C^{low} monocytes (Hettinger et al., 2013; Sunderkotter et al., 2004; Varol et al., 2007; Yona et al., 2013; Yrlid et al., 2006). However, there are a number of genetic studies that are in conflict with this model of Ly6C^{low} monocyte development. It has been reported that Ly6C^{low} monocytes can develop in the absence of Ly6C^{+} monocytes in *Irf8*-deficient and *Klf4*-deficient mice (Alder et al., 2008; Kurotaki et al., 2013). Furthermore, Hanna *et al.,*

demonstrated Ly6C^{low} monocyte differentiation and/or survival is dependent upon the transcription factor *Nr4a1*, whereas Ly6C^{+} monocytes are found at normal frequencies in *Nr4a1*-deficient mice (Hanna et al., 2011).

In this chapter, the development of Ly6C^{low} MHC II^{-} monocytes is systematically analysed using a number of genetic models, in particular *Csf1r*^{iCre} *Nr4a1*$^{fl/fl}$, in order to understand the development pathway of Ly6C^{low} MHC II^{-} monocytes and their relationship with Ly6C-expressing monocyte subsets by investigating *Irf8*- and *Ccr2*-deficient animal models.

4.3.1 Hypothesis and aims

Chapter 4 objective: To dissect the genetic requirements of blood and BM monocyte subsets using different gene knock out models.

The aims of this chapter are as follows:

1. To assess expression of NR4A1^{GFP} in haematopoietic and non-haematopoietic populations;

2. To analyse the effects of Nr4a1-deficiency in *Csf1r*^{iCre} *Nr4a1*$^{fl/fl}$ conditional deletion animals and in *Nr4a1*^{GFP} *Nr4a1*$^{-/-}$ double mutant animals;

3. To extend the analysis of monocyte subsets to other genetic ablation models including *Irf8*$^{-/-}$ and *Ccr2*$^{-/-}$.

4. To gain further understanding of Ly6C^{low} MHC II^{-} monocyte development using adoptive transfer and *in vitro* culture systems.

4.4 The role of *Nr4a1* in Ly6C^{low} MHC II^{-} monocyte development

4.4.1 Characterisation of NR4A1^{GFP} expression

The pattern of NR4A1^{GFP} expression in a BAC transgenic mouse line was shown to be consistent with endogenous NR4A1 expression (Moran et al., 2011), was used to analyse NR4A1 expression in blood, BM and tissue myeloid cells.

To start, NR4A1^{GFP} in haematopoietic stem cells in the BM was analysed. Lineage (CD3, CD4, CD8, CD11b, CD19, Gr1) negative Sca-1^{+} KIT^{+} long term HSCs (LT-HSCs; CD150^{+} CD48^{-}), short term HSCs (ST-HSCs; CD150^{-} CD48^{-}) and multipotent progenitors (MPPs; CD150^{-} CD48^{+}) all expressed low levels of NR4A1^{GFP} (Figure 4-1a).

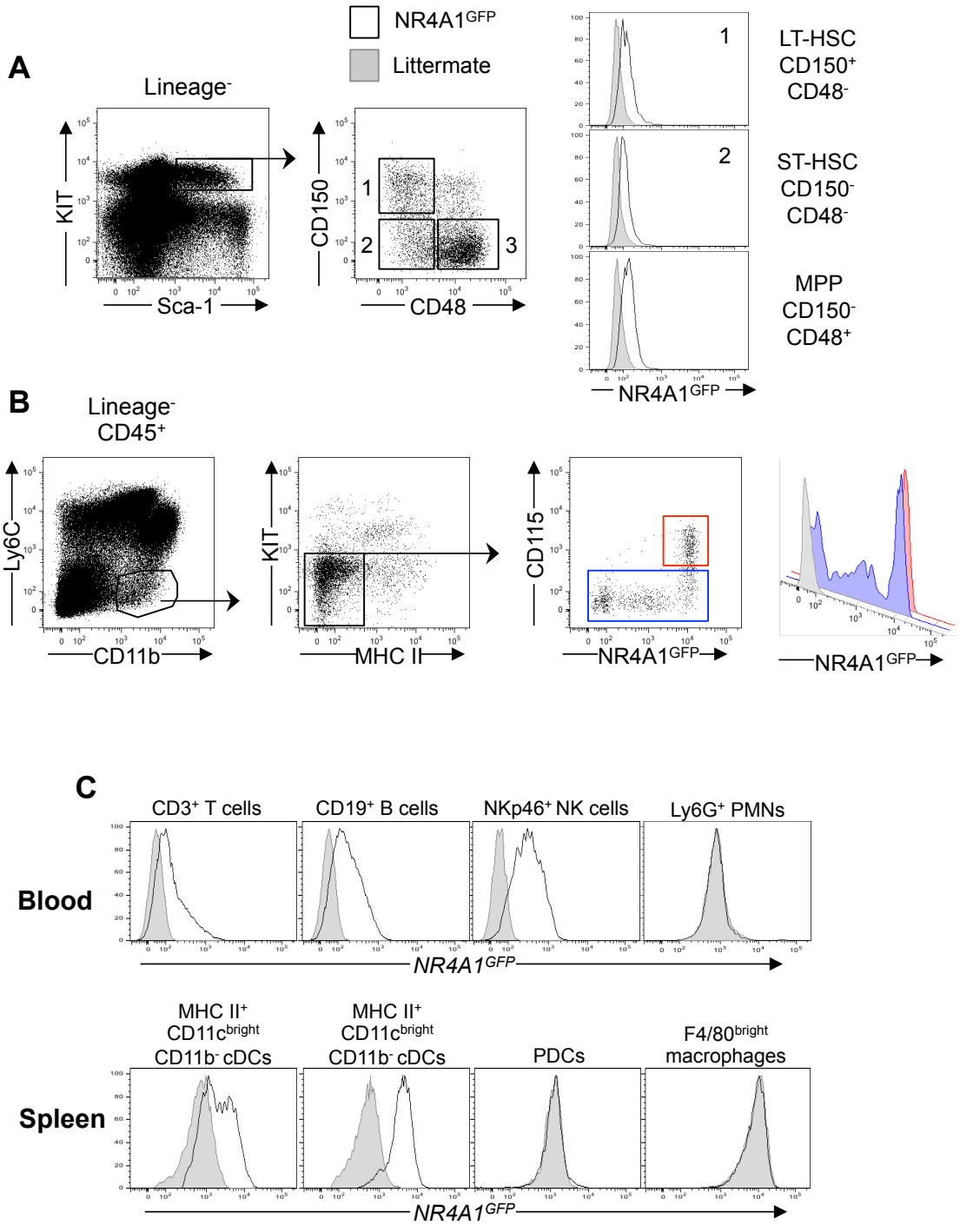

Figure 4-1 NR4A1^{GFP} expression in HSCs, lymphocytes, granulocytes, dendritic cells and splenic macrophages

(A) NR4A1 is expressed by LT-HSCs, ST-HSCs and MPPs, white histograms represent GFP^{+} animals, and grey histograms represent GFP^{-} littermate controls. **(B)** NR4A1^{GFP} is highly expressed by part of the CD11b^{+} CD115^{low} population (blue) and by Ly6C^{low} MHC II^{-} BM monocytes (red). **(C)** T cells, B cells, NK cells, and cDC subsets express NR4A1^{GFP} whereas granulocytes, PDCs and F4/80^{bright} macrophages do not, white histograms represent GFP^{+} animals, and grey histograms represent GFP^{-} littermate controls.

As previously discussed in Chapter 3, later BM progenitors, the MDP, cMoP, BM monocyte subsets and $CD115^{low}$ cells all express $NR4A1^{GFP}$ (See Chapter 3 section 3.2.2.2 and Figure 3-4). A proportion of the newly identified KIT^{-} $CD11b^{+}$ $CD115^{low}$ population expresses $NR4A1^{GFP}$ very brightly, and to the same level as $Ly6C^{low}$ MHC II^{-} monocytes (Figure 4-1b).

In the blood, T cells, B cells and NK cells express NR4A1 (Figure 4-1c), as do all three monocyte populations (Figure 3.2) however, PMNs do not (Figure 4-1c). In the spleen, both $CD11b^{-}$ and $CD11b^{+}$ subsets of cDCs express $NR4A1^{GFP}$ however; plasmacytoid dendritic cells (PDCs) and $F4/80^{bright}$ splenic macrophages do not (Figure 4-1c).

In order to characterise $NR4A1^{GFP}$ expression by tissue resident macrophages and myeloid cells within the tissues, brain, liver and lung were analysed by flow cytometry. As expected, classical, $F4/80^{bright}$ tissue resident macrophages in the brain, liver and lung did not express $NR4A1^{GFP}$ (Figure 4-2). However, some tissue $F4/80^{int}$ $CD11b^{+}$ populations did express NR4A1 in the liver and lung (Figure 4-2b and 4-2d). As the mice were not perfused prior to excision of tissues, it is likely that these NR4A1-expressing cells within the tissue are monocytes and other circulating leukocytes from within the tissue capillary network.

In addition, the skin from $NR4A1^{GFP}$ reporter mice was analysed. Epidermal sheets were taken for immunofluorescence and both dermis and epidermis were analysed by flow cytometry. Immunofluorescence staining and confocal imaging of the epidermis revealed widespread $NR4A1^{GFP}$ expression. Flow cytometry analysis confirmed that keratinocytes ($CD45^{-}$ $CD104^{+}$), Langerhans cells ($F4/80^{bright}$) and epidermal T cells ($CD3^{+}$) all expressed $NR4A1^{GFP}$ (Figure 4-2e). Furthermore, in the dermis, both dermal $CD45^{-}$ non-haematopoietic fraction and dermal macrophages were GFP^{+} (Figure 4-2f).

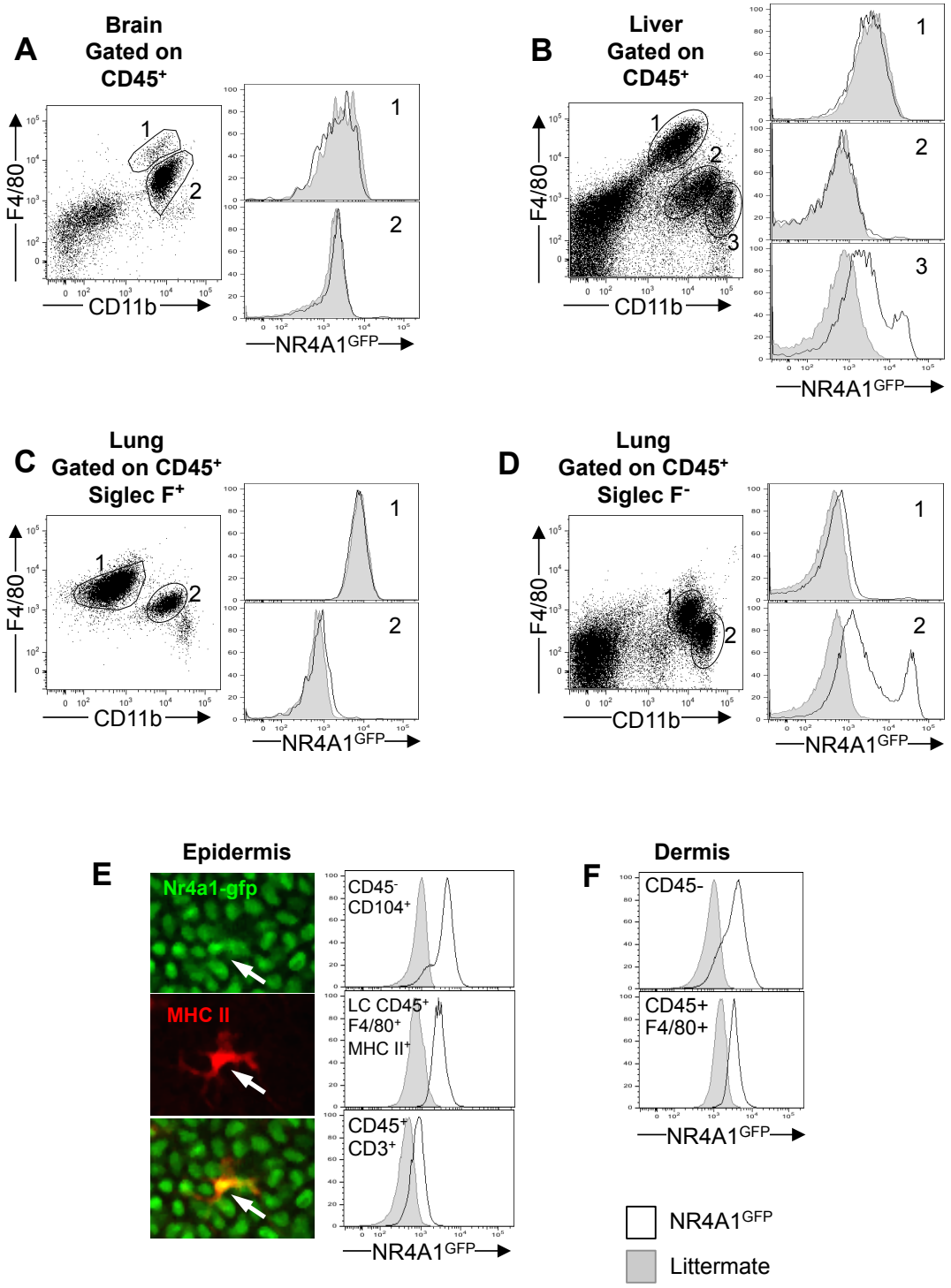

Figure 4-2 NR4A1^{GFP} expression in tissue cells

(A) NR4A1^{GFP} expression in brain F4/80^{bright} macrophages (1) and microglia (2). **(B)** NR4A1^{GFP} expression in liver F4/80^{bright} Kupffer cells (1) and liver myeloid cells (2 and 3). **(C)** NR4A1^{GFP} expression in alveolar macrophages (1) and lung eosinophils (2). **(D)** NR4A1^{GFP} expression in lung CD11b^{+} Siglec F^{-} lung myeloid cells. **(E)** NR4A1^{GFP} expression in epidermal haematopoietic and non-haematopoietic cells by immunofluorescence (left) and flow cytometry (right). **(F)** NR4A1^{GFP} expression in dermal macrophages and non-haematopoietic cells. White histograms represent GFP^{+} animals, and grey histograms represent GFP^{-} littermate controls

4.4.2 Characterisation of *Csf1r*^{iCre} as a driver for conditional Nr4a1 deletion

As discussed above, and previously widely reported, many different haematopoietic and non-haematopoietic cell types express *Nr4a1* (see above) (Davis and Puhl, 2011; Lee et al., 1995; Winoto and Littman, 2002). In addition, the *Nr4a1*-null mice were generated by the insertion of a phosphoglycerate kinase-neomycin resistance cassette (neo cassette) into the coding region of exon 2 of the *Nr4a1* gene (Lee et al., 1995). This neo cassette has not been excised from the genome of *Nr4a1*$^{-/-}$ animals, which may perturb expression of neighbouring genes (Meier et al., 2010; Pham et al., 1996; Rijli et al., 1994).

Furthermore, in the study by Hanna *et al.,* identifying the role of *Nr4a1* in Ly6C^{low} monocyte development, a statistically significant increase in granulocytes in *Nr4a1*-null mice, which may suggest an inflammatory phenotype (Hanna et al., 2011; Hanna et al., 2012). Thus, a cleaner, more targeted knockout system would be preferable to study the role of *Nr4a1* in monocyte development.

In order to generate such an improved model, to analyse the role of *Nr4a1* in the development of Ly6C^{low} MHC II^{-} and Ly6C^{int} MHC II^{+} monocytes, this study took advantage of the *Cre-lox* system. To generate conditional *Nr4a1*-knock out animals, mice harbouring the Cre recombinase under the control of the promoter for *Csf1r* (also known as CD115, *c-fms* or *M-csfr*) (Deng et al., 2010) were crossed to mice in which exons 2 and 4 of the *Nr4a1* gene (on chromosome 15) had been flanked by loxP sites (see Figure 2-2) (Boudreaux et al., 2012; Kadkhodaei et al., 2009).

In mature cells, CSF1R (CD115) expression is primarily restricted to monocytes and macrophages, although low-level expression on neutrophils has been reported (Sasmono

et al., 2007). Furthermore, the common dendritic cell progenitor (CDP) is defined, in part, by its expression of CSF1R. Consequently, it was important to ascertain where the *Csf1r*^{iCre} was active and which cells would be targeted by this approach. Thus, *Csf1r*^{iCre} mice were crossed to *Rosa26LSL*^{YFP} reporter mice. In these animals, any cell that expresses *Csf1r* and its progeny will have the lox-STOP-lox sequence excised and YFP will be expressed. HSCs and myeloid BM progenitors from *Csf1r*^{iCre} *Rosa*^{YFP} were analysed by flow cytometry (Figure 4-3).

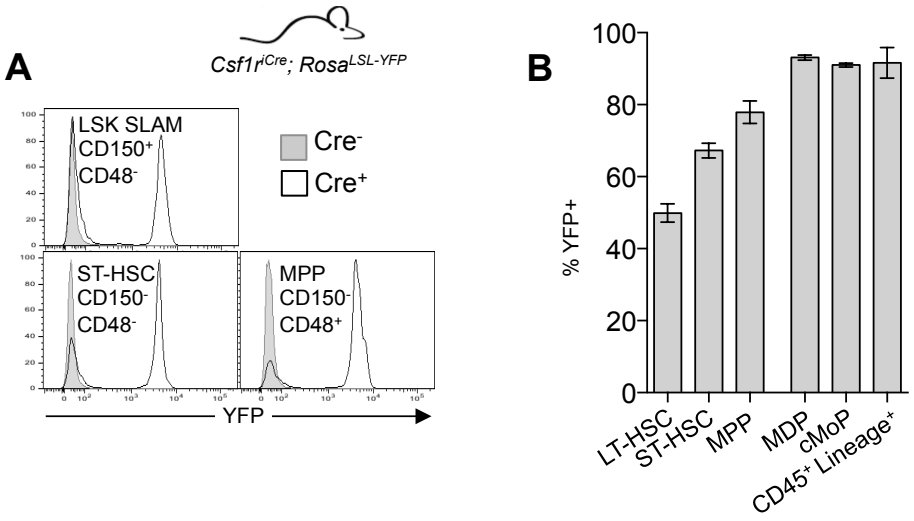

Figure 4-3 Assessment of *Csf1r*^{iCre} activity using *Rosa26LSL*^{YFP} reporter

(A) *Csf1r*^{iCre} activity in haematopoietic stem cell populations, white histograms represent iCre^{+} animals, grey histograms represent iCre^{-} littermate controls. **(B)** Quantification of proportion YFP^{+} HSCs, monocyte progenitors and in CD45^{+} lineage^{+} cells from *Csf1r*^{iCre} YFP^{+} animals, n=3 for each genotype.

It can be seen that 50% of LT-HSC have had the LSL sequence excised and express YFP and at the stage of MPP's 75% of cells are YFP positive. The MDP, cMoP and consequently all downstream progeny including BM monocytes are all >90% YFP positive. In addition, CD45^{+} lineage positive cells (including CD3 CD19 and NKp46) were also >90% YFP^{+}, providing an approximation of *Csf1r*^{iCre} mediated recombination in lymphocytes. This indicates that *Csf1r* mediated recombination at the Rosa locus is

highly efficient and effective resulting in pan-haematopoietic expression of Cre recombinase and consequently could also lead to pan-haematopoietic deletion of *Nr4a1*.

In order to validate the potential for efficient pan-haematopoietic deletion at the *Nr4a1* locus mediated by $Csf1r^{iCre}$ in the $Nr4a1^{fl/fl}$ model, a blood sample was taken from *Csf1r* $Nr4a1^{fl/+}$ (heterozygous, $iCre^-$); *Csf1r* $Nr4a1^{fl/fl}$ (homozygous, $iCre^-$); $Csf1r^{iCre}$ $Nr4a1^{\Delta/+}$ (heterozygous, $iCre^+$) and $Csf1r^{iCre}$ $Nr4a1^{\Delta/\Delta}$ (homozygous, $iCre^+$) littermates and an allele-specific PCR was carried out on this blood to assess deletion (Figure 4-4a). In this PCR, (detailed in Chapter 2: Materials and Methods) three primers are used to identify wild type DNA fragments (band at 215bp), the *Nr4a1*-floxed DNA fragments (band at 300bp) and the *Nr4a1*-deleted (Δ) DNA fragments after recombination (band at 425bp). In whole blood, the deletion of $Nr4a1^{fl/fl}$ was efficient with no residual bands (wild type or floxed) visible in the blood from $Csf1r^{iCre}$ animals (Figure 4-4a).

This PCR was repeated on purified (FACS sorted) cell populations from $Csf1r^{iCre}$ $Nr4a1^{\Delta/+}$, $Csf1r^{iCre}$ $Nr4a1^{\Delta/\Delta}$ and $Nr4a1^{fl/fl}$ animals. Sorted splenic $CD3^+$ T cells, $CD19^+$ B cells (Figure 4-4b), $CD11b^+$ and $CD11b^-$ cDCs, $PDCA1^+$ pDCs, $Ly6G^+$ granulocytes and $Ly6C^+$ monocytes (Figure 4-4c) all show efficient deletion of the *Nr4a1* gene with the only visible residual floxed band being present in pDCs, indicating incomplete recombination in this population. In addition, brain microglia and liver Kupffer cells were also sorted and analysed in the same manner, both populations show efficient deletion of the *Nr4a1* gene (Figure 4-4c). Collectively these deletion PCR data demonstrate *Csf1r* is effective and efficient at driving pan-haematopoietic deletion of *Nr4a1*.

In order to assess the level of deletion in haematopoietic vs. non-haematopoietic cells from within the same organ, epidermal Langerhans cells, $CD3^+$ T cells and $CD45^-$

$CD104^+$ (integrinβ_4) keratinocytes were FACS sorted and analysed using the same allele specific PCR. As shown in Figure 4-4d, *Nr4a1* is deleted in the $F4/80^+$ Langerhans cells and $CD3^+$ T cells in the $Nr4a1^{\Delta/\Delta}$ animals, as indicated by the DNA fragment band at 425bp whereas the $CD45^-$ $CD104^+$ keratinocytes have the undeleted floxed band at 300bp. These data confirm that $Csf1r^{iCre}$ is a good driver of pan-haematopoietic Nr4a1 deletion in this model and that $Csf1r^{iCre}$ is not expressed sufficiently in $CD45^-$ $CD104^+$ keratinocytes to mediate recombination at the loxP sites thus *Nr4a1* remains undeleted.

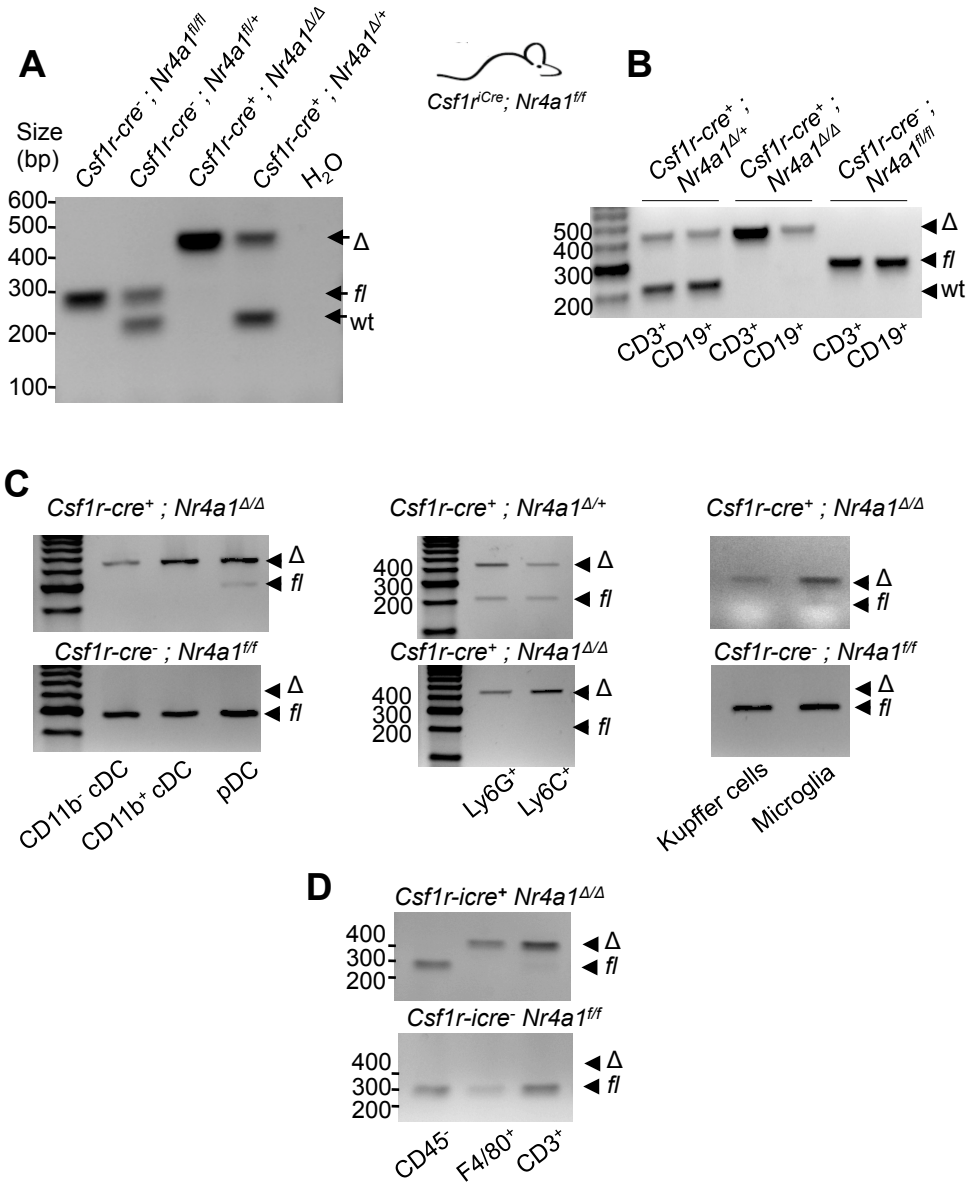

Figure 4-4 PCR analysis of *Nr4a1* deletion by *Csf1r*^{iCre}

Nr4a1 deletion in whole blood **(A),** sorted splenic T and B cells **(B)**, sorted splenic dendritic cell subsets, Ly6G^{+} granulocytes, Ly6C^{+} monocytes, liver Kupffer cells and brain microglia **(C).** *Nr4a1* deletion in non-haematopoietic and haematopoietic epidermal cell populations **(D).**

4.4.3 Characterisation of blood from *Csf1r^{iCre} Nr4a1$^{\Delta/\Delta}$* mice

In order to assess whether the *Csf1r^{iCre} Nr4a1$^{\Delta/\Delta}$* mice recapitulated the monocyte phenotype observed in the *Nr4a1$^{-/-}$* mice (Hanna et al., 2011), littermates were blood phenotyped by flow cytometry.

This analysis demonstrated Ly6C^{low} MHC II^{-} monocytes are selectively, and almost completely, dependent upon *Nr4a1* for their development, recapitulating the phenotype from the *Nr4a1$^{-/-}$* mice in a separate genetic model (Figure 4-5a and 4-5b). Ly6C^{+} and Ly6C^{int} MHC II^{+} monocytes were unaffected by *Nr4a1*-deficiency in this model. This is in contrast to the previously reported trend towards a slight reduction of Ly6C^{+} monocytes in *Nr4a1*-null animals (Hanna et al., 2011). As Ly6C^{int} MHC II^{+} cells were unaffected by *Nr4a1* deficiency (Figure 4-5a and 4-5b), it is likely that this population accounts for the residual cells within the Ly6C^{int}/Ly6C^{low} compartment observed in *Nr4a1$^{-/-}$* mice (Hanna et al., 2011).

Ly6C^{low} MHC II^{-} monocytes were shown to exhibit a strong gene dose effect: *Nr4a1$^{+/\Delta}$* mice have a reduction of 75% (p<0.0001) compared with *Nr4a1$^{fl/fl}$* littermate controls, and *Nr4a1$^{\Delta/\Delta}$* animals have a 98% reduction (p<0.0001) in Ly6C^{low} MHC II^{-} monocytes (Figure 4-5b).

Analysis of Ly6C^{low} MHC II^{-} monocytes from animals housed in conventional units compared to specific pathogen free (SPF) showed that conventional housing increased the number of Ly6C^{low} MHC II^{-} monocytes in littermate controls but failed to do so in the *Nr4a1$^{\Delta/\Delta}$* animals (Figure 4-5c). In addition, no differences in Ly6C^{low} MHC II^{-} monocytes were observed between male (blue circles) and female (red circles) littermates (Figure 4-5c).

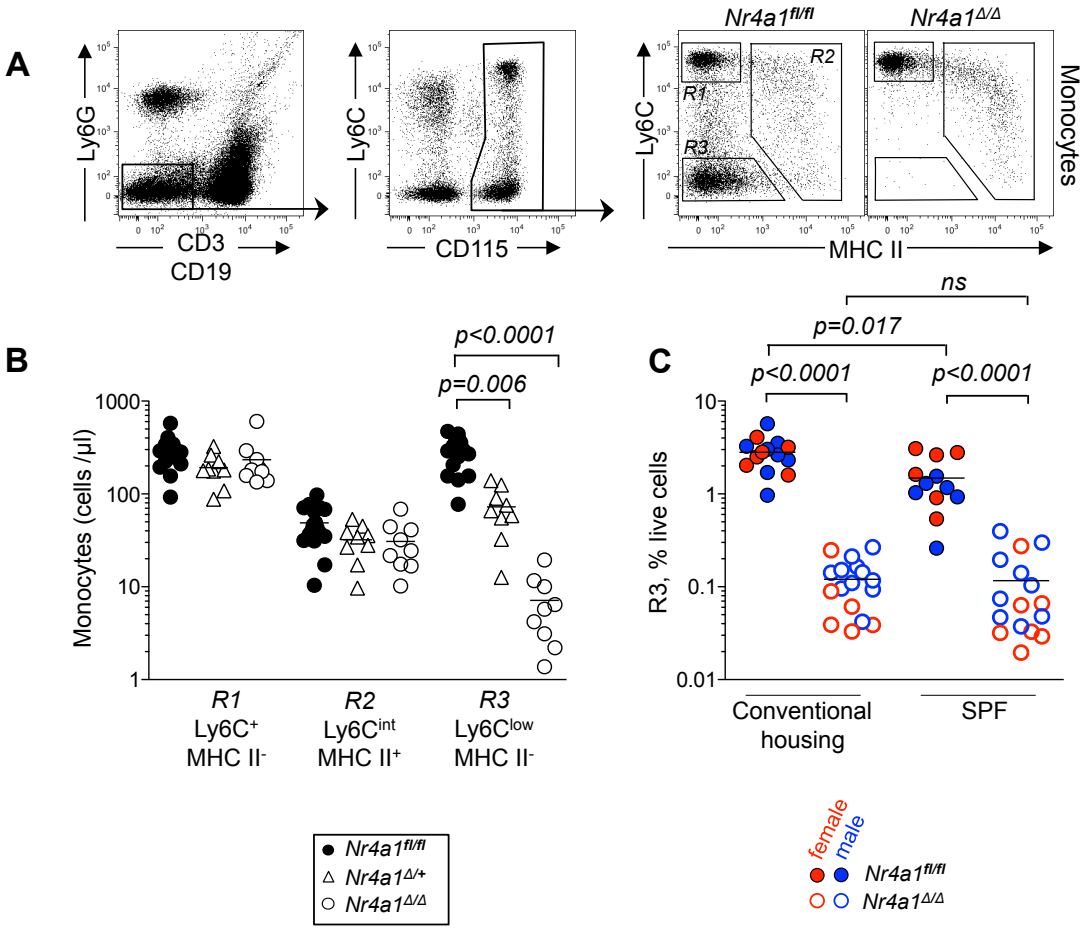

Figure 4-5 Analysis of blood granulocytes and monocytes from *Csf1r*^{iCre} *Nr4a1*$^{fl/fl}$ mice

(A) Representative dot plots illustrating gating strategy of blood CD115^{+} monocyte subsets in *Nr4a1*$^{\Delta/\Delta}$ mice and littermates. **(B)** Number/µL blood of CD115^{+} monocytes in *Nr4a1*$^{fl/fl}$ (closed circles, n=12), *Nr4a1*$^{\Delta/+}$ (open triangles, n=9) and *Nr4a1*$^{\Delta/\Delta}$ mice (open circles, n=9). **(C)** Frequency of Ly6C^{low} MHC II^{-} monocytes in *Nr4a1*$^{\Delta/\Delta}$ mice (open circles, n=20 males, n=13 females) and littermates (closed circles, n=14 males, n=12 females) under conventional and SPF housing conditions and colour coded by sex (males=blue, females=red). Symbols represent individual mice. Data analysed using unpaired t-test.

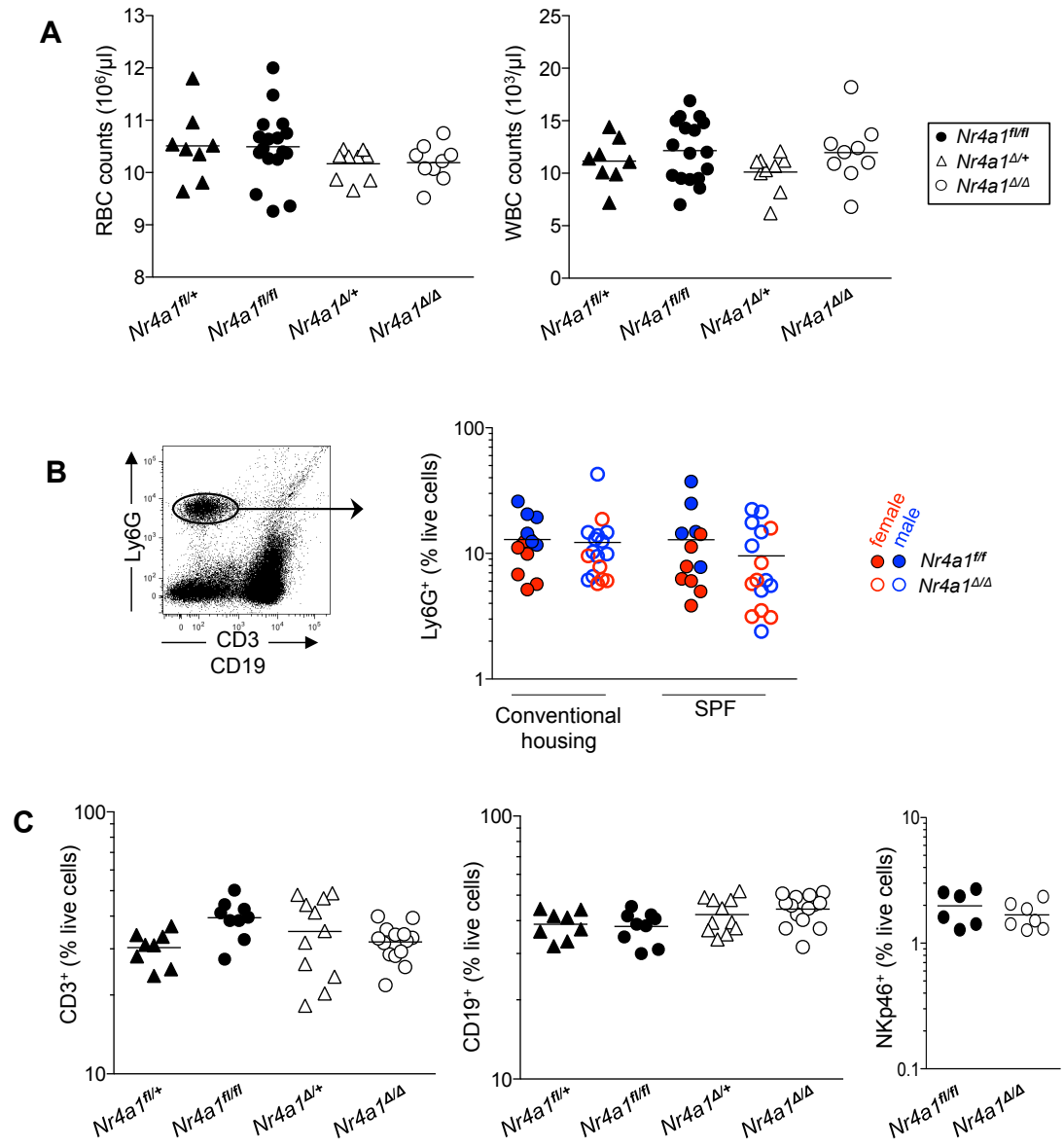

Figure 4-6 Blood analysis of *Csf1r*^{iCre} *Nr4a1*$^{fl/fl}$ littermates

(A) Total red blood cell (RBC) and white blood cell (WBC) counts from *Nr4a1*$^{+/fl}$ (closed triangles, n=8), *Nr4a1*$^{fl/fl}$ (closed circles, n=17), *Nr4a1*$^{+/\Delta}$ (open triangles, n=9) and *Nr4a1*$^{\Delta/\Delta}$ littermates (open circles, n=9). **(B)** Gating and frequency of Ly6G^{+} granulocytes in *Nr4a1*$^{\Delta/\Delta}$ (open circles, n=20 males, n=13 females) mice and littermates (closed circles, n=14 males, n=12 females) under conventional and SPF housing conditions and by sex (males = blue circles, females = red circles). **(C)** Frequency of CD3^{+} T cells, CD19^{+} B cells and NKp46^{+} NK cells in *Nr4a1*$^{\Delta/\Delta}$ mice (open circles, n=8-14) and *Nr4a1*$^{+/fl}$ (closed triangles, n=8), *Nr4a1*$^{fl/fl}$ (closed circles, n=6-9), *Nr4a1*$^{+/\Delta}$ (open triangles, n=11) littermates. Data analysed using unpaired t-test.

To confirm that the phenotype was selective for Ly6C^{low} MHC II^{-} monocytes total red blood cell (RBC) counts and white blood cell (WBC) counts in unlysed blood were analysed revealing no significant differences between the four phenotypes (Figure 4-6a).

Flow cytometry analysis of Ly6G^{+} granulocytes demonstrated that these cells are unaffected by *Csf1r*^{iCre} mediated deletion of *Nr4a1* (Figure 4-6b), in contrast to the reported increase observed in *Nr4a1*-null mice (Hanna et al., 2011). Thus, despite efficient deletion of the floxed alleles in granulocytes (Figure 4-4c) from *Nr4a1*$^{\Delta/\Delta}$ animals, the frequency of granulocytes amongst WBC was unperturbed (Figure 4-6b). This may suggest that the reported increase in granulocyte frequency in *Nr4a1*$^{-/-}$ mice could be due to *Nr4a1*-deficiency in non-haematopoietic cells.

To further confirm the specificity of *Nr4a1*-deficiency on Ly6C^{low} MHC II^{-} monocytes and to ensure that other blood cells were not affected by this deletion, CD3^{+} T cells, CD19^{+} B cells and NKp46^{+} NK cells were analysed. There were no differences detected in the cell frequencies of these populations between *Nr4a1*$^{fl/fl}$, *Nr4a1*$^{+/\Delta}$ and *Nr4a1*$^{\Delta/\Delta}$ littermates (Figure 4-6c).

Extending this analysis to the spleen showed that Ly6C^{low} MHC II^{-} monocytes were reduced in the spleen by 98% in *Nr4a1*$^{\Delta/\Delta}$ mice compared with littermate controls (Figure 4-7a and 4-7b). In contrast, all other spleen myeloid subsets were unaffected, including Ly6C^{+} and Ly6C^{int} MHC II^{+} monocyte subsets, conventional dendritic cell subsets and plasmacytoid dendritic cells (Figure 4-7b and 4-7c).

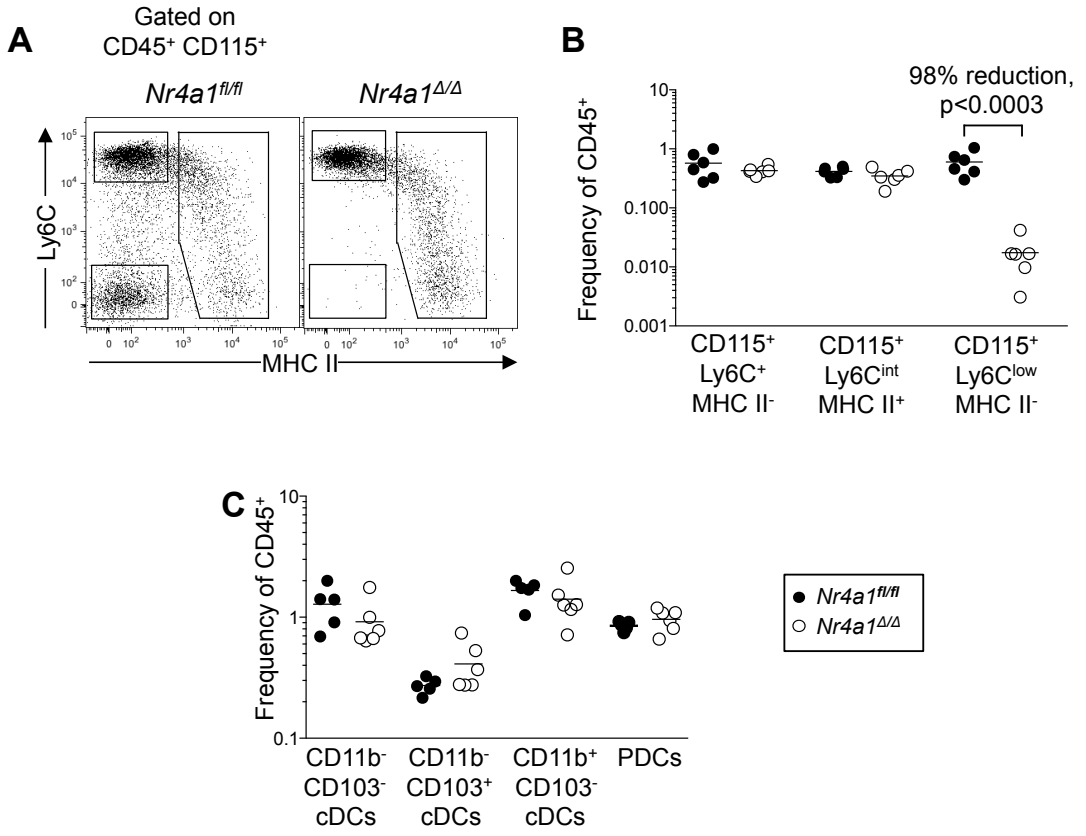

Figure 4-7 Splenic monocytes and DCs in *Csf1r*^{iCre} *Nr4a1*$^{fl/fl}$ mice

(A) Representative dot plots of splenic monocyte populations from *Nr4a1*$^{fl/fl}$ and *Nr4a1*$^{\Delta/\Delta}$ littermates **(B)** Frequency of splenic monocyte subsets among CD45$^+$ cells from *Nr4a1*$^{fl/fl}$ (n=6) and *Nr4a1*$^{\Delta/\Delta}$ (n=6) littermates. **(C)** Frequency of splenic DC subsets amongst CD45$^+$ cells from *Nr4a1*$^{fl/fl}$ (n=5) and *Nr4a1*$^{\Delta/\Delta}$ (n=6) littermates. Symbols represent individual animals. Data analysed using unpaired t-test

Together, these data confirmed and extend, using an independent genetic model, the dependency of Ly6C^{low} MHC II$^-$ monocytes on *Nr4a1* for their development. The use of Ly6C combined with MHC II allows the division of the CD115$^+$ monocyte compartment into three separate subsets, it can be seen that Ly6C^{low} MHC II$^-$ monocytes are almost completely absent in *Nr4a1*$^{\Delta/\Delta}$ and the residual cells that remained in the previous report (Hanna et al., 2011) can be accounted for by the MHC II$^+$ fraction of the monocyte compartment in both the blood and the spleen. In addition, these data

demonstrate strong haploinsufficiency in animals with only one copy of *Nr4a1* (*Nr4a1*$^{+/\Delta}$).

4.5 Bone marrow analysis of *Csf1r*^{iCre} *Nr4a1*$^{fl/fl}$ mice

4.5.1 Bone marrow frequencies of monocytes and their progenitors

The paper by Hanna *et al.,* (Hanna et al., 2011) demonstrated that Ly6C^{low} monocyte development was arrested in the BM. In order to confirm and extend these observations using the *Csf1r*^{iCre} *Nr4a1*$^{fl/fl}$ model, BM monocyte subsets and their progenitors were systematically analysed.

In line with the previously published data (Hanna et al., 2011), within the BM compartment, the MDP (KIT$^+$ CX$_3$CR1$^+$ CD115$^+$ Flt3 (CD135)$^+$ Ly6C$^-$ cells) (Auffray et al., 2009a; Fogg et al., 2006; Liu et al., 2009; Varol et al., 2007) and the cMoP (KIT$^+$ CX$_3$CR1$^+$ CD115$^+$ Flt3 (CD135)$^-$ Ly6C$^+$ cells) (Hettinger et al., 2013) were found in similar numbers in *Nr4a1*$^{\Delta/\Delta}$ and *Nr4a1*$^{+/\Delta}$ when compared with *Nr4a1*$^{fl/fl}$ wild type littermate controls (Figure 4-8a).

Analysis of the KIT$^-$ CD115$^+$ compartment showed that Ly6C$^+$ and Ly6C^{int} MHC II$^+$ BM monocytes were present in in normal numbers in *Nr4a1*$^{\Delta/\Delta}$ and *Nr4a1*$^{+/\Delta}$ when compared with *Nr4a1*$^{fl/fl}$ wild type littermate controls (Figure 4-8b and 4-8c). However, BM Ly6C^{low} MHC II$^-$ monocytes were markedly decreased by 72% in *Nr4a1*$^{+/\Delta}$ (p=0.007) and by 94% in *Nr4a1*$^{\Delta/\Delta}$ (p<0.0001) compared to littermate controls (Figure 4-8b and 4-8c).

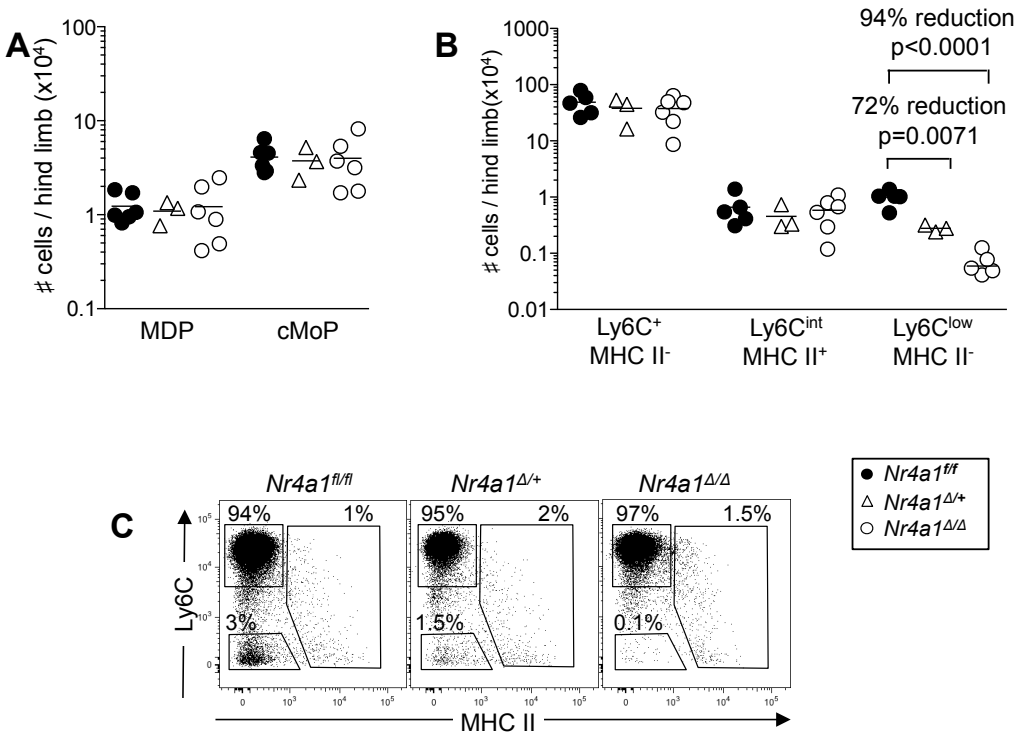

Figure 4-8 Selective loss of BM Ly6C^{low} MHC II^{-} monocytes in *Csf1r^{iCre} Nr4a1$^{fl/fl}$* animals

(**A** and **B**) MDP and cMoP **(A),** and BM monocyte **(B)** cell counts per hind limb from *Nr4a1$^{fl/fl}$* (closed circles, n=5), *Nr4a1$^{fl/Δ}$* (open triangles, n=3) and *Nr4a1$^{Δ/Δ}$* (open circles, n=6). **(C)** Representative dot plots of BM monocyte subsets from *Nr4a1$^{fl/fl}$*, *Nr4a1$^{fl/Δ}$* and *Nr4a1$^{Δ/Δ}$* animals. Symbols represent individual animals. Data analysed using unpaired t-test.

As previously described in Chapter 3, this study had identified a new population of CD11b^{+} CD115^{low} NR4A1^{+} cells within the Ly6C^{low} CD11b^{+} MHC II^{-} CD115^{low} BM compartment, thus the question arose as to whether this population is affected by *Nr4a1* deficiency. Accordingly, the lineage negative, KIT^{-} Ly6C^{low} CD11b^{+} MHC II^{-} CD115^{low} compartment was analysed. In this compartment it can be seen that the CD115^{low} population was decreased in the *Nr4a1$^{+/Δ}$* animals by 44% (p=0.035) and by 67% in *Nr4a1$^{Δ/Δ}$* (p=0.0004) (Figure 4-9), indicating a dependence on *Nr4a1* for their development and/or maintenance.

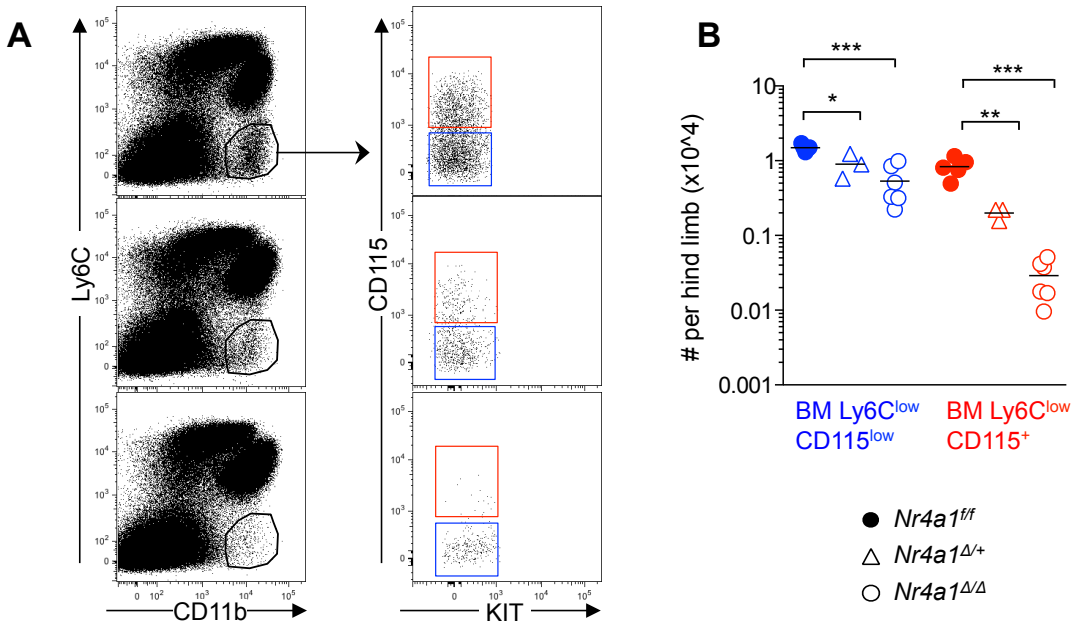

Figure 4-9 *Nr4a1*-deficiency leads to reduction of Ly6C^{low} MHC II^{-} CD11b^{+} CD115^{low} BM cells

(A) Representative dot plots showing Ly6C^{low} MHC II^{-} CD11b^{+} KIT^{-} populations in *Nr4a1*$^{fl/fl}$, *Nr4a1*$^{fl/\Delta}$ and *Nr4a1*$^{\Delta/\Delta}$ animals. **(B)** Number of cells per hind limb of CD11b^{+} CD115^{low} (blue) and BM Ly6C^{low} MHC II^{-} monocytes (red) from *Nr4a1*$^{fl/fl}$ (closed circles, n=5), *Nr4a1*$^{fl/\Delta}$ (open triangles, n=3) and *Nr4a1*$^{\Delta/\Delta}$ (open circles, n=6) animals. Symbols represent individual animals. Statistical significance assessed using unpaired t-test.

These data confirm that BM Ly6C^{low} MHC II^{-} monocytes require *Nr4a1* for their differentiation, in a gene dose dependent manner. In addition, the newly identified CD11b^{+} CD115^{low} population of cells that express high levels of *Nr4a1* were shown to exhibit similar dependency on *Nr4a1* as Ly6C^{low} MHC II^{-} monocytes for their development or survival. Thus, it was hypothesised that *Nr4a1* deficiency may cause a differentiation or maturation blockade within this subset.

4.5.2 Analysis of bone marrow monocytes and progenitors proliferation rates

It was previously reported that *Nr4a1*$^{-/-}$ BM Ly6C^{low} monocytes were unable to progress through cell cycle (Hanna et al., 2011). Consequently, it was important to assess

whether this cell cycle arrest could be seen in *Nr4a1*$^{\Delta/\Delta}$ compared with littermate controls. As shown before, Ki67/DAPI staining was used for cell cycle analysis.

As expected, the MDP and cMoP compartments in the BM were highly actively proliferating with approximately a quarter of both MDP and cMoP populations were in S+G_2M phases of cell cycle in *Nr4a1*$^{\Delta/\Delta}$, *Nr4a1*$^{+/\Delta}$ and wild type littermate controls (Figure 4-10a).

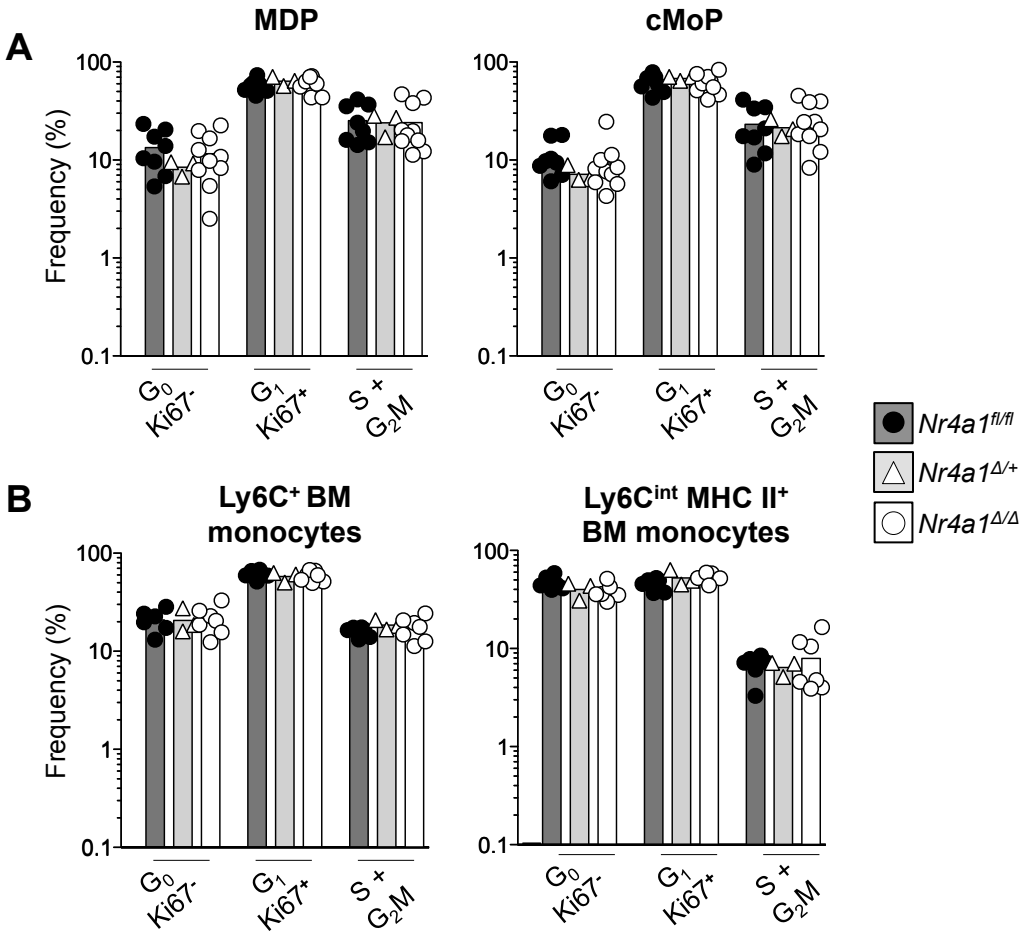

Figure 4-10 Cell cycle analysis of MDP, cMoP and BM LyC-expressing monocytes

(A) Frequency of cells in each cell cycle phase in monocyte progenitors MDP and cMoP. **(B)** Frequency of cells within each phase of cell cycle in BM Ly6C^{+} monocytes and BM Ly6C^{int} MHC II^{+} monocyte subsets from *Nr4a1*$^{fl/fl}$ (dark grey bars, closed circles, n=8), *Nr4a1*$^{fl/\Delta}$ (light grey bars, open triangles, n=3) and *Nr4a1*$^{\Delta/\Delta}$ (white bars, open circles, n=10) littermates. Symbols represent individual animals. Data analysed using unpaired t-test.

Moreover, in line with a previous report BM monocyte populations were also found to be proliferating (Shand et al., 2014). BM monocytes were found to be actively proliferating and no differences in proportion of the population in S+G_2M phases were detected between *Nr4a1*$^{\Delta/\Delta}$, *Nr4a1*$^{+/\Delta}$ and *Nr4a1*$^{fl/fl}$ littermate controls (18.33%, 18.70% and 17.57% respectively) (Figure 4-10b). The Ly6C^{int} MHC II^{+} BM monocyte population was also found to be actively cycling and no differences were detected between genotypes with 6.68% vs. 6.42% vs. 7.91% in S+G_2M phases in *Nr4a1*$^{fl/fl}$, *Nr4a1*$^{+/\Delta}$ and *Nr4a1*$^{\Delta/\Delta}$ respectively (Figure 4-10b).

In contrast, analysis of the cell cycle profile of the CD11b^{+} CD115^{low} population revealed a very small cycling proportion, 3.2% of cells in S+G_2M, in wild type littermates. However, the percentage of cells in S+G_2M doubled to 6.6% in *Nr4a1*$^{\Delta/+}$ and increased further to 19.5% in *Nr4a1*$^{\Delta/\Delta}$ animals (Figure 4-11a).

In addition, a negligible 0.8% of Ly6C^{low} MHC II^{-} BM monocytes were actively proliferating in wild type animals, which increased to 27% in the few remaining cells in *Nr4a1*$^{\Delta/\Delta}$ animals (Figure 4-11b). These data confirm the previous reports that BM monocytes are actively proliferating (Shand et al., 2014) and demonstrate that this proliferation is mostly attributable to Ly6C^{+} BM monocytes in wild type mice. However, in the absence of *Nr4a1* Ly6C^{low} MHC II^{-} monocytes exhibit increased proliferation (Figure 4-11b) confirming previously published data (Hanna et al., 2011). Nevertheless, it is clear from this genetic analysis and from the data presented in Chapter 3 that the vast majority of BM Ly6C^{low} MHC II^{-} monocytes do not actively proliferate wild type animals.

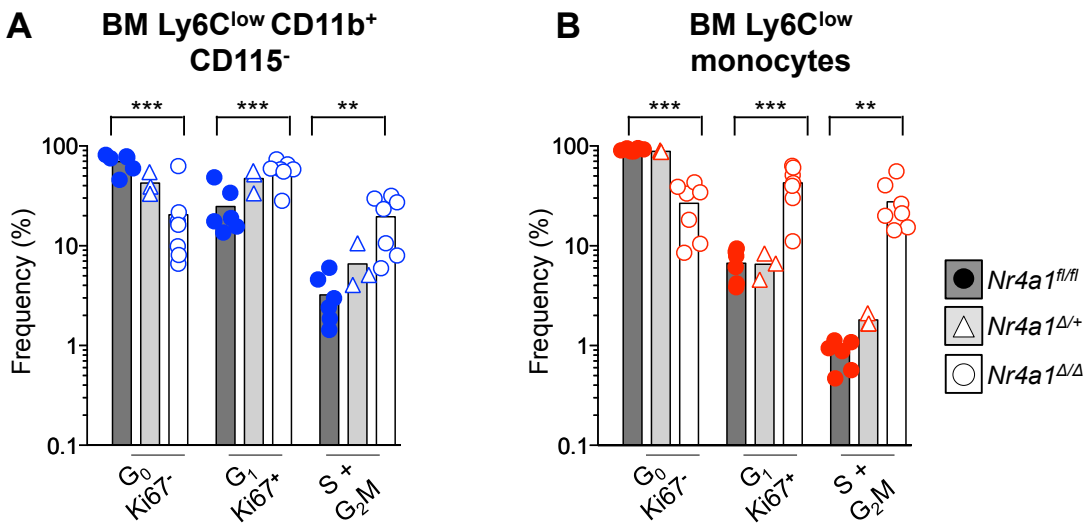

Figure 4-11 Cell cycle analysis within the Ly6C^{low} MHC II^{-} CD11b^{+} BM compartment in *Csf1r^{iCre} Nr4a1$^{fl/fl}$* animals

(A) CD11b^{+} CD115^{low} population cell cycle analysis. **(B)** Cell cycle analysis of Ly6C^{low} MHC II^{-} BM monocytes from *Nr4a1$^{fl/fl}$* (dark grey bars, closed circles, n=6), *Nr4a1$^{fl/\Delta}$* (light grey bars, open triangles, n=3) and *Nr4a1$^{\Delta/\Delta}$* (white bars, open circles, n=7) littermates. Symbols represent individual animals. Statistical significance assessed using unpaired t-test.

Thus, these data indicate that *Nr4a1* deficiency is associated with increased proliferation in both Ly6C^{low} CD11b^{+} CD115^{low} cells and Ly6C^{low} MHC II^{-} monocyte BM populations (Figure 4-10a and b). Interestingly, the Ly6C^{low} CD11b^{+} CD115^{low} population showed a slow turn over which drastically increase in *Nr4a1$^{\Delta/\Delta}$* mice, indicating a possible role as an intermediate population for *Nr4a1*-dependent Ly6C^{low} monocytes.

4.5.3 Kinetic analysis of monocytes and their progenitors in *Csf1r^{iCre} Nr4a1$^{\Delta/\Delta}$* mice and littermates

To confirm the increased proliferation of Ly6C^{low} MHC II^{-} monocytes in *Nr4a1$^{\Delta/\Delta}$* compared to their littermate controls and to gain insight into monocyte interrelationships in the absence of *Nr4a1,* the same BrdU pulse-chase methodology detailed in Chapter 3 was employed to complement the snapshot insight that Ki67/DAPI analysis provided with a time course analysis. *Nr4a1$^{fl/fl}$* and *Nr4a1$^{\Delta/\Delta}$* littermates were

injected with 1.5mg of BrdU and blood and BM were analysed at regular time points. In accordance with the cell cycle analysis, incorporation of BrdU in wild type littermate controls and *Nr4a1*$^{\Delta/\Delta}$ was identical in MDP, cMoP, BM Ly6C^{+} and BM Ly6C^{int} MHC II^{+} subsets (Figure 4-12a).

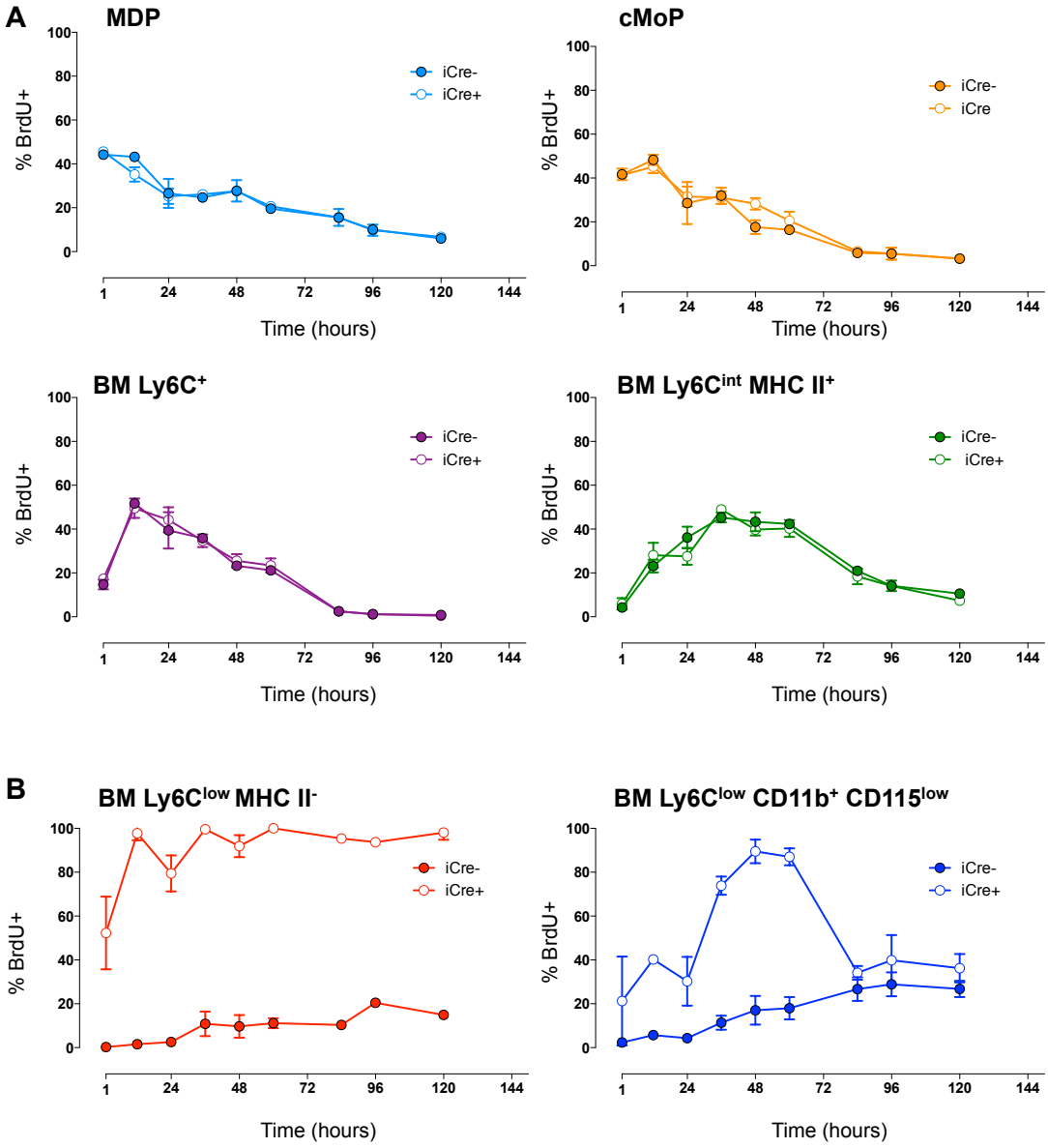

Figure 4-12 BrdU incorporation in BM from *Nr4a1*$^{fl/fl}$ and *Nr4a1*$^{\Delta/\Delta}$ mice

(A) Percentage of BrdU^{+} cells in MDP, cMoP, Ly6C^{+} and Ly6C^{int} BM monocyte compartments over time from *Nr4a1*$^{fl/fl}$ (closed circles) and *Nr4a1*$^{\Delta/\Delta}$ (open circles) animals. **(B)** Frequency of BrdU^{+} cells in BM Ly6C^{low} MHC II^{-} monocytes and BM Ly6C^{low} MHC II^{-} CD11b^{+} CD115^{low} cells from *Nr4a1*$^{fl/fl}$ (closed circles) and *Nr4a1*$^{\Delta/\Delta}$ (open circles) animals. n=3 per genotype per time point, error bars represent SD.

In contrast, the few remaining Ly6C^{low} MHC II^{-} BM monocytes in the *Nr4a1*$^{\Delta/\Delta}$ animals rapidly labelled – 80% BrdU^{+} Ly6C^{low} MHC II^{-} monocytes were detected at 48 hours compared to 10% labelling in wild type animals at the same time point (Figure 4-12b). Similarly, incorporation by CD115^{low} was increased four fold at 48 hours in *Nr4a1*$^{\Delta/\Delta}$ compared with littermate controls (80% versus 20%).

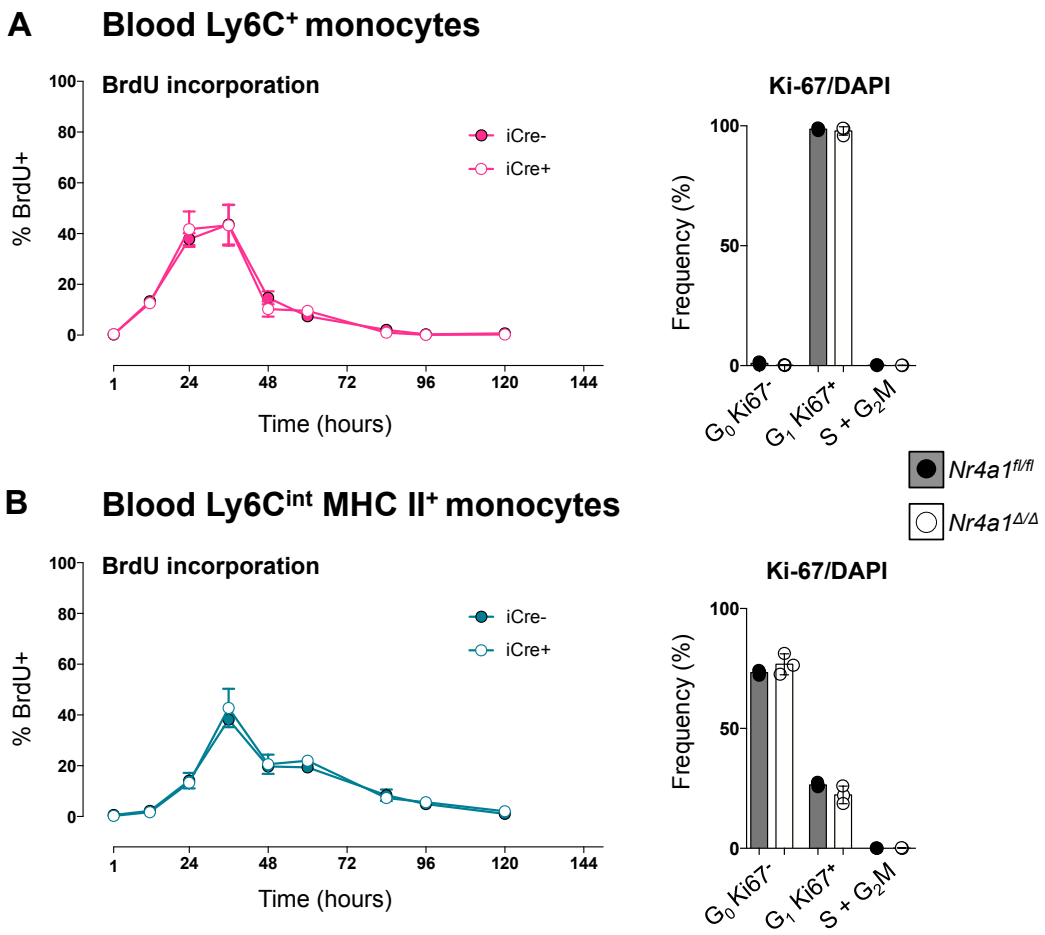

Figure 4-13 Blood monocyte BrdU labelling

(A) Frequency of BrdU^{+} Ly6C^{+} blood monocytes (left, n=3 mice per time point, error bars represent SD) and Ki-67/DAPI cell cycle analysis of Ly6C^{+} blood monocytes (right) from *Nr4a1*$^{fl/fl}$ (closed circles, n=3) and *Nr4a1*$^{\Delta/\Delta}$ (open circles, n=3) littermates. **(B)** Frequency of BrdU^{+} Ly6C^{int} MHC II^{+} blood monocytes (left, n=3 mice per time point, error bars represent SD) and Ki-67/DAPI cell cycle analysis of Ly6C^{int} MHC II^{+} blood monocytes (right) from *Nr4a1*$^{fl/fl}$ (closed circles, n=3) and *Nr4a1*$^{\Delta/\Delta}$ (open circles, n=3) littermates.

Blood Ly6C^{+} monocytes are widely regarded as the obligate precursor to blood Ly6C^{low} monocytes (Sunderkotter et al., 2004; Varol et al., 2007; Yona et al., 2013),

furthermore, it has been suggested that blood and BM Ly6C^{low} MHC II^{-} monocyte compartments develop and are maintained independently of each other (Yona et al., 2013). In light of these hypotheses it was reasoned that, in *Nr4a1*$^{\Delta/\Delta}$ animals where the development of Ly6C^{low} MHC II^{-} monocytes is defective in both the blood and the BM, there should be some perturbation in blood monocyte BrdU incorporation and/or cell cycle profile in *Nr4a1*$^{\Delta/\Delta}$ compared to littermate controls. Thus, the blood from *Nr4a1*$^{\Delta/\Delta}$ and littermate controls was analysed to assess BrdU incorporation and to assess Ki67/DAPI profile. It is not possible to compare Ly6C^{low} MHC II^{-} blood monocytes from *Nr4a1*$^{\Delta/\Delta}$ mice compared to littermates due to the absence of these cells in this model. However, Ly6C^{+} (Figure 4-13a) and Ly6C^{int} MHC II^{+} (Figure 4-13b) were analysed. No differences in BrdU incorporation were observed between *Nr4a1*$^{\Delta/\Delta}$ mice and littermates indicating that BrdU^{+} Ly6C^{+} monocytes do not accumulate in the blood because they are unable to differentiate into blood Ly6C^{low} MHC II^{-} monocytes.

Furthermore, no differences in Ki-67/DAPI profile were observed in *Nr4a1*$^{\Delta/\Delta}$ animals compared to littermate controls. Whilst it has already been noted that blood monocytes do not proliferate under homeostatic condition (Figure 3-7), this demonstrates that *Nr4a1*-deficiency does not induce Ly6C^{+} (or Ly6C^{int} MHC II^{+}) blood monocytes to proliferate (Figure 4-13a).

These data demonstrate that BrdU incorporation in the MDP, cMoP, and both BM and blood Ly6C^{+} and Ly6C^{int} MHC II^{+} monocytes are unaffected by *Nr4a1*-deficiency. The differentiation block that prevents the development of Ly6C^{low} MHC II^{-} monocytes appears to be within the Ly6C^{low} MHC II^{-} CD11b^{+} CD115^{low} compartment. The cells within this compartment of *Nr4a1*-deficient animals are more actively cycling, as confirmed by two independent methodologies, but maturation of Ly6C^{low} MHC II^{-} monocytes is blocked. Thus, it was reasoned that there must be increased apoptosis

within the Ly6C^{low} MHC II^{-} CD11b^{+} CD115^{low} compartment, otherwise an accumulation of cells would be observed. This reasoning prompted analysis of apoptotic particles within this compartment, defined as sub-2N (Pozarowski and Darzynkiewicz, 2004). Within the BrdU incorporation experiment, cells were stained with the nuclear dye 7AAD, which allows the measurement of DNA content. Ly6C^{low} MHC II^{-} CD11b^{+} CD115^{low} cells were analysed for the proportion of events that were BrdU^{+} and sub-2N, as a measure of BrdU-labelled, apoptotic fragments during early time points (Figure 4-14).

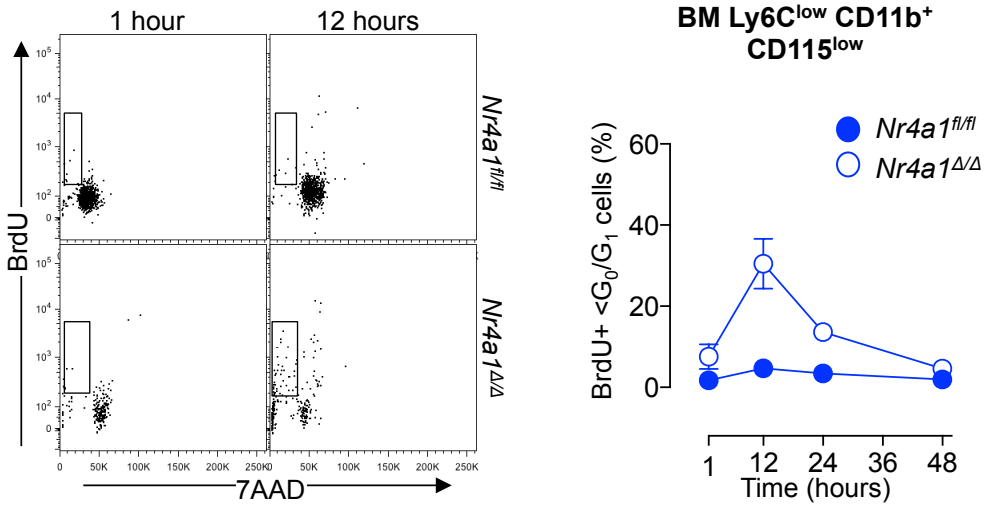

Figure 4-14 Measurement of apoptotic events in Ly6C^{low} MHC II^{-} CD11b^{+} CD115^{low} compartment

Linear acquisition of 7AAD allows quantification of apoptotic particles defined as sub-2N (left) and quantification of frequency of BrdU^{+} sub-2N particles from *Nr4a1*$^{fl/fl}$ (closed circles, n=3 mice per time point) and *Nr4a1*$^{\Delta/\Delta}$ (open circles, n=3 mice per time point). Error bars represent SD.

Within the Ly6C^{low} MHC II^{-} CD11b^{+} CD115^{low} population there were considerably increased frequencies of BrdU^{+} sub-2N events in *Nr4a1*$^{\Delta/\Delta}$ animals compared with littermate controls at 12 hours post-BrdU administration, demonstrating an increase in BrdU-labelled apoptotic particles within this compartment at this time (Figure 4-14).

Altogether, these data can be interpreted as an absolute requirement of *Nr4a1* for Ly6C^{low} MHC II^{-} monocyte maturation. Further, these data suggest that cells from *Nr4a1*-deficient mice undergo apoptosis within the BM during a maturation step from a Ly6C^{low} MHC II^{-} CD11b^{+} CD115^{low} NR4A1^{+} intermediate into BM Ly6C^{low} MHC II^{-} CD115^{+} monocytes. Finally, these data indicate that blood Ly6C^{low} MHC II^{-} monocytes are generated in the BM and not in the blood, as has previously been suggested and blood Ly6C^{low} MHC II^{-} monocytes do not seem to be derived from blood Ly6C^{+} or Ly6C^{int} MHC II^{+} monocytes in the blood.

4.6 *Nr4a1^{GFP} Nr4a1$^{-/-}$* mice analysis

4.6.1 Rationale for creating double mutants

One difficulty in analysing Ly6C^{low} MHC II^{-} monocytes is the lack of specific, positive marker for which there is a good and reliable antibody. However, Ly6C^{low} MHC II^{-} monocytes express very high levels of NR4A1^{GFP}, considerably higher than other cell types (Figures 3-2, 3-4 and 4-2). Furthermore, this reporter strain was made by microinjection of a BAC (Moran et al., 2011) rather than being a knock-in (in which one copy of GFP allele replaces an endogenous allele for the gene of interest). This fact made it possible to cross *Nr4a1^{GFP}* animals with *Nr4a1*-null animals (Lee et al., 1995) to generate double mutants: *Nr4a1^{GFP} Nr4a1$^{-/-}$* animals as well as *Nr4a1^{GFP} Nr4a1$^{+/-}$* and *Nr4a1^{GFP} Nr4a1$^{+/+}$* controls. Thus, this model provided a tool to analyse BM and blood monocytes whilst using NR4A1^{GFP} as a positive marker for Ly6C^{low} MHC II^{-} monocytes and combined with the ability to assess developmental dependency on *Nr4a1*.

4.6.2 Bone marrow analysis of *Nr4a1^{GFP} Nr4a1$^{-/-}$* animals

As expected, analysis of the BM Ly6C^{low} MHC II^{-} CD11b^{+} compartment in *Nr4a1^{GFP} Nr4a1$^{+/+}$*, *Nr4a1^{GFP} Nr4a1$^{+/-}$* and *Nr4a1^{GFP} Nr4a1$^{-/-}$* animals shows that the CD115^{+} Ly6C^{low} MHC II^{-} BM monocytes are significantly reduced in the heterozygous animals compared with wild type and almost completely absent from *Nr4a1^{GFP} Nr4a1$^{-/-}$* littermates (Figure 4-15).

Interestingly, the CD115^{low} NR4A1^{bright} cells are also reduced in the same manner, indeed the ratio of CD115^{+} cells to CD115^{low} cells remains consistent at approximately 70%:30% in heterozygous animals and wild type littermate controls, although the overall number of cells in heterozygous animals is significantly reduced (by 93%) when there is only one copy of endogenous *Nr4a1* (Figure 4-15).

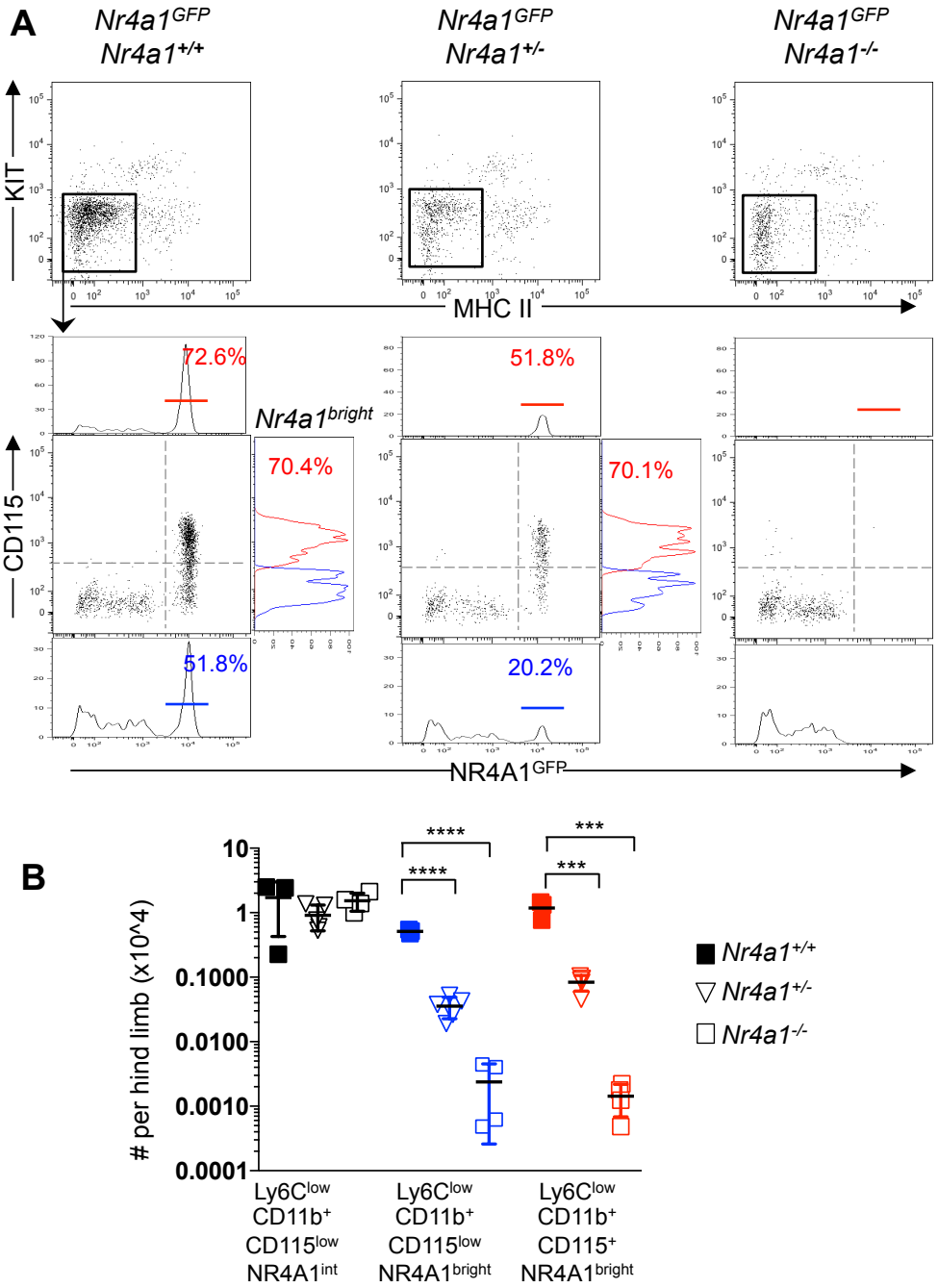

Figure 4-15 Analysis of Ly6C^{low} MHC II^{-} CD11b^{+} compartment of *Nr4a1^{GFP} Nr4a1$^{-/-}$* animals and littermate controls.

(A) Dot plot and histogram representations of *Nr4a1^{GFP}* and CD115 expression in CD45^{+} Lin^{-} Ly6C^{low} MHC II^{-} CD11b^{+} BM cells from *Nr4a1^{GFP} Nr4a1$^{+/+}$*, *Nr4a1^{GFP} Nr4a1$^{+/-}$*, *Nr4a1^{GFP} Nr4a1$^{-/-}$* littermates. **(B)** Quantified as absolute cell counts/hind limb BM from *Nr4a1^{GFP} Nr4a1$^{+/+}$* (closed squares, n=3), *Nr4a1^{GFP} Nr4a1$^{+/-}$* (open triangles, n=4), *Nr4a1^{GFP} Nr4a1$^{-/-}$* (open squares, n=4) littermates. Error bars represent SD, statistical significance determined using unpaired t-test.

This model allows the separation of Ly6C^{low} MHC II^{-} CD11b^{+} CD115^{low} NR4A1^{int} from of Ly6C^{low} MHC II^{-} CD11b^{+} CD115^{low} NR4A1^{bright}, providing a means to dissect *Nr4a1*-dependency within this compartment. The NR4A1^{int} cells did not vary between *Nr4a1*^{GFP} *Nr4a1*$^{+/+}$, *Nr4a1*^{GFP} *Nr4a1*$^{+/-}$ and *Nr4a1*^{GFP} *Nr4a1*$^{-/-}$ littermates (Figure 4-15) and therefore can develop independently of NR4A1. This suggests that Ly6C^{low} MHC II^{-} CD11b^{+} CD115^{low} NR4A1^{int} cells are not related to Ly6C^{low} MHC II^{-} monocytes.

This model has confirmed that the CD115^{low} NR4A1^{bright} BM population identified in this study behave in an identical manner to Ly6C^{low} MHC II^{-} BM monocytes with regards to *Nr4a1*, both in terms of dependency and high level of expression of NR4A1^{GFP} reporter. Taken together in conjunction with the apoptosis analysis (Figure 4-14), the few remaining GFP^{bright} cells that are found in the Ly6C^{low} MHC II^{-} CD11b^{+} compartment of *Nr4a1*$^{\Delta/\Delta}$ animals undergo apoptosis.

Altogether these data provide a genetic basis, from two independent models, for the hypothesis that the Ly6C^{low} MHC II^{-} monocyte maturation occurs in the BM and requires the transition through a CD115^{low} *Nr4a1*-dependent intermediate before surface expression of CD115 is upregulated. Thus, it was important to demonstrate that the Ly6C^{low} MHC II^{-} CD11b^{+} CD115^{low} cells are capable of upregulating CD115.

4.6.3 *In vitro* culture

In order to assess whether the NR4A1^{bright} CD11b^{+} CD115^{low} population is capable of upregulating cell surface expression of CD115, this study resorted to an *in vitro* culture system. Ly6C^{low} MHC II^{-} CD11b^{+} NR4A1^{int} CD115^{low} and Ly6C^{low} MHC II^{-} CD11b^{+} NR4A1^{bright} CD115^{low} populations from NR4A1^{GFP} (CD45.2 background) animals were FACS sorted. The sorted cells were cultured with unfractionated "feeder" BM cells from CD45.1 animals so that no cytokine was artificially added.

In the Ly6C^{low} MHC II^{-} CD11b^{+} NR4A1^{int} CD115^{low} population (black circles, Figure 4-16), expression of both CD115 and GFP remained at baseline low levels (Figure 4-16). In contrast, Ly6C^{low} MHC II^{-} CD11b^{+} NR4A1^{bright} CD115^{low} population (blue circles, Figure 4-16) had upregulated CD115 expression by 12 hours and by 48 hours in culture the whole population was CD115^{+}, and importantly remained NR4A1^{bright} throughout the experiment (Figure 4-16).

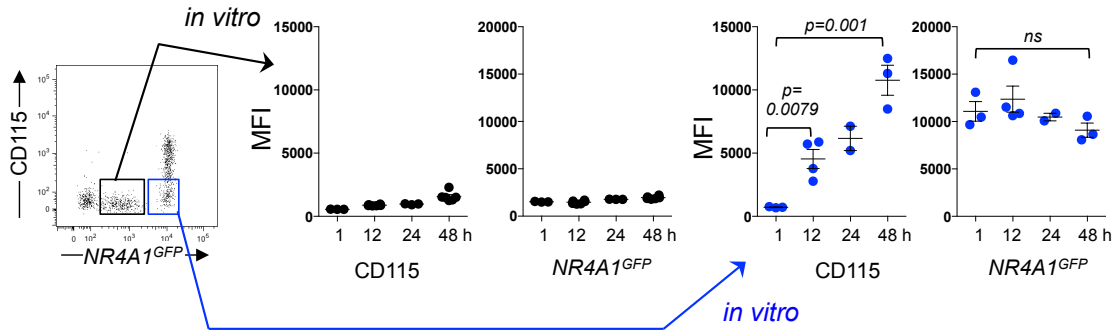

Figure 4-16 *in vitro* culture of CD115^{low} NR4A1^{GFP} populations.

Geometric mean fluorescence intensity of CD115 and NR4A1^{GFP} of sorted Ly6C^{low} MHC II^{-} CD11b^{+} CD115^{low} NR4A1^{int} (black) and NR4A1^{birght} (blue) populations after in vitro culture for 1, 12, 24 or 48 hours. Representative of two independent experiments, n=3 mice per experiment. Symbols represent average of duplicate wells; error bars represent SD. Statistical significance analysed using unpaired t-test.

This *in vitro* culture experiment provides evidence that Ly6C^{low} CD11b^{+} NR4A1^{bright} CD115^{low} cells have the capacity to upregulate CD115 to the cell surface *in vitro* whereas the NR4A1^{int} CD115^{low} population do not.

Altogether, these data indicate that the development of Ly6C^{low} CD11b^{+} NR4A1^{int} CD115^{low} cells is not affected by *Nr4a1*-deficiency nor can it upregulate NR4A1 or CD115 expression in this *in vitro* system. Thus making it unlikely that this population contributes to Ly6C^{low} MHC II^{-} monocyte development. On the contrary, the NR4A1^{bright} CD115^{low} population shows the same developmental dependency on *Nr4a1*

as Ly6C^{low} MHC II^{-} monocytes and upregulates CD115 expression, thus becoming phenotypically identical to a *bona fide* Ly6C^{low} MHC II^{-} monocyte in this *in vitro* system.

Collectively, the *in vitro* data combined with the *in vivo* genetic dependency of this population on NR4A1, establish Ly6C^{low} CD11b^{+} NR4A1^{bright} CD115^{low} cells as a novel BM intermediate in the Ly6C^{low} MHC II^{-} monocyte development pathway.

4.7 The effects of *Ccr2*- and *Irf8*- deficiency on Ly6C^{low} monocytes

4.7.1 *Ccr2*-deficency and Ly6C^{low} MHC II^{-} monocytes

4.7.1.1 Phenotypic analysis of CCR2$^{-/-}$ mice

The requirement of Ly6C^{+} monocytes on CCR2 receptor signalling for their BM egress has been well documented (Serbina et al., 2008; Serbina and Pamer, 2006), whereas the effect of *Ccr2*-deficiency on Ly6C^{low} monocytes is less well defined. Thus, *Ccr2*$^{-/-}$ animals and littermate controls were analysed to evaluate the effect of *Ccr2*-deficiency on both Ly6C^{low} MHC II^{-} and Ly6C^{int} MHC II^{+} monocyte subsets.

As expected, Ly6C^{+} monocytes were dramatically reduced in the blood of *Ccr2*$^{-/-}$ mice by 73% (Figure 4-17a). Interestingly, Ly6C^{int} MHC II^{+} monocytes were also reduced, by 51%, in the blood of *Ccr2*$^{-/-}$ mice and this may indicate that they also require CCR2 signalling to egress from the BM. In contrast, blood Ly6C^{low} MHC II^{-} monocytes were not significantly affected by *Ccr2*-deficiency (Figure 4-17a).

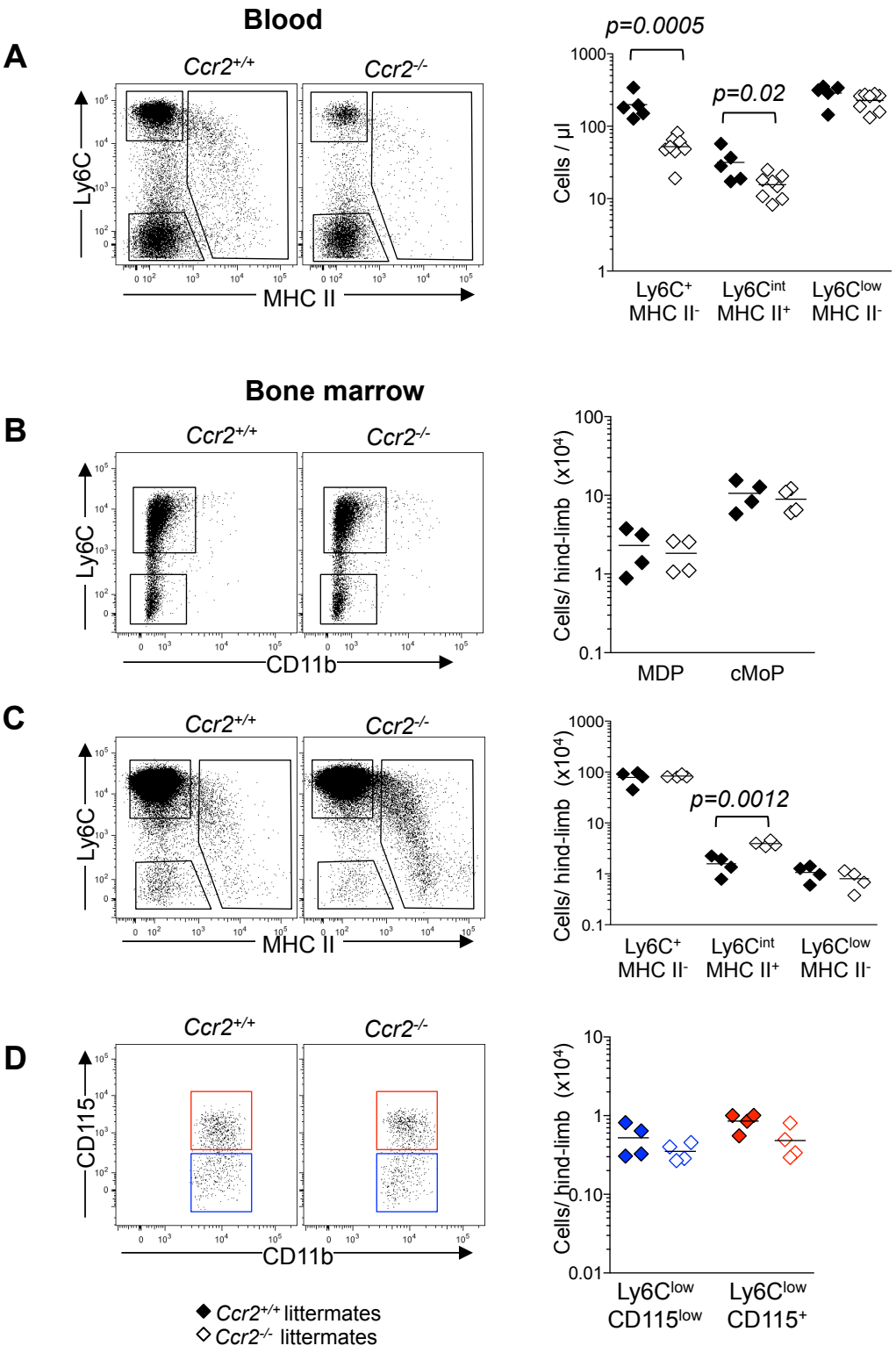

Figure 4-17 CCR2-deficiency in blood and BM monocyte subsets.

(A) Effect of CCR2-deficiency on blood monocyte subsets, closed diamond represent *Ccr2*$^{+/+}$(n=5); open diamonds represent *Ccr2*$^{-/-}$ (n=8) littermates. (**B-D**) BM analysis from *Ccr2*$^{+/+}$ (closed diamonds, n=4) and *Ccr2*$^{-/-}$ (open diamonds, n=4) littermates showing MDP and cMoP **(B)**; BM monocyte subsets **(C);** and BM Ly6C^{low} MHC II^{-} CD11b^{+} CD115^{low} (blue) and BM Ly6C^{low} MHC II^{-} monocytes (red) **(D)**. Symbols represent individual animals. Statistical significance analysed using unpaired t-test.

Additionally, MDP and cMoP populations were unaffected by *Ccr2*-deficiency (Figure 4-17b). Moreover, BM Ly6C^{+} monocytes were only slightly, and not significantly, increased in *Ccr2*-deficient animals as expected for steady state conditions (Tsou et al., 2007). Interestingly, the Ly6C^{int} MHC II^{+} BM monocyte subset showed significant accumulation under steady state conditions in the BM (Figure 4-17b), suggesting that Ly6C^{int} MHC II^{+} also require CCR2 signalling for their BM egress and that this population could represent a differentiation/maturation of Ly6C^{+} monocytes. Consistent with their blood phenotype, BM Ly6C^{low} MHC II^{-} monocytes were also unaltered in *Ccr2*-deficient animals (Figure 4-17c).

4.7.1.2 BrdU incorporation by Ccr2-deficient mice and littermates

Blocking of CCR2 with the antibody MC21, ablates blood Ly6C^{+} monocytes (Bruhl et al., 2007) but not BM Ly6C^{+} monocytes (Yona et al., 2013). It was demonstrated that administration of MC21 reduces BrdU labelling of blood Ly6C^{low} monocytes, thought to be due to the ablation of blood BrdU-labelled, *Ccr2*-expressing Ly6C^{+} monocytes (Yona et al., 2013). BM Ly6C^{+} monocytes are unaffected by MC21 and it was observed that BrdU labelling in the BM compartment was unaffected by MC21 treatment in either Ly6C^{+} or Ly6C^{low} monocyte subsets (Yona et al., 2013). However, the identification of a third monocyte subset with similar a requirement for CCR2-signalling to mediate it's BM egress as classical Ly6C^{+} monocytes prompted the reassessment of precursor-product relationships using BrdU incorporation in the context of CCR2 deficiency. As a consequence of the variability of Ly6C expression with the MHC II^{+} monocyte population, a proportion of these cells will fall into the gating of Ly6C^{low} monocytes when MHC II is not used as a marker, and be included in the analysis of Ly6C^{low} monocytes. Thus, the separation out of the MHC II^{+} cells can

provide new insights into the precursor-product relationships between monocyte subsets.

It was hypothesised that analysis of BrdU incorporation into monocyte subsets from *Ccr2*$^{-/-}$ animals and littermate controls should demonstrate whether Ly6C^{+} blood monocytes are the obligate precursor of *Nr4a1*-dependent Ly6C^{low} MHC II^{-} monocytes. If blood Ly6C^{low} MHC II^{-} monocytes arise from blood Ly6C^{+} monocytes, it was hypothesised that there would be a delay in blood Ly6C^{low} MHC II^{-} monocyte BrdU labelling to reflect considerably reduced Ly6C^{+} blood monocyte population. In contrast, BM labelling should be unaffected.

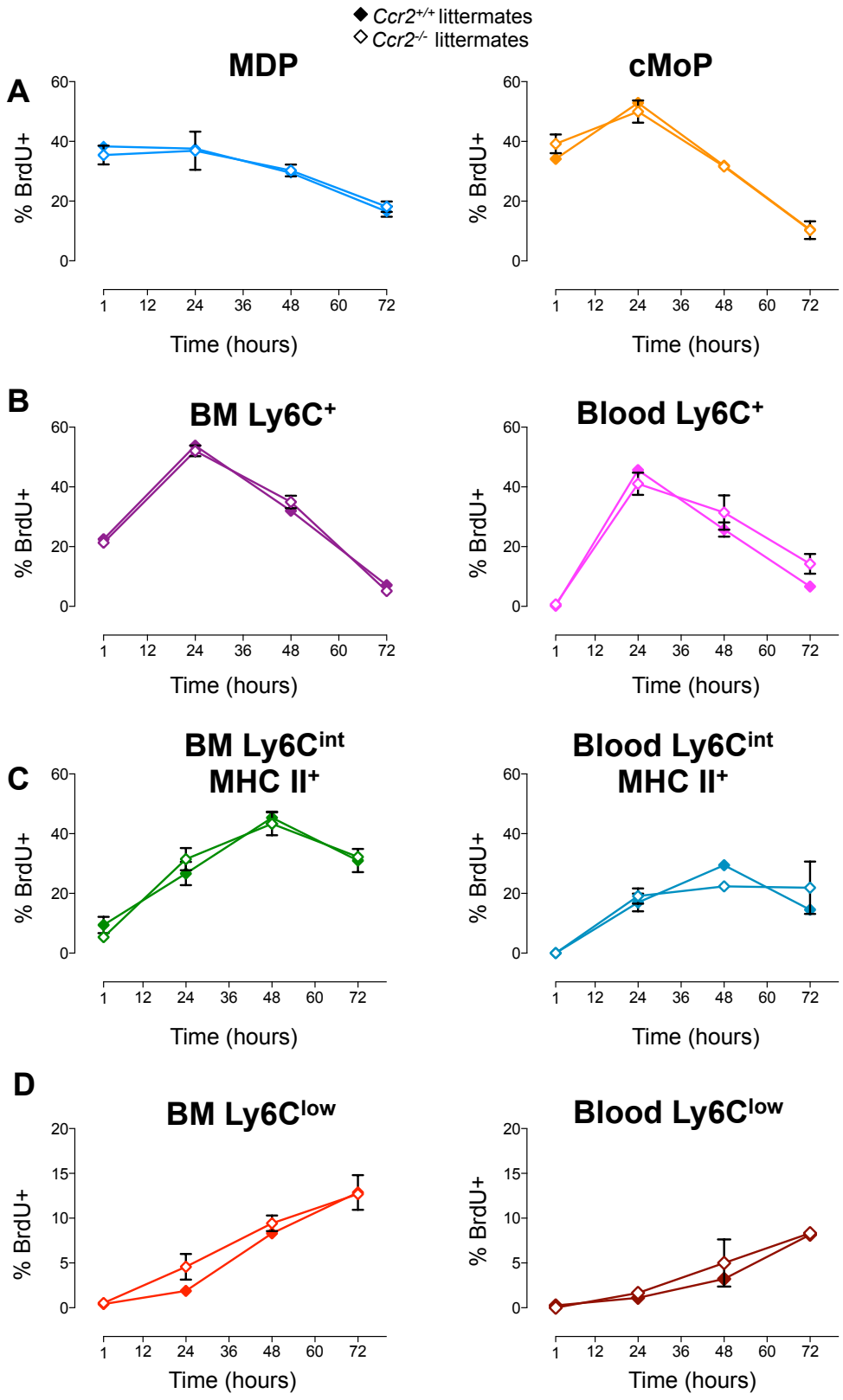

Figure 4-18 BrdU incorporation in *Ccr2*$^{-/-}$ animals and littermate controls.

(A-D) Frequency of BrdU^{+} monocytes and progenitors from *Ccr2*$^{+/+}$ animals (closed diamonds) and *Ccr2*$^{-/-}$ (open diamonds) littermates in **(A)** MDP and cMoP; **(B)** BM (left) and blood (right) Ly6C^{+} monocytes; **(C)** BM (left) and blood (right) Ly6C^{int} MHC II^{+} monocytes; **(D)** BM (left) and blood (right) Ly6C^{low} MHC II^{-} monocytes, n=3 mice per time point, error bars represent SD. Statistical significance assessed by unpaired t-test.

There were no differences observed in BrdU labelling between *Ccr2*$^{+/+}$ and *Ccr2*$^{-/-}$ littermates in the MDP and cMoP (Figure 4-18a), BM and blood Ly6C^{+} monocytes (Figure 4-18b), BM and blood Ly6C^{int} MHC II^{+} monocytes (Figure 4-18c) or BM and blood Ly6C^{low} MHC II^{-} monocytes. Indeed, Figure 4-18 demonstrates that, despite the reduction of Ly6C^{+} and Ly6C^{int} MHC II^{+} monocytes in the blood of *Ccr2*-deficient mice, the same proportion of each population is BrdU-labelled in *Ccr2*$^{-/-}$ animals as in wild type animals. These data fit with the notion that *Ccr2*-deficiency is an impairment of Ly6C^{+} monocyte mobilisation rather than an inherent developmental impairment.

Furthermore, Ly6C^{low} MHC II^{-} monocyte BrdU incorporation in the blood and BM was unaffected by *Ccr2*-deficiency and the predicted delay in Ly6C^{low} MHC II^{-} blood monocyte labelling was not observed. These data further support the contention that Ly6C^{low} MHC II^{-} monocytes develop in the BM and that their development is independent of blood Ly6C^{+} monocytes. However, as is demonstrated in Figure 4-17a, a small proportion of Ly6C^{+} monocytes do egress from the BM to the blood in *Ccr2*-deficient mice, thus an alternative interpretation of these results could be that these *Ccr2*-independent Ly6C^{+} monocytes give rise to blood Ly6C^{low} MHC II^{-} monocytes. To investigate these two possibilities further, characterisation of blood and BM monocyte subsets in *Irf8*-deficient animals was carried out.

4.7.2 *Irf8*-deficiency and Ly6C^{low} MHC II^{-} monocytes

It has been reported that *Irf8*$^{-/-}$ animals lack Ly6C^{+} monocytes while Ly6C^{low} MHC II^{-} monocytes remain, albeit at a lower frequency (Kurotaki et al., 2013). In light of the increased heterogeneity within the monocyte compartment established in this thesis, it was hypothesised that the reported reduction in Ly6C^{low} MHC II^{-} monocytes was due to a reduction in Ly6C^{int} MHC II^{+} monocytes.

Analysis of blood monocyte subsets from *Irf8*-deficient mice and wild type controls revealed that blood Ly6C^{low} MHC II^{-} monocytes were found at normal frequencies, unaffected by this deficiency (Figure 4-19a). In contrast, Ly6C^{+} were almost completely absent in the blood of *Irf8*$^{-/-}$ animals. Furthermore, Ly6C^{int} MHC II^{+} monocytes were also significantly decreased (Figure 4-19a).

Interestingly, the BM CD115^{+} KIT^{+} compartment, containing the MDP and the cMoP populations was greatly expanded (Figure 4-19b). This was in stark contrast to the BM CD115^{+} KIT^{-} compartment containing BM monocytes, which was dramatically reduced. This reduction was attributable to Ly6C^{+} BM monocytes, which were reduced by 95%. This suggests a differentiation block in the monocyte development pathway at the point of MDP/cMoP. Whilst it has previously been described that *Irf8* is critical for monocyte development (Kurotaki et al., 2013), these data identify the point at which *Irf8* is critical for Ly6C^{+} monocyte development.

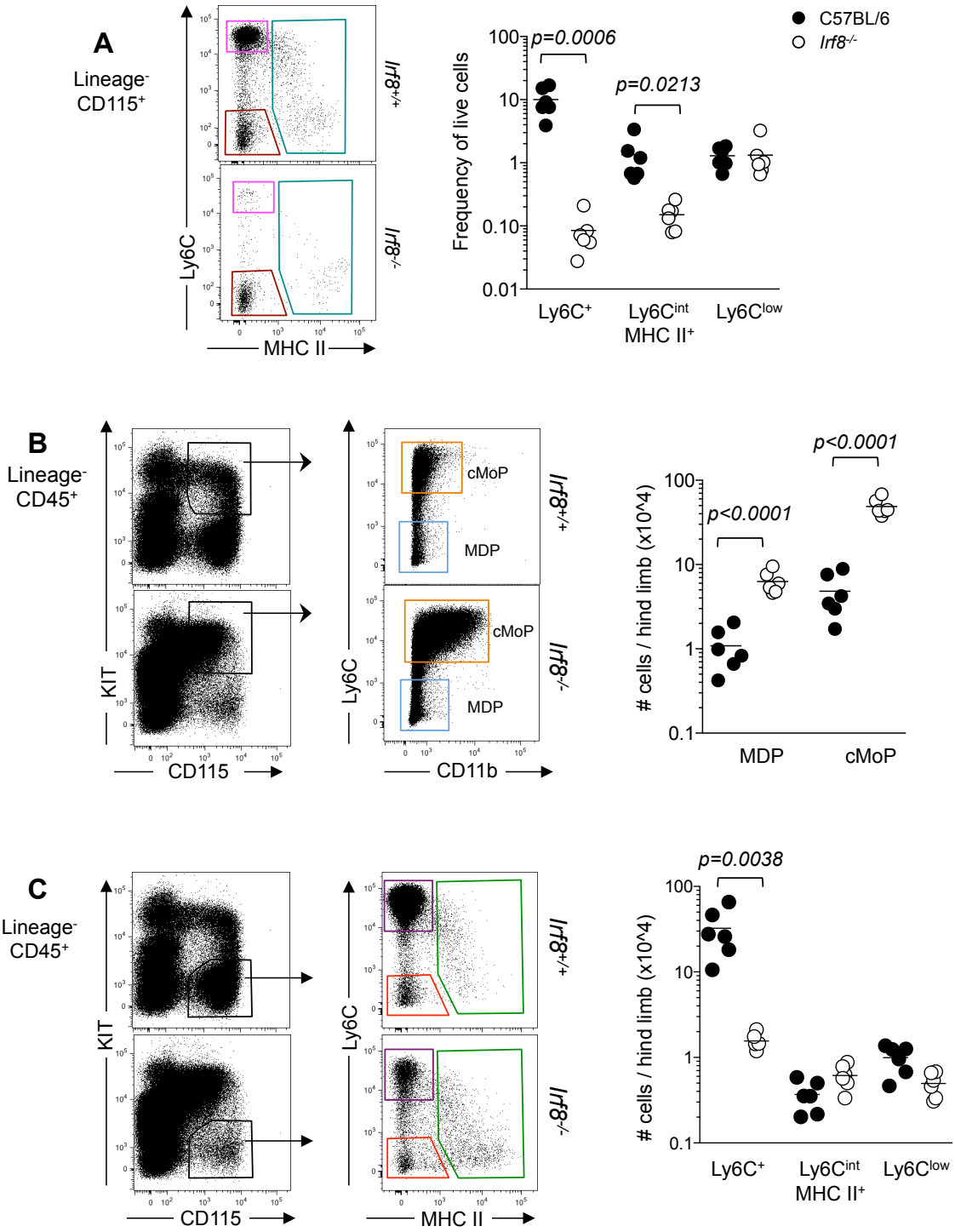

Figure 4-19 *Irf8*-deficiency in blood and BM monocytes and BM progenitors.

(A) Representative dot plots and quantification of blood monocyte frequency from C57BL/6 (closed circles, n=6) and *Irf8*$^{-/-}$ (open circles, n=6) animals. (**B-C**) Representative dot plots and quantification of BM cells per hind limb from C57BL/6 (closed circles, n=6) and *Irf8*$^{-/-}$ (open circles, n=6) animals of MDP and cMoP **(B)** and BM monocyte subsets **(C)**. Statistical significance was determined by unpaired t-test.

In contrast, Ly6C^{low} MHC II^{-} BM monocytes were unaffected by *Irf8* deficiency (Figure 4-19c and Figure 4-20), nor were CD11b^{+} CD115^{low} cells (Figure 4-20). Thus, confirming Ly6C^{low} MHC II^{-} monocytes and their proposed intermediate, the CD11b^{+} CD115^{low} population, develop independently of IRF8.

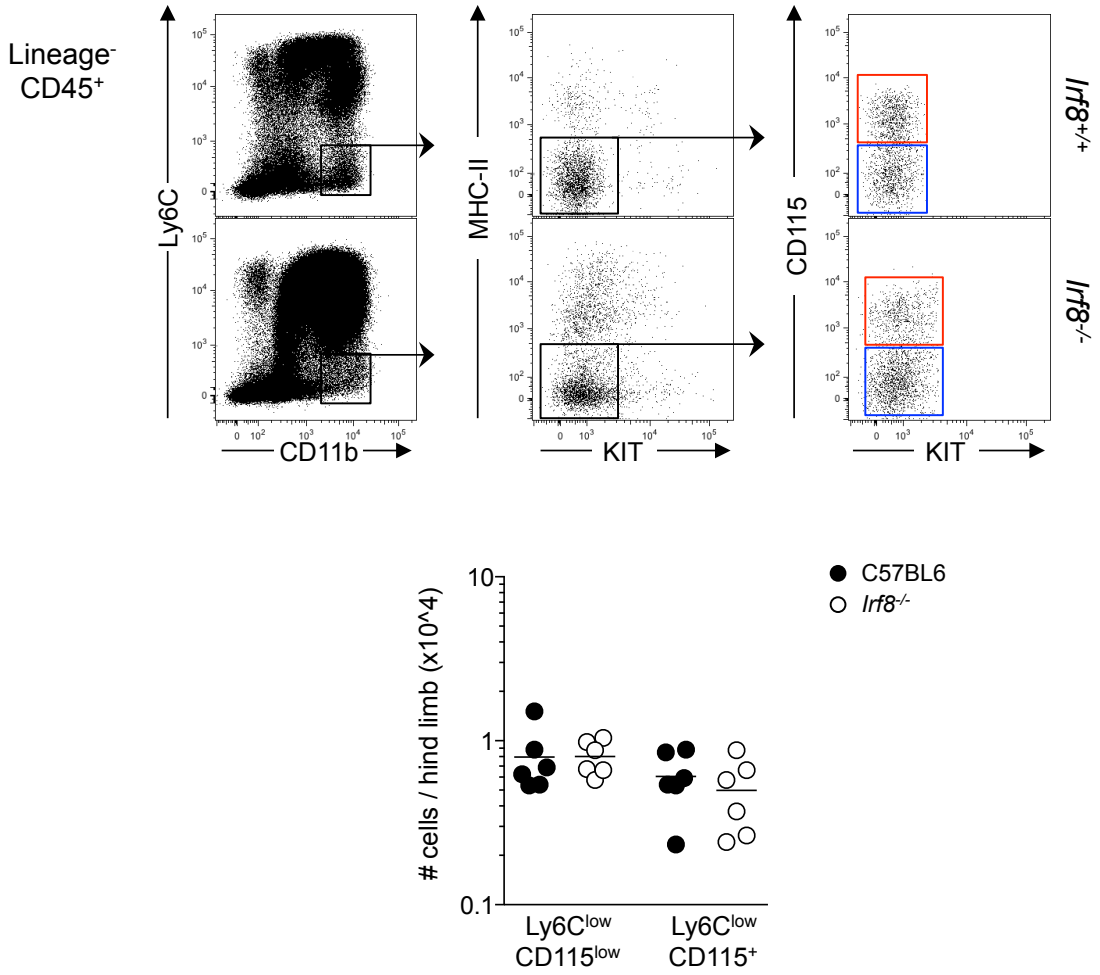

Figure 4-20 *Irf8* deficiency does not affect Ly6C^{low} MHC II^{-} BM monocytes or CD11b^{+} CD115^{low} cells.

Representative dot plots and quantification of Ly6C^{low} MHC II^{-} CD11b^{+} compartment (number of cells per hind limb) from *Irf8*$^{-/-}$ animals (open circles, n=6) and C57BL/6 controls (closed circles, n=6). Statistical significance was assessed by applying unpaired t-test.

Collectively, these analyses of three separate genetic models indicate a shared dependency on *Irf8* and *Ccr2* for Ly6C^{+} and Ly6C^{int} MHC II^{+} monocyte populations for their development into blood circulating cells. Conversely, Ly6C^{low} MHC II^{-} monocytes develop normally in *Irf8*- and *Ccr2*-deficient animals but are selectively and completely dependent upon *Nr4a1*.

Interestingly, the Ly6C^{+} BM monocyte dependency upon *Irf8* is not absolute and approximately 5% of BM Ly6C^{+} monocytes can develop independently of *Irf8* whereas blood Ly6C^{+} monocytes are almost completely absent (reduced by 99%) (Figure 4-19a and c). This raises the question of what happens to this remaining Ly6C^{+} BM monocyte fraction that appears to be *Irf8*-independent?

4.8 Relative compartment size

To enable side-by-side comparison of the divergent genetic requirements of monocyte subsets in the BM and blood, the relative compartment size of each population of wild type, *Irf8*$^{-/-}$, *Ccr2*$^{-/-}$ and *Nr4a1*$^{\Delta/\Delta}$ mice was represented graphically. The absolute cell numbers in each population were measured by flow cytometry (method for obtaining absolute cell counts described in Chapter 2, Materials and Methods). For BM populations, the BM from two hind limbs (femur and tibia, no iliac crest) was counted, analysed and considered to represent 20% of total BM cellularity (Colvin et al., 2004; Colvin et al., 2000; Lambert et al., 2000).

For blood populations, the total number of white blood cells per µl was obtained using a haemocytometer and the number of monocytes per µl was calculated from the flow cytometry data (as described in Chapter 2). Total blood volume was estimated at 80µl/g body weight, which for a 25g C57BL/6 mouse is 2ml total blood volume (Harkness and Wagner, 1995; Mitruka and Rawnsley, 1981). Using these calculations, it was possible

to extrapolate the average total number of cells within each compartment per animal. Each population was then represented as an area using the following formula (http://www.1728.org/diam.htm):

$$\text{Area of a circle} = \pi r^2 \text{ where } r=1 \text{ is equivalent to } 1\text{x}10^6 \text{ cells}$$

Figure 4-19 shows the graphical representation of the size of each population using the calculations outlined above where surface area is proportional to cell numbers in C57BL/6 wild type mice, *Irf8*$^{-/-}$, *Nr4a1*$^{\Delta/\Delta}$ and *Ccr2*$^{-/-}$ mice. This graphical representation provides an interesting insight into the compartment sizes.

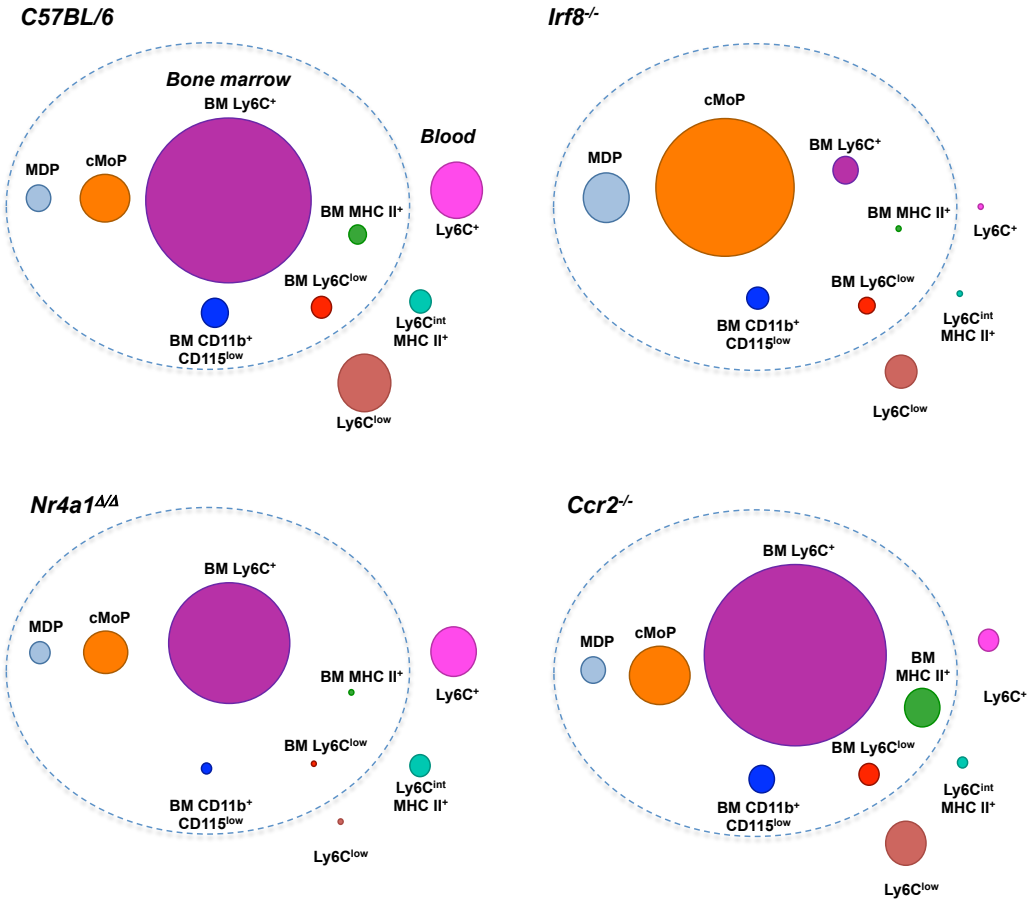

Figure 4-21 Relative compartment size of monocyte populations and their progenitors in different genetic models

Visualising compartment size in this manner highlights that the BM Ly6C^{low} MHC II^{-} population is considerably smaller than its blood counterpart in wild type animals, *Irf8*-deficient and *Ccr2*-deficient mice. This is in line with the long half-life calculated for Ly6C^{low} MHC II^{-} monocytes (see Figure 3-7d) (Yona et al., 2013). Thus, if blood Ly6C^{low} MHC II^{-} monocytes are replenished by BM Ly6C^{low} MHC II^{-} monocytes, it would logically follow that only a small number of cells is required for this replenishment.

Furthermore, this analysis reveals that the BM Ly6C^{+} population is disproportionately large in wild type animals, significantly larger than their blood counterpart. This potentially suggests that the BM Ly6C^{+} population may be a more complicated, as yet uncharacterised, heterogeneous population rather than simply the mature Ly6C^{+} BM monocyte counterpart but may be a precursor population in its own right. This observation led to the hypothesis that the possibility that the 5% of BM Ly6C^{+} monocytes that remain in *Irf8*-deficient mice could potentially be a precursor population for Ly6C^{low} MHC II^{-} monocytes. In turn, this raises the question of where the NR4A1^{bright} CD11b^{+} CD115^{low} population fits into the development pathway of Ly6C^{low} MHC II^{-} monocytes.

4.9 Adoptive transfer

In order to assess the potential of Ly6C^{+} BM and blood monocytes to generate Ly6C^{low} MHC II^{-} NR4A1^{bright} monocytes, BM and blood Ly6C^{+} monocytes from *Nr4a1*^{GFP} *Nr4a1*$^{+/+}$ and from *Nr4a1*^{GFP} *Nr4a1*$^{-/-}$ were adoptively transferred into non-irradiated, CD45.1 congenic animals. BM Ly6C^{+} monocytes transferred from *Nr4a1*^{GFP} *Nr4a1*$^{+/+}$ animals were found to give rise to CD115^{+} NR4A1^{bright} Ly6C^{low} MHC II^{-} monocytes in

the blood and spleen of CD45.1 congenic mice 3.5 days post transfer (Figure 4-22a). In addition, in the spleen a proportion of the NR4A1^{bright} cells had low expression levels of CD115. These data to demonstrate the maturation process of Ly6C^{low} MHC II^{-} monocytes from BM Ly6C^{+} monocytes via a CD115^{low} intermediate *in vivo,* although one consideration in interpreting these data must be that the CD115^{low} NR4A1^{bright} population have not been observed in the spleens of wild type mice. However, these experiments involved the artificial transfer of BM cells directly into the blood stream, thus it is feasible that immature cells home to the spleen in order to complete their maturation process.

In contrast, Ly6C^{+} BM monocytes from *Nr4a1^{GFP} Nr4a1$^{-/-}$* were unable to generate Ly6C^{low} MHC II^{-} NR4A1^{bright} cells (Figure 4-22a). In addition, neither *Nr4a1^{GFP} Nr4a1$^{+/+}$* nor *Nr4a1^{GFP} Nr4a1$^{-/-}$* Ly6C^{+} blood monocytes were capable of giving rise to "true" NR4A1^{bright} Ly6C^{low} MHC II^{-} monocytes (Figure 4-22b).

Whilst adoptive transfer is an inefficient system, these data clearly demonstrate in the absence of ionising radiation, Ly6C^{+} BM monocytes are capable of giving rise to Ly6C^{low} MHC II^{-} NR4A1^{bright} monocytes whereas blood Ly6C^{+} monocytes could not.

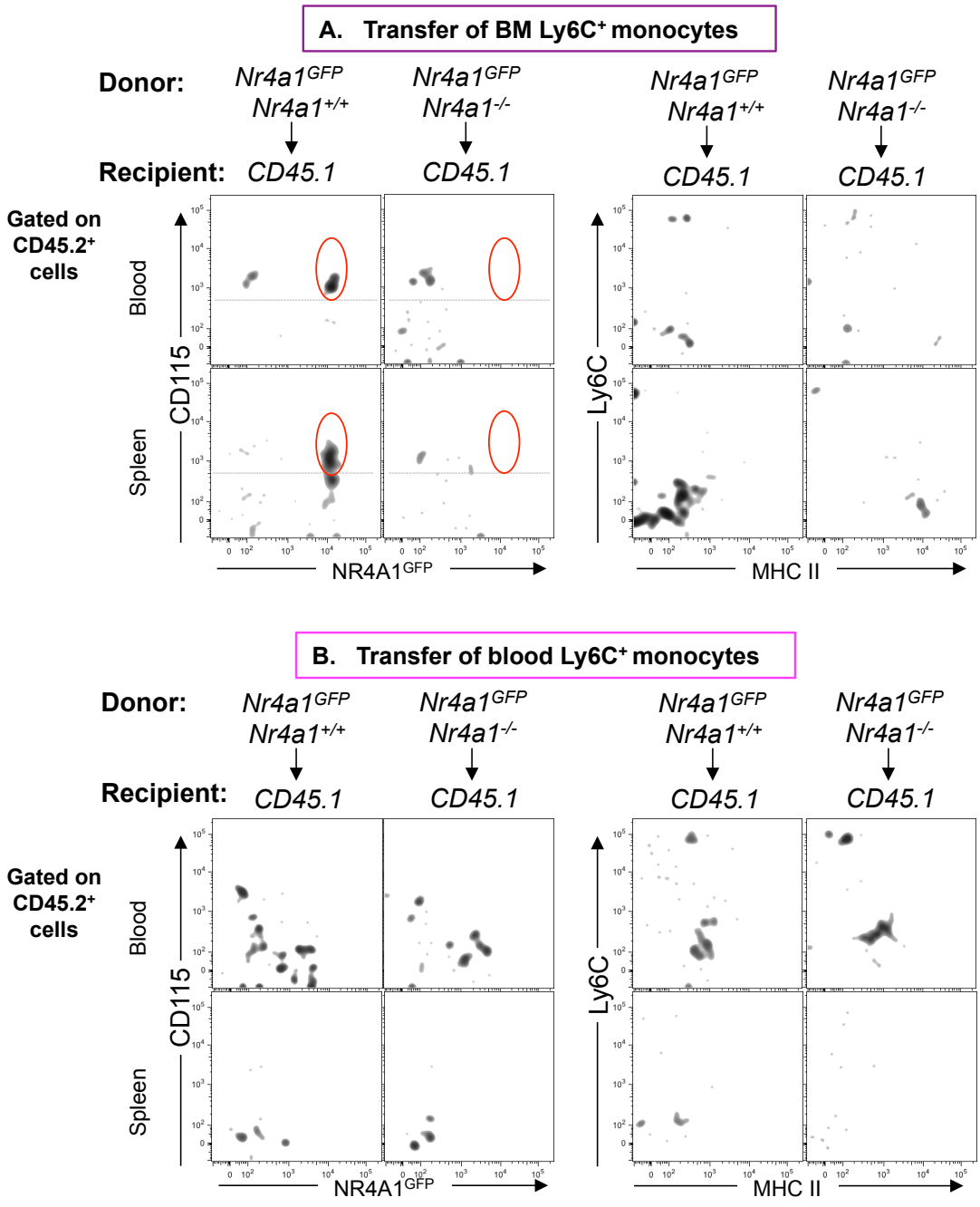

Figure 4-22 Adoptive transfer of BM and blood Ly6C$^+$ monocytes from *Nr4a1^{GFP} Nr4a1$^{+/+}$* and *Nr4a1^{GFP} Nr4a1$^{-/-}$* littermates.

(A) Analysis of blood and spleen from CD45.1 mice 3.5 days after adoptive transfer of BM Ly6C$^+$ monocytes from *Nr4a1^{GFP} Nr4a1$^{+/+}$* and *Nr4a1^{GFP} Nr4a1$^{-/-}$* littermates. **(B)** Analysis of blood and spleen from CD45.1 mice 3.5 days after adoptive transfer of blood Ly6C$^+$ monocytes from *Nr4a1^{GFP} Nr4a1$^{+/+}$* and *Nr4a1^{GFP} Nr4a1$^{-/-}$* littermates. Data are representative of 3 independent experiments.

Interestingly, some donor CD45.2^{+} Ly6C^{low} MHC II^{-} cells that could be seen in the blood and spleen of animals transferred with blood Ly6C^{+} monocytes from both *Nr4a1*^{GFP} *Nr4a1*$^{+/+}$ and *Nr4a1*^{GFP} *Nr4a1*$^{-/-}$. However, these cells were very few and did not express the characteristically high levels of NR4A1^{GFP} expected of true Ly6C^{low} MHC II^{-} monocytes and therefore could not be considered as such.

4.10 Overview and Discussion

4.10.1 *Nr4a1* as a genetic tool for understanding Ly6C^{low} MHC II^{-} monocytes

The data presented in this chapter confirm and extend the previously published data that Ly6C^{low} MHC II^{-} monocytes are selectively dependent upon the transcription factor *Nr4a1* for their development (Hanna et al., 2011). Furthermore, Ly6C^{low} MHC II^{-} monocytes express *Nr4a1*^{GFP} at an appreciably higher level than other monocyte subsets, lymphocytes, dendritic cells, or tissue macrophages. Thus, *Nr4a1*^{GFP} is a marker that enables clearer identification of *bona fide* Ly6C^{low} MHC II^{-} patrolling monocytes separate from Ly6C^{+} or Ly6C^{int} MHC II^{+} monocytes better than was possible with *Cx3cr1*^{GFP} transgenic animals. Furthermore, the double mutant *Nr4a1*^{GFP} *Nr4a1*$^{-/-}$ animals provide a critical tool for analysing the genetic dependency of Ly6C^{low} MHC II^{-} monocytes on *Nr4a1* for their development in conjunction with a specific reporter signal for this subset.

Using *Nr4a1* transgenic and knockout animals as tools for understanding Ly6C^{low} MHC II^{-} monocytes has provided evidence of a population of NR4A1^{bright} CD115^{low} cells within the Ly6C^{low} CD11b^{+} BM compartment that shares the same dependency for development on *Nr4a1*. Further more the data presented here indicate that this population is a developmental intermediate of BM Ly6C^{low} MHC II^{-} monocytes.

4.10.2 Genetic evidence for increased monocyte heterogeneity

The data presented here have provided genetic evidence for a third, previously uncharacterised MHC II^+ monocyte subset. Using *Ccr2*- and *Irf8*-deficient in alongside *Nr4a1*$^{\Delta/\Delta}$ animals has demonstrated that this $Ly6C^{int}$ MHC II^+ develops independently of *Nr4a1* expression. As the expression of Ly6C in this subset is variable, ranging from $Ly6C^+$ to $Ly6C^{low}$, it has been previously included in the analysis of both the classical and patrolling monocyte subsets, which is likely to account for the conflicting theories of $Ly6C^{low}$ monocyte development. Analysis of the genetic models here clearly demonstrates that $Ly6C^{int}$ MHC II^+ monocytes are dependent upon *Irf8* for their development and *Ccr2* for their BM egress, whereas they develop normally in the absence of *Nr4a1*. These genetic requirements mirror those of $Ly6C^+$ monocytes, which indicate that $Ly6C^+$ and $Ly6C^{int}$ MHC II^+ monocytes are part of a single development pathway. In contrast, $Ly6C^{low}$ MHC II^- are absolutely dependent upon *Nr4a1* for their development but independent of *Irf8* and do not require *Ccr2* to mediate their BM egress, demonstrating a distinct developmental lineage. Furthermore, this study has demonstrated that the point at which $Ly6C^{low}$ MHC II^- monocytes diverge from $Ly6C^+$ and $Ly6C^{int}$ MHC II^+ is at the point of BM $Ly6C^+$ monocytes.

4.10.3 A new proposal for $Ly6C^{low}$ MHC II^- monocyte development

The data presented here show that the BM $Ly6C^+$ monocyte population is actively proliferating and can give rise to all three blood monocyte subsets, demonstrating that these cells represent a *bona fide* BM precursor population, and not equivalent to mature blood $Ly6C^+$ monocytes. Thus, based on these data the model of monocyte development can be updated, and this study demonstrates that all three monocyte subsets are generated in the BM, arising from the BM $Ly6C^+$ monocyte subset before egress to the periphery. Thus, we propose that BM $Ly6C^+$ monocytes be renamed

"common pro-monocyte" to reflect their precursor potential to give rise to at least three separate blood monocyte subsets.

Furthermore, this study demonstrates the presence of a slowly proliferating, BM KIT^{-} $Ly6C^{low}$ $CD11b^{+}$ $CD115^{low}$ $NR4A1^{bright}$ population and establishes it as the transitional intermediate between BM $Ly6C^{+}$ common pro-monocytes and mature $Ly6C^{low}$ MHC II^{-} monocytes.

5 Ly6C^{low} MHC II^{-} monocytes contribution to tissue resident macrophages

5.1 Introduction, aims and objectives

5.1.1 Ly6C^{low} monocytes as a potential steady state precursor for tissue macrophages

Over the last few years, there has been an enormous paradigm shift in our understanding of the development of tissue resident macrophage (TRM) populations. The basis of the MPS was data from inflammatory and irradiation chimera models, demonstrating that monocytes give rise to tissue resident macrophages (Ebert and Florey, 1939; van Furth et al., 1972). However, it is now understood that macrophages arise in the steady state from yolk sac derived precursors (Schulz et al., 2012; Yona et al., 2013). However, this understanding raised questions of replenishment by HSC-derived cells or self-maintenance TRM populations by proliferation in the steady state.

Ly6C^{low} monocytes have often been considered the blood-circulating precursor for tissue resident "M2" type macrophages (Auffray et al., 2009b; Geissmann et al., 2003). Early work into monocyte heterogeneity described the different migratory behaviours of monocyte subsets and suggested that Ly6C^{low} monocytes may be the precursors to certain TRM populations (Geissmann et al., 2003). However, with more recent appreciation of the yolk sac origin of macrophages, this hypothesis has not been borne out. An additional layer of confusion has been the use Ly6C as a marker for distinguishing macrophage subsets, with the assumption that Ly6C^{+} macrophages arising from Ly6C^{+} monocytes and likewise Ly6C^{-} macrophages arising from Ly6C^{-} monocytes. Several studies have shown this assumption does not stand up to experimental scrutiny (Hilgendorf et al., 2014; Varga et al., 2013). However, it remains to be confirmed whether Ly6C^{low} monocytes contribute to adult tissue resident macrophage populations in the steady state. As mounting evidence demonstrates, the maintenance of TRM populations is varied (Bain et al., 2014; Chorro et al., 2009;

Davies et al., 2011). It has been reported previously that Ly6C^{low} monocytes contribute to tissue macrophages/ DCs in tissues such as the lung and gut (Jakubzick et al., 2008; Landsman et al., 2007; Yrlid et al., 2006).

5.1.1.1 Hypothesis and aims

Chapter 5 objective: to address whether Ly6C^{low} monocytes represent a blood-circulating progenitor for tissue myeloid populations. It was hypothesised that using the conditional *Nr4a1*-deletion model that selectively lacks Ly6C^{low} monocytes would enable assessment of their contribution to tissue myeloid conditions in steady state. Furthermore, this model would avoid the inflammatory phenotype associated with stromal deletion of *Nr4a1* (Chao et al., 2013; Hanna et al., 2011).

The aims of this chapter are as follows

1. To systematically analyse the contribution of *Nr4a1*-dependent Ly6C^{low} MHC II^{-} monocytes to tissue resident macrophage populations in adult mice under steady state conditions;

2. To investigate the contribution of yolk sac derived macrophages and HSC derived macrophages in the thymic and peritoneal macrophage populations

5.2 Ly6C^{low} MHC II^{-} monocytes do not contribute to tissue macrophage homeostasis

To systematically assess the contribution of *Nr4a1*-dependent Ly6C^{low} MHC II^{-} monocytes to extravascular pools of myeloid cells in the steady state, the lung, liver, brain and skin from hematopoietic-specific *Csf1r*^{iCre} *Nr4a1*$^{\Delta/\Delta}$ mice and their wild-type *Csf1r*^{iCre} *Nr4a1*$^{+/+}$ littermates were analysed (all gating strategies can be found in Appendix 1). It was hypothesised that any macrophage populations to which Ly6C^{low}

MHC II$^-$ monocytes contributed would be reduced in an animal model that selectively lacked circulating Ly6C^{low} MHC II$^-$ monocytes.

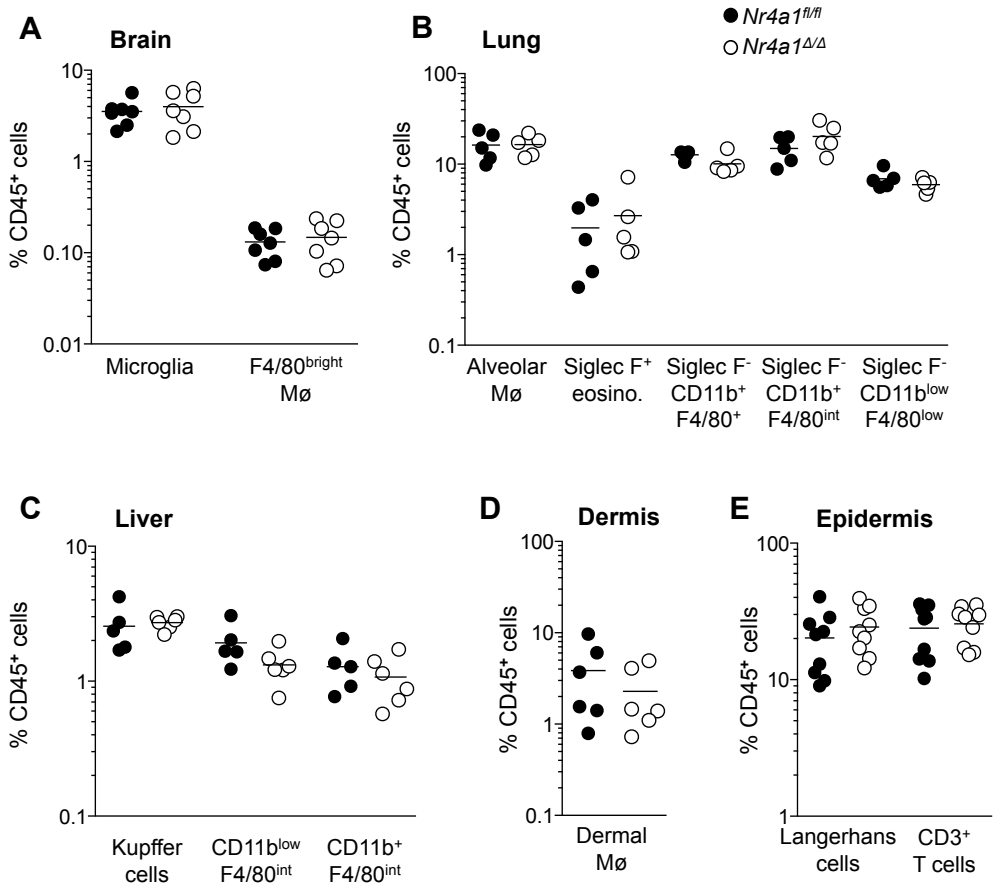

Figure 5-1 Tissue resident myeloid populations in brain, lung, liver and skin.

(A-D) Frequencies of myeloid and macrophage populations in the brain **(A)**, lung **(B)**, liver **(C)** and dermal macrophages **(D)** amongst CD45$^+$ cells and **(E)** Epidermal Langerhans cells and CD3$^+$ T cells from *Nr4a1*$^{fl/fl}$ (closed circles) and *Nr4a1*$^{\Delta/\Delta}$ (open circles) littermates.

There were no significant differences were detected in frequencies of macrophages and myeloid populations amongst CD45$^+$ (haematopoietic) cells in the brain, lung, liver or skin (Figure 5-1). This included alveolar macrophages a population to which it has been suggested that Ly6C^{low} MHC II$^-$ monocytes may contribute (Landsman et al., 2007) (Figure 5-1).

It has been shown in the gut, that circulating monocytes constantly replenish the gut macrophage pool in adult mice (Bain et al., 2014). Thus, the question arose as to

whether Ly6C^{low} MHC II^{-} monocytes contribute to this replenishment. Furthermore, it has been suggested that Ly6C^{low} monocytes contribute to a proportion of intestinal lymph DCs (Yrlid et al., 2006). Consequently, the myeloid populations from the small intestine and the colon lamina propria were analysed (Figure 5-2).

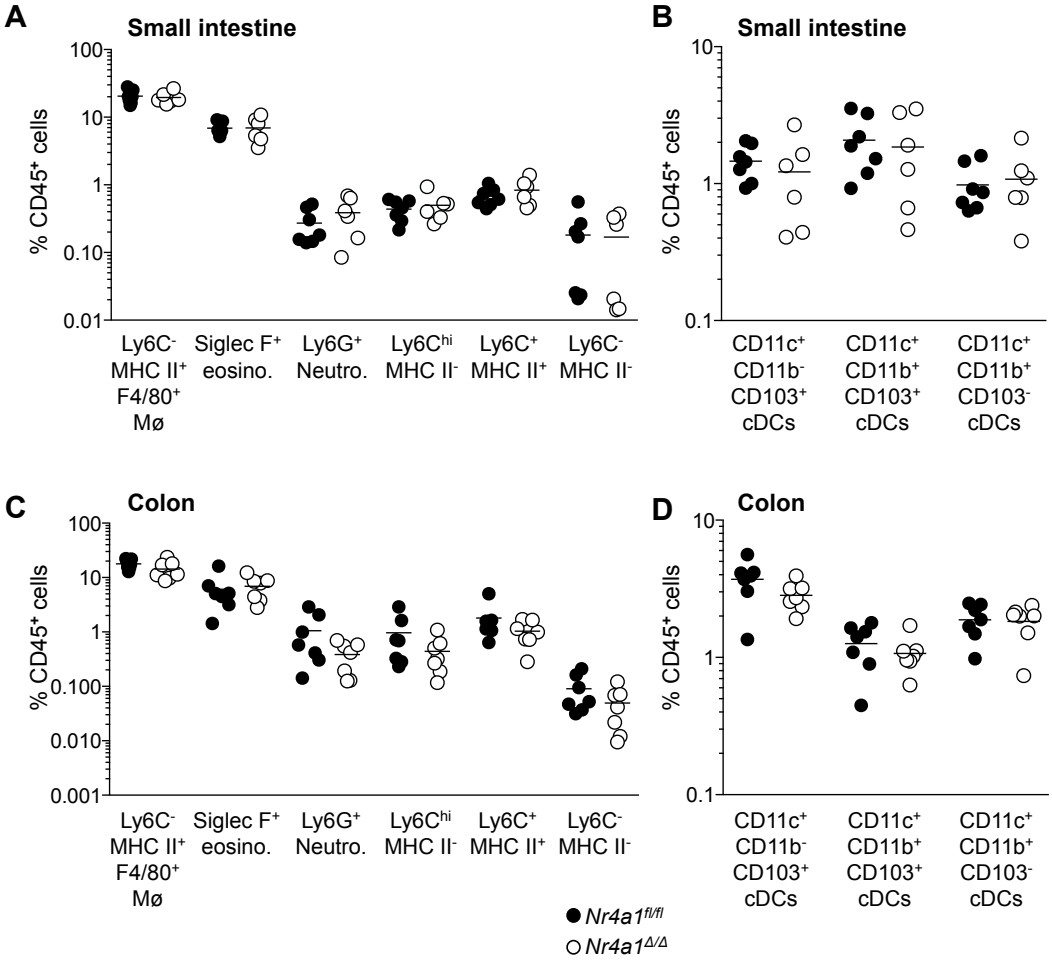

Figure 5-2 Gut myeloid populations from *Nr4a1*$^{\Delta/\Delta}$ mice and littermates

(A-B) Small intestine frequencies of macrophages, granulocytic and monocytic populations **(A)** and dendritic cell subsets **(B);** Colon frequencies of macrophages, granulocytic and monocytic populations **(C)** and dendritic cell subsets **(D)** from *Nr4a1*$^{fl/fl}$ (closed circles) and *Nr4a1*$^{\Delta/\Delta}$ (open circles) littermates. *This analysis was done in collaboration with Dr Calum Bain, University of Glasgow*.

Gut myeloid cells, including macrophages, granulocytic populations, monocytic cells and DCs are not affected by a lack of circulating Ly6C^{low} MHC II^{-} monocytes or haematopoietic deletion of *Nr4a1* (Figure 5-2). This demonstrates that gut myeloid

populations do not require *Nr4a1* for their development nor do they rely on contributions from Ly6C^{low} MHC II^{-} monocytes in the steady state confirming that the continual replenishment of gut macrophages is a result of differentiation of Ly6C^{+} monocytes and with no contribution from Ly6C^{low} MHC II^{-} monocyte subset (Bain et al., 2014).

5.2.1 Secondary lymphoid tissue macrophage populations

5.2.1.1 Splenic macrophage populations

Secondary lymphoid structures have highly defined organised structures. The spleen is the largest secondary lymphoid organ structurally similar to lymph nodes except the spleen lacks high endothelial venules. The spleen structured around the branches of the splenic artery, which open out into venous sinusoids, surrounded by a layer of lymphoid tissue consisting of B cell follicles and T cell zones (den Haan and Kraal, 2012). The highly structured organisation of the spleen enables functionally discrete niches within one organ and different macrophage subpopulations can be identified associated with specific anatomical niches (den Haan and Kraal, 2012; MacLennan, 1994; Mebius and Kraal, 2005; Taylor et al., 2005).

In order to assess whether *Nr4a1*-deficiency affected tissue resident macrophage populations found in the spleen two complimentary methods of analysis were utilised. Red pulp macrophages (RPM) defined as F4/80^{bright} CD11b^{low}, were analysed by flow cytometry (Figure 5-3a and b). This population is established prenatally (Schulz et al., 2012; Yona et al., 2013), their principal function is to phagocytose aged erythrocytes as they move through the red pulp (den Haan and Kraal, 2012), was found to be unaffected by *Nr4a1*-deficiency (Figure 5-3a).

To assess marginal zone macrophages and metallophilic macrophages in addition to checking that the splenic microarchitecture was also unaffected by *Nr4a1*-deficiency, *in situ* immunofluorescent staining was carried out.

Marginal zone macrophages were defined by their expression of macrophage receptor with collagenous structure (MARCO) and metallophilic macrophages, defined by their expression of MOMA1 (CD169). Both marginal zone and metallophilic macrophages function to capture blood borne antigens passing through the spleen (Davies et al., 2013a; den Haan and Kraal, 2012; Mebius and Kraal, 2005). Immunofluorescent staining demonstrated that the splenic microarchitecture remained intact and that neither marginal zone nor metallophilic macrophage populations were altered in *Nr4a1*-deficient mice compared with littermate controls (Figure 5-3c and d).

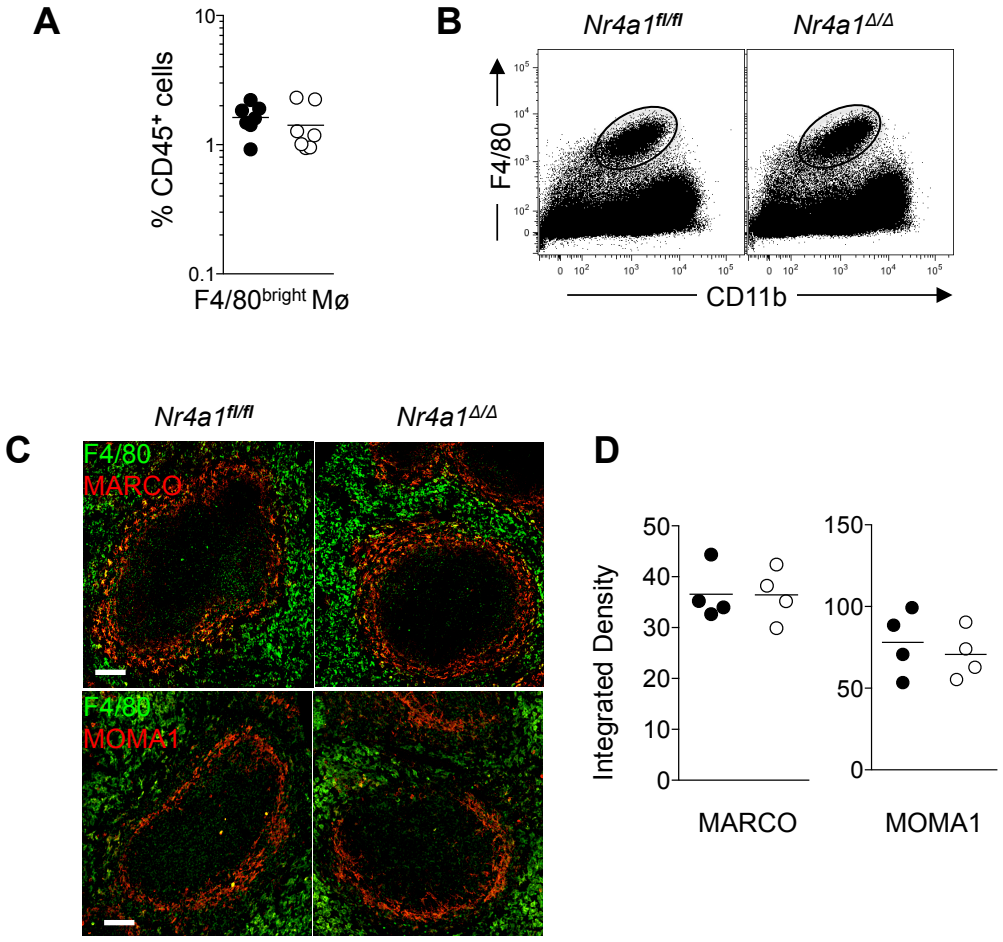

Figure 5-3 Splenic macrophage populations in *Nr4a1*$^{fl/fl}$ and *Nr4a1*$^{\Delta/\Delta}$ littermates

(A and B) Flow cytometry analysis of F4/80^{bright} CD11b^{low} splenic macrophages from *Nr4a1*$^{fl/fl}$ (closed circles, n=7) and *Nr4a1*$^{\Delta/\Delta}$ (open circles, n=7). **(C)** Immunofluorescence staining of splenic cryosections shows splenic microarchitecture. **(D)** MARCO^{+} and MOMA1^{+} populations quantified by integrated density. Scale bar = 50µm. Symbols represent individual animals, closed circles represent *Nr4a1*$^{fl/fl}$ mice (n=4), open circles represent *Nr4a1*$^{\Delta/\Delta}$ mice (n=4). Statistical significance as assessed using unpaired t-test.

5.2.1.2 Lymph node macrophage populations

As mentioned above, lymph nodes (LN) are highly organised structures and studies using both *in situ* staining and flow cytometry have revealed several different macrophage subsets (Gray and Cyster, 2012; Phan et al., 2009; Phan et al., 2007). These macrophage subpopulations can be divided into medullary (CD169^{+} F4/80^{+}) macrophages and subcapsular sinus (CD169^{+} F4/80^{-}) macrophages. Both types of LN

macrophages were analysed by flow cytometry from *Nr4a1*$^{\Delta/\Delta}$ animals and littermate controls as were LN dendritic cell populations (Figure 5-4).

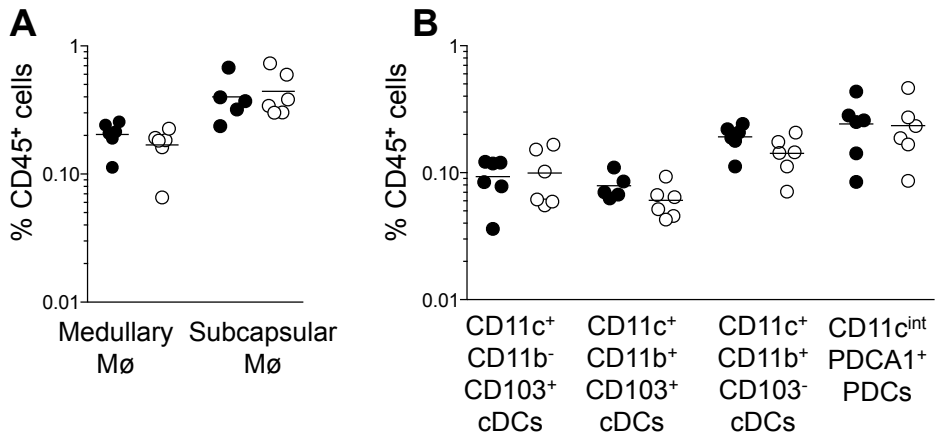

Figure 5-4 LN macrophage and dendritic cell populations

(A) Medullary (CD169^{+} F4/80^{+}) and subcapsular (CD169^{+} F4/80^{-}) macrophages from *Nr4a1*$^{fl/fl}$ (closed circles, n=5) and *Nr4a1*$^{\Delta/\Delta}$ (open circles, n=6) littermates were analysed and quantified by flow cytometry. **(B)** LN DC populations from *Nr4a1*$^{fl/fl}$ (closed circles, n=6) and *Nr4a1*$^{\Delta/\Delta}$ (open circles, n=6) littermates were analysed and quantified by flow cytometry. Symbols represent individual animals. Statistical significance was tested using unpaired t-test.

Thus it can be seen that neither medullary CD169^{+} F4/80^{+} nor subcapsular CD169^{+} F4/80^{-} macrophages were affected by *Nr4a1*-deficiency. LN DCs were similarly unaffected by the mutation. These data further demonstrate that Ly6C^{low} MHC II^{-} monocytes do not contribute to tissue macrophage or DC populations in the steady state.

5.3 Thymic macrophage populations

5.3.1 A novel macrophage population is reduced in the thymus of *Nr4a1*$^{\Delta/\Delta}$ animals

Nr4a1 has been widely investigated in terms of progenitor thymocytes and T cell antigen receptor (TCR) engagement in the thymus (Cheng et al., 1997; Lee et al., 1995; Sekiya et al., 2013). Indeed, Nr4a family members have been shown to have essential roles in regulatory T cell development (Sekiya et al., 2013). , Thymic macrophages have a vital role in the phagocytosis of apoptotic thymocytes during positive and negative T cell selection in the thymus (Esashi et al., 2003; Odaka and Mizuochi, 2002; Surh and Sprent, 1994). Although some level of functional redundancy between Nr4a family members during this process of T cell education has been reported (Sekiya et al., 2013), it is not known whether *Nr4a1*-deficiency would impact the phenotype of specific macrophage populations. Thus, it was important to investigate whether a lack Ly6C^{low} monocytes, or lack of haematopoietic *Nr4a1,* altered any of the thymic myeloid populations.

Within the F4/80^{+} TIM4^{+} CD64^{+} macrophage compartment of the thymus, two separate populations could be isolated: classical F4/80^{bright} CD11b^{+} thymic macrophage populations and a novel F4/80^{+} CD11b^{-} population (Figure 5-5a). This novel population was reduced by 45% in *Nr4a1*$^{\Delta/\Delta}$ animals compared with wild type littermate controls (Figure 5-5b). Thymic dendritic cell subsets were also analysed and found to be unaffected in frequency by *Nr4a1*-deficiency (Figure 5-5c).

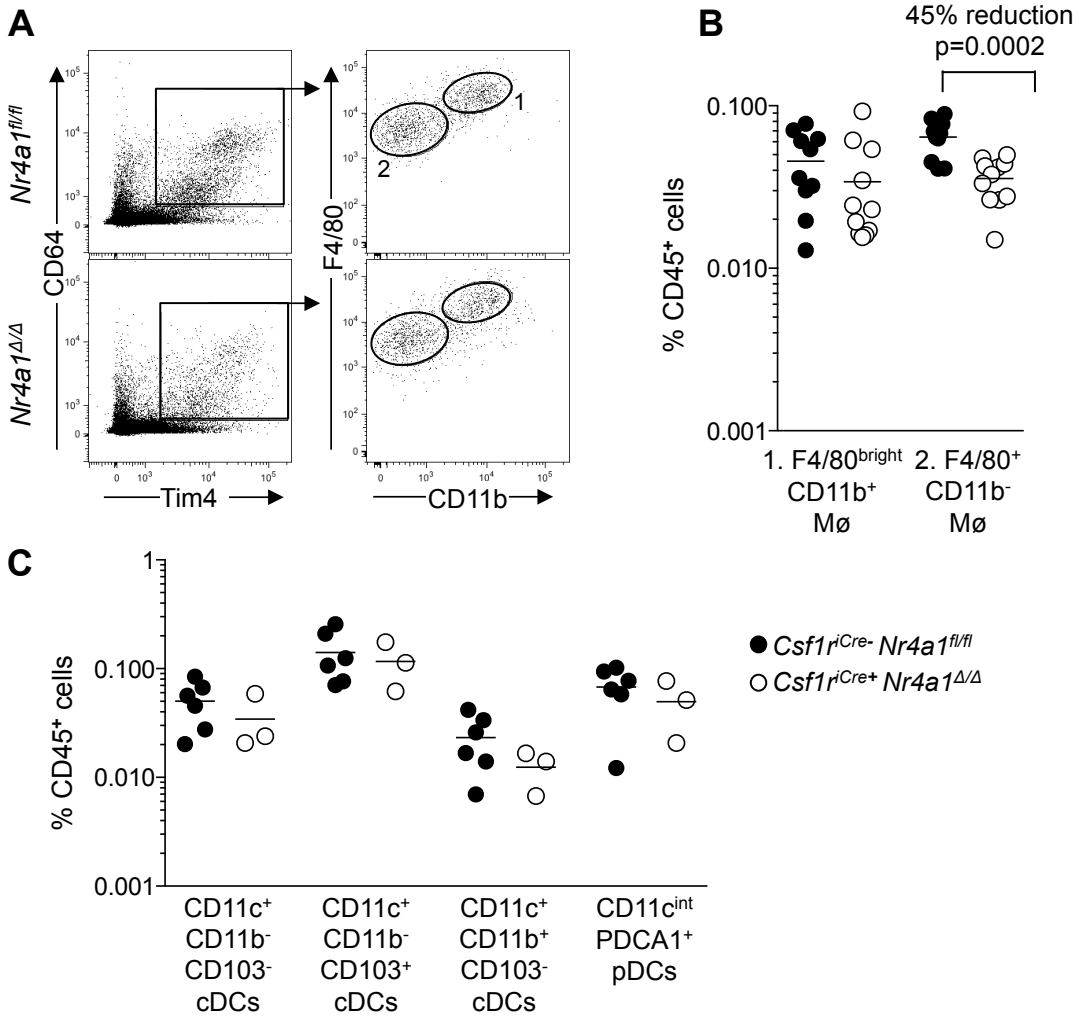

Figure 5-5 Thymic macrophage and dendritic cell populations

(A-B) Representative dot plots **(A)** of thymic macrophages from *Nr4a1*$^{fl/fl}$ (closed circles) and *Nr4a1*$^{\Delta/\Delta}$ (open circles) mice: (1) F4/80^{bright} CD11b^{+} classical macrophages and (2) F4/80^{+} CD11b^{-} macrophages and quantification **(B)**. **(C)** Thymic dendritic cells from *Nr4a1*$^{fl/fl}$ (closed circles) and *Nr4a1*$^{\Delta/\Delta}$ (open circles) mice.

The role of this novel macrophage population was investigated thoroughly by collaborators (Tacke et al., 2015), thus this project focused on investigating the origin of this population.

5.3.1.1 Are thymic macrophages yolk sac or bone marrow derived?

As the reduction of the F4/80^{+} CD11b^{-} thymic population was 45% compared with littermates, it seemed unlikely that Ly6C^{low} monocytes act as progenitor cells for this population due to the almost total loss of Ly6C^{low} monocytes in *Nr4a1*$^{\Delta/\Delta}$. However, as

this model uses *Csf1r*^{iCre} to delete *Nr4a1*, which is expressed by both YS- and HSC-derived macrophages (Gomez Perdiguero et al., 2015; Schulz et al., 2012), it does not rule out either yolk sac or BM origins for this population.

First, it was assessed whether this population expressed *Nr4a1* using NR4A1^{GFP} reporter mice. As can be seen in the top panel of Figure 5-6a, F4/80^{bright} macrophages did not express NR4A1^{GFP} and the F4/80^{+} CD11b^{-} population only expressed very low levels of NR4A1^{GFP}. In addition, *Csf1r*^{iCre} *Rosa26*^{YFP} reporter mice were analysed as a proxy for analysing deletion. It was confirmed that *Csf1r*^{iCre} expression is sufficient to mediate recombination at the *Rosa26* locus in both of these macrophage populations (Figure 5-6a). Whilst it cannot be assumed that recombination by *Csf1r*^{iCre} at the *Nr4a1* locus is equal to that at the *Rosa26* locus, this data demonstrates that *Csf1r*^{iCre} is expressed and active in thymic macrophage population.

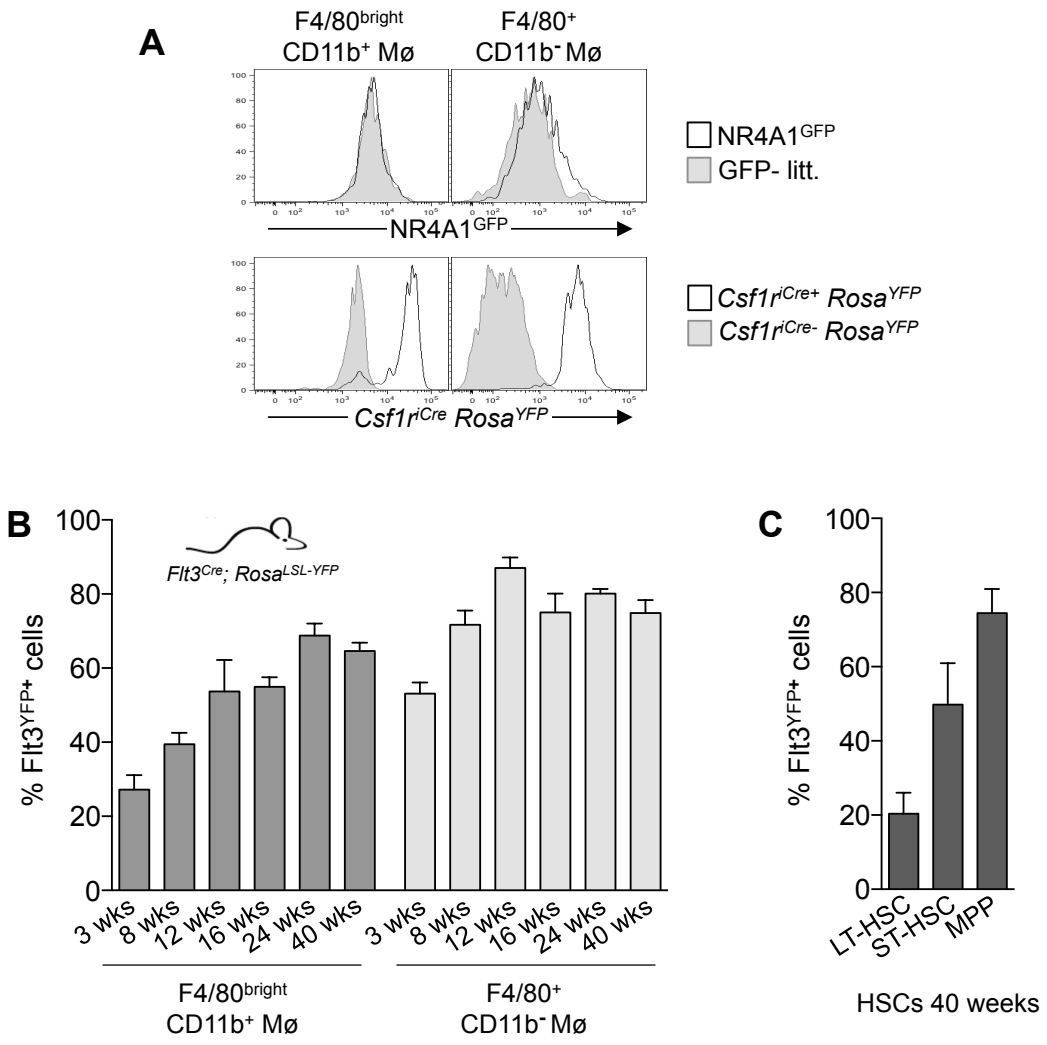

Figure 5-6 Fate mapping thymic macrophage populations

(A) Expression of *Nr4a1*^{GFP} (top) and *Csf1r*^{iCre} *Rosa*^{YFP} (bottom) by thymic macrophage populations. **(B)** Frequency of *Flt3*^{Cre} *Rosa*$^{YFP+}$ cells in thymic macrophage populations over time from weaning to 40 weeks of age. **(C)** Frequency of *Flt3*^{Cre} *Rosa*$^{YFP+}$ HSCs at 40 weeks; n=3-6 in each age group, error bars represent SD.

In order to the ascertain whether thymic macrophage populations are the progeny of YS or HSC progenitors, thymic macrophage populations from *Flt3*^{Cre} *Rosa26*^{YFP} reporter mice were assessed. *Flt3*^{Cre} *Rosa26*^{YFP} reporter mice labels foetal liver and adult HSC derived MPPs (Christensen and Weissman, 2001; Gomez Perdiguero et al., 2015; Schulz et al., 2012) and their progeny. (Full *Flt3*^{Cre} *Rosa26*^{YFP} fate mapping of HSCs is available in Appendix 2).

This facilitates lineage tracing of BM derived populations therefore thymic macrophage populations were analysed from this reporter strain at 3, 8, 12, 16, 24 and 40 weeks of age. In dark grey bars of Figure 5-6b show the percentage of *Flt3*$^{YFP+}$ in F4/80^{bright} CD11b^{+} macrophages. At three weeks of age, 27% (±3% SD) of this population expresses YFP, indicating that only 27% of this population is HSC derived and the remaining 70% of the population develops independently of Flt3. The most likely interpretation of this data is that the majority of F4/80^{bright} CD11b^{+} macrophages are yolk sac derived. Over time, the frequency of YFP^{+} cells in this population gradually increases over time, reaching around 64% (±2% SD) at 40 weeks suggesting contribution from HSCs over time. However, the frequency of YFP^{+} cells in the F4/80^{bright} CD11b^{+} macrophage population has not quite equilibrated with MPPs (74% (±6% SD) YFP^{+}, Figure 5-6c) 40 weeks of age. In contrast, the F4/80^{+} CD11b^{-} thymic macrophage population does equilibrate with the MPPs by 12 weeks, suggesting that in adulthood, this population is principally made up of BM derived cells.

Collectively, these data demonstrate the presence of a novel macrophage subset within the thymus that is partially dependent up *Nr4a1* for its development. Furthermore, these data indicate the dual origins of macrophage populations within the thymus. The Flt3 labelling allows lineage tracing of populations that are of HSC origin and demonstrates that by 12 weeks of age, this novel F4/80^{+} CD11b^{-} population consists mainly of HSC derived cells, although in early life this population may have contribution from YS-derived cells.

5.4 Peritoneal macrophages

5.4.1 Characterisation of peritoneal macrophage populations

The peritoneal cavity is used extensively to study macrophage populations due to the abundance of macrophages in this compartment, their relative ease of isolation and the large influx of inflammatory cells when this compartment is challenged. Furthermore, it has been demonstrated that there are two distinct macrophage populations within the peritoneal cavity: large peritoneal macrophages (LPM) and small peritoneal macrophages (SPM) (Ghosn et al., 2010). LPM are defined as F4/80^{bright} CD11b^{+} MHC II^{low} cells whereas SPM are defined as F4/80^{+} CD11b^{+} MHC II^{+} (Ghosn et al., 2010). Additionally, it is thought that the in the context of inflammation, the SPM is monocyte-derived pool of cells, making it an interesting macrophage pool to check for Ly6C^{low} MHC II^{-} monocyte contribution.

Initially to ensure that these peritoneal populations are indeed macrophages, they were isolated using CD115 (*Csf1r)*, F4/80, and TIM4 staining. TIM4 is a member of T-cell immunoglobin mucin protein family that binds phosphatidylserine on the surface of apoptotic cells (Kobayashi et al., 2007; Miyanishi et al., 2007), which is reportedly important for peritoneal macrophage homeostasis (Wong et al., 2010).

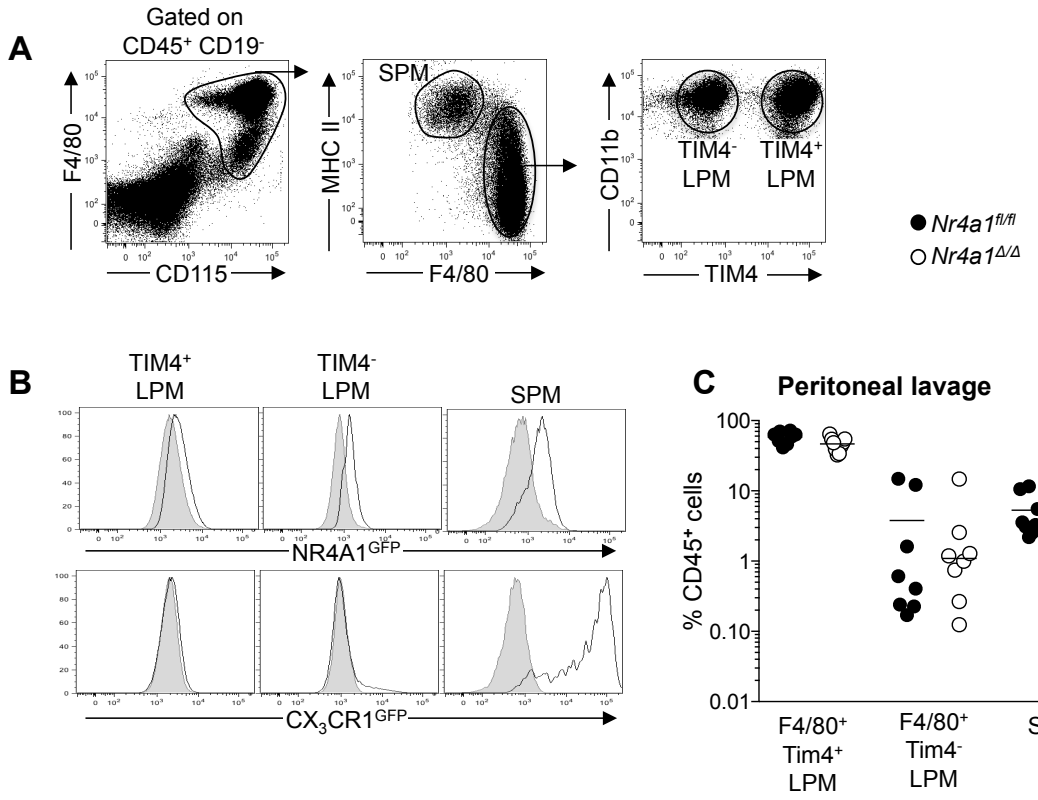

Figure 5-7 Peritoneal macrophage populations

(A) Gating strategy to isolate peritoneal macrophage populations: F4/80^{+} MHC II^{+} SPM, F4/80^{bright} MHC II^{low} TIM4^{+} LPM and F4/80^{bright} MHC II^{low} TIM4^{-} LPM. **(B)** NR4A1^{GFP} and CX_3CR1^{GFP} expression of LPM populations and SPM, grey histograms represent GFP^{-}, white histograms represent GFP^{+} mice. **(C)** Quantification of peritoneal macrophage populations from *Nr4a1*$^{fl/fl}$ (closed circles, n=8) and *Nr4a1*$^{\Delta/\Delta}$ (open circles, n=8) animals. Statistical significance was assessed using unpaired t-test.

Analysis of peritoneal macrophage populations including the marker TIM4 revealed the presence of two separate LPM populations (Figure 5-7a). The TIM4^{-} population is a minor population that, to our knowledge, has not previously been described. Figure 5-7b shows that NR4A1^{GFP} expression in all three subsets is low. Conversely, SPM expressed high levels of CX_3CR1^{GFP} (Figure 5-7b), which prompted investigation into whether SPM relied on Ly6C^{low} monocyte contribution.

In order to assess whether any of the peritoneal macrophage populations had some contribution from Ly6C^{low} monocytes, the peritoneal lavage from *Nr4a1*$^{\Delta/\Delta}$ animals and littermate controls was analysed. Figure 5-7c demonstrates that neither LPM population

nor the SPM population were significantly reduced by lack of circulating Ly6C^{low} monocytes.

It can be seen that the size of the TIM4^{-} varies dramatically between littermates, although the distribution is comparable between iCre^{-} and iCre^{+} littermates. This vast variation between mice raised the possibility that the TIM4^{+} and TIM4^{-} are the same population but the TIM4^{-} fraction represents a portion of the population that is undergoing receptor internalisation due to activation. To address this question, the origins of the different populations were investigated using the *Flt3^{Cre} Rosa^{YFP}* mice.

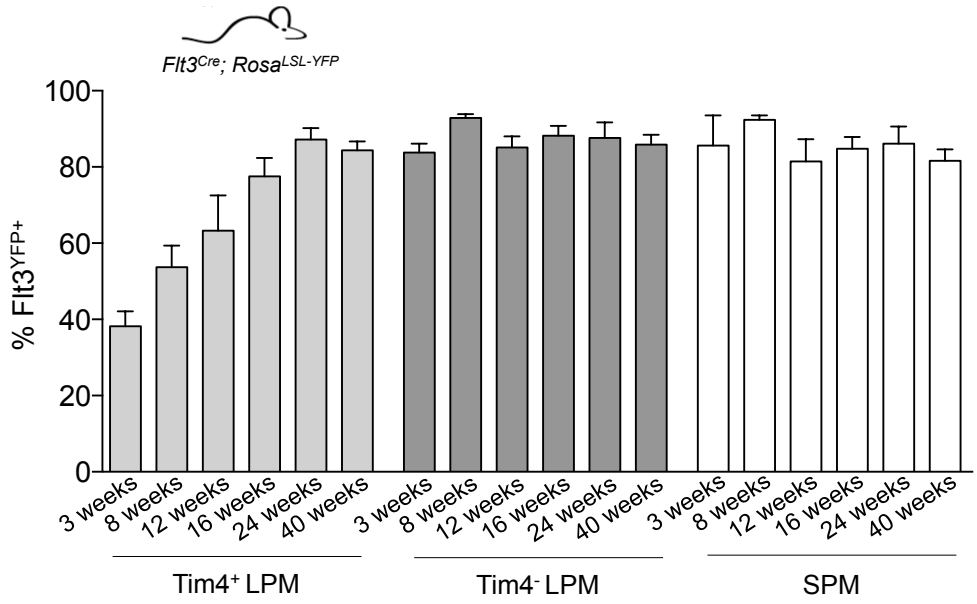

Figure 5-8 Fate mapping of peritoneal macrophage populations

Frequency of *Flt3^{YFP+}* cells in the peritoneal TIM4^{+} LPM (light grey bars), TIM4^{-} LPM (dark grey bars) and SPM (white bars) at 3, 8, 12, 16, 24 and 40 weeks of age, n=3-6 mice per age group; error bars represent standard deviation.

Figure 5-8 demonstrates that, at 3 weeks of age, the TIM4^{+} macrophage population is only around 35% comes from an Flt3^{+} progenitor, indicating that ~65% of the population are Flt3-independent and therefore do not come from HSCs. However, by 24 weeks of age, this population has equilibrated with the MPPs suggesting that HSC-

derived cells replenish this population. An alternative interpretation of these results could be that TIM4^{+} macrophages upregulate Flt3 over time.

In contrast, the TIM4^{-} LPM and the SPM both exhibited high level of excision of the LSL cassette and subsequent expression of YFP. Thus, both of these populations are mostly derived from HSC-derived progenitors. These data demonstrate two independent development pathways between LPM subpopulations, with the TIM4^{+} population having dual origin in adulthood whereas the TIM4^{-} population is dependent upon HSC progenitors. This makes it unlikely that the TIM4^{-} population represents an activation state of the TIM4^{+} population. Rather, this data shows that there is heterogeneity with the LPM compartment. In addition, these data show that whilst SPM are HSC-derived, they have no contribution from Ly6C^{low} MHC II^{-} monocytes in the steady state.

5.5 Overview and discussion

5.5.1 Ly6C^{low} MHC II^{-} monocytes do not contribute tissue resident macrophages under steady state conditions

This chapter demonstrates that Ly6C^{low} MHC II^{-} monocytes do not contribute to tissue macrophage populations in the steady state. Systematic analysis of macrophage populations from the brain, liver, lung, skin, gut, spleen, LN and peritoneum reveals that, even in the total absence of Ly6C^{low} MHC II^{-} monocytes in *Nr4a1*$^{\Delta/\Delta}$ animals, tissue resident macrophage populations in these organs are found at similar frequencies to *Nr4a1*$^{fl/fl}$ littermate controls. In addition, the splenic microarchitecture was unchanged between *Nr4a1*$^{\Delta/\Delta}$ and littermates.

Interestingly, a novel population of thymic macrophages was found to be reduced by a half in *Nr4a1*$^{\Delta/\Delta}$ animals compared to littermates. This finding was confirmed and validated by collaborators in an independent genetic model (*Nr4a1*$^{-/-}$) and demonstrated

that this population is important for the effective clearance of apoptotic thymocytes (Tacke et al., 2015). As this population is halved in *Nr4a1*$^{\Delta/\Delta}$ animals, it was reasoned that it was unlikely that the reduction was due to lack of Ly6C^{low} MHC II^{-} monocytes, rather that this population is partially dependent on *Nr4a1* for its development.

Furthermore, the data presented here indicate that this novel thymic macrophage population in adult mice is HSC-derived, whereas classical tissue resident thymic macrophages are a mixture of YS- and HSC-derived cells. However, the interpretation of the *Flt3*^{Cre} *Rosa*^{YFP} data must be considered with caution. As yet, we do not have a specific, positive marker for YS-derived macrophages and in this model we infer the absence of labelling indicates YS-origin but to be certain of this, it would be necessary to investigate using a reporter strain that was specific for YS-derived macrophages. In addition, the increase of YFP labelling over time is interpreted as being a reflection of HSC-derived cells infiltrating macrophage populations. However the possibility cannot be excluded that YS-derived macrophages upregulate Flt3 over time sufficiently to enable recombination of the Lox-STOP-Lox motif and subsequent expression of YFP.

Finally, this chapter investigates the macrophages of the peritoneal cavity and demonstrates that large peritoneal macrophages consist of two subsets with distinct origins. The TIM4^{+} LPM population in young mice is a mixed population of YS- and HSC-derived macrophages whereas the TIM4^{-} LPM population were entirely HSC-derived, interpreting the *Flt3*^{Cre} *Rosa*^{YFP} data with the same caveats as discussed above.

Thus, the data presented in this chapter demonstrate that Ly6C^{low} MHC II^{-} monocytes do not contribute to tissue macrophage populations in the steady state of the organs that were investigated here. It cannot be excluded that Ly6C^{low} MHC II^{-} monocytes do not contribute to any macrophage populations, as these examinations were by no means

exhaustive. Furthermore, this chapter characterises the origin of macrophage subsets from the thymus and peritoneum, highlighting the complexity of macrophage origins within a single tissue.

6 Discussion

6.1 Summary of findings

Firstly, this thesis describes the phenotypic and genetic validation of a third, MHC II^+ monocyte subset that can be found in the blood, spleen and BM of adult mice.

Secondly, the data presented in this thesis suggest an updated maturation pathway of monocyte subsets that takes into account previously published reports and the findings here of a third, distinct subset.

Thirdly, this study demonstrates that $Ly6C^{low}$ MHC II^- monocytes do not contribute to the tissue macrophage pool in the steady state, which suggests that the fate of this population is to remain in the vasculature in order to carry out their effector functions.

The next section will discuss the value of studying murine monocyte development and discuss the interpretation of each of the principal findings, considering alternative interpretations and discussing the limitations of the experiments presented in the present study.

6.2 Murine model for understanding monocyte development

6.2.1 Conserved function between human and murine monocytes

Our understanding of the origin and function of human patrolling monocytes is even more limited than our understanding of murine patrolling monocytes. However, human $CD14^{dim}$ $CD16^+$ monocytes are considered to be analogous to murine $Ly6C^{low}$ monocytes on account of some phenotypic characteristics including high CX_3CR1 expression (Geissmann et al., 2003) but also conserved patrolling behaviour (Auffray et al., 2007). Furthermore, it has been demonstrated that $CD14^{dim}$ $CD16^+$ monocytes express higher levels of NR4A1 by RT-qPCR than the other two subsets: $CD14^+$ $CD16^-$ and $CD14^+$ $CD16^+$ monocytes (Hanna et al., 2012). Thus, it seems that high *Nr4a1*

expression is conserved between species in patrolling monocytes which may indicate *Nr4a1* could be a candidate gene for involved in susceptibility to infectious disease, inflammatory diseases and autoimmunity via it's control of monocyte differentiation. Accordingly, understanding Ly6C^{low} monocyte ontogeny and the molecular mechanisms that control murine monocyte development and survival can provide *in vivo* clues for *ex vivo* research human monocyte development and survival. Given the incompletely elucidated roles of monocyte subsets in inflammatory diseases, infection and cancer understanding the mechanisms that control functional heterogeneity are essential to identify potential future therapeutic targets. Several studies directly comparing gene and/or protein expression profiles from human and murine monocytes (Cros et al., 2010; Ingersoll et al., 2010; Schmidl et al., 2014) show that there is significant homology but also important differences which serves as a reminder that findings from one species cannot be directly translated to another. Furthermore, CD14^{dim} CD16^{+} monocytes, like their murine Ly6C^{low} counterpart appear to carry out their effector functions from within the vasculature, patrolling the luminal side of blood vessels and scavenging microparticles (Auffray et al., 2007; Carlin et al., 2013; Cros et al., 2010).

Thus, understanding murine monocyte development can act as tool for identifying potential avenues of interest in addition to aiding our understanding of basic biology.

6.3 Monocyte heterogeneity

6.3.1 Two distinct genetic lineages within the monocyte compartment

Monocyte heterogeneity has been appreciated for many years now (Geissmann et al., 2003; Passlick et al., 1989). In mice it is generally considered that there are two

monocyte subsets, the Ly6C^{+} "classical" or "inflammatory" subset and the Ly6C^{low} "patrolling" subset but their relationship to each other has remained a topic of debate.

This thesis establishes, in wild type mice that the monocyte compartment can be divided into three distinct subsets based the cell surface expression of Ly6C and MHC II, which is underscored by differing genetic requirements for development. As a consequence, the data presented here can be used to understand the seemingly conflicting reports of distinct genetic dependencies (Alder et al., 2008; Debien et al., 2013; Hanna et al., 2011; Kurotaki et al., 2013) and the current model of monocyte conversion in the blood (Hettinger et al., 2013; Sunderkotter et al., 2004; Varol et al., 2007; Yona et al., 2013; Yrlid et al., 2006).

As described in previous studies, we found that Ly6C^{+} monocytes depend upon *Irf8* for their development (Alder et al., 2008; Kurotaki et al., 2013) and *Ccr2* for their migration from the BM to the periphery (Serbina and Pamer, 2006). Interestingly, it was found that Ly6C^{int} MHC II^{+} monocytes also have the same genetic requirements for their development and BM egress. In contrast, Ly6C^{low} MHC II^{-} monocytes were found to develop independently of *Irf8* and did not require *Ccr2* to exit the BM (Figures 4-17 and 4-19). Moreover, as previously described by Hanna *et al.,* Ly6C^{low} MHC II^{-} monocytes were completely dependent upon *Nr4a1* for successful BM development (Hanna et al., 2011). Taken together, these genetic dependencies reveal two separate developmental lineages of mature monocyte subsets: one which is dependent upon *Irf8* and *Ccr2* and generates Ly6C^{+} and Ly6C^{int} MHC II^{+} monocytes and a second which is dependent upon *Nr4a1* and gives rise to Ly6C^{low} MHC II^{-} monocytes. Seemingly contradictory previously published reports regarding Ly6C^{low} monocyte development pathways can be explained by the overlap within the Ly6C^{low} monocyte compartment between Ly6C^{low} MHC II^{-} and Ly6C^{int} MHC II^{+} subsets. Thus, the observation that

Ly6C^{low} monocytes can still develop in the absence of Ly6C^{+} monocytes in *Irf8*$^{-/-}$ animals (Kurotaki et al., 2013) can be accounted for by the *Nr4a1*-dependent, *Irf8*-independent Ly6C^{low} MHC II^{-} monocyte subset. Furthermore, the residual Ly6C^{low} monocytes observed in *Nr4a1*$^{-/-}$ animals in the paper by Hanna *et al.,* are *Nr4a1*-independent Ly6C^{int} MHC II^{+} monocytes (Hanna et al., 2011) (See Figure 4-5).

The genetic confirmation of monocyte heterogeneity supports the notion that there are at least two distinct monocyte lineages in the blood, away from relying only on cell surface markers (Figure 6-1).

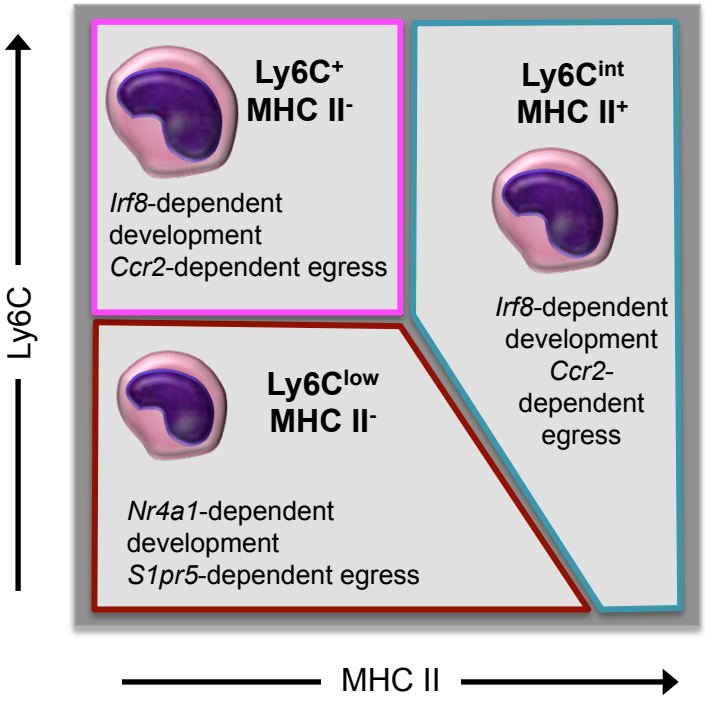

Figure 6-1 Murine monocyte heterogeneity

The murine monocyte compartment consists of at least two genetically distinct lineages. One, which is dependent upon *Irf8* for monocyte development and *Ccr2* for BM egress and the second, which depends on *Nr4a1* for development and *S1pr5* for BM egress

Furthermore, these differing genetic requirements have important consequences for our understanding of the molecular control of monocyte functional heterogeneity. The functions of Ly6C^{int} MHC II^{+} monocytes remain to be described, however, one could

speculate that, as they express MHC II^+, CD11c and Flt3, it would be very interesting to investigate whether this subset has DC-like functions *in vivo*.

6.3.2 *Nr4a1^{GFP}* as a positive marker for Ly6C^{low} MHC II$^-$ monocytes

In this study we utilise the high level of $NR4A1^{GFP}$ expression that is selectively observed in $Ly6C^{low}$ monocytes. Whilst CX_3CR1^{GFP} has been critical for the progress of understanding myeloid biology, the difference in CX_3CR1^{GFP} MFI between $Ly6C^+$ and $Ly6C^{low}$ MHC II^- monocytes is a 4-fold increase and the difference between $Ly6C^{int}$ MHC II^+ and $Ly6C^{low}$ MHC II^- monocytes is a 2-fold increase (Figure 3-2). $Ly6C^+$ monocytes are often referred to in the literature as having intermediate Cx3cr1 expression levels whereas $Ly6C^{low}$ MHC II^- monocytes are described as CX_3CR1^{bright}. In reality, this marked difference in expression levels does not allow clear distinction between subsets in flow cytometry.

In contrast, the $NR4A1^{GFP}$ MFI of the blood $Ly6C^{low}$ MHC II^- subset is 25-fold higher than $Ly6C^+$ monocytes and 10-fold higher than $Ly6C^{int}$ MHC II^+ subsets (Figure 3-2). Thus, whilst many different cell populations express *Nr4a1,* the selective high level of expression observed on $Ly6C^{low}$ MHC II^- proved very useful in separating monocyte populations from each other and using $NR4A1^{GFP}$ as positive marker for *Nr4a1*-dependent monocytes.

The increase in GFP of both *Cx3cr1* and *Nr4a1* as Ly6C expression decreases. GFP reporter lines should be a direct reflection of cellular expression of protein of interest. However, as was already noted, GFP protein has a long half-life and the increase in GFP MFI could be interpreted as an accumulation of protein within the cells as they convert from $Ly6C^+$ through to $Ly6C^{int}$ MHC II^+ until finally maturing into $Ly6C^{low}$ MHC II^- monocytes. However, in light of the differing genetic dependencies of $Ly6C^+$

and Ly6C^{int} MHC II^{+} subsets compared to Ly6C^{low} MHC II^{-} monocytes evidenced here, it would seem unlikely. However, one possibility that hasn't been excluded is that *Nr4a1*-dependent Ly6C^{low} MHC II^{-} monocytes can upregulate MHC II^{+}, contributing to this compartment. In addition, the possibility cannot be excluded that investigations with further genetic models and with additional cell surface markers that the heterogeneity within the monocyte compartment will increase still further.

6.4 Monocyte dynamics

In the present study monocyte dynamics in the blood and BM were characterised using two different techniques: cell cycle analysis using Ki-67/DAPI staining and BrdU incorporation analysis.

Cell cycle analysis using Ki-67/DAPI staining provided information regarding the proportion of each population actively cycling at any one time, however, as discussed in chapter 3, cell cycle analysis in this manner provides a snapshot of proliferation activity at that particular time and does not provide information regarding the rate at which a population turns over. Thus the combination with BrdU pulse-chase analysis provided information about the length of time it takes for a population to be completely replaced with unlabelled cells.

The half-lives on monocyte subsets in the blood and BM were analysed using exponential curve fitting to the rate of decay of BrdU signal over time. It was clear that as blood monocytes were not actively cycling themselves all BrdU signal must come from their progenitor population replenishing the blood monocyte compartment. In contrast, BM Ly6C^{+} monocytes were found to be actively cycling, with approximately 15% of the population in S+G_2M phase. Thus, the BrdU^{+} fraction of BM Ly6C^{+} monocytes will have a combination of cells that are BrdU-labelled because they

themselves incorporated BrdU and others that have come into the BM Ly6C^{+} monocyte compartment from upstream progenitors. Nevertheless, the BrdU incorporation by MDP, cMoP, Ly6C^{+} BM monocytes and Ly6C^{int} MHC II^{+} BM monocytes all have very related kinetics: rapid incorporation of BrdU and rapid dilution of BrdU labelling in the compartment. The previously characterised development sequence of MDP upregulating Ly6C to become the cMoP, which in turn down regulate KIT to differentiate into BM Ly6C^{+} monocyte which then enter the blood as mature Ly6C^{+} monocytes (Auffray et al., 2009a; Fogg et al., 2006; Hettinger et al., 2013) show an anticipated delay as BrdU labelling moves downstream away from earlier progenitors. Interestingly, the Ly6C^{int} MHC II^{+} monocyte subset also follows this pattern and BrdU is incorporated into this subset rapidly following Ly6C^{+} monocytes. Analysis of the role of the chemokine receptor *Ccr2* is also consistent with this interpretation. Here, we demonstrate that *Ccr2* deficiency does not affect egress of the Ly6C^{low} MHC II^{-} monocytes: previously published data demonstrating a dramatic increase in the half-life of Ly6C^{low} monocytes after blocking of *Ccr2* with the antibody MC21, was interpreted as a possible compensatory survival of Ly6C^{low} monocytes in the absence of their precursor (Yona et al., 2013). In light of the data presented here, it seems probable that this observation corresponded to the decrease of the short lived Ly6C^{int} MHC II^{+} monocytes in the blood, thus, allowing the analysis of long-lived Ly6C^{low} MHC II^{-} monocytes without the influence of short lived Ly6C^{int} MHC II^{+} on half-life calculations.

The genetic and kinetic analyses of Ly6C^{int} MHC II^{+} monocytes indicate that this subset is the progeny of Ly6C^{+} monocytes. However, it is not clear whether the upregulation of MHC II and downregulation of Ly6C only occurs in the BM or if Ly6C^{+} monocytes can also undergo this differentiation step in the blood as well.

BrdU labelling of Ly6C^{low} MHC II^{-} monocytes in the blood begins after blood Ly6C^{+} monocytes have almost completely diluted out the BrdU labelling in that subset. In addition, BM Ly6C^{low} MHC II^{-} BrdU labelling appears to precede the blood labelling in a related manner. This was interpreted here, in conjunction with genetic data and adoptive transfer experiments, that blood Ly6C^{+} monocytes do not give rise to Ly6C^{low} MHC II^{-} monocytes in the blood. However, although not evidenced here, the possibility cannot be completely excluded that a small proportion of Ly6C^{+} monocytes do give rise to Ly6C^{low} MHC II^{-} monocytes within the blood. This is, in part, due to the few remaining Ly6C^{+} monocytes that are observed in the blood of *Irf8* and *Ccr2* deficient animals.

The identification of a cell surface marker specific for Ly6C^{low} MHC II^{-} monocytes would be incredibly useful, particularly for the BrdU incorporation experiments. The protocol involves several fixation/ permeablisation steps, which can pose a problem for combining with GFP-reporter cells as it is well documented that fixation/ permeabilisation protocols can cause leakage of cytoplasmic GFP. Whilst the *Nr4a1*^{GFP} transgene is fused to a Cre codon which in principal should ensure it's nuclear localisation (Shimshek et al., 2002), BrdU protocols require DNA denaturation to expose the BrdU signal. In optimising the BrdU incorporation experiment, this denaturation step was found to greatly reduce GFP signal. Thus the identification of a specific marker for Ly6C^{low} MHC II^{-} monocytes and their BM Ly6C^{low} CD11b^{+} intermediate would improve accuracy of analysis.

One limitation of the kinetic analysis experiments presented in this study is that we cannot label a single cell and trace it through its life span to fully understand its fate from HSC to maturity. An interesting way to establish the exact fate of monocytes from their progenitors would be to make use genetic barcoding techniques that have been

utilised in haematopoietic lineage tracing (Lu et al., 2011; Naik et al., 2013; Naik et al., 2014).

6.5 An updated model of the Ly6C^{low} monocyte development pathway

6.5.1 Bone marrow Ly6C^{+} monocytes – a progenitor population?

The results in this study indicate that Ly6C^{+} BM monocytes are a precursor population in there own right, capable of giving rise to at least three different blood monocyte populations. Calculating the relative compartment size of monocytes and their progenitors demonstrated that the BM Ly6C^{+} monocyte population is disproportionately expanded compared with blood Ly6C^{+} monocytes suggesting that it may be a precursor population to more than just blood monocyte populations. An interesting postulation is that this population is the direct precursor to gut macrophage populations, which are constantly replenished by *Ccr2*-dependent Ly6C^{+} monocytes (Bain et al., 2014). To clearly distinguish BM Ly6C^{+} monocytes as a bona fide precursor population, capable of giving rise to a number of different subsets, we suggest that it could be referred to as "common pro-monocyte" (cProM), following Shand *et al.,* who referred to BM monocytes as "pro-monocytes" (Shand et al., 2014) and with the prefix "common" to reflect the ability of this cell type to generate several distinct monocyte populations.

Further investigations into the cProM could provide great insight into the precursor potential and also inform on the heterogeneity within this population. This study has demonstrated that there are cells within the cProM with at least two different genetic dependencies: the majority of the population is *Irf8*- and *Ccr2*-dependent but a fraction of the population develops independently of these genes. An interesting way of investigating this could be by utilising the technology of mass cytometry (CyTOF),

which combines the resolution capabilities of mass spectrometry at the single cell level with traditional flow cytometry techniques but without the limitations of spectral overlap. Mass cytometry can allow analysis of multiple different antigens; both internal such as phosphoproteins and external cell surface markers, facilitating multiparameter single-cell characterisation of complex populations (Bendall et al., 2011).

6.5.2 A novel Ly6C^{low} CD11b^{+} NR4A1^{bright} monocyte intermediate

In the present study, it was possible to identify in the absence of irradiation and *in vivo* using two independent *Nr4a1*-deficient models, a novel BM *Nr4a1*-dependent Ly6C^{low} CD11b^{+} MHC II^{-} NR4A1^{bright} CX$_3$CR1^{bright} population. Systematic analysis of this population revealed that the differentiation block observed in the BM of *Nr4a1*-deficient animals (Hanna et al., 2011) occurs at this step in the Ly6C^{low} MHC II^{-} monocyte development pathway. Whilst this population is considerably reduced in *Nr4a1*-deficient animals, the few remaining cells were actively cycling yet were unable to fully mature, instead undergoing apoptosis, similarly to Ly6C^{low} MHC II^{-} BM monocytes. Furthermore, this population was slowly proliferating, in line with being an intermediate of a long-lived cell population and was shown to be capable of upregulating CD115 *in vitro*. Altogether, these data demonstrate the presence of an intermediate BM population between the "cProM" and BM Ly6C^{low} MHC II^{-} monocytes leading to the updated monocyte development pathway outlined below (Figure 6-2).

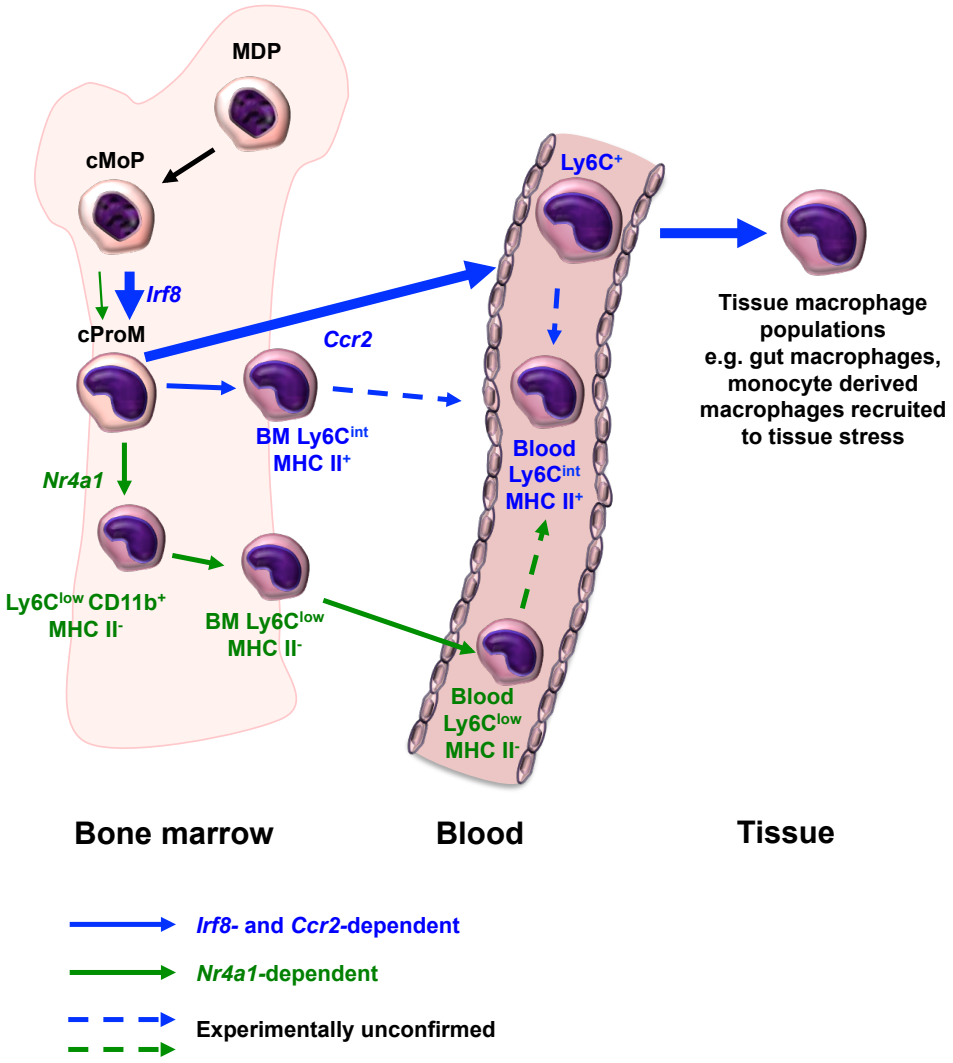

Figure 6-2 An updated model of monocyte development

6.6 The fate of Ly6C^{low} MHC II^{-} monocytes in steady state

This study further demonstrated that Ly6C^{low} MHC II^{-} monocytes are distinct from Ly6C^{+} monocytes in fate in the periphery. Interestingly, Ly6C^{low} MHC II^{-} monocytes were shown not contribute to tissue myeloid cells in a steady state, but apparently spend their lifespan within the vasculature, congruent with the reported 'patrolling' role of *Nr4a1*-dependent Ly6C^{low} monocytes as scavengers of the micro-vasculature (Auffray et al., 2007; Carlin et al., 2013; Devi et al., 2013; Michaud et al., 2013; Sumagin et al.,

2010). Ly6C^{low} MHC II^{-} monocytes, and their human CD14^{dim} CD16^{+} counterparts (Cros et al., 2010), have been shown to mediate intravascular inflammatory responses to viruses and nucleic acid signals, facilitate IgG-dependent effector functions and are implicated in diseases with nucleic acid aetiology, such as viral infections and Systemic Lupus Erythematosus (Amano et al., 2005; Biburger et al., 2011; Carlin et al., 2013; Cros et al., 2010; Daley-Bauer et al., 2014; Devi et al., 2013; Santiago-Raber et al., 2009).

This study investigated a number of different tissue myeloid populations including brain, spleen, liver and skin; it is by no means exhaustive analysis of all tissue macrophage populations, therefore it is impossible to conclude that Ly6C^{low} MHC II^{-} monocytes do not contribute to any tissue macrophage populations in the steady state. However, we infer that it seems highly unlikely as the evidence presented here demonstrates that absence of Ly6C^{low} MHC II^{-} monocytes did not directly affect any of the macrophage populations analysed. Thus, it can be inferred from the data presented here that Ly6C^{low} MHC II^{-} monocytes remain in the circulation throughout their life span, and their effector functions in steady state are carried out from within blood vessels.

6.7 What genes does *Nr4a1* regulate during monopoiesis?

Nr4a family members are known to regulate gene expression and are involved in a wide range of physiological processes (Bonta et al., 2006; Boudreaux et al., 2012; Liu et al., 2003; Sekiya et al., 2013). The absolute requirement of *Nr4a1* for Ly6C^{low} MHC II^{-} monocytes is interesting as there is a level of functional redundancy within the *Nr4a* family, which is partly attributed to the ability of all three family members to trans-activate the same Nur-response element (Chao et al., 2013; Cheng et al., 1997; Sekiya et

al., 2013). However, the data presented here demonstrate that for Ly6C^{low} MHC II^{-} monocyte development, *Nr4a1* is essential and that other Nr4a family members cannot compensate its absence. Furthermore, a strong haploinsufficiency was observed, a finding that is reminiscent of the gene dosage effect reported for other members of the Nr4a family during haematopoiesis (Ramirez-Herrick et al., 2011). The molecular mechanisms and control of gene expression that *Nr4a1* exerts during Ly6C^{low} MHC II^{-} monocyte development would be extremely interesting to investigate further.

The transcriptional activity of Nr4a family members is thought to be regulated by their expression levels in combination with co-activators (Rambaud et al., 2009; Rosenfeld et al., 2006; Wansa et al., 2002; Wansa et al., 2003; Wansa and Muscat, 2005), co-repressors (Sohn et al., 2001) and post translational modifications (Hermanson et al., 2002; Kang et al., 2010; Katagiri et al., 1997). One such regulator of *Nr4a1* activity is the member of the small interferon stimulated gene family, *Isg12* (interferon stimulatory gene 12) (Papac-Milicevic et al., 2012). ISG12 is an interaction partner of NR4A1 and upon its upregulation, ISG12 has been shown to mediate the translocation of NR4A1 from the nucleus to the cytoplasm, thus reducing the availability of NR4A1 to bind DNA thus activating transcription (Papac-Milicevic et al., 2012; Uhrin et al., 2013). It would be interesting to investigate whether *Isg12*$^{-/-}$ mice have a phenotype in the Ly6C^{low} MHC II^{-} monocyte compartment.

An unbiased approach would to be to use genome wide analysis to investigate the transcriptional and epigenetic networks of the differing monocyte subsets using high-throughput genome-wide sequencing assays such as RNA-sequencing (RNA-seq), chromatin immunoprecipitation sequencing (ChIP-seq) and assay for trasnposase accessible chromatin sequencing (ATAC-seq). RNA-seq would information on the global gene expression profiles of monocyte subsets (RNA-seq), genome wide profiling

of histone modifications (ChIP-seq) and analysis of open (therefore accessible for protein binding) chromatin regions. Together, these data could shed interesting light into the cellular identity of monocyte subsets, which could potentially provide further information on their ontogeny.

6.8 General conclusion

To conclude; within the monocyte compartment, there are at least two genetically distinct monocyte lineages, one which requires *Irf8* for development and *Ccr2* for migration from the BM to the periphery and a second lineage which is completely dependent upon *Nr4a1* for its development in the BM from the Ly6C^{+} common pro-monocyte.

The loss of *Nr4a1* resulted in the absence of Ly6C^{low} MHC II^{-} monocytes in the BM and periphery due to a differentiation block in the BM at the point of a newly identified BM Ly6C^{low} CD11b^{+} CD115^{low} NR4A1^{bright} intermediate. This intermediate population was also shown to be the transitional step between Ly6C^{+} common pro-monocyte population and Ly6C^{low} MHC II^{-} monocytes.

Finally, this thesis demonstrates that the fate of Ly6C^{low} MHC II^{-} monocytes is to remain within the circulation and these cells do not contribute to tissue macrophage populations in the steady state.

7 References

Adolfsson, J., Mansson, R., Buza-Vidas, N., Hultquist, A., Liuba, K., Jensen, C.T., Bryder, D., Yang, L., Borge, O.J., Thoren, L.A*., et al.* (2005). Identification of Flt3+ lympho-myeloid stem cells lacking erythro-megakaryocytic potential a revised road map for adult blood lineage commitment. Cell *121*, 295-306.

Akashi, K., Kondo, M., Cheshier, S., Shizuru, J., Gandy, K., Domen, J., Mebius, R., Traver, D., and Weissman, I.L. (1999). Lymphoid development from stem cells and the common lymphocyte progenitors. Cold Spring Harb Symp Quant Biol *64*, 1-12.

Akashi, K., Traver, D., Miyamoto, T., and Weissman, I.L. (2000). A clonogenic common myeloid progenitor that gives rise to all myeloid lineages. Nature *404*, 193-197.

Alder, J.K., Georgantas, R.W., 3rd, Hildreth, R.L., Kaplan, I.M., Morisot, S., Yu, X., McDevitt, M., and Civin, C.I. (2008). Kruppel-like factor 4 is essential for inflammatory monocyte differentiation in vivo. J Immunol *180*, 5645-5652.

Aldridge, J.R., Jr., Moseley, C.E., Boltz, D.A., Negovetich, N.J., Reynolds, C., Franks, J., Brown, S.A., Doherty, P.C., Webster, R.G., and Thomas, P.G. (2009). TNF/iNOS-producing dendritic cells are the necessary evil of lethal influenza virus infection. Proc Natl Acad Sci U S A *106*, 5306-5311.

Amano, H., Amano, E., Santiago-Raber, M.L., Moll, T., Martinez-Soria, E., Fossati-Jimack, L., Iwamoto, M., Rozzo, S.J., Kotzin, B.L., and Izui, S. (2005). Selective expansion of a monocyte subset expressing the CD11c dendritic cell marker in the Yaa model of systemic lupus erythematosus. Arthritis Rheum *52*, 2790-2798.

Ancuta, P., Autissier, P., Wurcel, A., Zaman, T., Stone, D., and Gabuzda, D. (2006). CD16+ monocyte-derived macrophages activate resting T cells for HIV infection by producing CCR3 and CCR4 ligands. J Immunol *176*, 5760-5771.

Ancuta, P., Moses, A., and Gabuzda, D. (2004). Transendothelial migration of CD16+ monocytes in response to fractalkine under constitutive and inflammatory conditions. Immunobiology *209*, 11-20.

Ancuta, P., Rao, R., Moses, A., Mehle, A., Shaw, S.K., Luscinskas, F.W., and Gabuzda, D. (2003). Fractalkine preferentially mediates arrest and migration of CD16+ monocytes. J Exp Med *197*, 1701-1707.

Auffray, C., Fogg, D., Garfa, M., Elain, G., Join-Lambert, O., Kayal, S., Sarnacki, S., Cumano, A., Lauvau, G., and Geissmann, F. (2007). Monitoring of blood vessels and tissues by a population of monocytes with patrolling behavior. Science *317*, 666-670.

Auffray, C., Fogg, D.K., Narni-Mancinelli, E., Senechal, B., Trouillet, C., Saederup, N., Leemput, J., Bigot, K., Campisi, L., Abitbol, M*., et al.* (2009a). CX3CR1+ CD115+ CD135+ common macrophage/DC precursors and the role of CX3CR1 in their response to inflammation. J Exp Med *206*, 595-606.

Auffray, C., Sieweke, M.H., and Geissmann, F. (2009b). Blood monocytes: development, heterogeneity, and relationship with dendritic cells. Annu Rev Immunol *27*, 669-692.

Bain, C.C., Bravo-Blas, A., Scott, C.L., Gomez Perdiguero, E., Geissmann, F., Henri, S., Malissen, B., Osborne, L.C., Artis, D., and Mowat, A.M. (2014). Constant replenishment from circulating monocytes maintains the macrophage pool in the intestine of adult mice. Nat Immunol.

Barbalat, R., Lau, L., Locksley, R.M., and Barton, G.M. (2009). Toll-like receptor 2 on inflammatory monocytes induces type I interferon in response to viral but not bacterial ligands. Nat Immunol *10*, 1200-1207.

Bendall, S.C., Simonds, E.F., Qiu, P., Amir el, A.D., Krutzik, P.O., Finck, R., Bruggner, R.V., Melamed, R., Trejo, A., Ornatsky, O.I.*, et al.* (2011). Single-cell mass cytometry of differential immune and drug responses across a human hematopoietic continuum. Science *332*, 687-696.

Benz, C., Martins, V.C., Radtke, F., and Bleul, C.C. (2008). The stream of precursors that colonizes the thymus proceeds selectively through the early T lineage precursor stage of T cell development. J Exp Med *205*, 1187-1199.

Bertrand, J.Y., Jalil, A., Klaine, M., Jung, S., Cumano, A., and Godin, I. (2005). Three pathways to mature macrophages in the early mouse yolk sac. Blood *106*, 3004-3011.

Biburger, M., Aschermann, S., Schwab, I., Lux, A., Albert, H., Danzer, H., Woigk, M., Dudziak, D., and Nimmerjahn, F. (2011). Monocyte subsets responsible for immunoglobulin G-dependent effector functions in vivo. Immunity *35*, 932-944.

Biburger, M., Trenkwald, I., and Nimmerjahn, F. (2015). yThree blocks are not enough - Blocking of the murine IgG receptor FcgammaRIV is crucial for proper characterization of cells by FACS analysis. Eur J Immunol.

Biswas, S.K., and Mantovani, A. (2010). Macrophage plasticity and interaction with lymphocyte subsets: cancer as a paradigm. Nat Immunol *11*, 889-896.

Boisset, J.C., van Cappellen, W., Andrieu-Soler, C., Galjart, N., Dzierzak, E., and Robin, C. (2010). In vivo imaging of haematopoietic cells emerging from the mouse aortic endothelium. Nature *464*, 116-120.

Bonta, P.I., van Tiel, C.M., Vos, M., Pols, T.W., van Thienen, J.V., Ferreira, V., Arkenbout, E.K., Seppen, J., Spek, C.A., van der Poll, T.*, et al.* (2006). Nuclear receptors Nur77, Nurr1, and NOR-1 expressed in atherosclerotic lesion macrophages reduce lipid loading and inflammatory responses. Arterioscler Thromb Vasc Biol *26*, 2288-2294.

Boring, L., Gosling, J., Chensue, S.W., Kunkel, S.L., Farese, R.V., Jr., Broxmeyer, H.E., and Charo, I.F. (1997). Impaired monocyte migration and reduced type 1 (Th1) cytokine responses in C-C chemokine receptor 2 knockout mice. J Clin Invest *100*, 2552-2561.

Boudreaux, S.P., Ramirez-Herrick, A.M., Duren, R.P., and Conneely, O.M. (2012). Genome-wide profiling reveals transcriptional repression of MYC as a core component of NR4A tumor suppression in acute myeloid leukemia. Oncogenesis *1*, e19.

Bruhl, H., Cihak, J., Plachy, J., Kunz-Schughart, L., Niedermeier, M., Denzel, A., Rodriguez Gomez, M., Talke, Y., Luckow, B., Stangassinger, M.*, et al.* (2007). Targeting of Gr-1+,CCR2+ monocytes in collagen-induced arthritis. Arthritis Rheum *56*, 2975-2985.

Bruttger, J., Karram, K., Wortge, S., Regen, T., Marini, F., Hoppmann, N., Klein, M., Blank, T., Yona, S., Wolf, Y.*, et al.* (2015). Genetic Cell Ablation Reveals Clusters of Local Self-Renewing Microglia in the Mammalian Central Nervous System. Immunity *43*, 92-106.

Busch, K., Klapproth, K., Barile, M., Flossdorf, M., Holland-Letz, T., Schlenner, S.M., Reth, M., Hofer, T., and Rodewald, H.R. (2015). Fundamental properties of unperturbed haematopoiesis from stem cells in vivo. Nature *518*, 542-546.

Carlin, L.M., Stamatiades, E.G., Auffray, C., Hanna, R.N., Glover, L., Vizcay-Barrena, G., Hedrick, C.C., Cook, H.T., Diebold, S., and Geissmann, F. (2013). Nr4a1-dependent Ly6Clow monocytes monitor endothelial cells and orchestrate their disposal. Cell *153*, 362-375.

Carrel, A., and Ebeling, A.H. (1926). The Fundamental Properties of the Fibroblast and the Macrophage : Ii. The Macrophage. J Exp Med *44*, 285-305.

Challen, G.A., Boles, N., Lin, K.K., and Goodell, M.A. (2009). Mouse hematopoietic stem cell identification and analysis. Cytometry Part A : the journal of the International Society for Analytical Cytology *75*, 14-24.

Chao, L.C., Soto, E., Hong, C., Ito, A., Pei, L., Chawla, A., Conneely, O.M., Tangirala, R.K., Evans, R.M., and Tontonoz, P. (2013). Bone marrow NR4A expression is not a dominant factor in the development of atherosclerosis or macrophage polarization in mice. J Lipid Res *54*, 806-815.

Chawla, A., Nguyen, K.D., and Goh, Y.P. (2011). Macrophage-mediated inflammation in metabolic disease. Nat Rev Immunol *11*, 738-749.

Chen, G., Zhuchenko, O., and Kuspa, A. (2007). Immune-like phagocyte activity in the social amoeba. Science *317*, 678-681.

Chen, M.J., Yokomizo, T., Zeigler, B.M., Dzierzak, E., and Speck, N.A. (2009). Runx1 is required for the endothelial to haematopoietic cell transition but not thereafter. Nature *457*, 887-891.

Cheng, L.E., Chan, F.K., Cado, D., and Winoto, A. (1997). Functional redundancy of the Nur77 and Nor-1 orphan steroid receptors in T-cell apoptosis. EMBO J *16*, 1865-1875.

Chorro, L., Sarde, A., Li, M., Woollard, K.J., Chambon, P., Malissen, B., Kissenpfennig, A., Barbaroux, J.B., Groves, R., and Geissmann, F. (2009). Langerhans cell (LC) proliferation mediates neonatal development, homeostasis, and inflammation-associated expansion of the epidermal LC network. J Exp Med *206*, 3089-3100.

Christensen, J.L., and Weissman, I.L. (2001). Flk-2 is a marker in hematopoietic stem cell differentiation: a simple method to isolate long-term stem cells. Proc Natl Acad Sci U S A *98*, 14541-14546.

Colucci, F., Samson, S.I., DeKoter, R.P., Lantz, O., Singh, H., and Di Santo, J.P. (2001). Differential requirement for the transcription factor PU.1 in the generation of natural killer cells versus B and T cells. Blood *97*, 2625-2632.

Colvin, G.A., Lambert, J.F., Abedi, M., Hsieh, C.C., Carlson, J.E., Stewart, F.M., and Quesenberry, P.J. (2004). Murine marrow cellularity and the concept of stem cell competition: geographic and quantitative determinants in stem cell biology. Leukemia *18*, 575-583.

Colvin, G.A., Lambert, J.F., Carlson, J.E., and Quesenberry, P.J. (2000). Total murine marrow cellularity and the concept of marrow stem cell competition. Blood *96*, 116B-116B.

Combadiere, C., Potteaux, S., Rodero, M., Simon, T., Pezard, A., Esposito, B., Merval, R., Proudfoot, A., Tedgui, A., and Mallat, Z. (2008). Combined inhibition of CCL2, CX3CR1, and CCR5 abrogates Ly6C(hi) and Ly6C(lo) monocytosis and almost abolishes atherosclerosis in hypercholesterolemic mice. Circulation *117*, 1649-1657.

Cooper, A.M. (2009). Cell-mediated immune responses in tuberculosis. Annu Rev Immunol *27*, 393-422.

Corish, P., and Tyler-Smith, C. (1999). Attenuation of green fluorescent protein half-life in mammalian cells. Protein engineering *12*, 1035-1040.

Crisan, M., Kartalaei, P.S., Vink, C., Yamada-Inagawa, T., Bollerot, K., van, I.W., van der Linden, R., de Sousa Lopes, S.M., Monteiro, R., Mummery, C.*, et al.* (2015). BMP signalling differentially regulates distinct haematopoietic stem cell types. Nature communications *6*, 8040.

Cros, J., Cagnard, N., Woollard, K., Patey, N., Zhang, S.Y., Senechal, B., Puel, A., Biswas, S.K., Moshous, D., Picard, C.*, et al.* (2010). Human CD14dim monocytes patrol and sense nucleic acids and viruses via TLR7 and TLR8 receptors. Immunity *33*, 375-386.

Cross, M.A., and Enver, T. (1997). The lineage commitment of haemopoietic progenitor cells. Curr Opin Genet Dev *7*, 609-613.

Cumano, A., and Godin, I. (2007). Ontogeny of the hematopoietic system. Annu Rev Immunol *25*, 745-785.

D'Agostino, R.B., and Stephens, M.A. (1986). Goodness-of-fit techniques (New York ; Basel: Marcel Dekker).

Dai, X.M., Ryan, G.R., Hapel, A.J., Dominguez, M.G., Russell, R.G., Kapp, S., Sylvestre, V., and Stanley, E.R. (2002). Targeted disruption of the mouse colony-stimulating factor 1 receptor gene results in osteopetrosis, mononuclear phagocyte deficiency, increased primitive progenitor cell frequencies, and reproductive defects. Blood *99*, 111-120.

Dakic, A., Metcalf, D., Di Rago, L., Mifsud, S., Wu, L., and Nutt, S.L. (2005). PU.1 regulates the commitment of adult hematopoietic progenitors and restricts granulopoiesis. J Exp Med *201*, 1487-1502.

Daley-Bauer, L.P., Roback, L.J., Wynn, G.M., and Mocarski, E.S. (2014). Cytomegalovirus hijacks CX3CR1(hi) patrolling monocytes as immune-privileged vehicles for dissemination in mice. Cell host & microbe *15*, 351-362.

Davies, L.C., Jenkins, S.J., Allen, J.E., and Taylor, P.R. (2013a). Tissue-resident macrophages. Nat Immunol *14*, 986-995.

Davies, L.C., Rosas, M., Jenkins, S.J., Liao, C.T., Scurr, M.J., Brombacher, F., Fraser, D.J., Allen, J.E., Jones, S.A., and Taylor, P.R. (2013b). Distinct bone marrow-derived and tissue-resident macrophage lineages proliferate at key stages during inflammation. Nature communications *4*, 1886.

Davies, L.C., Rosas, M., Smith, P.J., Fraser, D.J., Jones, S.A., and Taylor, P.R. (2011). A quantifiable proliferative burst of tissue macrophages restores homeostatic macrophage populations after acute inflammation. Eur J Immunol *41*, 2155-2164.

Davis, M.I., and Puhl, H.L., 3rd (2011). Nr4a1-eGFP is a marker of striosome-matrix architecture, development and activity in the extended striatum. PLoS One *6*, e16619.

Dawson, T.C., Beck, M.A., Kuziel, W.A., Henderson, F., and Maeda, N. (2000). Contrasting effects of CCR5 and CCR2 deficiency in the pulmonary inflammatory response to influenza A virus. Am J Pathol *156*, 1951-1959.

Debien, E., Mayol, K., Biajoux, V., Daussy, C., De Aguero, M.G., Taillardet, M., Dagany, N., Brinza, L., Henry, T., Dubois, B.*, et al.* (2013). S1PR5 is pivotal for the homeostasis of patrolling monocytes. Eur J Immunol.

den Haan, J.M., and Kraal, G. (2012). Innate immune functions of macrophage subpopulations in the spleen. J Innate Immun *4*, 437-445.

Deng, L., Zhou, J.F., Sellers, R.S., Li, J.F., Nguyen, A.V., Wang, Y., Orlofsky, A., Liu, Q., Hume, D.A., Pollard, J.W.*, et al.* (2010). A novel mouse model of inflammatory bowel disease links mammalian target of rapamycin-dependent hyperproliferation of colonic epithelium to inflammation-associated tumorigenesis. Am J Pathol *176*, 952-967.

Devi, S., Li, A., Westhorpe, C.L., Lo, C.Y., Abeynaike, L.D., Snelgrove, S.L., Hall, P., Ooi, J.D., Sobey, C.G., Kitching, A.R.*, et al.* (2013). Multiphoton imaging reveals a new leukocyte recruitment paradigm in the glomerulus. Nat Med *19*, 107-112.

Diserbo, M., Agin, A., Lamproglou, I., Mauris, J., Staali, F., Multon, E., and Amourette, C. (2002). Blood-brain barrier permeability after gamma whole-body irradiation: an in vivo microdialysis study. Can J Physiol Pharmacol *80*, 670-678.

Dominguez, P.M., and Ardavin, C. (2010). Differentiation and function of mouse monocyte-derived dendritic cells in steady state and inflammation. Immunol Rev *234*, 90-104.

Doyle, A.G., Herbein, G., Montaner, L.J., Minty, A.J., Caput, D., Ferrara, P., and Gordon, S. (1994). Interleukin-13 alters the activation state of murine macrophages in vitro: comparison with interleukin-4 and interferon-gamma. Eur J Immunol *24*, 1441-1445.

Eaves, C.J. (2015). Hematopoietic stem cells: concepts, definitions, and the new reality. Blood *125*, 2605-2613.

Ebert, R.H., and Florey, H.W. (1939). The extravascular development of the monocyte observed in vivo. British journal of experimental pathology *20*, 342-356.

Ehrlich, P. (1956). Collected papers of Paul Ehrlich; in four volumes including a complete bibliography (London, New York,: Pergamon Press).

Enver, T., Heyworth, C.M., and Dexter, T.M. (1998). Do stem cells play dice? Blood *92*, 348-351; discussion 352.

Esashi, E., Sekiguchi, T., Ito, H., Koyasu, S., and Miyajima, A. (2003). Cutting Edge: A possible role for CD4+ thymic macrophages as professional scavengers of apoptotic thymocytes. J Immunol *171*, 2773-2777.

Fang, F.C. (2004). Antimicrobial reactive oxygen and nitrogen species: concepts and controversies. Nat Rev Microbiol *2*, 820-832.

Feinberg, M.W., Wara, A.K., Cao, Z., Lebedeva, M.A., Rosenbauer, F., Iwasaki, H., Hirai, H., Katz, J.P., Haspel, R.L., Gray, S.*, et al.* (2007). The Kruppel-like factor KLF4 is a critical regulator of monocyte differentiation. EMBO J *26*, 4138-4148.

Fogg, D.K., Sibon, C., Miled, C., Jung, S., Aucouturier, P., Littman, D.R., Cumano, A., and Geissmann, F. (2006). A clonogenic bone marrow progenitor specific for macrophages and dendritic cells. Science *311*, 83-87.

Franklin, R.A., Liao, W., Sarkar, A., Kim, M.V., Bivona, M.R., Liu, K., Pamer, E.G., and Li, M.O. (2014). The cellular and molecular origin of tumor-associated macrophages. Science *344*, 921-925.

Galkina, E., and Ley, K. (2009). Immune and inflammatory mechanisms of atherosclerosis (*). Annu Rev Immunol *27*, 165-197.

Gazzinelli, R.T., Hieny, S., Wynn, T.A., Wolf, S., and Sher, A. (1993). Interleukin 12 is required for the T-lymphocyte-independent induction of interferon gamma by an intracellular parasite and induces resistance in T-cell-deficient hosts. Proc Natl Acad Sci U S A *90*, 6115-6119.

Geissmann, F., Jung, S., and Littman, D.R. (2003). Blood monocytes consist of two principal subsets with distinct migratory properties. Immunity *19*, 71-82.

Gerrity, R.G., Naito, H.K., Richardson, M., and Schwartz, C.J. (1979). Dietary induced atherogenesis in swine. Morphology of the intima in prelesion stages. Am J Pathol *95*, 775-792.

Ghosn, E.E., Cassado, A.A., Govoni, G.R., Fukuhara, T., Yang, Y., Monack, D.M., Bortoluci, K.R., Almeida, S.R., Herzenberg, L.A., and Herzenberg, L.A. (2010). Two

physically, functionally, and developmentally distinct peritoneal macrophage subsets. Proc Natl Acad Sci U S A *107*, 2568-2573.

Giese, N.A., Gabriele, L., Doherty, T.M., Klinman, D.M., Tadesse-Heath, L., Contursi, C., Epstein, S.L., and Morse, H.C., 3rd (1997). Interferon (IFN) consensus sequence-binding protein, a transcription factor of the IFN regulatory factor family, regulates immune responses in vivo through control of interleukin 12 expression. J Exp Med *186*, 1535-1546.

Girgis, N.M., Gundra, U.M., Ward, L.N., Cabrera, M., Frevert, U., and Loke, P. (2014). Ly6C(high) monocytes become alternatively activated macrophages in schistosome granulomas with help from CD4+ cells. PLoS Pathog *10*, e1004080.

Golub, R., and Cumano, A. (2013). Embryonic hematopoiesis. Blood Cells Mol Dis *51*, 226-231.

Gomez Perdiguero, E., Klapproth, K., Schulz, C., Busch, K., Azzoni, E., Crozet, L., Garner, H., Trouillet, C., de Bruijn, M.F., Geissmann, F.*, et al.* (2015). Tissue-resident macrophages originate from yolk-sac-derived erythro-myeloid progenitors. Nature *518*, 547-551.

Gomez Perdiguero, E., Schulz, C., and Geissmann, F. (2013). Development and homeostasis of "resident" myeloid cells: the case of the microglia. Glia *61*, 112-120.

Gordon, S. (2008). Elie Metchnikoff: father of natural immunity. Eur J Immunol *38*, 3257-3264.

Gordon, S., and Martinez, F.O. (2010). Alternative activation of macrophages: mechanism and functions. Immunity *32*, 593-604.

Gordon, S., and Taylor, P.R. (2005). Monocyte and macrophage heterogeneity. Nat Rev Immunol *5*, 953-964.

Grage-Griebenow, E., Flad, H.D., and Ernst, M. (2001a). Heterogeneity of human peripheral blood monocyte subsets. J Leukoc Biol *69*, 11-20.

Grage-Griebenow, E., Flad, H.D., Ernst, M., Bzowska, M., Skrzeczynska, J., and Pryjma, J. (2000). Human MO subsets as defined by expression of CD64 and CD16 differ in phagocytic activity and generation of oxygen intermediates. Immunobiology *202*, 42-50.

Grage-Griebenow, E., Zawatzky, R., Kahlert, H., Brade, L., Flad, H., and Ernst, M. (2001b). Identification of a novel dendritic cell-like subset of CD64(+) / CD16(+) blood monocytes. Eur J Immunol *31*, 48-56.

Gray, E.E., and Cyster, J.G. (2012). Lymph node macrophages. J Innate Immun *4*, 424-436.

Hahn, C., and Schwartz, M.A. (2009). Mechanotransduction in vascular physiology and atherogenesis. Nat Rev Mol Cell Biol *10*, 53-62.

Halpern, B.N. (1959). The role and function of the reticulo-endothelial system in immunological processes. J Pharm Pharmacol *11*, 321-338.

Hambleton, S., Salem, S., Bustamante, J., Bigley, V., Boisson-Dupuis, S., Azevedo, J., Fortin, A., Haniffa, M., Ceron-Gutierrez, L., Bacon, C.M., *et al.* (2011). IRF8 mutations and human dendritic-cell immunodeficiency. N Engl J Med *365*, 127-138.

Hanna, R.N., Carlin, L.M., Hubbeling, H.G., Nackiewicz, D., Green, A.M., Punt, J.A., Geissmann, F., and Hedrick, C.C. (2011). The transcription factor NR4A1 (Nur77) controls bone marrow differentiation and the survival of Ly6C- monocytes. Nat Immunol *12*, 778-785.

Hanna, R.N., Shaked, I., Hubbeling, H.G., Punt, J.A., Wu, R., Herrley, E., Zaugg, C., Pei, H., Geissmann, F., Ley, K., *et al.* (2012). NR4A1 (Nur77) deletion polarizes macrophages toward an inflammatory phenotype and increases atherosclerosis. Circ Res *110*, 416-427.

Harkness, J.E., and Wagner, J.E. (1995). The biology and medicine of rabbits and rodents, 4th edn (Baltimore: Williams & Wilkins).

Hashimoto, D., Chow, A., Noizat, C., Teo, P., Beasley, M.B., Leboeuf, M., Becker, C.D., See, P., Price, J., Lucas, D., *et al.* (2013). Tissue-resident macrophages self-maintain locally throughout adult life with minimal contribution from circulating monocytes. Immunity *38*, 792-804.

Havran, W.L., and Allison, J.P. (1988). Developmentally ordered appearance of thymocytes expressing different T-cell antigen receptors. Nature *335*, 443-445.

Havran, W.L., and Allison, J.P. (1990). Origin of Thy-1+ dendritic epidermal cells of adult mice from fetal thymic precursors. Nature *344*, 68-70.

Herbert, D.R., Orekov, T., Roloson, A., Ilies, M., Perkins, C., O'Brien, W., Cederbaum, S., Christianson, D.W., Zimmermann, N., Rothenberg, M.E., *et al.* (2010). Arginase I suppresses IL-12/IL-23p40-driven intestinal inflammation during acute schistosomiasis. J Immunol *184*, 6438-6446.

Herbomel, P., Thisse, B., and Thisse, C. (1999). Ontogeny and behaviour of early macrophages in the zebrafish embryo. Development *126*, 3735-3745.

Hermanson, O., Glass, C.K., and Rosenfeld, M.G. (2002). Nuclear receptor coregulators: multiple modes of modification. Trends Endocrinol Metab *13*, 55-60.

Herzenberg, L.A., and Herzenberg, L.A. (1989). Toward a layered immune system. Cell *59*, 953-954.

Hettinger, J., Richards, D.M., Hansson, J., Barra, M.M., Joschko, A.C., Krijgsveld, J., and Feuerer, M. (2013). Origin of monocytes and macrophages in a committed progenitor. Nat Immunol *14*, 821-830.

Hilgendorf, I., Gerhardt, L.M., Tan, T.C., Winter, C., Holderried, T.A., Chousterman, B.G., Iwamoto, Y., Liao, R., Zirlik, A., Scherer-Crosbie, M., *et al.* (2014). Ly-6Chigh monocytes depend on Nr4a1 to balance both inflammatory and reparative phases in the infarcted myocardium. Circ Res *114*, 1611-1622.

Hoeffel, G., Chen, J., Lavin, Y., Low, D., Almeida, F.F., See, P., Beaudin, A.E., Lum, J., Low, I., Forsberg, E.C., *et al.* (2015). C-Myb(+) erythro-myeloid progenitor-derived fetal monocytes give rise to adult tissue-resident macrophages. Immunity *42*, 665-678.

Holtschke, T., Lohler, J., Kanno, Y., Fehr, T., Giese, N., Rosenbauer, F., Lou, J., Knobeloch, K.P., Gabriele, L., Waring, J.F., *et al.* (1996). Immunodeficiency and chronic myelogenous leukemia-like syndrome in mice with a targeted mutation of the ICSBP gene. Cell *87*, 307-317.

http://phenome.jax.org. Monocyte differential (percent of total WBC) [%].

http://www.1728.org/diam.htm. Circle, sphere & cylinder calculator.

Hu, M., Krause, D., Greaves, M., Sharkis, S., Dexter, M., Heyworth, C., and Enver, T. (1997). Multilineage gene expression precedes commitment in the hemopoietic system. Genes & development *11*, 774-785.

Ikuta, K., Kina, T., MacNeil, I., Uchida, N., Peault, B., Chien, Y.H., and Weissman, I.L. (1990). A developmental switch in thymic lymphocyte maturation potential occurs at the level of hematopoietic stem cells. Cell *62*, 863-874.

Ingersoll, M.A., Spanbroek, R., Lottaz, C., Gautier, E.L., Frankenberger, M., Hoffmann, R., Lang, R., Haniffa, M., Collin, M., Tacke, F., *et al.* (2010). Comparison of gene expression profiles between human and mouse monocyte subsets. Blood *115*, e10-19.

Iwasaki, H., Somoza, C., Shigematsu, H., Duprez, E.A., Iwasaki-Arai, J., Mizuno, S., Arinobu, Y., Geary, K., Zhang, P., Dayaram, T., *et al.* (2005). Distinctive and indispensable roles of PU.1 in maintenance of hematopoietic stem cells and their differentiation. Blood *106*, 1590-1600.

Jakubzick, C., Gautier, E.L., Gibbings, S.L., Sojka, D.K., Schlitzer, A., Johnson, T.E., Ivanov, S., Duan, Q., Bala, S., Condon, T., *et al.* (2013). Minimal differentiation of classical monocytes as they survey steady-state tissues and transport antigen to lymph nodes. Immunity *39*, 599-610.

Jakubzick, C., Tacke, F., Ginhoux, F., Wagers, A.J., van Rooijen, N., Mack, M., Merad, M., and Randolph, G.J. (2008). Blood monocyte subsets differentially give rise to CD103+ and CD103- pulmonary dendritic cell populations. J Immunol *180*, 3019-3027.

Jenkins, S.J., Ruckerl, D., Cook, P.C., Jones, L.H., Finkelman, F.D., van Rooijen, N., MacDonald, A.S., and Allen, J.E. (2011). Local macrophage proliferation, rather than recruitment from the blood, is a signature of TH2 inflammation. Science *332*, 1284-1288.

Jenkins, S.J., Ruckerl, D., Thomas, G.D., Hewitson, J.P., Duncan, S., Brombacher, F., Maizels, R.M., Hume, D.A., and Allen, J.E. (2013). IL-4 directly signals tissue-resident macrophages to proliferate beyond homeostatic levels controlled by CSF-1. J Exp Med *210*, 2477-2491.

Jia, T., Leiner, I., Dorothee, G., Brandl, K., and Pamer, E.G. (2009). MyD88 and Type I interferon receptor-mediated chemokine induction and monocyte recruitment during Listeria monocytogenes infection. J Immunol *183*, 1271-1278.

Jia, T., Serbina, N.V., Brandl, K., Zhong, M.X., Leiner, I.M., Charo, I.F., and Pamer, E.G. (2008). Additive roles for MCP-1 and MCP-3 in CCR2-mediated recruitment of inflammatory monocytes during Listeria monocytogenes infection. J Immunol *180*, 6846-6853.

Jung, S., Aliberti, J., Graemmel, P., Sunshine, M.J., Kreutzberg, G.W., Sher, A., and Littman, D.R. (2000). Analysis of fractalkine receptor CX(3)CR1 function by targeted deletion and green fluorescent protein reporter gene insertion. Mol Cell Biol *20*, 4106-4114.

Kadkhodaei, B., Ito, T., Joodmardi, E., Mattsson, B., Rouillard, C., Carta, M., Muramatsu, S., Sumi-Ichinose, C., Nomura, T., Metzger, D*., et al.* (2009). Nurr1 is required for maintenance of maturing and adult midbrain dopamine neurons. J Neurosci *29*, 15923-15932.

Kanda, H., Tateya, S., Tamori, Y., Kotani, K., Hiasa, K., Kitazawa, R., Kitazawa, S., Miyachi, H., Maeda, S., Egashira, K*., et al.* (2006). MCP-1 contributes to macrophage infiltration into adipose tissue, insulin resistance, and hepatic steatosis in obesity. J Clin Invest *116*, 1494-1505.

Kang, S.A., Na, H., Kang, H.J., Kim, S.H., Lee, M.H., and Lee, M.O. (2010). Regulation of Nur77 protein turnover through acetylation and deacetylation induced by p300 and HDAC1. Biochem Pharmacol *80*, 867-873.

Katagiri, Y., Hirata, Y., Milbrandt, J., and Guroff, G. (1997). Differential regulation of the transcriptional activity of the orphan nuclear receptor NGFI-B by membrane depolarization and nerve growth factor. J Biol Chem *272*, 31278-31284.

Kierdorf, K., Erny, D., Goldmann, T., Sander, V., Schulz, C., Perdiguero, E.G., Wieghofer, P., Heinrich, A., Riemke, P., Holscher, C*., et al.* (2013a). Microglia emerge from erythromyeloid precursors via Pu.1- and Irf8-dependent pathways. Nat Neurosci *16*, 273-280.

Kierdorf, K., Katzmarski, N., Haas, C.A., and Prinz, M. (2013b). Bone marrow cell recruitment to the brain in the absence of irradiation or parabiosis bias. PLoS One *8*, e58544.

Kobayashi, N., Karisola, P., Pena-Cruz, V., Dorfman, D.M., Jinushi, M., Umetsu, S.E., Butte, M.J., Nagumo, H., Chernova, I., Zhu, B*., et al.* (2007). TIM-1 and TIM-4 glycoproteins bind phosphatidylserine and mediate uptake of apoptotic cells. Immunity *27*, 927-940.

Kodama, H., Yamasaki, A., Nose, M., Niida, S., Ohgame, Y., Abe, M., Kumegawa, M., and Suda, T. (1991). Congenital osteoclast deficiency in osteopetrotic (op/op) mice is cured by injections of macrophage colony-stimulating factor. J Exp Med *173*, 269-272.

Kondo, M., Weissman, I.L., and Akashi, K. (1997). Identification of clonogenic common lymphoid progenitors in mouse bone marrow. Cell *91*, 661-672.

Kratz, A., Ferraro, M., Sluss, P.M., and Lewandrowski, K.B. (2004). Case records of the Massachusetts General Hospital. Weekly clinicopathological exercises. Laboratory reference values. N Engl J Med *351*, 1548-1563.

Kurakula, K., Koenis, D.S., van Tiel, C.M., and de Vries, C.J. (2014). NR4A nuclear receptors are orphans but not lonesome. Biochim Biophys Acta *1843*, 2543-2555.

Kurihara, T., Warr, G., Loy, J., and Bravo, R. (1997). Defects in macrophage recruitment and host defense in mice lacking the CCR2 chemokine receptor. J Exp Med *186*, 1757-1762.

Kurotaki, D., Osato, N., Nishiyama, A., Yamamoto, M., Ban, T., Sato, H., Nakabayashi, J., Umehara, M., Miyake, N., Matsumoto, N.*, et al.* (2013). Essential role of the IRF8-KLF4 transcription factor cascade in murine monocyte differentiation. Blood *121*, 1839-1849.

Lacaud, G., Gore, L., Kennedy, M., Kouskoff, V., Kingsley, P., Hogan, C., Carlsson, L., Speck, N., Palis, J., and Keller, G. (2002). Runx1 is essential for hematopoietic commitment at the hemangioblast stage of development in vitro. Blood *100*, 458-466.

Laiosa, C.V., Stadtfeld, M., and Graf, T. (2006). Determinants of lymphoid-myeloid lineage diversification. Annu Rev Immunol *24*, 705-738.

Lambert, J.F., Carlson, J.E., Colvin, G.A., and Quesenberry, P.J. (2000). Evaluation of mouse whole body bone marrow cellularity and distribution of hematopoietic progenitors. Experimental hematology *28*, 1493-1493.

Lancrin, C., Sroczynska, P., Serrano, A.G., Gandillet, A., Ferreras, C., Kouskoff, V., and Lacaud, G. (2010). Blood cell generation from the hemangioblast. Journal of molecular medicine *88*, 167-172.

Landsman, L., Varol, C., and Jung, S. (2007). Distinct differentiation potential of blood monocyte subsets in the lung. J Immunol *178*, 2000-2007.

Lawrence, T., and Natoli, G. (2011). Transcriptional regulation of macrophage polarization: enabling diversity with identity. Nat Rev Immunol *11*, 750-761.

Lee, S.L., Wesselschmidt, R.L., Linette, G.P., Kanagawa, O., Russell, J.H., and Milbrandt, J. (1995). Unimpaired thymic and peripheral T cell death in mice lacking the nuclear receptor NGFI-B (Nur77). Science *269*, 532-535.

Leuschner, F., Rauch, P.J., Ueno, T., Gorbatov, R., Marinelli, B., Lee, W.W., Dutta, P., Wei, Y., Robbins, C., Iwamoto, Y.*, et al.* (2012). Rapid monocyte kinetics in acute myocardial infarction are sustained by extramedullary monocytopoiesis. J Exp Med *209*, 123-137.

Lewis, M.R. (1925). The Formation of Macrophages, Epithelioid Cells and Giant Cells from Leucocytes in Incubated Blood. Am J Pathol *1*, 91-100 101.

Ley, K., Miller, Y.I., and Hedrick, C.C. (2011). Monocyte and macrophage dynamics during atherogenesis. Arterioscler Thromb Vasc Biol *31*, 1506-1516.

Lim, J.K., Obara, C.J., Rivollier, A., Pletnev, A.G., Kelsall, B.L., and Murphy, P.M. (2011). Chemokine receptor Ccr2 is critical for monocyte accumulation and survival in West Nile virus encephalitis. J Immunol *186*, 471-478.

Lin, H., Lee, E., Hestir, K., Leo, C., Huang, M., Bosch, E., Halenbeck, R., Wu, G., Zhou, A., Behrens, D.*, et al.* (2008). Discovery of a cytokine and its receptor by functional screening of the extracellular proteome. Science *320*, 807-811.

Liu, D., Jia, H., Holmes, D.I., Stannard, A., and Zachary, I. (2003). Vascular endothelial growth factor-regulated gene expression in endothelial cells: KDR-mediated induction of Egr3 and the related nuclear receptors Nur77, Nurr1, and Nor1. Arterioscler Thromb Vasc Biol *23*, 2002-2007.

Liu, K., Victora, G.D., Schwickert, T.A., Guermonprez, P., Meredith, M.M., Yao, K., Chu, F.F., Randolph, G.J., Rudensky, A.Y., and Nussenzweig, M. (2009). In vivo analysis of dendritic cell development and homeostasis. Science *324*, 392-397.

Liu, K., Waskow, C., Liu, X., Yao, K., Hoh, J., and Nussenzweig, M. (2007). Origin of dendritic cells in peripheral lymphoid organs of mice. Nature immunology.

Loke, P., Nair, M.G., Parkinson, J., Guiliano, D., Blaxter, M., and Allen, J.E. (2002). IL-4 dependent alternatively-activated macrophages have a distinctive in vivo gene expression phenotype. BMC Immunol *3*, 7.

Lu, R., Neff, N.F., Quake, S.R., and Weissman, I.L. (2011). Tracking single hematopoietic stem cells in vivo using high-throughput sequencing in conjunction with viral genetic barcoding. Nat Biotechnol *29*, 928-933.

MacDonald, K.P., Rowe, V., Bofinger, H.M., Thomas, R., Sasmono, T., Hume, D.A., and Hill, G.R. (2005). The colony-stimulating factor 1 receptor is expressed on dendritic cells during differentiation and regulates their expansion. J Immunol *175*, 1399-1405.

MacLennan, I.C. (1994). Germinal centers. Annu Rev Immunol *12*, 117-139.

Mansson, R., Hultquist, A., Luc, S., Yang, L., Anderson, K., Kharazi, S., Al-Hashmi, S., Liuba, K., Thoren, L., Adolfsson, J.*, et al.* (2007). Molecular evidence for hierarchical transcriptional lineage priming in fetal and adult stem cells and multipotent progenitors. Immunity *26*, 407-419.

Marchesi, V.T., and Florey, H.W. (1960). Electron micrographic observations on the emigration of leucocytes. Q J Exp Physiol Cogn Med Sci *45*, 343-348.

Marquis, J.F., LaCourse, R., Ryan, L., North, R.J., and Gros, P. (2009). Disseminated and rapidly fatal tuberculosis in mice bearing a defective allele at IFN regulatory factor 8. J Immunol *182*, 3008-3015.

Martinez, F.O., and Gordon, S. (2014). The M1 and M2 paradigm of macrophage activation: time for reassessment. F1000Prime Rep *6*, 13.

Mazurier, F., Fontanellas, A., Salesse, S., Taine, L., Landriau, S., Moreau-Gaudry, F., Reiffers, J., Peault, B., Di Santo, J.P., and de Verneuil, H. (1999). A novel immunodeficient mouse model--RAG2 x common cytokine receptor gamma chain double mutants--requiring exogenous cytokine administration for human hematopoietic stem cell engraftment. J Interferon Cytokine Res *19*, 533-541.

McKenzie, I.F., Gardiner, J., Cherry, M., and Snell, G.D. (1977). Lymphocyte antigens: Ly-4, Ly-6, and Ly-7. Transplant Proc *9*, 667-669.

McKercher, S.R., Torbett, B.E., Anderson, K.L., Henkel, G.W., Vestal, D.J., Baribault, H., Klemsz, M., Feeney, A.J., Wu, G.E., Paige, C.J*., et al.* (1996). Targeted disruption of the PU.1 gene results in multiple hematopoietic abnormalities. EMBO J *15*, 5647-5658.

Mebius, R.E., and Kraal, G. (2005). Structure and function of the spleen. Nat Rev Immunol *5*, 606-616.

Medvinsky, A., and Dzierzak, E. (1996). Definitive hematopoiesis is autonomously initiated by the AGM region. Cell *86*, 897-906.

Meier, I.D., Bernreuther, C., Tilling, T., Neidhardt, J., Wong, Y.W., Schulze, C., Streichert, T., and Schachner, M. (2010). Short DNA sequences inserted for gene targeting can accidentally interfere with off-target gene expression. FASEB J *24*, 1714-1724.

Metcalf, D. (2007). On hematopoietic stem cell fate. Immunity *26*, 669-673.

Metchnikoff, E. (1884a). The Ancestral History of the Inflammatory Process. Quarterly Journal of Microscopical Science, 112-117.

Metchnikoff, E. (1884b). Researches on the Intracellular Digestion of Invertebrates. Quarterly Journal of Microscopical Science, 89-111.

Metchnikoff, E. (1891). Lecture on Phagocytosis and Immunity. British medical journal *1*, 213-217.

Metchnikoff, E. (1892). Leçons sur la pathologie comparée de l'inflammation, Faites à l'Institut Pasteur in 1891 / par Elie Metchnikoff (Paris: Masson).

Metchnikoff, E. (1893). Lectures on the comparative pathology of inflammation : delivered at the Pasteur Institute in 1891 (London: Kegan Paul, Trench, Trübner).

Metchnikoff, E. (1968). Lectures on the comparative pathology of inflammation; delivered at the Pasteur Institute in 1891 (New York,: Dover Publications).

Michaud, J.P., Bellavance, M.A., Prefontaine, P., and Rivest, S. (2013). Real-time in vivo imaging reveals the ability of monocytes to clear vascular amyloid beta. Cell reports *5*, 646-653.

Michaud, J.P., Richard, K.L., and Rivest, S. (2011). MyD88-adaptor protein acts as a preventive mechanism for memory deficits in a mouse model of Alzheimer's disease. Mol Neurodegener *6*, 5.

Mildner, A., and Jung, S. (2014). Development and function of dendritic cell subsets. Immunity *40*, 642-656.

Mildner, A., Schmidt, H., Nitsche, M., Merkler, D., Hanisch, U.K., Mack, M., Heikenwalder, M., Bruck, W., Priller, J., and Prinz, M. (2007). Microglia in the adult

brain arise from Ly-6C(hi)CCR2(+) monocytes only under defined host conditions. Nat Neurosci *10*, 1544-1553.

Mills, C.D. (2012). M1 and M2 Macrophages: Oracles of Health and Disease. Crit Rev Immunol *32*, 463-488.

Mills, C.D., Kincaid, K., Alt, J.M., Heilman, M.J., and Hill, A.M. (2000). M-1/M-2 macrophages and the Th1/Th2 paradigm. J Immunol *164*, 6166-6173.

Misharin, A.V., Cuda, C.M., Saber, R., Turner, J.D., Gierut, A.K., Haines, G.K., 3rd, Berdnikovs, S., Filer, A., Clark, A.R., Buckley, C.D.*, et al.* (2014). Nonclassical Ly6C(-) monocytes drive the development of inflammatory arthritis in mice. Cell reports *9*, 591-604.

Mitruka, B.M., and Rawnsley, H.M. (1981). Clinical biochemical and hematological reference values in normal experimental animals and normal humans, 2nd edn (New York: Masson Pub. USA).

Miyamoto, T., Iwasaki, H., Reizis, B., Ye, M., Graf, T., Weissman, I.L., and Akashi, K. (2002). Myeloid or lymphoid promiscuity as a critical step in hematopoietic lineage commitment. Dev Cell *3*, 137-147.

Miyanishi, M., Tada, K., Koike, M., Uchiyama, Y., Kitamura, T., and Nagata, S. (2007). Identification of Tim4 as a phosphatidylserine receptor. Nature *450*, 435-439.

Moniuszko, M., Bodzenta-Lukaszyk, A., Kowal, K., Lenczewska, D., and Dabrowska, M. (2009). Enhanced frequencies of CD14++CD16+, but not CD14+CD16+, peripheral blood monocytes in severe asthmatic patients. Clin Immunol *130*, 338-346.

Montecino-Rodriguez, E., Leathers, H., and Dorshkind, K. (2006). Identification of a B-1 B cell-specified progenitor. Nat Immunol *7*, 293-301.

Moran, A.E., Holzapfel, K.L., Xing, Y., Cunningham, N.R., Maltzman, J.S., Punt, J., and Hogquist, K.A. (2011). T cell receptor signal strength in Treg and iNKT cell development demonstrated by a novel fluorescent reporter mouse. J Exp Med *208*, 1279-1289.

Morrison, S.J., Wandycz, A.M., Hemmati, H.D., Wright, D.E., and Weissman, I.L. (1997). Identification of a lineage of multipotent hematopoietic progenitors. Development *124*, 1929-1939.

Morrison, S.J., and Weissman, I.L. (1994). The long-term repopulating subset of hematopoietic stem cells is deterministic and isolatable by phenotype. Immunity *1*, 661-673.

Mosmann, T.R., and Coffman, R.L. (1989). TH1 and TH2 cells: different patterns of lymphokine secretion lead to different functional properties. Annu Rev Immunol *7*, 145-173.

Mossadegh-Keller, N., Sarrazin, S., Kandalla, P.K., Espinosa, L., Stanley, E.R., Nutt, S.L., Moore, J., and Sieweke, M.H. (2013). M-CSF instructs myeloid lineage fate in single haematopoietic stem cells. Nature *497*, 239-243.

Mosser, D.M., and Edwards, J.P. (2008). Exploring the full spectrum of macrophage activation. Nat Rev Immunol *8*, 958-969.

Mucenski, M.L., McLain, K., Kier, A.B., Swerdlow, S.H., Schreiner, C.M., Miller, T.A., Pietryga, D.W., Scott, W.J., Jr., and Potter, S.S. (1991). A functional c-myb gene is required for normal murine fetal hepatic hematopoiesis. Cell *65*, 677-689.

Mukouyama, Y., Chiba, N., Mucenski, M.L., Satake, M., Miyajima, A., Hara, T., and Watanabe, T. (1999). Hematopoietic cells in cultures of the murine embryonic aorta-gonad-mesonephros region are induced by c-Myb. Curr Biol *9*, 833-836.

Muller, A.M., Medvinsky, A., Strouboulis, J., Grosveld, F., and Dzierzak, E. (1994). Development of hematopoietic stem cell activity in the mouse embryo. Immunity *1*, 291-301.

Munder, M., Eichmann, K., and Modolell, M. (1998). Alternative metabolic states in murine macrophages reflected by the nitric oxide synthase/arginase balance: competitive regulation by CD4+ T cells correlates with Th1/Th2 phenotype. J Immunol *160*, 5347-5354.

Murray, P.J., Allen, J.E., Biswas, S.K., Fisher, E.A., Gilroy, D.W., Goerdt, S., Gordon, S., Hamilton, J.A., Ivashkiv, L.B., Lawrence, T.*, et al.* (2014). Macrophage activation and polarization: nomenclature and experimental guidelines. Immunity *41*, 14-20.

Naik, S.H., Perie, L., Swart, E., Gerlach, C., van Rooij, N., de Boer, R.J., and Schumacher, T.N. (2013). Diverse and heritable lineage imprinting of early haematopoietic progenitors. Nature *496*, 229-232.

Naik, S.H., Sathe, P., Park, H.Y., Metcalf, D., Proietto, A.I., Dakic, A., Carotta, S., O'Keeffe, M., Bahlo, M., Papenfuss, A.*, et al.* (2007). Development of plasmacytoid and conventional dendritic cell subtypes from single precursor cells derived in vitro and in vivo. Nat Immunol *8*, 1217-1226.

Naik, S.H., Schumacher, T.N., and Perie, L. (2014). Cellular barcoding: a technical appraisal. Exp Hematol *42*, 598-608.

Nair, M.G., Cochrane, D.W., and Allen, J.E. (2003). Macrophages in chronic type 2 inflammation have a novel phenotype characterized by the abundant expression of Ym1 and Fizz1 that can be partly replicated in vitro. Immunol Lett *85*, 173-180.

Nakatani, K., Yoshimoto, S., Iwano, M., Asai, O., Samejima, K., Sakan, H., Terada, M., Hasegawa, H., Nose, M., and Saito, Y. (2010). Fractalkine expression and CD16+ monocyte accumulation in glomerular lesions: association with their severity and diversity in lupus models. Am J Physiol Renal Physiol *299*, F207-216.

Nascimento, M., Huang, S.C., Smith, A., Everts, B., Lam, W., Bassity, E., Gautier, E.L., Randolph, G.J., and Pearce, E.J. (2014). Ly6Chi monocyte recruitment is responsible for Th2 associated host-protective macrophage accumulation in liver inflammation due to schistosomiasis. PLoS Pathog *10*, e1004282.

Nathan, C.F., Murray, H.W., Wiebe, M.E., and Rubin, B.Y. (1983). Identification of interferon-gamma as the lymphokine that activates human macrophage oxidative metabolism and antimicrobial activity. J Exp Med *158*, 670-689.

Nerlov, C., and Graf, T. (1998). PU.1 induces myeloid lineage commitment in multipotent hematopoietic progenitors. Genes & development *12*, 2403-2412.

Nimmerjahn, F., and Ravetch, J.V. (2008). Fcgamma receptors as regulators of immune responses. Nat Rev Immunol *8*, 34-47.

O'Garra, A., and Murphy, K. (1994). Role of cytokines in determining T-lymphocyte function. Curr Opin Immunol *6*, 458-466.

Odaka, C., and Mizuochi, T. (2002). Macrophages are involved in DNA degradation of apoptotic cells in murine thymus after administration of hydrocortisone. Cell Death Differ *9*, 104-112.

Olefsky, J.M., and Glass, C.K. (2010). Macrophages, inflammation, and insulin resistance. Annu Rev Physiol *72*, 219-246.

Onai, N., Obata-Onai, A., Schmid, M.A., Ohteki, T., Jarrossay, D., and Manz, M.G. (2007). Identification of clonogenic common Flt3(+)M-CSFR(+) plasmacytoid and conventional dendritic cell progenitors in mouse bone marrow. Nat Immunol *8*, 1207-1216.

Osawa, M., Hanada, K., Hamada, H., and Nakauchi, H. (1996). Long-term lymphohematopoietic reconstitution by a single CD34-low/negative hematopoietic stem cell. Science *273*, 242-245.

Palframan, R.T., Jung, S., Cheng, G., Weninger, W., Luo, Y., Dorf, M., Littman, D.R., Rollins, B.J., Zweerink, H., Rot, A.*, et al.* (2001). Inflammatory chemokine transport and presentation in HEV: a remote control mechanism for monocyte recruitment to lymph nodes in inflamed tissues. J Exp Med *194*, 1361-1373.

Palis, J., Robertson, S., Kennedy, M., Wall, C., and Keller, G. (1999). Development of erythroid and myeloid progenitors in the yolk sac and embryo proper of the mouse. Development *126*, 5073-5084.

Pamer, E.G. (2004). Immune responses to Listeria monocytogenes. Nat Rev Immunol *4*, 812-823.

Papac-Milicevic, N., Breuss, J.M., Zaujec, J., Ryban, L., Plyushch, T., Wagner, G.A., Fenzl, S., Dremsek, P., Cabaravdic, M., Steiner, M.*, et al.* (2012). The interferon stimulated gene 12 inactivates vasculoprotective functions of NR4A nuclear receptors. Circ Res *110*, e50-63.

Passlick, B., Flieger, D., and Ziegler-Heitbrock, H.W. (1989). Identification and characterization of a novel monocyte subpopulation in human peripheral blood. Blood *74*, 2527-2534.

Pesce, J.T., Ramalingam, T.R., Mentink-Kane, M.M., Wilson, M.S., El Kasmi, K.C., Smith, A.M., Thompson, R.W., Cheever, A.W., Murray, P.J., and Wynn, T.A. (2009). Arginase-1-expressing macrophages suppress Th2 cytokine-driven inflammation and fibrosis. PLoS Pathog *5*, e1000371.

Peters, W., Cyster, J.G., Mack, M., Schlondorff, D., Wolf, A.J., Ernst, J.D., and Charo, I.F. (2004). CCR2-dependent trafficking of F4/80dim macrophages and

CD11cdim/intermediate dendritic cells is crucial for T cell recruitment to lungs infected with Mycobacterium tuberculosis. J Immunol *172*, 7647-7653.

Pham, C.T., MacIvor, D.M., Hug, B.A., Heusel, J.W., and Ley, T.J. (1996). Long-range disruption of gene expression by a selectable marker cassette. Proc Natl Acad Sci U S A *93*, 13090-13095.

Phan, T.G., Green, J.A., Gray, E.E., Xu, Y., and Cyster, J.G. (2009). Immune complex relay by subcapsular sinus macrophages and noncognate B cells drives antibody affinity maturation. Nat Immunol *10*, 786-793.

Phan, T.G., Grigorova, I., Okada, T., and Cyster, J.G. (2007). Subcapsular encounter and complement-dependent transport of immune complexes by lymph node B cells. Nat Immunol *8*, 992-1000.

Plump, A.S., and Breslow, J.L. (1995). Apolipoprotein E and the apolipoprotein E-deficient mouse. Annu Rev Nutr *15*, 495-518.

Pozarowski, P., and Darzynkiewicz, Z. (2004). Analysis of cell cycle by flow cytometry. Methods Mol Biol *281*, 301-311.

Qu, C., Edwards, E.W., Tacke, F., Angeli, V., Llodra, J., Sanchez-Schmitz, G., Garin, A., Haque, N.S., Peters, W., van Rooijen, N.*, et al.* (2004). Role of CCR8 and other chemokine pathways in the migration of monocyte-derived dendritic cells to lymph nodes. J Exp Med *200*, 1231-1241.

Raes, G., De Baetselier, P., Noel, W., Beschin, A., Brombacher, F., and Hassanzadeh Gh, G. (2002). Differential expression of FIZZ1 and Ym1 in alternatively versus classically activated macrophages. J Leukoc Biol *71*, 597-602.

Rambaud, J., Desroches, J., Balsalobre, A., and Drouin, J. (2009). TIF1beta/KAP-1 is a coactivator of the orphan nuclear receptor NGFI-B/Nur77. J Biol Chem *284*, 14147-14156.

Ramirez-Herrick, A.M., Mullican, S.E., Sheehan, A.M., and Conneely, O.M. (2011). Reduced NR4A gene dosage leads to mixed myelodysplastic/myeloproliferative neoplasms in mice. Blood *117*, 2681-2690.

Randolph, G.J., Inaba, K., Robbiani, D.F., Steinman, R.M., and Muller, W.A. (1999). Differentiation of phagocytic monocytes into lymph node dendritic cells in vivo. Immunity *11*, 753-761.

Rijli, F.M., Dolle, P., Fraulob, V., LeMeur, M., and Chambon, P. (1994). Insertion of a targeting construct in a Hoxd-10 allele can influence the control of Hoxd-9 expression. Dev Dyn *201*, 366-377.

Robbins, C.S., Chudnovskiy, A., Rauch, P.J., Figueiredo, J.L., Iwamoto, Y., Gorbatov, R., Etzrodt, M., Weber, G.F., Ueno, T., van Rooijen, N.*, et al.* (2012). Extramedullary hematopoiesis generates Ly-6C(high) monocytes that infiltrate atherosclerotic lesions. Circulation *125*, 364-374.

Robbins, C.S., Hilgendorf, I., Weber, G.F., Theurl, I., Iwamoto, Y., Figueiredo, J.L., Gorbatov, R., Sukhova, G.K., Gerhardt, L.M., Smyth, D.*, et al.* (2013). Local

proliferation dominates lesional macrophage accumulation in atherosclerosis. Nat Med *19*, 1166-1172.

Rosen, H., Gordon, S., and North, R.J. (1989). Exacerbation of murine listeriosis by a monoclonal antibody specific for the type 3 complement receptor of myelomonocytic cells. Absence of monocytes at infective foci allows Listeria to multiply in nonphagocytic cells. J Exp Med *170*, 27-37.

Rosenfeld, M.G., Lunyak, V.V., and Glass, C.K. (2006). Sensors and signals: a coactivator/corepressor/epigenetic code for integrating signal-dependent programs of transcriptional response. Genes & development *20*, 1405-1428.

Ross, R. (1999). Atherosclerosis--an inflammatory disease. N Engl J Med *340*, 115-126.

Roszer, T., Menendez-Gutierrez, M.P., Cedenilla, M., and Ricote, M. (2013). Retinoid X receptors in macrophage biology. Trends Endocrinol Metab *24*, 460-468.

Salazar-Mather, T.P., Orange, J.S., and Biron, C.A. (1998). Early murine cytomegalovirus (MCMV) infection induces liver natural killer (NK) cell inflammation and protection through macrophage inflammatory protein 1alpha (MIP-1alpha)-dependent pathways. J Exp Med *187*, 1-14.

Sans-Fons, M.G., Yeramian, A., Pereira-Lopes, S., Santamaria-Babi, L.F., Modolell, M., Lloberas, J., and Celada, A. (2013). Arginine transport is impaired in C57Bl/6 mouse macrophages as a result of a deletion in the promoter of Slc7a2 (CAT2), and susceptibility to Leishmania infection is reduced. J Infect Dis *207*, 1684-1693.

Santiago-Raber, M.L., Amano, H., Amano, E., Baudino, L., Otani, M., Lin, Q., Nimmerjahn, F., Verbeek, J.S., Ravetch, J.V., Takasaki, Y.*, et al.* (2009). Fcgamma receptor-dependent expansion of a hyperactive monocyte subset in lupus-prone mice. Arthritis Rheum *60*, 2408-2417.

Santiago-Raber, M.L., Baudino, L., Alvarez, M., van Rooijen, N., Nimmerjahn, F., and Izui, S. (2011). TLR7/9-mediated monocytosis and maturation of Gr-1(hi) inflammatory monocytes towards Gr-1(lo) resting monocytes implicated in murine lupus. J Autoimmun *37*, 171-179.

Sasmono, R.T., Ehrnsperger, A., Cronau, S.L., Ravasi, T., Kandane, R., Hickey, M.J., Cook, A.D., Himes, S.R., Hamilton, J.A., and Hume, D.A. (2007). Mouse neutrophilic granulocytes express mRNA encoding the macrophage colony-stimulating factor receptor (CSF-1R) as well as many other macrophage-specific transcripts and can transdifferentiate into macrophages in vitro in response to CSF-1. J Leukoc Biol *82*, 111-123.

Sasmono, R.T., Oceandy, D., Pollard, J.W., Tong, W., Pavli, P., Wainwright, B.J., Ostrowski, M.C., Himes, S.R., and Hume, D.A. (2003). A macrophage colony-stimulating factor receptor-green fluorescent protein transgene is expressed throughout the mononuclear phagocyte system of the mouse. Blood *101*, 1155-1163.

Scharton-Kersten, T., Contursi, C., Masumi, A., Sher, A., and Ozato, K. (1997). Interferon consensus sequence binding protein-deficient mice display impaired

resistance to intracellular infection due to a primary defect in interleukin 12 p40 induction. J Exp Med *186*, 1523-1534.

Schmidl, C., Renner, K., Peter, K., Eder, R., Lassmann, T., Balwierz, P.J., Itoh, M., Nagao-Sato, S., Kawaji, H., Carninci, P.*, et al.* (2014). Transcription and enhancer profiling in human monocyte subsets. Blood *123*, e90-99.

Schulz, C., Gomez Perdiguero, E., Chorro, L., Szabo-Rogers, H., Cagnard, N., Kierdorf, K., Prinz, M., Wu, B., Jacobsen, S.E., Pollard, J.W.*, et al.* (2012). A lineage of myeloid cells independent of Myb and hematopoietic stem cells. Science *336*, 86-90.

Scott, E.W., Simon, M.C., Anastasi, J., and Singh, H. (1994). Requirement of transcription factor PU.1 in the development of multiple hematopoietic lineages. Science *265*, 1573-1577.

Scott, H.M., and Flynn, J.L. (2002). Mycobacterium tuberculosis in chemokine receptor 2-deficient mice: influence of dose on disease progression. Infect Immun *70*, 5946-5954.

Segre, J.A., Bauer, C., and Fuchs, E. (1999). Klf4 is a transcription factor required for establishing the barrier function of the skin. Nat Genet *22*, 356-360.

Sekiya, T., Kashiwagi, I., Yoshida, R., Fukaya, T., Morita, R., Kimura, A., Ichinose, H., Metzger, D., Chambon, P., and Yoshimura, A. (2013). Nr4a receptors are essential for thymic regulatory T cell development and immune homeostasis. Nat Immunol *14*, 230-237.

Serbina, N.V., Cherny, M., Shi, C., Bleau, S.A., Collins, N.H., Young, J.W., and Pamer, E.G. (2009). Distinct responses of human monocyte subsets to Aspergillus fumigatus conidia. J Immunol *183*, 2678-2687.

Serbina, N.V., Jia, T., Hohl, T.M., and Pamer, E.G. (2008). Monocyte-mediated defense against microbial pathogens. Annu Rev Immunol *26*, 421-452.

Serbina, N.V., Kuziel, W., Flavell, R., Akira, S., Rollins, B., and Pamer, E.G. (2003a). Sequential MyD88-independent and -dependent activation of innate immune responses to intracellular bacterial infection. Immunity *19*, 891-901.

Serbina, N.V., and Pamer, E.G. (2006). Monocyte emigration from bone marrow during bacterial infection requires signals mediated by chemokine receptor CCR2. Nat Immunol *7*, 311-317.

Serbina, N.V., Salazar-Mather, T.P., Biron, C.A., Kuziel, W.A., and Pamer, E.G. (2003b). TNF/iNOS-producing dendritic cells mediate innate immune defense against bacterial infection. Immunity *19*, 59-70.

Serbina, N.V., Shi, C., and Pamer, E.G. (2012). Monocyte-mediated immune defense against murine Listeria monocytogenes infection. Adv Immunol *113*, 119-134.

Shand, F.H., Ueha, S., Otsuji, M., Koid, S.S., Shichino, S., Tsukui, T., Kosugi-Kanaya, M., Abe, J., Tomura, M., Ziogas, J.*, et al.* (2014). Tracking of intertissue migration reveals the origins of tumor-infiltrating monocytes. Proc Natl Acad Sci U S A *111*, 7771-7776.

Sheng, J., Ruedl, C., and Karjalainen, K. (2015). Most Tissue-Resident Macrophages Except Microglia Are Derived from Fetal Hematopoietic Stem Cells. Immunity *43*, 382-393.

Shimshek, D.R., Kim, J., Hubner, M.R., Spergel, D.J., Buchholz, F., Casanova, E., Stewart, A.F., Seeburg, P.H., and Sprengel, R. (2002). Codon-improved Cre recombinase (iCre) expression in the mouse. Genesis *32*, 19-26.

Silverstein, A.M. (2009). A history of immunology, 2nd ed. edn (London: Elsevier/Academic Press).

Skrzeczynska-Moncznik, J., Bzowska, M., Loseke, S., Grage-Griebenow, E., Zembala, M., and Pryjma, J. (2008). Peripheral blood CD14high CD16+ monocytes are main producers of IL-10. Scand J Immunol *67*, 152-159.

Sohn, Y.C., Kwak, E., Na, Y., Lee, J.W., and Lee, S.K. (2001). Silencing mediator of retinoid and thyroid hormone receptors and activating signal cointegrator-2 as transcriptional coregulators of the orphan nuclear receptor Nur77. J Biol Chem *276*, 43734-43739.

Sorokin, S.P., Hoyt, R.F., Jr., Blunt, D.G., and McNelly, N.A. (1992). Macrophage development: II. Early ontogeny of macrophage populations in brain, liver, and lungs of rat embryos as revealed by a lectin marker. The Anatomical record *232*, 527-550.

Soza-Ried, C., Hess, I., Netuschil, N., Schorpp, M., and Boehm, T. (2010). Essential role of c-myb in definitive hematopoiesis is evolutionarily conserved. Proc Natl Acad Sci U S A *107*, 17304-17308.

Spain, L.M., Guerriero, A., Kunjibettu, S., and Scott, E.W. (1999). T cell development in PU.1-deficient mice. J Immunol *163*, 2681-2687.

Spangrude, G.J., Heimfeld, S., and Weissman, I.L. (1988). Purification and characterization of mouse hematopoietic stem cells. Science *241*, 58-62.

Sponaas, A.M., Freitas do Rosario, A.P., Voisine, C., Mastelic, B., Thompson, J., Koernig, S., Jarra, W., Renia, L., Mauduit, M., Potocnik, A.J*., et al.* (2009). Migrating monocytes recruited to the spleen play an important role in control of blood stage malaria. Blood *114*, 5522-5531.

Srinivas, S., Watanabe, T., Lin, C.S., William, C.M., Tanabe, Y., Jessell, T.M., and Costantini, F. (2001). Cre reporter strains produced by targeted insertion of EYFP and ECFP into the ROSA26 locus. BMC Dev Biol *1*, 4.

Stein, M., Keshav, S., Harris, N., and Gordon, S. (1992). Interleukin 4 potently enhances murine macrophage mannose receptor activity: a marker of alternative immunologic macrophage activation. J Exp Med *176*, 287-292.

Steinman, R.M., Adams, J.C., and Cohn, Z.A. (1975). Identification of a novel cell type in peripheral lymphoid organs of mice. IV. Identification and distribution in mouse spleen. J Exp Med *141*, 804-820.

Steinman, R.M., and Cohn, Z.A. (1973). Identification of a novel cell type in peripheral lymphoid organs of mice. I. Morphology, quantitation, tissue distribution. J Exp Med *137*, 1142-1162.

Steinman, R.M., Lustig, D.S., and Cohn, Z.A. (1974). Identification of a novel cell type in peripheral lymphoid organs of mice. 3. Functional properties in vivo. J Exp Med *139*, 1431-1445.

Steinman, R.M., and Witmer, M.D. (1978). Lymphoid dendritic cells are potent stimulators of the primary mixed leukocyte reaction in mice. Proc Natl Acad Sci U S A *75*, 5132-5136.

Sumagin, R., Prizant, H., Lomakina, E., Waugh, R.E., and Sarelius, I.H. (2010). LFA-1 and Mac-1 define characteristically different intralumenal crawling and emigration patterns for monocytes and neutrophils in situ. J Immunol *185*, 7057-7066.

Sumner, R., Crawford, A., Mucenski, M., and Frampton, J. (2000). Initiation of adult myelopoiesis can occur in the absence of c-Myb whereas subsequent development is strictly dependent on the transcription factor. Oncogene *19*, 3335-3342.

Sunderkotter, C., Nikolic, T., Dillon, M.J., Van Rooijen, N., Stehling, M., Drevets, D.A., and Leenen, P.J. (2004). Subpopulations of mouse blood monocytes differ in maturation stage and inflammatory response. J Immunol *172*, 4410-4417.

Surh, C.D., and Sprent, J. (1994). T-cell apoptosis detected in situ during positive and negative selection in the thymus. Nature *372*, 100-103.

Swirski, F.K., Libby, P., Aikawa, E., Alcaide, P., Luscinskas, F.W., Weissleder, R., and Pittet, M.J. (2007). Ly-6Chi monocytes dominate hypercholesterolemia-associated monocytosis and give rise to macrophages in atheromata. J Clin Invest *117*, 195-205.

Tacke, F., and Randolph, G.J. (2006). Migratory fate and differentiation of blood monocyte subsets. Immunobiology *211*, 609-618.

Tacke, R., Hilgendorf, I., Garner, H., Waterborg, C., Park, K., Nowyhed, H., Hanna, R.N., Wu, R., Swirski, F.K., Geissmann, F*., et al.* (2015). The transcription factor NR4A1 is essential for the development of a novel macrophage subset in the thymus. Scientific reports *5*, 10055.

Takahashi, K., Yamamura, F., and Naito, M. (1989). Differentiation, maturation, and proliferation of macrophages in the mouse yolk sac: a light-microscopic, enzyme-cytochemical, immunohistochemical, and ultrastructural study. J Leukoc Biol *45*, 87-96.

Tamura, T., Nagamura-Inoue, T., Shmeltzer, Z., Kuwata, T., and Ozato, K. (2000). ICSBP directs bipotential myeloid progenitor cells to differentiate into mature macrophages. Immunity *13*, 155-165.

Taylor, P.R., and Gordon, S. (2003). Monocyte heterogeneity and innate immunity. Immunity *19*, 2-4.

Taylor, P.R., Martinez-Pomares, L., Stacey, M., Lin, H.H., Brown, G.D., and Gordon, S. (2005). Macrophage receptors and immune recognition. Annu Rev Immunol *23*, 901-944.

Till, J.E., McCulloch, E.A., and Siminovitch, L. (1964). A Stochastic Model of Stem Cell Proliferation, Based on the Growth of Spleen Colony-Forming Cells. Proc Natl Acad Sci U S A *51*, 29-36.

Tober, J., McGrath, K.E., and Palis, J. (2008). Primitive erythropoiesis and megakaryopoiesis in the yolk sac are independent of c-myb. Blood *111*, 2636-2639.

Traynor, T.R., Kuziel, W.A., Toews, G.B., and Huffnagle, G.B. (2000). CCR2 expression determines T1 versus T2 polarization during pulmonary Cryptococcus neoformans infection. J Immunol *164*, 2021-2027.

Tsou, C.L., Peters, W., Si, Y., Slaymaker, S., Aslanian, A.M., Weisberg, S.P., Mack, M., and Charo, I.F. (2007). Critical roles for CCR2 and MCP-3 in monocyte mobilization from bone marrow and recruitment to inflammatory sites. J Clin Invest *117*, 902-909.

Turcotte, K., Gauthier, S., Malo, D., Tam, M., Stevenson, M.M., and Gros, P. (2007). Icsbp1/IRF-8 is required for innate and adaptive immune responses against intracellular pathogens. J Immunol *179*, 2467-2476.

Uhrin, P., Perkmann, T., Binder, B., and Schabbauer, G. (2013). ISG12 is a critical modulator of innate immune responses in murine models of sepsis. Immunobiology *218*, 1207-1216.

van Furth, R. (1970). Origin and kinetics of monocytes and macrophages. Semin Hematol *7*, 125-141.

van Furth, R. (1980). The mononuclear phagocyte system. Verh Dtsch Ges Pathol *64*, 1-11.

van Furth, R., and Cohn, Z.A. (1968). The origin and kinetics of mononuclear phagocytes. J Exp Med *128*, 415-435.

van Furth, R., Cohn, Z.A., Hirsch, J.G., Humphrey, J.H., Spector, W.G., and Langevoort, H.L. (1972). The mononuclear phagocyte system: a new classification of macrophages, monocytes, and their precursor cells. Bull World Health Organ *46*, 845-852.

Varga, T., Mounier, R., Gogolak, P., Poliska, S., Chazaud, B., and Nagy, L. (2013). Tissue LyC6- macrophages are generated in the absence of circulating LyC6- monocytes and Nur77 in a model of muscle regeneration. J Immunol *191*, 5695-5701.

Varol, C., Landsman, L., Fogg, D.K., Greenshtein, L., Gildor, B., Margalit, R., Kalchenko, V., Geissmann, F., and Jung, S. (2007). Monocytes give rise to mucosal, but not splenic, conventional dendritic cells. J Exp Med *204*, 171-180.

Varol, C., Vallon-Eberhard, A., Elinav, E., Aychek, T., Shapira, Y., Luche, H., Fehling, H.J., Hardt, W.D., Shakhar, G., and Jung, S. (2009). Intestinal lamina propria dendritic cell subsets have different origin and functions. Immunity *31*, 502-512.

Wansa, K.D., Harris, J.M., and Muscat, G.E. (2002). The activation function-1 domain of Nur77/NR4A1 mediates trans-activation, cell specificity, and coactivator recruitment. J Biol Chem *277*, 33001-33011.

Wansa, K.D., Harris, J.M., Yan, G., Ordentlich, P., and Muscat, G.E. (2003). The AF-1 domain of the orphan nuclear receptor NOR-1 mediates trans-activation, coactivator recruitment, and activation by the purine anti-metabolite 6-mercaptopurine. J Biol Chem *278*, 24776-24790.

Wansa, K.D., and Muscat, G.E. (2005). TRAP220 is modulated by the antineoplastic agent 6-Mercaptopurine, and mediates the activation of the NR4A subgroup of nuclear receptors. J Mol Endocrinol *34*, 835-848.

Waskow, C., Liu, K., Darrasse-Jeze, G., Guermonprez, P., Ginhoux, F., Merad, M., Shengelia, T., Yao, K., and Nussenzweig, M. (2008). The receptor tyrosine kinase Flt3 is required for dendritic cell development in peripheral lymphoid tissues. Nat Immunol *9*, 676-683.

Weber, C., Belge, K.U., von Hundelshausen, P., Draude, G., Steppich, B., Mack, M., Frankenberger, M., Weber, K.S., and Ziegler-Heitbrock, H.W. (2000). Differential chemokine receptor expression and function in human monocyte subpopulations. J Leukoc Biol *67*, 699-704.

Weber, C., Zernecke, A., and Libby, P. (2008). The multifaceted contributions of leukocyte subsets to atherosclerosis: lessons from mouse models. Nat Rev Immunol *8*, 802-815.

Weisberg, S.P., Hunter, D., Huber, R., Lemieux, J., Slaymaker, S., Vaddi, K., Charo, I., Leibel, R.L., and Ferrante, A.W., Jr. (2006). CCR2 modulates inflammatory and metabolic effects of high-fat feeding. J Clin Invest *116*, 115-124.

Weisberg, S.P., McCann, D., Desai, M., Rosenbaum, M., Leibel, R.L., and Ferrante, A.W., Jr. (2003). Obesity is associated with macrophage accumulation in adipose tissue. J Clin Invest *112*, 1796-1808.

Weissman, I.L. (2000). Stem cells: units of development, units of regeneration, and units in evolution. Cell *100*, 157-168.

Wiktor-Jedrzejczak, W., Bartocci, A., Ferrante, A.W., Jr., Ahmed-Ansari, A., Sell, K.W., Pollard, J.W., and Stanley, E.R. (1990). Total absence of colony-stimulating factor 1 in the macrophage-deficient osteopetrotic (op/op) mouse. Proc Natl Acad Sci U S A *87*, 4828-4832.

Wiktor-Jedrzejczak, W., and Gordon, S. (1996). Cytokine regulation of the macrophage (M phi) system studied using the colony stimulating factor-1-deficient op/op mouse. Physiol Rev *76*, 927-947.

Winoto, A., and Littman, D.R. (2002). Nuclear hormone receptors in T lymphocytes. Cell *109 Suppl*, S57-66.

Wong, K., Valdez, P.A., Tan, C., Yeh, S., Hongo, J.A., and Ouyang, W. (2010). Phosphatidylserine receptor Tim-4 is essential for the maintenance of the homeostatic state of resident peritoneal macrophages. Proc Natl Acad Sci U S A *107*, 8712-8717.

Wong, K.L., Tai, J.J., Wong, W.C., Han, H., Sem, X., Yeap, W.H., Kourilsky, P., and Wong, S.C. (2011). Gene expression profiling reveals the defining features of the classical, intermediate, and nonclassical human monocyte subsets. Blood *118*, e16-31.

Woollard, K.J., and Geissmann, F. (2010). Monocytes in atherosclerosis: subsets and functions. Nat Rev Cardiol *7*, 77-86.

Wynn, T.A., Chawla, A., and Pollard, J.W. (2013). Macrophage biology in development, homeostasis and disease. Nature *496*, 445-455.

Xu, H., Barnes, G.T., Yang, Q., Tan, G., Yang, D., Chou, C.J., Sole, J., Nichols, A., Ross, J.S., Tartaglia, L.A.*, et al.* (2003). Chronic inflammation in fat plays a crucial role in the development of obesity-related insulin resistance. J Clin Invest *112*, 1821-1830.

Yamada, M., Naito, M., and Takahashi, K. (1990). Kupffer cell proliferation and glucan-induced granuloma formation in mice depleted of blood monocytes by strontium-89. J Leukoc Biol *47*, 195-205.

Yamamoto, R., Morita, Y., Ooehara, J., Hamanaka, S., Onodera, M., Rudolph, K.L., Ema, H., and Nakauchi, H. (2013). Clonal analysis unveils self-renewing lineage-restricted progenitors generated directly from hematopoietic stem cells. Cell *154*, 1112-1126.

Yang, L., Bryder, D., Adolfsson, J., Nygren, J., Mansson, R., Sigvardsson, M., and Jacobsen, S.E. (2005). Identification of Lin(-)Sca1(+)kit(+)CD34(+)Flt3- short-term hematopoietic stem cells capable of rapidly reconstituting and rescuing myeloablated transplant recipients. Blood *105*, 2717-2723.

Yona, S., and Gordon, S. (2015). From the Reticuloendothelial to Mononuclear Phagocyte System - The Unaccounted Years. Front Immunol *6*, 328.

Yona, S., Kim, K.W., Wolf, Y., Mildner, A., Varol, D., Breker, M., Strauss-Ayali, D., Viukov, S., Guilliams, M., Misharin, A.*, et al.* (2013). Fate mapping reveals origins and dynamics of monocytes and tissue macrophages under homeostasis. Immunity *38*, 79-91.

Yoshida, H., Hayashi, S., Kunisada, T., Ogawa, M., Nishikawa, S., Okamura, H., Sudo, T., Shultz, L.D., and Nishikawa, S. (1990). The murine mutation osteopetrosis is in the coding region of the macrophage colony stimulating factor gene. Nature *345*, 442-444.

Yrlid, U., Jenkins, C.D., and MacPherson, G.G. (2006). Relationships between distinct blood monocyte subsets and migrating intestinal lymph dendritic cells in vivo under steady-state conditions. J Immunol *176*, 4155-4162.

Zawada, A.M., Rogacev, K.S., Rotter, B., Winter, P., Marell, R.R., Fliser, D., and Heine, G.H. (2011). SuperSAGE evidence for CD14++CD16+ monocytes as a third monocyte subset. Blood *118*, e50-61.

Zernecke, A., Bot, I., Djalali-Talab, Y., Shagdarsuren, E., Bidzhekov, K., Meiler, S., Krohn, R., Schober, A., Sperandio, M., Soehnlein, O.*, et al.* (2008). Protective role of CXC receptor 4/CXC ligand 12 unveils the importance of neutrophils in atherosclerosis. Circ Res *102*, 209-217.

Zhang, S.H., Reddick, R.L., Piedrahita, J.A., and Maeda, N. (1992). Spontaneous hypercholesterolemia and arterial lesions in mice lacking apolipoprotein E. Science *258*, 468-471.

Ziegler-Heitbrock, H.W., Passlick, B., and Flieger, D. (1988). The monoclonal antimonocyte antibody My4 stains B lymphocytes and two distinct monocyte subsets in human peripheral blood. Hybridoma *7*, 521-527.

Ziegler-Heitbrock, L. (2014). Monocyte subsets in man and other species. Cell Immunol *289*, 135-139.

Ziegler-Heitbrock, L., Ancuta, P., Crowe, S., Dalod, M., Grau, V., Hart, D.N., Leenen, P.J., Liu, Y.J., MacPherson, G., Randolph, G.J., *et al.* (2010). Nomenclature of monocytes and dendritic cells in blood. Blood *116*, e74-80.

8 Appendix 1

Spleen macrophage/monocyte gating strategy

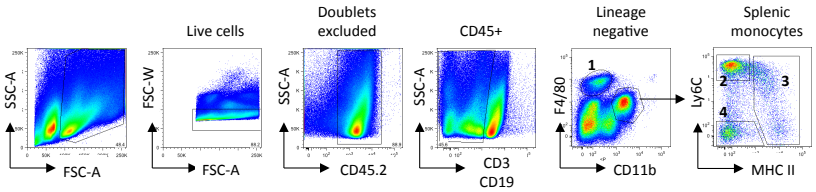

1. F4/80^{bright} Red Pulp Mø

2. Splenic Ly6C^{+}
3. Splenic Ly6C^{int} MHC II^{+}
4. Splenic Ly6C^{low} MHC II^{-}

Spleen dendritic cell gating strategy

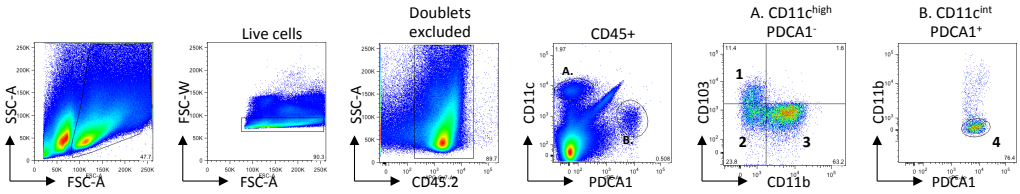

1. CD11c^{high} PDCA1^{-} CD11b^{-} CD103^{+}
2. CD11c^{high} PDCA1^{-} CD11b^{-} CD103^{-}
3. CD11c^{high} PDCA1^{-} CD11b^{+} CD103^{-}

4. CD11c^{int} PDCA1^{+}

Liver: Gating strategy

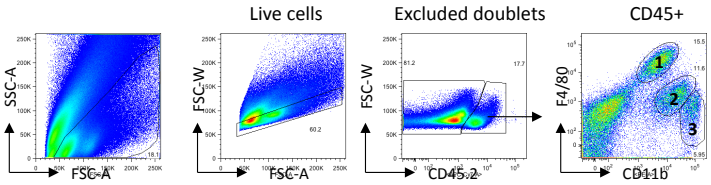

1. Kupffer Cells
2. F4/80^{+} CD11b^{+}
3. F4/80^{-} CD11b^{+}

Lung: Gating strategy

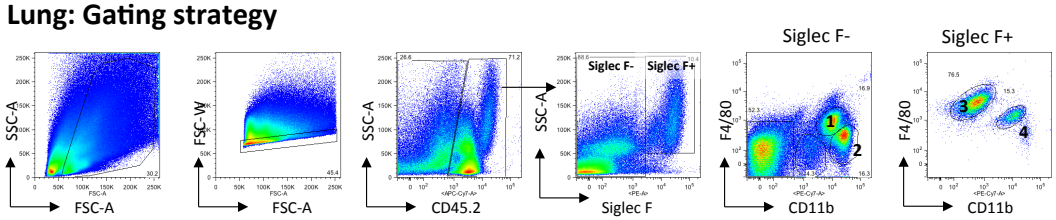

1. Siglec F^{-} F4/80^{+} CD11b^{+}
2. Siglec F^{-} F4/80^{-} CD11b^{+}

3. Siglec F^{+} F4/80^{+} CD11b^{-} alveolar Mø
4. Siglec F^{+} F4/80^{low} CD11b^{+} eosinophils

Brain: Gating strategy

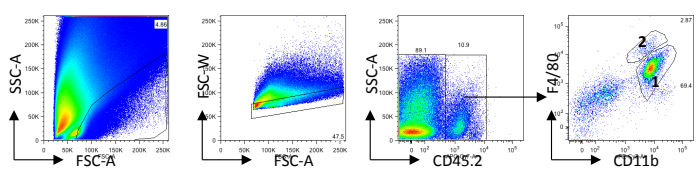

1. Microglia
2. F4/80^{bright} CD11b^{+}

Lymph node dendritic cells and medullary macrophages gating strategy

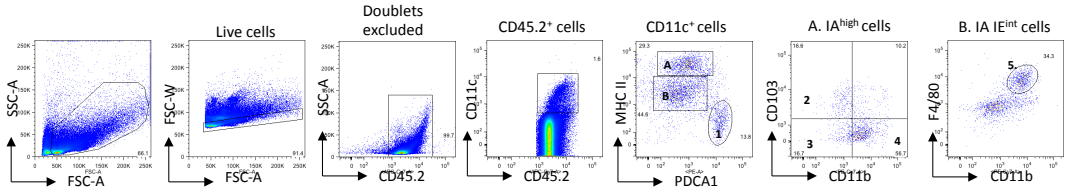

1. CD11c⁺ PDCA1⁺ pDCs

2. CD11c^high PDCA1⁻ CD11b⁻ CD103⁺

3. CD11c^high PDCA1⁻ CD11b⁻ CD103⁻

4. CD11c^high PDCA1⁻ CD11b⁺ CD103⁻

5. Medullary macrophages

Lymph node subcapsular macrophages gating strategy

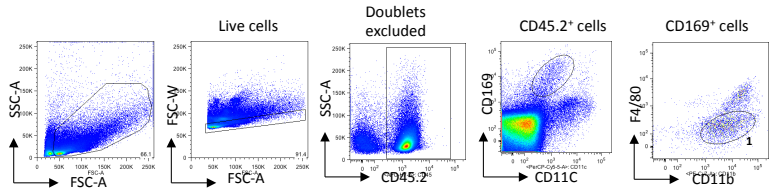

1. Sucapsular macrophages

Thymus macrophage gating strategy

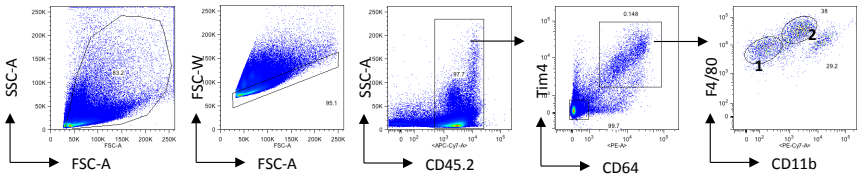

1. Tim4⁺ CD64⁺ F4/80⁺ CD11b^low

2. Tim4⁺ CD64⁺ F4/80^bright CD11b⁺

Thymus dendritic cell gating strategy

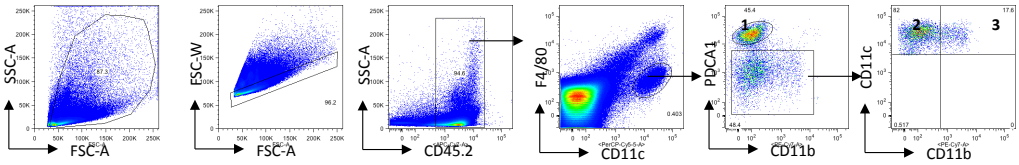

1. CD11c⁺ PDCA1⁺ pDCs

2. CD11c⁺ PDCA1⁻ CD11b⁻

2. CD11c⁺ PDCA1⁻ CD11b⁺

Dermis macrophage gating strategy

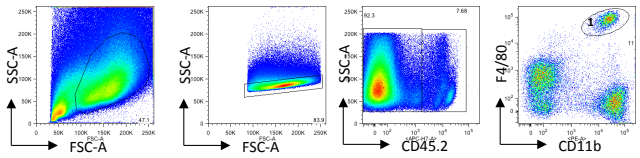

1. F4/80^{bright} macrophages

Dermis dendritic cell gating strategy

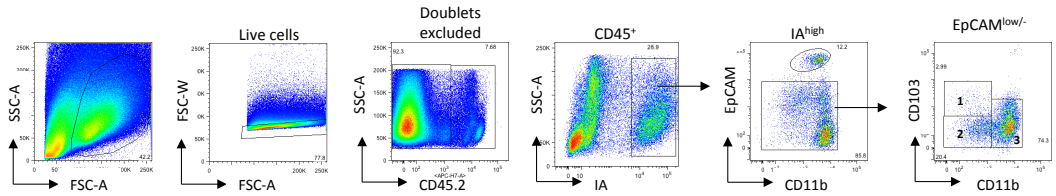

1. CD103$^+$ CD11b$^-$
2. CD103$^-$ CD11b$^-$
3. CD103$^-$ CD11b$^+$

Epidermis gating strategy

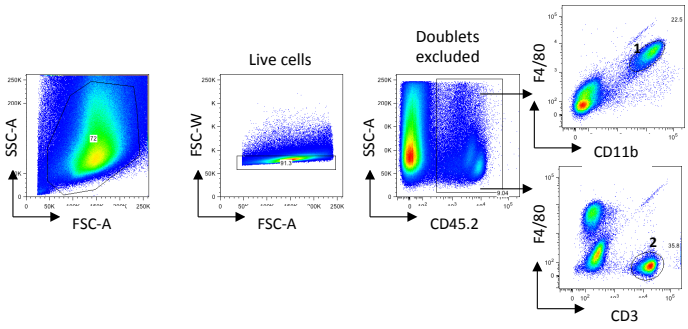

1. Langerhans cells
2. T cells

Small intestine lamina propria /colon gating strategy myeloid cells

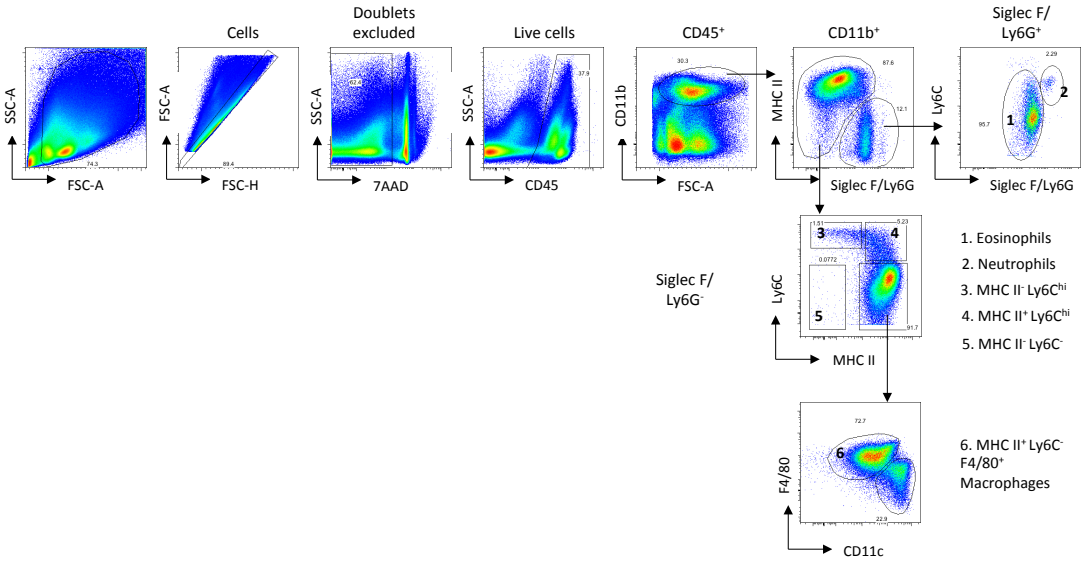

Small intestine lamina propria /colon gating strategy dendritic cells

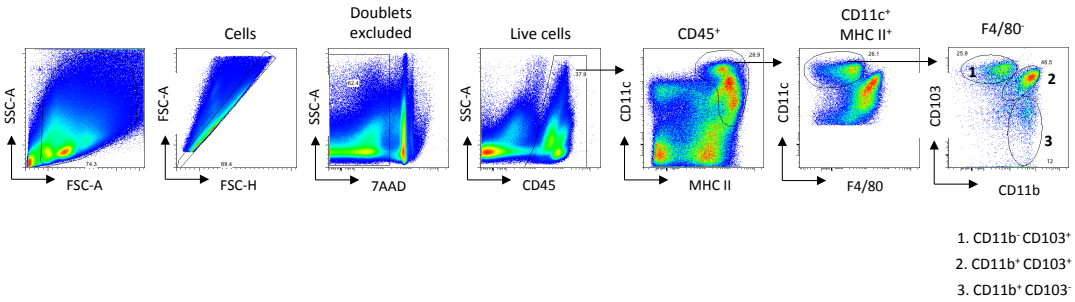

Appendix 1- 1 Gating strategies used in flow cytometry analysis in this thesis

Gating strategies used for analysing tissue myeloid populations in this thesis with the exception of blood, BM and peritoneal lavage, the gating strategies for these are included in the main body of the text.

9 Appendix 2

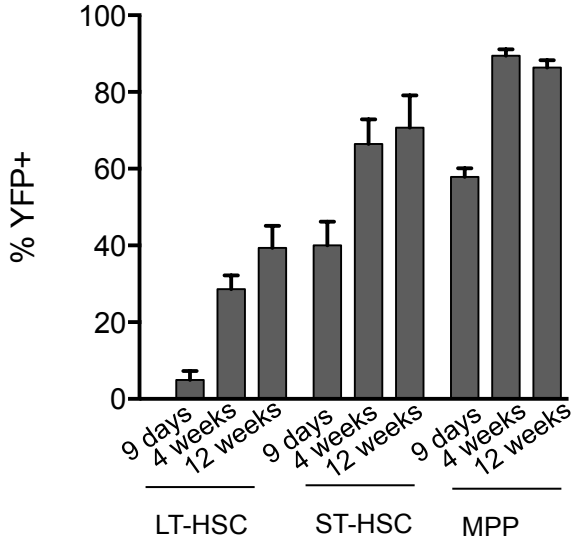

Appendix 1- 2 *Flt3*^{Cre} *Rosa*^{YFP} labelling of HSCs

Frequency of YFP^{+} HSCs at 9 days, 4 weeks and 12 weeks of age, n=3-6 per age group, error bars represent standard deviation.